Polyelectrolyte Templating in Langmuir-Blodgett Films : Enhanced Second Harmonic Generation in Molecular Materials and Chain Organization in Polymer Assemblies

A Thesis
Submitted for the Degree of
DOCTOR OF PHILOSOPHY

by

M. Sharath Chandra

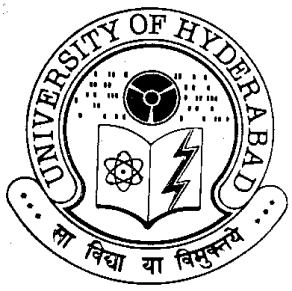

School of Chemistry
University of Hyderabad
Hyderabad 500 046
INDIA

June 2005

To
Ayee and Naanna

DECLARATION

I hereby declare that the matter embodied in this thesis is the result of investigations carried out by me in the School of Chemistry, University of Hyderabad, Hyderabad under the supervision of Prof. T. P. Radhakrishnan.

In keeping with the general practice of reporting scientific observations, due acknowledgements have been made wherever the work described is based on the findings of other investigators.

M. Sharath Chandra

CERTIFICATE

This is to certify that the work described in this thesis entitled "**Polyelectrolyte Templated Langmuir-Blodgett Films : Enhanced Second Harmonic Generation in Molecular Materials and Chain Organization in Polymer Assemblies**" has been carried out by M. Sharath Chandra, under my supervision and the same has not been submitted elsewhere for any degree.

Prof. T. P. Radhakrishnan
(Thesis Supervisor)

DEAN
School of Chemistry
University of Hyderabad
Hyderabad 500 046

ACKNOWLEDGEMENTS

I take this opportunity to express my deep sense of gratitude to Prof. T. P. Radhakrishnan, my thesis supervisor for his constant encouragement and support during my research work. His commitment towards work, discipline, honesty and patience are highly admirable and motivating. My association with him has been an enriching experience.

I would like to thank the present and past Deans, School of Chemistry for the facilities and infrastructure in the department. I thank all the faculty members for their cooperation. My special thanks are due to all my M. Sc teachers for their excellent teaching. I specially thank Prof. E. D. Jemmis and Prof. D. Basavaiah for their useful suggestions and encouragement. I also thank Prof. K. C. Kumaraswamy for his care and concern. I thank Prof. M. Durga Prasad for some fruitful discussions. I am very grateful to Prof. M. J. Swamy, for his suggestions and support at various stages of my research. I am deeply indebted to all my teachers through out my academics for their wonderful teaching and education.

I thank Prof. D. Narayana Rao, Dr. M. G. Krishna (School of Physics, University of Hyderabad) and Dr. Murali Sastry (NCL, Pune) for their help. I thank all the non-teaching staff, School of Chemistry for their cooperation.

My special thanks are due to Prof. Jun Kawamata (Yamaguchi University, Japan), for his help in carrying out SHG experiments and hospitality during my stay in Japan. I would also like to thank his research group especially Dr. Y. Ogata and Mr. H. Mimata for their help. I thank Prof. T. Nakamura and Prof. Akutagawa for some useful tips with the AFM. My special thanks to Prof. Ishiguro and his family for their hospitality and affection during my stay with them at Yamaguchi, Japan. I thank Prof. P. Ugliengo (Italy) for fruitful discussions regarding the MOLDRAW program. Technical help for the LB trough from Prof. Grunfeld (Nima Technology, UK) and Nanofilm, Germany for the Brewster angle microscope are greatly acknowledged.

I thank CSIR, New Delhi for fellowship and a foreign travel grant to attend ICONO'7/ICOPE-2003. UGC for the UPE program and DST for the National Single

Crystal X-ray Diffractometer facility at our school are acknowledged. Special thanks to DST and JSPS for supporting some of the research projects.

It is indeed a pleasure to thank my seniors Dr. Palash Gangopadhyay, Dr. Sonika Sharma, Dr. Jayanty Subbalakshimi and Mr. Philip Anthony for their love and cooperation. Thanks Prakash, Shatabdi, Abhijit and Rajesh for maintaining a lively environment in the lab. I also thank Srinivas, Manoj, Joseph and other laser lab friends for their help. I thank some of the M.Sc project students, Kishore, Mishra, Saritha, Anish, Shyama and Basavaiah for their cheerful presence in the lab. I would like to thank all the colleagues in the department and friends for their smiles, and making my stay on the campus a memorable one.

I dedicate my thesis to my parents, without whose committed efforts, constant support and love I would have not reached this stage today. I am at loss of words to express my gratitude to them. I am very thankful to my sister and brother for their love, affection and support. My special thanks to my brother-in-law and Namish, who has filled joy in our lives. I thank all the members of Mahavadi and Koride families for their love. My special thanks to my parent-in-law for their affection. I would also like to thank all the other members of the Meduri family. I thank my cousin sister Ms. Anita, who is one of my first teachers, her family and the Pendyala family for their support on various occasions. On this occasion I would like to remember my cousin sister Late Ms. Haritha for her love and care.

I thank all my school and college friends for their encouragement. My special thanks to Harsha, Vasulu, Phani, Nagesh, Desigan, Santosh, Banala, Sabitha and Sheena for their support and encouragement.

Finally I thank my best friend, wife Padmaja, for her support and affection. I specially thank her for her patience and understanding without which it would have not been possible to finish this thesis in time. She has always been the driving force to give my best.

M. Sharath Chandra

COMMON ABBREVIATIONS

AFM	atomic force microscope
AM1	Austin Model 1
BAM	Brewster angle microscope
BDEP	N-*n*-butyl[2-(4-dimethylaminophenyl)ethenyl] pyridinium
CI	configuration interaction
CMC	carboxymethyl cellulose
COSMO	conductor-like screening model
d	doublet
D, A	donor, acceptor
DNA	deoxyribonucleic acid
dec	decomposition
LB	Langmuir-Blodgett
LS	Langmuir-Schaefer
m	multiplet
M.P.	melting point
NLO	nonlinear optical
NOA	N-*n*-octadecylaniline
ODEP	N-*n*-octadecyl[2-(4-dimethylaminophenyl)ethenyl] pyridinium
ODP	N-*n*-octadecyl(4-dimethylamino)pyridinium
PNOA	poly(N-*n*-octadecylaniline)
PSS	poly(sodium (4-styrenesulfonate))
11PSSM	poly(sodium 1:1 (4-styrenesulfonate-*co*-maleic acid))
31PSSM	poly(sodium 3:1 (4-styrenesulfonate-*co*-maleic acid))
PVS	poly(potassium vinylsulfate)
s	singlet
SHG	second harmonic generation
t	triplet
TR	transfer ratio

CONTENTS

CHAPTER 1

Introduction

Prof. Irving Langmuir

Dr. Katherine Blodgett

Prof. Irwing Langmuir (1881-1957) and Dr. Katherine Blodgett (1898-1979) investigated extensively and systematically for the first time, the behavior and properties of molecules assembled at the air-water interface, subsequently transferring them onto solid substrates. The technique of studying the structure and behavior of molecular assemblies on a liquid surface and transferring of the molecular layers onto solid supports is named after these two pioneers and is popularly known as the 'Langmuir-Blodgett' technique.

Scope

Organizing molecules in a desired fashion is a challenging and fascinating problem and forms the essential basis for the design of molecular materials. Judicious choice of molecules and their organized assembly leads to the realization of a wide range of materials properties such as electronic, magnetic and optical. While a number of approaches are known for assembling molecules into materials, the Langmuir-Blodgett method stands out as one of the most elegant techniques, due to the simplicity of the concept and the high level of control it affords. The Langmuir-Blodgett technique has been the subject of extensive scientific research for several decades and has found extensive applications in a wide range of disciplines. The technique is often used in materials fabrication; it is also a favourite approach to model biological supramolecular systems. This thesis addresses some fundamental problems associated with the Langmuir-Blodgett mode of molecular assembly. An important theme is the development of a simple and efficient methodology that facilitates significant control on the monolayer organization at the air-water interface. The materials aspect focussed on, in several of the investigations, is the quadratic nonlinear optical effect of second harmonic generation.

In this chapter we provide a brief overview of the evolution of materials in general and the emergence of molecular materials in particular (Sec. 1.1). In Sec. 1.2, the basic concepts of nonlinear optics of interest in a good part of the thesis is presented. The Langmuir-Blodgett technique is introduced in Sec. 1.3. Following a brief historical perspective, the experimental technique, some fundamental problems associated with the technique and the different types of Langmuir-Blodgett films are discussed in detail. Characterization methods for Langmuir and Langmuir-Blodgett films as well as potential applications of the technique are listed. The layout of the thesis is given in Sec. 1.4.

1.1. Molecules to Materials

1.1.1. *Historical perspective*

The quality of life through the ages has been greatly influenced by the kind of materials that were in vogue. There exists a close parallel between the evolution of materials and human civilization. The earliest materials like stone and wood were

directly adopted from nature and restructured and reshaped physically to suit specific needs such as weaponary, utensils, clothing and shelter. One of the earliest materials fabrication process dates back to the eighth millenium BC, the baking of clay for ceramics like porcelain. Extraction of metals from their ores, fabrication of alloys and glass-making are some of the early breakthroughs in the history of materials; these processes involve chemical reactions in addition to the physical transformations. The early utilization of materials was mostly based on their structural, mechanical, optical and thermal properties. Synthetic polymers, a major achievement of modern synthetic chemistry, added a new dimension to the world of materials. The electrically insulating nature coupled with light weight and mechanical flexibility made polymers uniquely suited to a range of applications. Development of quantum theory brought about a deeper understanding of the microscopic nature of the matter in the beginning of the twentieth century. Discovery of semiconductors and superconductors marked the beginning of a new era in the field of materials. Paralleling the new developments in fundamental science was the fabrication of new materials, where concepts like purity and specificity emerged as key factors that determined the properties and applications of the materials. Growth of the electronic industry and the advances in semiconductor physics made challenging demands on the specificity and precision of materials properties. The stringent demands on materials made by the emergence of a wide range of new applications have led to the exploration of new types and classes of materials such as composites, thin films and nanostructures. Traditionally, materials are often classified into general classes such as metals, semiconductors, ceramics, polymers and composites. These classes of materials, except polymers are all built up as an assembly of atoms or ions. In the case of polymers,[1] covalently bound long chain molecules are the basic building blocks. Nanomaterials form the important state between the atomic / molecular extreme and the bulk materials.

1.1.2. *Molecular materials*

A significant departure from the course taken in the development of materials is the growth of a new family of materials which have small molecules and molecular ions as their building blocks and these are popularly known as molecular materials.[2] The significant factors distinguishing molecular materials from other classes of materials are listed in Table 1.1. Polymeric solids with extended covalently bonded macromolecular

building blocks are half way between molecular solids based on small molecules and traditional covalent solids. The unique electronic structural features such as π - electrons delocalized over the molecular framework make molecular materials promising candidates for several technological applications. Molecular materials afford wide flexibility in the approaches to their design and fabrication and can be tailored to suit a vast range of applications. Fundamental to the design of such materials is the interplay between recognition and organization, a factor which also forms the basis for the construction of functional supramolecular systems.[3]

Table 1.1. *Significant factors distinguishing molecular materials from other classes of materials.*

	Molecular materials	**Other materials**
Building blocks	Molecules or molecular ions	Atoms or ions
Bonding/Interactions	Primarily noncovalent - dispersion forces, H-bonds, π-stacking, ionic	Ionic, covalent, metallic
Fabrication Techniques	Two-stage process - synthesis followed by crystallization/electric field poling/LB technique/layer-by-layer assembly etc.	Ceramic methods, soft chemical routes, melt quench process, chemical vapor deposition, calcinations, sintering etc.
Flexibility	Can be disassembled into the molecular constituents maintaining their individuality	Not easily separated into the building blocks with independent existence
Properties	Often directly related to the additive contribution of the constituent molecules or molecular ions	Usually not a sum of the contributions from the constituent atoms or ions

The tunability of the subtle and relatively weak interactions make molecular materials highly versatile. Molecular materials fabrication can be achieved by a variety of means like controlled crystallization,[4] electric field poling of polymers and molecules embedded in polymers,[5] formation of Langmuir-Blodgett (LB) films,[6] host-guest complexation,[7] self assembly using layer-by-layer methodology[8] and organic molecular beam deposition (OMBD).[9] Among these, crystallization is perhaps the most popular

method of organizing molecules into bulk materials. However, many molecules, especially sterically hindered or conformationally mobile ones are often difficult to crystallize. An elegant method that entails a molecular level control over the organization of molecules is the LB film formation; however amphiphilicity is a prerequisite for molecules to form ordered monolayers, typically at the air-water interface. Methods like OMBD offer a convenient way to materials fabrication ensuring high purity without having to modify the molecular design; however the molecules should possess good thermal stability and should be amenable to sublimation. Several of the methodologies used for molecular materials synthesis can be adapted for the assembly of nanostructures of great current interest.

The discussion above illustrates that the evolution of materials fabrication techniques reflects the progress of technology. Starting with crude mechanical approaches to materials structuring, more sophisticated thermal, electrical, chemical and electrochemical techniques have evolved. In the current scenario development of new materials with desired properties necessarily involves significant inputs from chemists, physicists, biologists and engineers. Such multidisciplinary activities have led to the emergence of a wide range of materials. With the advancement of technology the quest for miniaturization appears to be heading to its logical conclusion through the development of molecular devices. It is believed that the future information technology will be based on photonics, where photons instead of electrons are used to acquire, process and transmit information. Considering the higher speed and large frequency range they straddle, photons are superior carriers of information. At this point it is highly instructive to look for connecting links between apparently separated disciplines such as life sciences and materials science, as there is increasing interest in developing new materials which simulate natural supramolecular systems and in learning more from the organization of such natural supramolecular entities to guide the design of entirely new classes of materials. Chemistry as a central science, influences various disciplines and its impact is significant as a bridge between the materials and life sciences. Chemical principles provide explanation for the formation of functional nanostructures with biological molecules and simultaneously provide tools to synthesize analogous structures in the nonbiological environment. We believe that LB films serve as one of the best forums to realize such relations. The ultrathin films formed by the LB technique have great application potential in catalysis, sensors and separation

technology. Monolayers are useful models for simulating various membrane processes. The major constituent of biological cell membranes, phospholipids, form stable monolayers at the air-water interface and have been studied extensively for their organization and recognition properties. The recent examples of molecular switching devices utilizing these membrane constituents once again show a connecting link between life sciences and materials science.[10]

We are interested in using the LB technique for the organization of nonlinear optical (NLO) chromophores and realizing quadratic NLO effects. We have explored the utility of polyelectrolyte templating in effecting such molecular assemblies and obtaining enhanced materials properties. The following section provides an overview of the basic concepts of NLO effects at the molecular and materials level.

1.2. Nonlinear Optics – Basic Concepts and Materials

Nonlinear optical phenomena allow the manipulation of the fundamental properties of laser light and hence are of great technological importance in areas such as optical data processing and storage. The NLO phenomena arise due to the interaction of the intense electromagnetic field of the laser light with matter, which causes the modification of optical characteristics of matter such as the refractive index. Linear and quadratic electric field induced changes in the refractive index, popularly known as the Pockels and Kerr effects respectively are NLO effects observed early on. With the advent of lasers the interest and activity in nonlinear optics grew exponentially. The use of optical fibers in telecommunications has led to extensive practical application of NLO devices. In addition, NLO effects are increasingly used to investigate physical and chemical processes in atoms, molecules, crystals, thin films and polymers. An interesting survey of the historical developments of NLO materials has been provided by Bloembergen.[11] The volumes edited by Chemla and Zyss[12] on the NLO properties of organic molecules and their crystals is a basic text in the subject. There is now a vast literature on molecular NLO materials; a selection of them is listed in Reference 13.

1.2.1. *Basic concepts of nonlinear optics*

Electric field of electromagnetic radiation typically in the range of optical frequencies interacting with a molecule or material will induce electronic polarization. The electric displacement induced in the medium by the electric field can be written as,

$$D = \epsilon_r\epsilon_0 E \quad \text{or} \quad D = \epsilon_0 E + P$$

where ϵ_0 is the permitivity of free space (8.854 X 10^{-12} Fm^{-1}) and ϵ_r is the dielectric constant, a second rank tensor. P is the polarization induced in the material by the electric field. Polarization is the induced dipole moment per unit volume; the units are (Cm^{-2}). When E is relatively small, the polarization is linearly related to the electric field (Fig. 1.1) *i.e.,*

$$P = \epsilon_r\epsilon_0\chi E$$

where χ is the second rank susceptibility tensor. However, when E is large, P varies nonlinearly with E (Fig. 1.1) and it is appropriate to consider the full series,

$$\frac{P}{\varepsilon_0} = \chi^{(1)}E + \chi^{(2)}E.E + \chi^{(3)}E.E.E + ...$$

$\chi^{(2)}$ is the second-order susceptibility tensor and $\chi^{(3)}$ the third-order susceptibility tensor. At high fields, typically those associated with lasers, contribution from these higher order (nonlinear) terms become significant.[14] The second-order term is responsible for effects such as second harmonic generation (SHG, frequency doubling) and the linear electrooptic effect, while the third order term is responsible for third harmonic generation and the quadratic electrooptic effect. The phenomenon of SHG can be visualized as arising from an applied electric field of frequency ω, represented by a function $\sin(\omega t)$ and the quadratic response with a 2ω dependence as follows.

$$E \propto \sin \omega t$$

$$E^2 \propto \sin^2 \omega t \left(= \frac{1}{2}(1-\cos 2\omega t)\right)$$

The basic requirement for a material to show second order nonlinear susceptibility $\chi^{(2)}$ is that it should be noncentrosymmetric. If the material possesses inversion symmetry (centrosymmetric material), $\chi^{(2)}$ vanishes. A molecule subjected to the electric field of a radiation experiences a polarizing effect leading to a change in its dipole moment μ. At the molecular level, we can express this using a similar equation as the earlier one:

$$\mu = \alpha E + \beta E.\ E + \gamma E.\ E.\ E + \ldots.$$

α is the linear polarizability and β, γ etc. (all tensor quantities) are the higher order polarizabilities or hyperpolarizabilities. Centrosymmetric molecules will respond to the electric field of the optical wave to give equal and opposite polarization as the phase of the wave changes through 180° and therefore will have zero β coefficient. Large β coefficients can arise through the presence of an asymmetric mobile π-electron system and low lying charge transfer states in molecules; such molecules are of great interest in SHG applications.

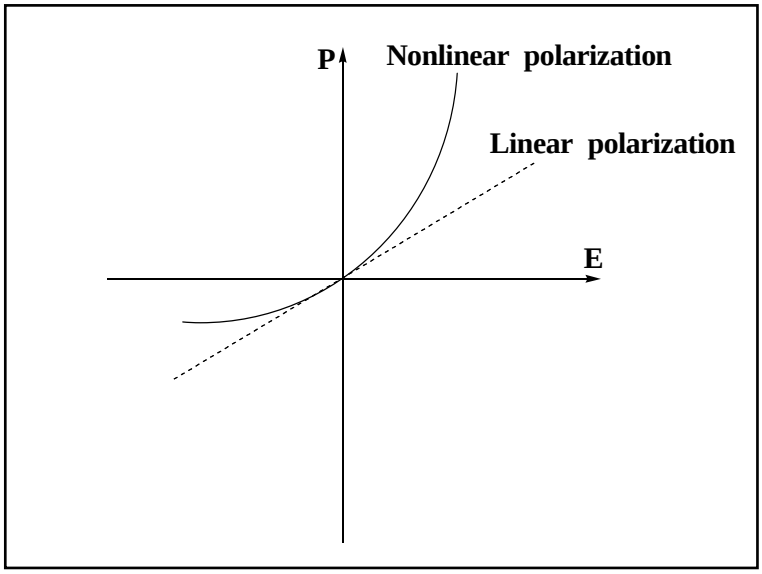

Figure 1.1. *Nonlinear polarization at high electric fields; the linearity at low fields is shown using the dashed line.*

A large number of organic molecules developed for second order nonlinear optics are based on the framework - donor group/π-electron system/acceptor group (D-π-A). The physical mechanism of charge transfer that leads to the NLO effect in such

molecules can be understood in terms of the Mulliken resonance structures. When the molecule is subjected to an applied field parallel to the dipolar axis, the electronic polarization response will be unsymmetric as a result of the cooperative influence of the donor and acceptor groups; this can be contrasted with the symmetric response of an unsubstituted benzene. The asymmetry in the polarization gives rise to the harmonic frequencies of the field radiated by the molecular dipole oscillations. These simple considerations have led to the developments of a vast number of organic molecular crystals and polymers as candidates for NLO applications.

A good number of molecules that show quadratic NLO response are based on donor-acceptor substituted aromatics. Some of the extensively studied classes of NLO chromophores of this type are 1,4-disubstituted benzenes and stilbenes,[15,16] 4-nitroanilines and 4-(N,N-dimethylamino)-4'-nitrostilbene(DANS).[17] Dulcic and Sauteret[18] were the first to study the substituent effect in para disubstituted benzene derivatives and Ouder and Leperson reported on the effect of conjugation length by using stilbene in place of the benzene system.[19] Since then several systematic investigations have been carried out on the structure-property relationship of NLO chromophores. Compounds with conjugating bridges such as tolans,[16] diazostilbenes,[20] polyenes,[21,22] polyphenylenes,[23] as well as heteroatomic 5- or 6- membered rings like thiophenes and azoles[24] have been investigated. Other systems studied include organometallic compounds[25] and calixarenes.[26] In order to overcome the problem of absorption at 2ω, Mignani and coworkers have developed an interesting approach of linking donor and acceptor groups through s-p conjugative units, such as silanes and polysilanes.[27] A variety of salts especially with pyridinium and stilbazolium cations have been studied for their second order NLO properties.

Since D-π-A type systems often tend to prefer centrosymmetric organization in the bulk, there has been considerable interest in exploring octupolar molecules.[28] NLO chromophores with through space or through σ-bond (as opposed to π conjugative) interactions between the donor and acceptor groups which show improved absorption characteristics have been developed.[29] Supramolecular assemblies, especially those with helical organization showing enhanced nonlinearity have been reported.[30]

1.2.2. *Quadratic nonlinear optical effects at the molecular level*

The first hyperpolarizability, β quantifies the second order NLO effect at the molecular level. In most of the D-π-A systems, which are also known as 'push-pull' molecules, major component of the β tensor lies along the charge transfer axis or the dipole axis. Two methodologies[31] are often adopted to compute the β: (i) generalized finite field method in which the perturbation due to the field is explicitly included in the Hamiltonian (the finite field (FF) and coupled perturbed Hatree-Fock (CPHF) methods) and (ii) perturbative schemes in which the calculations are carried out on the free (independent of field) molecules and the response involves the coupling of excited states (the sum-over-states (SOS) method). The CPHF method is equivalent to the time dependent Hatree-Fock approximation (TDHF) for static calculations. The simplest model to take into account the contribution of charge transfer resonance within a molecule to the first hyperpolarizability is the two-level model proposed by Ouder and Chemla.[17,32] An increased β often results from a red shift in the absorption spectrum due to a large conjugation length or lower energy charge transfer between the donor and acceptor substituents.[33]

Experimental determination of β is often carried out in solution phase. Since the molecular motion in solution leads to an average centre of symmetry, high electric fields are applied to break the symmetry of the isotropic solution, in the approach called 'electric field induced second harmonic generation (EFISHG)'.[34] In another technique called the hyper-Rayleigh scattering (HRS),[35] local anisotropy within the solution is used to produce incoherent harmonic scattering which allows the determination of β. The latter technique is applicable to charged and octupolar compounds that are not amenable to EFISHG studies.

1.2.3. *Quadratic nonlinear optical effects at the materials level*

As noted earlier, a material has to be noncentrosymmetric to exhibit quadratic NLO effects. Further, optimal assembly of molecules in a noncentrosymmetric lattice is required for enhanced NLO responses. Within the spirit of the two-stage development of molecular materials involving the synthesis of molecules followed by their assembly into materials, the molecular β values can be related to the bulk crystal NLO

coefficients through the oriented gas model[36] which provides guidelines for the optimal arrangement of molecules to achieve maximum SHG capability.

Molecular crystals of push-pull chromophores generally show a strong predilection towards centrosymmetric organization. Therefore the assembly of molecules in a noncentrosymmetric manner is itself, a nontrivial problem. Several approaches have been developed towards this target. Some of the strategies are inclusion of chirality,[21,37] exploitation of the weak as well as strong intermolecular forces,[38] inclusion of NLO-phores into the host lattices such as urea, perhydrotriphenylene (PHTP) or thiourea, formation of host-guest systems,[39] optimization of the chain length of the alkyl group on the NLO-phore[40] and coordination of the organic moiety to metals.[41] Contribution of remote functional groups on the active NLO-phore[42] has been shown to support noncentrosymmetric packing of the molecules in a crystal. Polymer films with large second order nonlinearities can be produced by the poling process.[5,43] In this approach, an efficient NLO chromophore is either doped in a host polymer matrix or covalently linked as pendent groups on a polymer backbone and a film is fabricated by the spin coating technique. Subsequently the film is subjected to a strong external dc electric field and heated to the glass transition temperature of the polymer. At this point, the chromophores are aligned parallel by the field and locked into position when the film is cooled to room temperature with the external field on. High optical quality can be achieved in such polymeric films so that they can be used for waveguided electrooptic devices.[44] However depoling in the absence of the external field is often a problem, and needs to be tackled by further chemical treatements like cross-linking to lock the poled structure. Recently, self assembly techniques involving covalent linkages and layer-by-layer fabrication has been reported to yield robust noncentric systems, suited for applications like SHG and electrooptic effects.[45] In addtion, sol-gel synthesis[8,46] and salt formation[47] can also lead to the noncentrosymmetric structures. Another systematic approach for the construction of efficient thin film based SHG materials has been to incorporate NLO chromophores into acentric X or Z type LB films.[48] This approach offers far greater net chromophore alignment than is possible in a poling field where net alignment is statistical.

1.3. Langmuir and Langmuir-Blodgett Films

Spreading of oils on the water surface is a phenomenon known for ages all over the world.[49] The effect of these films in calming ripples on the ocean has been exploited by fishermen and sailors. The scientific origin of Langmuir and LB films may be traced to the report of Benjamin Franklin at the British royal society[50] in which he wrote " *….the oil, though not more than a teaspoonful…..spread amazingly…making all that quarter of the pond, perhaps half an acre, as smooth as a looking glass.*" The systematic study of spread films started with the experiments of Agnes Pockels in Germany in the year 1882. Giles and Forrester have provided an account of her fascinating work;[51] her classical papers[52] laid the foundation for the trough technique, the use of volatile solvents and pressure-area isotherms, which form the basis of the LB technique as practised even today. Rayleigh predicted that the layers are monomolecular thick and the investigation of their properties by Hardy, Devaux and Mercelin have contributed largely to this field.

Irving Langmuir studied systematically, the monolayers of amphiphilic compounds at the air-water interface.[53] In 1919, Langmuir presented a paper[54] before a meeting of the Faraday Society where he described the transfer of monolayers onto solid supports. The seminal paper[55] of Katharine Blodgett on sequential transfer of these monolayers appeared in 1934. The technique is now popularly known as Langmuir-Blodgettry. The term 'Langmuir Film' is usually reserved for a floating monolayer. It is pertinent to recall that Langmuir was awarded Noble prize for his pioneering work, in the year 1933.

Technological and scientific interest in LB films was revived by the extensive work carried out by Hans Kuhn. Along with his collegues, Kuhn proved that LB films could be fabricated with the characteristics required for information processing technology in which individual molecules perform distinct functions. They also demonstrated ways in which LB films can be manipulated[56] and showed that these films form with very low defects.[57] This work and the book entitled 'Insoluble Monolayers at Liquid-Gas Interfaces' by Gaines,[58] published in 1966 initiated the current extensive research in this field.

LB film assembly[6,59,60] is a simple, elegant and efficient organization protocol of great potential for the fabrication of organic thin films and nanostructures for a variety of advanced technologies including sensors, detectors, NLO, microelectronic and light emiting devices and liquid crystals. LB technique enables the production of electrically, optically and biologically active components on a nanometer scale with the added advantages like (i) the precise control of the thickness of monolayer (ii) homogeneous deposition of the monolayer over large areas (iii) multilayer structures with varying layer composition and (iv) the flexibility to deposit on several kinds of solid supports. In addition to allowing organizational control at the molecular level, LB films can also serve as ideal model systems to study intermolecular interactions in membranes. This is of fundamental interest in the simulation of biological processes and the developnment of biosensors.

1.3.1. *Molecules at the air-water interface*

Insoluble molecules can orient themselves at the interface between gas and liquid or liquid and liquid to minimize the free energy of the interface. The resulting film at the surface is typically one molecule thick and is popularly known as monomolecular layer or monolayer. For a closer look at the phenomenon, we consider the air-water boundary (Fig. 1.2). Such a boundary shows a transition between the composition and properties of two bulk phases. The molecules in the bulk liquid are subject to intermolecular interactions from all the sides. The attractive force, also known as cohesion, in the bulk liquid is uniform in all the directions. However, a molecule at the interface will experience this force from fewer directions and less number of molecules compared to the bulk liquid phase. Therefore a net attractive force exists towards the bulk liquid (water in this case), and the air-water interface will tend to minimize its area and contract. In other words, more molecules will diffuse initially away from the surface, increasing the mean atomic separation between the surface molecules. As a result the activation energy for a surface molecule escaping into bulk will increase until it is equal to that of molecules diffusing from the bulk to the interface. A state of equilibrium is achieved at this point; the line force acting on the surface molecule is referred to as the surface tension, γ and is quantified as a force/length.

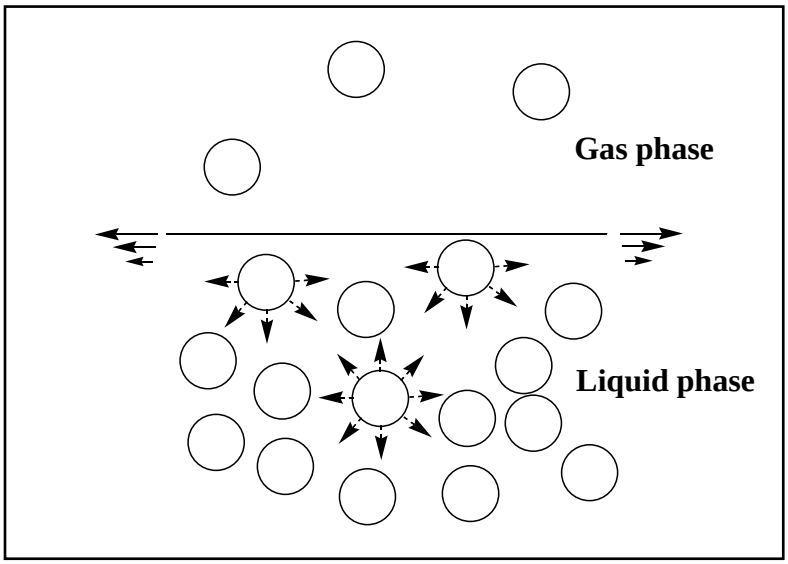

Figure 1.2. *Forces experienced by molecules in the bulk of a liquid and at the liquid/gas interface (Figure adapted from Ref. 6a).*

At thermodynamic equilibrium, surface tension of a plain interface can be expressed as,

$$\gamma = \left(\partial F / \partial A\right)_{T,V,n_i} = \left(\partial G / \partial A\right)_{T,P,n_i}$$

For a liquid in equilibrium with its standard vapors at a planar interface, surface tension equals the excess 'Helmholtz' free energy per unit area,

$$\gamma = \frac{F^S}{A}$$

where F^S refers to the surface excess free energy and A is the area. Surface tension can also be referred to as cohesive energy present at an interface. The common units for surface tension are dyne/cm or mN/m.

Polar liquids will have strong intermolecular interactions and thus they have high surface tension. Any factor which decreases the strength of this interaction will decrease the surface tension; increase in the temperature and contamination with

surfactants are common causes. LB technique is based on the latter effect. In the LB technique, the term 'surface pressure' is commonly used. The surface pressure π is the reduction of the pure liquid surface tension by the presence of a surfactant film.

$$\pi = \gamma_0 - \gamma$$

γ_0 is the surface tension of the pure liquid and γ is the surface tension with the films covering the surface.

1.3.2. *Surfactants*

These are molecules which reside at surfaces such as the air-water boundary, stabilizing the surface water molecules, but not dissolving in the bulk water (Fig. 1.3). Generally, they possess a long hydrophobic tail and a hydrophilic headgroup; they are also known as amphiphiles. Amphiphiles are ideal systems to study through the LB technique and to fabricate LB films. The hydrophobic tail is often about 18-20 carbon chain long. The hydrophilic headgroup is needed to anchor the molecules on to the water surface and generally has chemical functionalities like -COOH, $-NH_2$, -OH, $-NO_2$ and –CN. Dispersion interactions between the hydrocarbon chain is a dominant force in the close packed 2-dimensional structures. Other forces like π interactions may also contribute to the lateral interactions. In-plane order is improved when the side groups in the hydrophilic part also interact leading to long range ordering. Appropriate molecular design for interplanar connections can facilitate the transfer of electrons or other molecular species. Amphiphiles are often synthesized with specific functionalities to

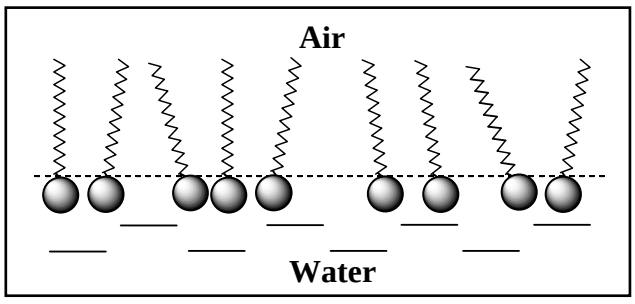

Figure 1.3. *A schematic representation of a monolayer of surfactant molecules at the air-water interface.*

achieve desired properties or to effect particular tasks with the LB films. In addition to the structural requirement, the purity of amphiphiles is critical for stable and reproducible LB film fabrication.

1.3.3. *LB Trough and monolayer compression and monitoring*

Many different approaches are known for the design of equipment for the fabrication of LB films. The basic requirement is the subphase container, the Langmuir or Langmuir-Blodgett trough. LB troughs are usually fabricated from a material such as PTFE (teflon) which is inert and sufficiently stable to withstand the organic solvents used for monolayer spreading and cleaning under harsh conditions such as strong acids or bases. Most of the troughs are either rectangular or circular in shape with a 'well' for the transfer of the floating layer on to a solid substrate. There are three common types of barriers used to compress the monolayer at the surface; the lateral sliding barrier on the rectangular trough, rotating sliding barrier on the circular trough and a constant perimeter barrier. These troughs are usually operated in a clean room environment with controlled temperature. The other basic accessories attached to an LB trough are the pressure sensor and the dipper. The pressure is often measured using a Wilhelmy plate (typically a clean piece of Whatmann 1 filter paper) which is dangled into the subphase from the sensor unit. The dipper provides for vertical motion of the substrate and is controlled by a motor. Fig. 1.4 shows a typical LB trough design. Details of the trough used in this thesis work is provided in Appendix. B.

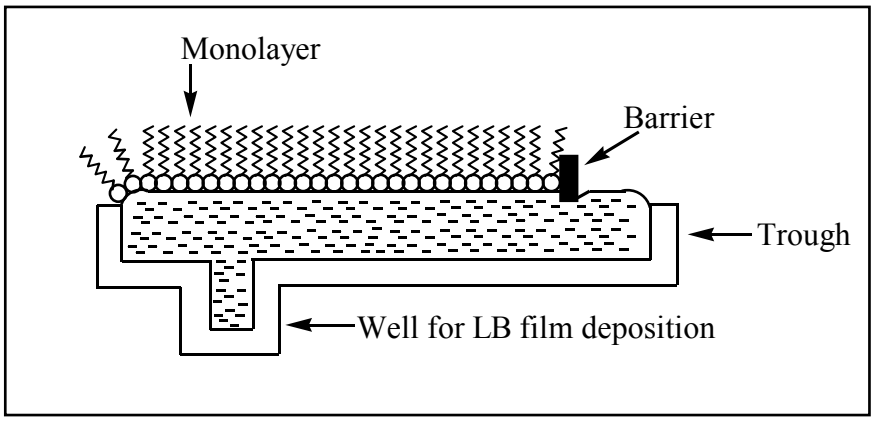

Figure 1.4. *Cross section of an LB trough with a single barrier and a well to facilitate LB film deposition (Figure adapted from Ref. 6a).*

1.3.4. *Subphase*

The most common subphase is water although mercury and other liquids such as ethylene glycol and glycerol have also been used. The water should be of very high purity with a typical resistivity of 18.2 x 10^6 Ω cm. Deviations from the standard value of surface tension of 72.8 mN/m at 25°C, normally indicates surface contamination.

1.3.5. *Surface pressure measurement*

Absolute measurement of π is made by suspending a plate from a sensitive balance so as to contact the monolayer. There are two main methods to measure the surface pressure during monolayer compression: the Langmuir balance and the Wilhelmy plate. Both have similar sensitivities (≈ 10^{-3} mN/m). The first one is essentially a differential measurement, in which a clean water surface is separated from the surface covered with the monolayer by a float (usually a movable PTFE partition) connected to a conventional balance that measures the force acting on the float.[61] The Wilhelmy method is perhaps the more popular approach; it is an absolute method in which the forces acting on the plate (usually made of platinum or filter paper) partially immersed in the subphase, are measured.

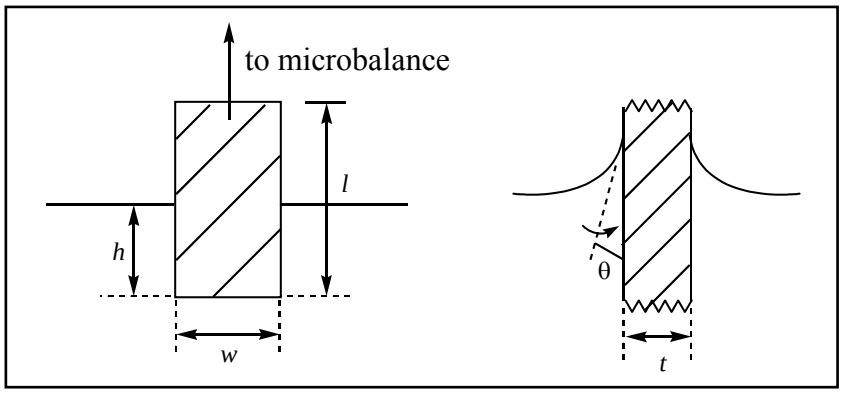

Figure 1.5. *Front and side views of a Wilhelmy plate.*

The forces acting on the plate are due to gravity and surface tension downwards and buoyancy due to displaced water upwards. For a rectangular plate of dimensions l, w and t (Fig. 1.5) and of material of density, ρ_W immersed to a depth h in a liquid of density, ρ_L, the net downward force F is given by

$$F = \rho_w glwt - \rho_L ghwt + 2\gamma(t+w)\cos\theta$$
(force = weight – upthrust + surface tension)

where γ is the surface tension of the liquid, θ is the contact angle on the solid plate and g is the gravitational constant. The usual procedure is to choose a plate that is completely wetted by the liquid so that $\theta = 0$ and to measure the change in F for a stationary plate. The difference in downward force, ΔF, experienced by the Wilhelmy plate between immersion in pure water and immersion in surfactant-covered water is given by:

$$\Delta F = 2(\gamma^o - \gamma)(t+w)$$

γ^o being the surface tension of pure, clean water (72.8 mN/m). If the plate is considered to be of negligible thickness compared to its width this can be simplified to:

$$\frac{\Delta F}{w} = 2\Delta\gamma$$

where $\Delta\gamma$ is the difference between the surface tension of pure water and that of surfactant covered water. As noted earlier, $\Delta\gamma$ is the surface pressure, π, so that,

$$\frac{\Delta F}{w} = 2\pi$$

For a 10mm wide paper plate (with 0^o contact angle), the measured force (in mg) is twice the surface pressure (in mN/m), if g is taken as 10 m/s^2. The forces acting on the plate are normally measured with a sensitive electrobalance. Some of the precautions needed with the Wilhelmy method are discussed by Middleton et al.[62]

1.3.6. *Pressure - Area isotherms*

In a typical LB experiment, dilute solutions (10^{-6} M) of an amphiphile in a volatile solvent such as $CHCl_3$ or hexane is spread on the water surface/subphase in the trough. The amount of amphiphile taken should not exceed what is required to form a monomolecular layer in the area available. High purity of the solvents is to be ensured to avoid residues being left behind upon solvent evaporation. Monolayers of molecules upon evaporation of solvents would resemble a 2-dimensional gas due to the relatively

large distances between the molecules. After the solvent evaporation the film is compressed and the variation of the pressure with area of monolayer (pressure-area isotherm) is recorded. During this compression the monolayer will undergo various phase transitions which are analogous to the transitions between gases, liquids and solids in 3-dimensional space. These phase changes can be followed by monitoring the pressure-area isotherms, which is the 2-dimensional equivalent of the pressure-volume isotherm for gas-liquid-solid. In this plot, area per molecule 'a' can be expressed by dividing the film area by the total number of molecules on the water surface.

$$a = \frac{AM}{CN_A V} = \frac{A}{cN_A V}$$

where A is the area of the film, M is the molecular weight of the monolayer material, C is the concentration of the spreading solution in mass per unit volume, c is the specific molar concentration of the solution and V is its volume. N_A is the Avogadro number.

The different phases in the pressure – area isotherm are described as the (i) gaseous phase (ii) expanded phase and (iii) condensed phase (Fig. 1.6). In the gaseous phase the molecules are far apart on the water surface and they exert very little force on one another. Monolayers at this stage can be modelled using a 2-dimensional variation of conventional kinetic theory. The average translational kinetic energy is kT/2 for each degree of freedom. So the ideal gaseous monolayer equation is:

$$\pi A = kT$$

where A and π are equivalent to V and p in the 3-dimensional case. As the barrier moves, the molecules are pushed closer. Decreasing the intermolecular distances leads to contacts and the surface pressure increases; this is called the expanded phase. The area per molecule in the expanded monolayer is much less than that expected in gaseous monolayers but is significantly greater than the area associated with the cross section of the cylindrical shaped amphiphilic molecule.

In the expanded phase the area per molecule varies considerably with the surface pressure and there is no apparent relation between the observed molecular area and the dimensions of the constituent molecules. If we compress the film further, it will reach an incompressible condensed state. In this state, the molecules are forced to organize in

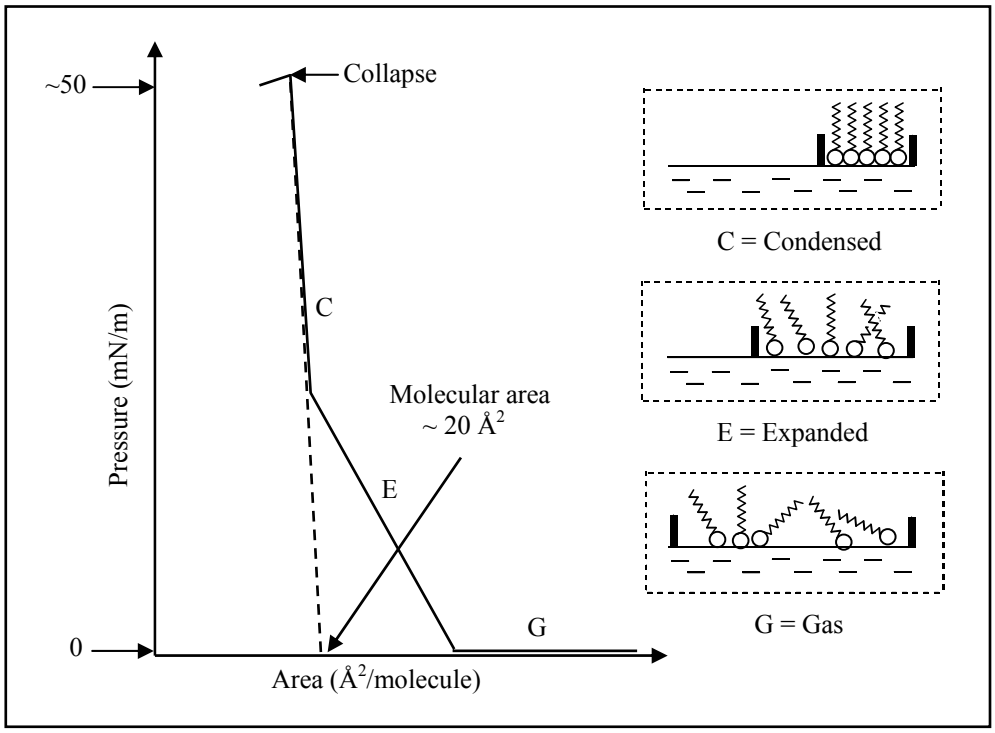

Figure 1.6. *A schematic illustration of a typical pressure-area isotherm and the organization of amphiphiles in different phases. The values of collapse pressure and molecular area are typical of long chain fatty acids.*

a close packed array and like most solids they are nearly incompressible. At this stage molecules form a solid floating monolayer called the 'Langmuir film'. If this region is extrapolated across the area axis (x-axis) the absolute area per molecule can be obtained. The molecular arrangement in this region are similar to that in smectic liquid crystals.[63] More details of the mesophases in the condensed phase are described in a book by Gray and Goody.[64]

In some cases a plateau region or constant pressure region is observed between the expanded and condensed phases. This constant pressure region indicates a first order thermodynamic phase transition. This is not observed in many isotherms for which various factors contribute.[65] The position of the plateau region is affected by factors like chain length and the temperature. An increase in the temperature or decrease in the chain length will increase the surface pressure of the phase transition and *vice versa*.

When the condensed phase is compressed too much, the monolayer will collapse due to mechanical instability and a pressure decrease or no increase in the pressure is observed. The forces acting on the monolayer at this point are quite high. The maximum pressure sustained is called the collapse pressure. When collapse occurs molecules are forced out of the monolayer as illustrated in Fig. 1.7. There are materials like polypeptides which exhibit two instances of collapse pressure, first collapse into a bilayer[66] which subsequently collapses into microcrystallites.

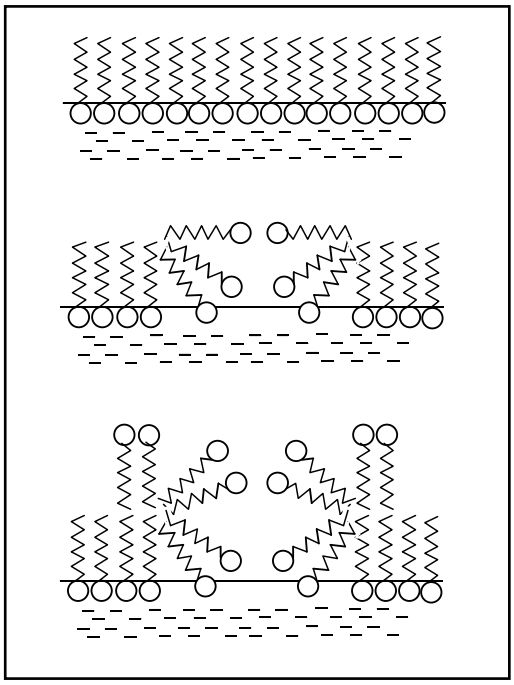

Figure 1.7. *Various stages of collapse of a monolayer are shown from the top to the bottom (Figure adapted from Ref. 6a).*

The pressure-area isotherm is rich in information on the stability of monolayer, reorientation of the molecules, phase transitions, conformational changes *etc*. The behavior of a particular material can vary greatly depending on the experimental conditions such as temperature, time delay between spreading and commencement of compression, pH of the subphase and the speed at which the barriers are closed.[67-69] Several studies on biologically important amphiphilic molecules like phospholipids have explored mixtures containing members of the family with different chain length or different amphiphiles like fatty acids and fatty alcohols. Such studies model the

interactions occurring in the living cells. The mixtures[70] behave as miscible, immiscible or partially miscible systems providing insight into the nature of intermolecular interactions using various thermodynamic parameters;[71] in some cases this provides important information on physiological processes as well.[72]

1.3.7. *Langmuir films to Langmuir-Blodgett films*

The properties of transferred LB films may differ from those of the corresponding Langmuir films as the factors governing the equilibrium packing arrangement of the molecules in Langmuir and LB films could be different, and the molecules can reorganize during or immediately after transfer to a more stable arrangement on a solid support. The observation of transition from an X-type to a Y-type film during monolayer transfer is known as 'detach-turnover-reattach' mechanism when the film is inside the subphase water. So the comparison between Langmuir and LB films is possible only if one can account for the change of interface and the possibility of molecular reorganization. Other parameters like the level of mixing between the components in a mixed monolayer and the composition of the monolayer and the degree of ionization of headgroups, in general do not change during the transfer. Information from the surface pressure-area isotherms are useful to optimize the parameters for the film transfer. Knowledge of monolayer quality and the presence of pin-holes, defects, irregular domains and patches can be inferred through '*in situ*' microscopic techniques; this can help to identify optimum surface pressure-area conditions for the transfer of good-quality LB films. The monolayer stability is very important for the choice of adequate deposition pressure and for the transfer ratio (TR) to be measured more accurately and reliably.

1.3.8. *Langmuir-Blodgett films*

The LB technique was first introduced by Langmuir[54] and applied extensively by Blodgett; it involves the vertical movement of a solid substrate through the monolayer-air interface.[55] LB films are often deposited on hydrophilic surfaces of glass or quartz. Other hydrophilic substrates used are Al, Cr, Au, silicon wafer and freshly cleaved mica. Glass, quartz or silicon surfaces can be made hydrophobic by treating with hexamethyldisilazane or trichlorosilane; such surfaces are also commonly used for LB

film transfer. CaF_2 substrates are preferred when spectroscopic studies such as infra red absorption are to be carried out on the LB film. Depending on the nature of the substrate surface, the first layer is coated while going up (in hydrophilic case, Fig. 1.8a) or while going down (in hydrophobic case, Fig. 1.8b).

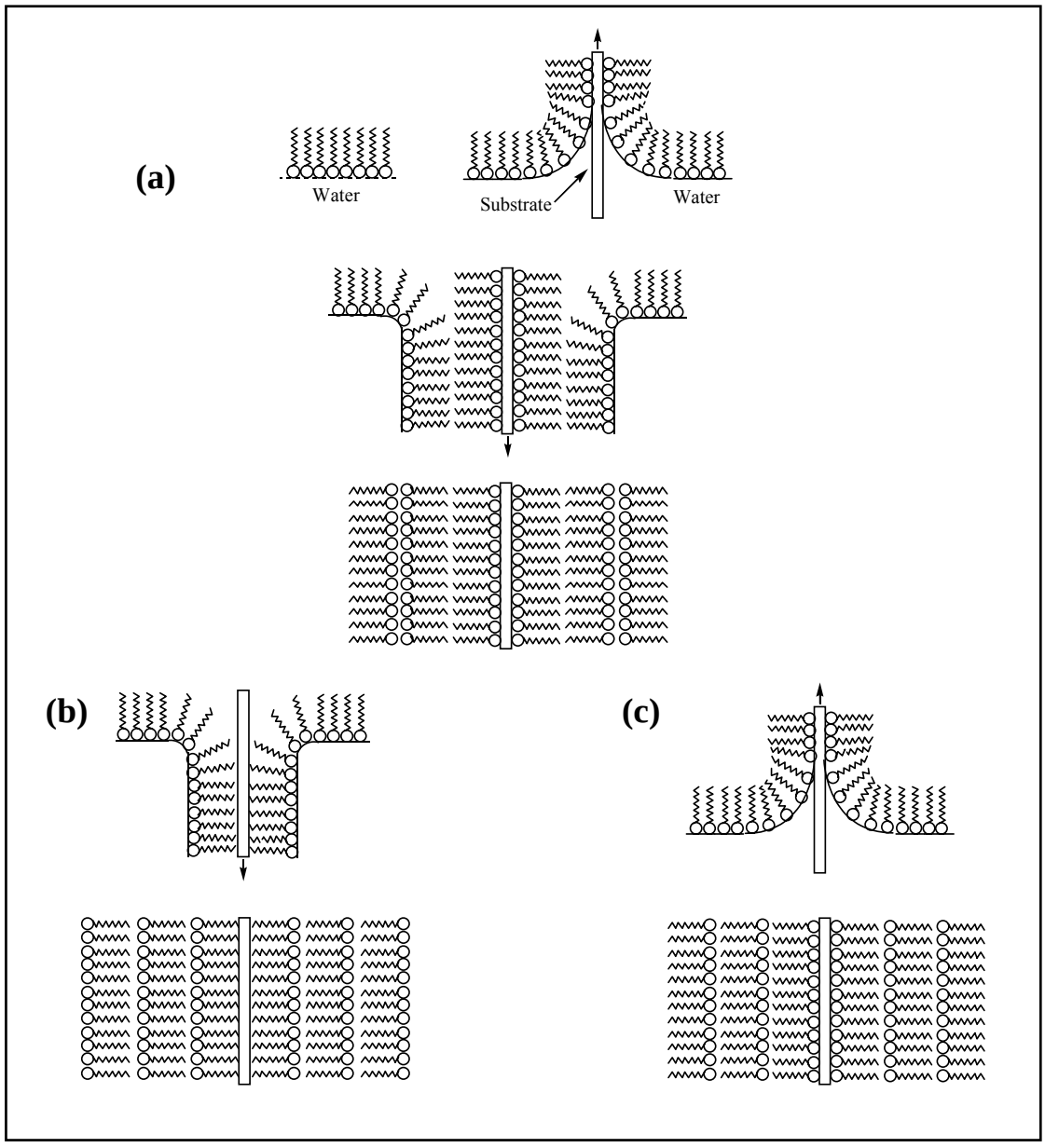

Figure 1. 8. *Langmuir-Blodgett film depostion-**(a)** Y- type; **(b)** X-type and **(c)** Z-type.*

Multilayers formed by multiple dipping of the substrate are usually of three kinds, known as the X, Y and Z type depending on the sequence in which amphiphiles are attached (Fig. 1.8). X-type film has molecules in every layer aligned with their hydrophobic tails towards the substrate and Z-type films have the hydrophilic headgroups in every layer towards the substrate. X and Z type films are noncentrosymmetric. When layer transfer occurs by up and down strokes during repeated dippings through the same Langmuir film, Y-type film with head-to-head and tail-to-tail attachments between the layers is obtained; these structures tend to be centrosymmetric if the molecules are oriented normal to the substrate plane. Noncentrosymmetric films can be fabricated by coating alternatively NLO active and inactive molecules or using an alternate trough to impose X or Z type structures. X-type depositon is also possible with suitable changes in the dipping conditions. X-type deposition is generally favoured by high pH values. Appropriate choice of dipping conditions also enables long chain esters to be deposited as either X-type or Y-type layers.[61] There are many reports of Z-type films. Typically, these concern aromatic molecules with short or no hydrocarbon chains that do not form true monolayers at the air-water interface.

During the LB film deposition the first monomolecular layer will be transferred onto a solid substrate of a different material, so this is called heterogeneous crystal growth.[73] For subsequent monolayers, transferring onto existing monolayer, the deposition will be homogeneous. So the chemical and physical nature of the first layer will be different from that of subsequent layers.[74] In the case of fatty acids it is known from electron diffraction studies that each monolayer has the same local orientation of molecular lattice as that of underlying monolayer; however it does not guarantee translational order from layer to layer.[75] Quality of the LB film depends on the monolayer stability as well as parameters like the dipping speed and nature of the substrate. The extent of film transfer is expressed as the transfer ratio, which is the ratio of the reduction in the monolayer area to the area of the substrate moved through the monolayer. TR should be ideally unity or 100%.

A comprehensive report on LB film structure has been published by Schwartz.[76] As found in molecular crystals, polymorphism does exist in LB films as well. Different packing structures of Langmuir and LB films in fatty acids have been revealed through

electron diffraction studies, X-ray reflectivity/diffraction, polarized reflection microscopy and FTIR techniques. Floating monolayers on aqueous subphase have been shown to exhibit complex polymorphism with phases whose structures may be compared to those of smectic mesophases. LB films normally show phases that exist at high surface pressure. Study of polymorphism helps to optimize the experimental conditions for better quality LB films. Structure of fatty acids and their salts in the LB films has been reviewed by Petty *et. al*.[77]

1.3.9. *Post deposition treatments*

Following LB deposition, the films may be treated in several ways ranging from storing in the desiccator to remove water, to cross-linking the monomer molecules in an array. Skeletonization is a common procedure for films containing long chain fatty acid and its salt; the LB film is soaked in a suitable solvent to dissolve the free acid alone. If the deposited LB film is immersed in a dilute aqueous solution of polyvalent cations,[58] the outer surface becomes polar as a result of the removal or overturning of molecules in the outer layers of the LB structure. In general, the long alkyl chains in the classical LB films reduces the thermal stability of the system and further, can dilute the effect of electrical or optical functionalities in the film. In such cases, the hydrocarbon chains are eliminated thermally. This technique has been used to prepare polyamide and polyphenylenevinylene LB films.[78]

1.3.10. *Large-scale Langmuir-Blodgett film deposition*

Langmuir-Blodgettry was conventionally used for the fundamental investigation of molecular interactions at the 2-dimensional level in various disciplines. The technology available for the LB film synthesis is mostly useful for the small-scale fabrication and none are well suited for large-scale manufacturing where continuous film depostion process would be desirable. Fig. 1.9 shows a recent design of a continuous LB deposition device that could be used for the large-scale production of LB films.[79] This device contains four stages (i) a spreading area (ii) a compression stage (iii) a deposition stage and (iv) an ageing control stage.

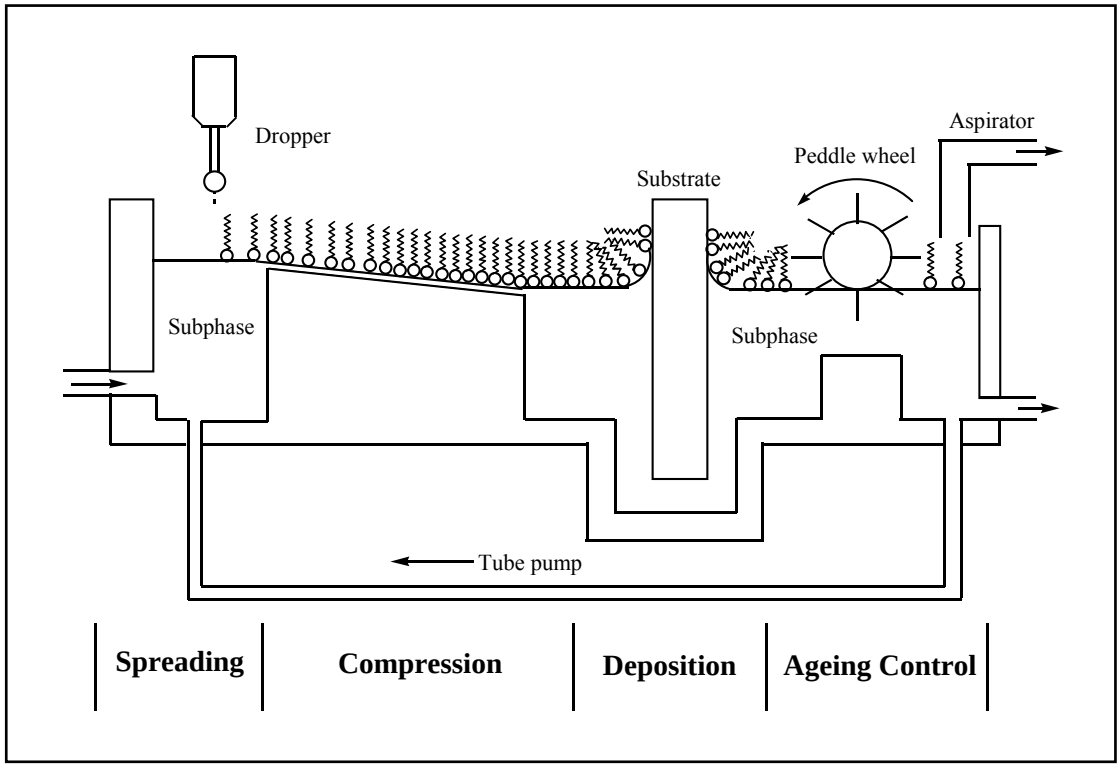

Figure 1.9. *Experimental design of a continuous LB film deposition apparatus (Figure adapted from Ref. 79).*

After spreading on the water surface, the surfactant molecules are carried along with a circulating subphase to a compression stage, where they flow down to combine with a compressed layer at the bottom. The surface pressure of the film will be controlled by two experimental variables, angle of the slope and the flow rate of the subphase. Later the compressed monolayer will be deposited onto a suitable substrate. In the fourth stage the unused surfactants will be removed at a constant rate from the deposition area. Such a trough can self-replenish the surfactant, maintain a constant surface pressure and remove aged film from the dipping area.

1.3.11. *Related thin film deposition techniques*

Apart from the standard LB technique there are some related techniques available to transfer the floating molecular film onto solid substrates. Highly rigid amphiphilic monolayers are transferred onto solid supports by the Langmuir-Schaefer

(LS) method[61,80] in which the substrates are horizontally lowered onto a floating monolayers for transfering the film. Organic multilayer films can also be fabricated chemically;[81] the popular method is the one developed by Sagiv and coworkers. In this procedure a monomolecular layer is adsorbed onto the solid substrate and the headgroup reacts with the substrate to give a permanent chemical attachment and each subsequent layer is chemically attached to the one before in a very similar way as that used in the supported synthesis of proteins. Another approach developed by Decher *et al.* [81] involves multilayer buildup through ionic interaction between opposite charges as the driving force. In general polyelectrolyte multilayer films are built up like this, in the layer-by-layer assembly process.

1.3.12. *Molecules for Langmuir / Langmuir-Blodgett films*

The most common and classical amphiphilic molecules for LB film formation are fatty acids,[83] phospholipids,[84] sterols,[85] ionophores,[77] dyes[86] and porphyrins.[87] These systems in the pure state or in mixtures are convenient model systems for various biological processes. Phthalocyanines[88] and dendrimers[89] have been studied as LB films with device applications as the ultimate goal. Several amphiphiles are potential candidates for a variety of materials applications such as molecular conductors[90] and magnets.[91] Studies involving polyelectrolytes[92] in the subphase have been directed towards an understanding of adsorption processes. Various cyanine dyes are studied for energy transfer processes.[86b] Chemoionophores are more sophisticated versions of simple dyes. They contain two functionally different chemical groups: an ionophore to recognize specific ions and a chromophore to transduce the chemical information produced by the ionophore into an optical signal.[93]

In this thesis, we describe a new methodology we have developed to enhance and stabilize the SHG potential of an NLO-phore and explore the possibility of controlling the polymerization process at the interfaces leading to polymer chain alignment in LB films. Therefore, various SHG active materials based on LB films and different polymers and polymerization methods at the air-water interface are discussed below.

Materials for SHG

A large number of studies have been carried out on LB films of amphiphilic dye molecules exhibiting NLO characteristics either in the pure state or as mixtures with fatty acids. SHG observed in the herringbone Y-type films of DCANP, a nitropyridine derivative has been reported by Decher *et al*.[94] Even though 4-nitroaniline is the prototypical dipolar NLO-phore, its amphiphilic derivatization generally do not form good films on their own.[95] Nalwa *et al.*[96] have shown that LB films of 2-dimensional charge transfer systems based on dinitrodiamino derivatives show stronger SHG than their 1-dimensional analogs. Ashwell and coworkers have reported SHG studies of quinolinium dyes,[97] centrosymmetrically substituted squarines[98] and zwitterionic tricyanoquinodimethanes.[99] NLO chromophores attached to polymer backbones like polysiloxanes, polyisocyanides,[100] polyethers and copolymers like styrene-maleic anhydride[59,60,101] have been studied. Polymers are less tractable than their monomeric versions; this has led to the development of oligomeric materials.[102] Other amphiphilic

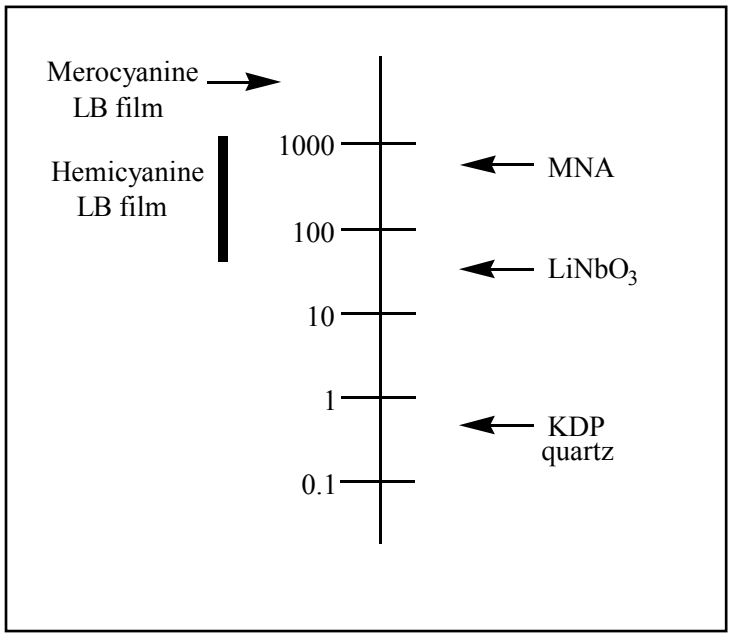

Figure 1.10. *Scale showing relative values of $\chi^{(2)}$ of various organic and inorganic materials (KDP: potassium dihydrogen phosphate; MNA: 2-methyl-4-nitroaniline). The bar indicates the range of values reported for the hemicyanine LB film (Figure is adapted from Ref. 6a).*

systems and LB films used in NLO studies are based on organometallic compounds,[103] azobenzene,[104] indanone[105] and some nonpolar compounds.[106] Fig. 1.10 compares the second harmonic coefficients of some inorganic and organic materials with that of well-known LB films.[107] Merocyanine dye possesses a very high second order nonlinear susceptibility, but this compound is unstable in air and gets protonated upon exposure to moisture in the atmosphere, which results in the reduction of the nonlinear activity. Hemicyanine dyes[86a,108] show pronounced NLO properties. Amphiphilic hemicyanine derivatives have been extensively studied; but the nonlinear coefficients measured with 1064 nm incident laser for the well studied candidate is approximately an order of magnitude less than that of merocyanine dye. However, no short term chemical reactions are reported for this compound. So it is often used as a standard against which new materials are compared. It is interesting that if this compound is diluted with fatty acids then the SHG is enhanced. This results from the effect of deaggregation. In this thesis we will focus on some of these aspects in Chapters 2 and 3.

Polymers

Polymeric materials are generally more robust than simple amphiphilic long chain compounds; therefore they have attracted more attention from a technological perspective. There are various methods to make multilayer structures of polymers using the LB technique. Either the monomers spread at the air-water interface can be polymerized and the polymer transferred onto solid substrate or after transferring the monomer monolayer onto a solid substrate, the oriented monomers can be polymerized. Typical examples are polymerization of aniline in Langmuir film[109] and cross-linking 22-tricosenoic acid transferred onto the substrate.[110] An alternative method is to build up LB films of pre-formed polymer monolayers.

There is growing interest in conjugated polymers because of the wide range of commercial applications they can be put to. Prior to the discovery of conducting polymers[111] in the 1970's, polymer science and technology was largely based on saturated polymers. Applications of these polymers are largely based on their mechanical and thermal properties; they do not show any special electronic or NLO properties. Conjugated polymers on the other hand possess overlapping π-orbitals leading to extended π-electron delocalization. The resulting band structure bestows

semiconducting or metallic properties on these materials. The classic example is polyacetylene, $(CH)_n$. Conjugated polymers with chain structures and extended π-electron conjugation can be considered as quasi 1-dimensional conductors.[112] The conductivity of the conjugated polymers are usually very sensitive to the extent of electron or hole doping. Polymers such as polyvinyl ferrocene, polyvinyl carbazole and tetrathiafulvalene substituted polystyrene[113] can be described as redox polymers and can be subjected to doping; however these are less suitable for electrical conduction than polymers with extended conjugation.

Conducting polymers combine many of the electrical and optical properties of metals and semiconductors and the mechanical attributes of conventional plastics. Thus they are unique materials poised for major applications in current and future technologies. The electrical conductivity of these polymers arise due to a variety of nonlinear excitations such as solitons, polarons and bipolarons generated by chain relaxation or deformation as well as doping.[112] One of the important features of these materials is the feasibility of fine-tuning the conductivity by controlling the doping levels. This has significant implications for applications of conducting polymers as sensor elements. Conducting polymers find application in other areas as well, such as electromagnetic radiation shields, anticorrosion coatings, smart windows and solid electrolytes.

Polyaniline (PANI) is one of the most popular conjugated polymers. The simple preparation and the thermal as well as environmental stability make it one of the most versatile among conducting polymers. Its superior advantage stems from the ease of controlling its electrical and optical characteristics. The various states of polyaniline are shown in Fig. 1.11.

Research on polyaniline has been extensive and multifaceted. It has been the subject of fundamental studies as well as a wide range of applications. Some of the recent investigations of polyaniline are the following. It has been deposited on self assembled monolayers for micron scale patterning.[114] PANI-PVA composite films[115] have been utilized in humidity sensing; at high humidity, polyaniline exists in the emaraldine salt form, but transforms to the non-conducting base form with decreasing environmental humidity. The conductivity of novel polyaniline - inorganic salt

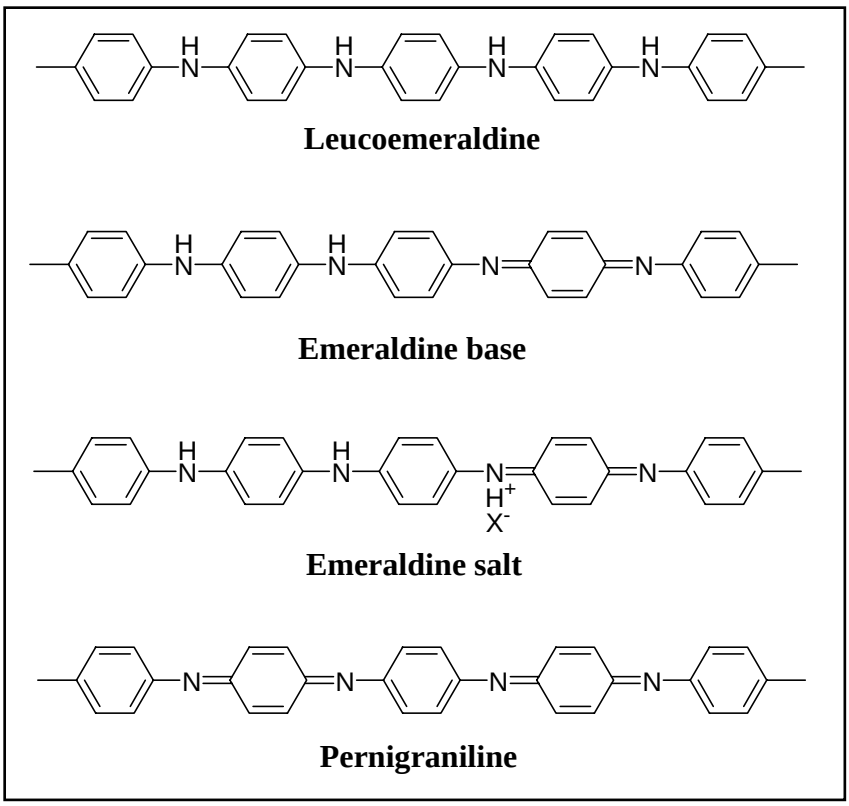

Figure 1.11. *Various oxidation states of the polyaniline.*

composites[116] have been analyzed via percolation theory. Nanocomposites with transition metal oxides[117] prepared by direct intercalation methods possess good electrical conductivity. Nanoscopic polyaniline particles with good crystallinity have been successfully synthesized in water-oil emulsion.[118] Novel polyaniline nanotubes have been used as a second order template[119] by encapsulating iron nanowires and their magnetic behavior has been investigated. Polyaniline nanowires were obtained by electropolymerization of liquid crystalline phases[120] and chiral polyaniline nanotubes were obtained by template-free methods.[121] Polyaniline–metal chelate blends synthesized recently[122] are promising candidates for cathodes in lithium batteries. Control of the alignment of polymer chains is an important consideration in the research of conducting polymers. We will discuss our efforts on the preparation of polyaniline at the air-water interface and the control it affords on the chain alignment, in Chapter 4.

1.3.13. *Characterization methods*

There are several techniques available to characterize Langmuir and LB films; some of these are of specific interest to particular applications. Information of basic interest include molecular orientation and domain structures, film coverage, thickness, density, atomic composition, chemical group composition, chemical structure, order and the content of defects or pinholes. A combination of two or more complementary techniques can be employed to probe several characteristics simultaneously. Many of the techniques are used in a qualitative or semiquantitative manner. Quantitative analysis is often based on post-measurement mathematical analysis and molecular modeling.

Pressure-area (π-A) isotherm is the simplest and immediate characterization of a Langmuir film. Other techniques for monitoring the film as it is compressed include surface potential or conductance measurements and a range of microscopic, diffraction, spectroscopic and NLO methods; a recent review of interest is the one by Dynarowicz *et al*.[123] SHG studies on Langmuir layers[124] are useful to characterize the orientation of molecules at the air-water interface. A brief description of some of the commonly used techniques for Langmuir and LB film characterization is given below.

Techniques such as Brewster angle microscopy (BAM) and Nomarski differential interface contrast microscopy are used to investigate inhomogeneity in the films. Fluorescence microscopy[125] provides useful information on domain structures. Scanning probe microscopies like scanning tunneling microscopy (STM),[126] atomic force microscopy (AFM) and friction force microscopy (FFM) are ideally suited to study the surface structures and defects in LB films with nearly atomic level resolution. Electron microscopies like transmission electron microscopy (TEM) can also provide a great deal of useful information on the in-plane structure. Scanning electron microscopy (SEM)[127] can be used to detect defects like microcrystal formation. X-ray scattering techniques like small angle X-ray scattering (SAXS) and grazing incidence X-ray diffraction (GIXD)[128] provide information on the layer structure of the film, type of molecular packing and molecular orientation.

Ellipsometric methods are often used to estimate the thickness of LB films.[129] Neutron reflectivity measurements can also give monolayer thickness and provide information regarding monolayer-counterion interactions. If the molecules in the LB film contain chromophore groups that absorb in the UV or visible region electronic absorption spectra provide a simple characterization. Linear variation of the absorbance with the number of layers gives preliminary information on the quality of the films. Polarized absorption spectra reveal the orientation of the chromophore with respect to the substrate plane and dipping direction. Vibrational spectroscopy is commonly employed to characterize LB films. Monolayer ordering, chain conformation and information regarding the functional groups can be obtained from Raman spectroscopy measurements. Three modes of FTIR[130] measurements are often used; transmission, grazing incidence reflection and attenuated total reflection (ATR). In transmission FTIR, information of relative amount and the conformations of various groups are obtained whereas grazing incidence and ATR can provide also details of the orientation of the molecular groups on the substrate. Since the beam can be polarized, it is possible to obtain dichroic ratios of various absorption bands.

If the molecules have appreciable hyperpolarizability and the packing is noncentrosymmetric, LB films can be characterized by their SHG. Normally the substrate is rotated to vary the angle of incidence of the laser beam on the substrate plane. This provides an interference pattern resulting from the signals generated from the film coated on either side of the substrate. The analysis of the SHG signal can be performed to yield an effective $\chi^{(2)}$ parameter for the thin film by comparison with standards such as Y-cut quartz crystal. The $\chi^{(2)}$ together with the knowledge of molecular organization can be used to estimate the molecular hyperpolarizability.[131] Homogeneous growth of LB multilayers in X or Z form is usually indicated by a quadratic increase of SHG with respect to the number of layers.

1.3.14. *Applications*

Langmuir and LB films have found innumerable applications in a variety of research areas as it is one of the simplest techniques available which permits the manipulation of materials at the molecular level. The LB process is relatively unique in its ability to organize molecules in mono or multilayer structures. Thus highly ordered

superlattice structures can be produced which are difficult to form by other means. In the case of second order nonlinear optics, the LB method offers a means of aligning the molecules in a film of micrometer dimensions. The fabrication of simple biological mimics for sensing applications is opening up new possibilities. A comprehensive account of potential applications of LB films has been given by Roberts[6] and Petty.[101] Some typical examples are listed below.

Sensors

The amenability of LB film structures to tuning by molecular engineering strategies and the versatility of synthetic chemistry make organic multilayer systems interesting candidates for the sensing element in a variety of novel transducers. The ultrathin nature of LB films and the organized assembly of molecules in these films result in enhanced response and short recovery time making them potentially interesting candidates for sensor applications. Starting from the early days of Langmuir several applications have been reported. In fact, Langmuir and Schaefer proposed a device for the detection of antigens and antibodies by means of light interference.[132] Moriizum *et al.*[133] have described a sensor in which glucose oxidase is immobilized on the headgroups of a lipid. LB films have been used in a wide variety of gas and ion sensors,[134] biosensors,[135] and molecular recognition[136] applications.

Membrane models

Large number of biological molecules are known to form stable monolayers[137] on the water surface. The close resemblence of monolayer and multilayer films to naturally occurring biological membranes is apparent. Phospholipids and proteins which are major constituents of biological structures can form monolayers or can be incorporated in multilayers. Investigations of nanostructures of lipid films at interfaces help to model various biological processes such as the functions of selective barriers for a variety of molecular and ionic species as in membranes or hybridization of DNA[138] useful for DNA-drug interaction or gene therapy.

Electronic devices

Molecular rectification using monolayer and multilayer films is one of the most interesting potential application in electronic devices.[139] Other applications include switching and memory devices, electroluminescent display,[140] photovoltaic energy conversion and optical data storage systems.[141]

Nonlinear optical materials

The LB technique facilitates the organization of NLO-phore based amphiphiles in a noncentrosymmetric manner, which is a neccessary prerequisite for observing second order NLO effects. LB films for second order NLO devices need to possess high second order nonlinear susceptibility $\chi^{(2)}$, good transperency over the wavelength range needed for the application and thickness of a few microns appropriate for application to optical devices such as waveguides. Many amphiphilic dye molecules have been synthesized and their monolayer and multilayer films investigated for NLO responses. Several examples were cited in Sec. 1.3.12. Some of the studies have been successful in providing films which fulfill the requirements for device applications. LB films of pyrazine derivatives[142] alternating with fatty acids have been shown to be of interest in waveguide devices.

1.3.15. *Drawbacks and remedies*

The main challenge for the practical application of LB films has been the delicate nature and the mechanical, structural or chemical instabilities. Even though the LB technique is an elegant approach, it is often plagued by several technical difficulties. One of the common problems is the instability and collapse of the monolayer at the air-water interface. Molecular aggregation in the Langmuir film can alter the molecular organization and adversely affect practical applications. Metastabilty of the deposited film makes them susceptible to structural modifications with or without external stimuli. Several approaches have been explored to tackle these problems. In this thesis we will be addressing some of these issues through simple chemical approaches.

Instability of monolayers at the air-water interface

Most molecules designed for specific applications do not form stable monolayer at the air-water interface and even when derivatized with long alkyl chain to form amphiphiles they may not form monolayer that can be compressed and transferred on to a suitable substrate. If the amphiphilic balance is not maintained properly it will form either micells or vesicles based on which character of the amphiphile is dominant. A common solution adopted is to mix the amphiphile of interest with fatty acids,[143] or other amphiphiles which are known to form very stable films. Phospholipids and fatty alcohols are known to act as stabilizing host matrices in the case of systems like phthalocyanines and other biomolecules.[144,145] Monolayers of NLO chromophore based amphiphiles have been stabilized using clay[146] in the subphase. We have demonstrated the dramatic effect of polyelectrolytes in the subphase, in stabilizing monolayers of cationic amphiphiles.[147] Amphiphiles with ionisable polar groups like –COOH utilize the ion-pair interactions[148] in the subphase to achieve monolayer stabilization. The classical work of Blodgett illustrates the improved stability of fatty acid monolayers achieved by the presence of divalent metal cations in the subphase.[149] Exploiting electrostatic interactions across the air-water interface for stabilization of monolayers has the advantage of not reducing the density of the active molecules in the film as would happen in the case of stabilization through the use of amphiphilic host matrices. The use of polyelectrolytes in the subphase is popularly known as gluing. We will be describing in the subsequent chapters the utility of this approach in addressing various problems in film fabrication and the stabilization and enhancement of NLO responses.

Molecular aggregation

There has been extensive interest in using LB technique to make molecular aggregated structures for specific applications;[150] however in some instances, molecular aggregation can also adversely affect some physical properties of the systems.[143,151] These kinds of aggregates can arise due to a number of intermolecular interactions ranging from strong electrostatic forces to weaker van der Waals forces between the molecules. These aggregates are quite common in concentrated dye solutions and is often difficult to avoid when the molecules are organized in the form of Langmuir or LB film.

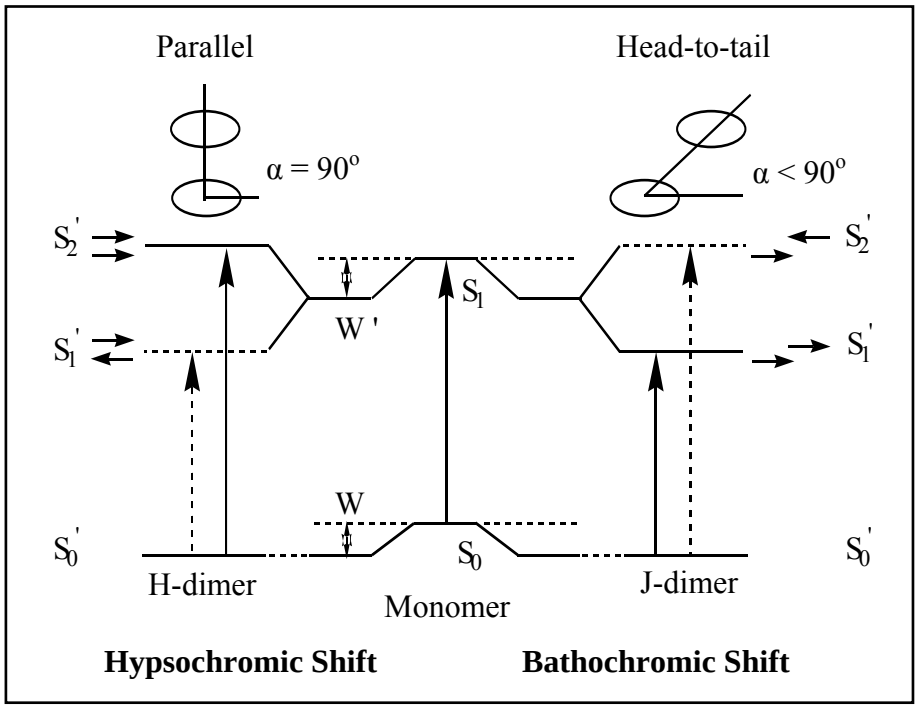

Figure 1.12. *Schematic representation of the relationship between chromophore arrangement in a dimer and spectral shift based on the molecular exciton theory (see text for details).*

Molecular aggregation in the case of chromophoric systems can have a strong impact on the spectroscopic properties. The interactions between dye molecules is usually explained by considering energetically delocalized states termed excitons. In Fig. 1.12, S_0 and S_1 are the unperturbed energy levels of an isolated molecule in dilute solution (monomer). When these molecules are brought close together the dipoles interact and multiple excitation energy levels are obtained. The splitting of energy levels (Davydov splitting) is determined by the difference between the interacting transition dipole moments, their relative orientation and the number of interacting molecules. For a simple dimer, the transition energies are given by

$$\Delta E_{dimer} = \Delta E_{monomer} + D \pm \varepsilon$$

ΔE represents the transition energies to the excited state of the dimer or monomer, ε is the interaction energy and D is a dispersion energy given by W-W' in Fig. 1.12. From the above equation it is clear that for a dimer, the excited energy state has two possible

levels. These can be related to the phase relationship between the transition dipole moments. If the moments of the two molecules are parallel as shown on the left side of the figure with $\alpha = 90^{o}$ (α is the angle between the dipole vector of the molecule and the vector connecting the centers of the two molecules), the net transition moment of the dimer to the energy state S_1' is zero and this transition is forbidden. Transition to the higher energy state S_2' alone is allowed, leading to a hypsochromic shift (H-band) which is quite common in LB films. If the transition dipoles are in line, *i.e.,* $\alpha = 0$ in the right side of the figure, transitions to the S_2' state are forbidden and a bathochromic shift (J-band) is observed in the spectrum. These will show up as intense narrow absorptions.[152] H and J-forms are two extreme forms of molecular aggregation and in reality transition dipoles can be oriented with some angle with respect to each other leading to more complex spectral changes. As noted earlier, the common practice to avoid aggregate formation in LB films is to admix the amphiphile of interest with amphiphiles like fatty acids or phospholipids which can form very stable films. We discuss the utility of the alternate approach of 'gluing' to avoid the aggregation problem in Chapter 3.

Thermodynamic instability of transferred films

A floating monomolecular film is stable in that form only under the existing compressive force. The deposited LB film devoid of the compressing force, is no longer neccessarily in a thermodynamically stable state.[76] It can undergo molecular rearrangement immediately after transfer or after drying as the equilibrium controlling parameters are now different from that in the Langmuir film. In a Y-type multilayer film, the hydrophilic headgroups are separated by nearly twice the length of the hydrocarbon chain. So there is enough room for the molecules to move around and rearrange themselves. Spontaneous molecular rearrangements in deposited LB films is well documented.[153] Exposure to external stimuli can further enhance rearrangement or the formation of aggregated structures depending on the strength of the intermolecular interactions. Thermally induced effects involve molecular rearragement in the LB films, leading to either aggregation or deaggregation. Changes in the molecular packing can be monitored by simple UV absorption spectroscopy or SHG studies. In the case of hemicyanines heating may lead to either aggregation[154] or deaggregation;[155] both these effects have been demonstrated through SHG measurements. In 4-nitroaniline derivatives heat treatment lead to the emergence of SHG.[156] In the case

tetracyanoquinodimethane[156] derivatives heating leads to the collapse of multilayer films. Laser irradiation can also lead to changes in molecular organization in LB films.[155,158] We demonstrate the impact of laser irradiation on a hemicyanine based LB film in Chapter 3.

1.4. Layout of the Thesis

The main objective of this thesis is the exploration of the utility of a simple templating methodology in the fabrication of Langmuir and LB films. We address specifically, the issue of instability and molecular aggregation and the control of polymerization process in the ultrathin films. Polyelectrolytes introduced from the aqueous subphase act as templates for the assembly of ionic amphiphiles at the air-water interface. The utility of the polyelectrolytes in stabilizing Langmuir films and achieving enhanced and stable SHG capability in the LB films through effective molecular deaggregation is demonstrated. The polyelectrolyte templates are also shown to exert a profound influence on the kinetics of polymerization in Langmuir films and lead to polymer chain alignment in the deposited LB film. This thesis consists of five chapters. The basic concepts of molecular materials, nonlinear optics, and the Langmuir – Blodgett technique are reviewed in the previous sections of this chapter. The salient features of the subsequent chapters are summarized below.

Chapter 2

This chapter presents two aspects of a general study on polyelectrolyte templating. The first part focusses on the impact of small anions and polyanions on the stabilization of a cationic pyridinium based amphiphile at the air-water interface. Characterization of the Langmuir films and the fabrication of LB films to gain insight into the amphiphile-polyelectrolyte interaction are discussed. In the second part, the complexation between the cationic amphiphiles and the polyanion at the interface is analyzed using semiempirical quantum chemical computations on model systems. The crucial role of the environment in modulating these interactions is highlighted.

Chapter 3

Extension of the methodology developed in Chapter 2 to LB films of a hemicyanine dye, is presented in this chapter. LB films of hemicyanine based amphiphiles have been extensively studied because of the strong hyperpolarizability of this chromophore unit; however the aggregation of the molecules at the air-water interface leading to the reduction of its SHG capability is a well-known problem. We have analyzed the molecular aggregation problem using computational studies on dimers extracted from the crystal structure of a model hemicyanine system. At the experimantal level, we have observed that the aggregation of these amphiphiles in Langmuir films is influenced by the rate of equilibration of the monolayer after spreading. We have used the polyelectrolyte templates to circumvent this problem. The aggregation of the cationic amphiphile is effectively limited by the introduction of different polyanions in the subphase. SHG studies of the LB films shows clear enhancement in the SHG of the polyelectrolyte complex, giving a direct proof of the presence of increased number of non-aggregated NLO phores.

Laser irradiation of the LB films of the hemicyanine dye during SHG studies revealed the marked instability of the LB films, by the systematic growth of the aggregates as indicated by the electronic absorption spectra recorded after each laser irradiation; the spectra show the growth of the peak assignable to the chromophore dimer. This has the significant influence of diminishing the SHG response from the film as well. Interestingly, templating by polyelectrolytes introduced from the subphase reduces considerably or even arrests completely, the SHG decay. Atomic force microscopy of the pure and complexed LB films show characteristic morphology variations which provide insight into the involvement of the polyelectrolytes. These studies clearly establish that polyelectrolytes play a definitive role in preventing aggregation in the Langmuir and LB films and enhancing and stabilizing their SHG capability.

Chapter 4

This chapter describes our studies of the polymerization of a novel amphiphilic molecule, N-*n*-octadecylaniline (NOA) in Langmuir film at the air-water interface and

the influence of polyelectrolyte templating on this process. A simple methodology is developed to follow the kinetics of the polymerization reaction without some ambiguities inherent in the protocols used in earlier investigations. Our procedure also allows the polymerization to be initiated after preorienting the monomers in the Langmuir film. Brewster angle microscopy was used effectively to probe morphology changes through the polymerization process and the impact of the polyelectrolyte templates. Atomic force microscope imaging of the deposited LB films clearly demonstrated the enhanced alignment of the polyaniline chains, induced by the polyelectrolyte complexaton.

In the second part of this chapter we present the synthesis of the same polyaniline at a liquid-liquid (organic-aqueous) interface. The influence of the polyelectrolytes in modifying the morphological and mechanical characteristics of the polymer are discussed.

Chapter 5

The final chapter presents a brief overview of the various investigations presented in the thesis and highlights the salient achievements of the polyelectrolyte templating methodology we have developed for the fabrication of LB films. The essential inferences are the following : (i) polyelectrolyte templating has a dramatic influence on the stabilization and molecular deaggregation in Langmuir monolayers as well as the transferred LB films; this should enhance the feasibility of using LB films as potential candidates for the fabrication of molecular scale devices; (ii) synthesis of polymers at the air-water interface and organization of the polymer chain in LB film, fine-tuned by polyelectrolyte templating, holds promise for areas such as nanolevel patterning.

Relevant information regarding the instrumentation and details of the experimental procedures are provided in the appendices.

References

1. (a) Seymour, R. B.; Carraher.Jr. C. E. *Polymer Chemistry,* Marcel Dekker Inc: New York, 1981; (b) Cowie, J. M. G. *Polymers*: *Chemistry and Physics of Modern Materials* 2nd Edn., Chapmann and Hall: London, 1991.
2. Simon, J.; Bassoul, P. *Design of Molecular Materials : Supramolecular Engineering* John Wiley: Chichester, 2000.
3. (a) Lehn, J. –M. *Supramolecular Chemistry: Concepts and Perspectives* VCH: Weinheim, 1995; (b) Steed, J. W.; Atwood, J. L. *Supramolecular Chemistry* John Wiley: Chichester, 2000.
4. Hulliger, J. *Angew. Chem. Int. Ed. Engl.* **1994**, *33*, 143.
5. *Poled Polymers and their Applications to SHG and EO Devices* Miyata, S.; Sasabe, H. (Eds.), Gordon and Breach Science Publishers: Amsterdam, 1997.
6. (a) Petty, M. C. *Langmuir-Blodgett Films : An Introduction* University Press : Cambridge, 1996; (b) Roberts, G. G. *Langmuir-Blodgett Films* Plenum Press: New York, 1990.
7. Williams, D. J. in *Nonlinear Optical Properties of Organic Molecules and Crystals* Chemla, D. S.; Zyss, J. (Eds.), Acadamic Press: New York, 1987, p. 405.
8. Ulman, A. *Chem. Rev.* **1996**, *96*, 1533.
9. Forrest, S. R. *Chem. Rev.* **1997**, *97*, 1793.
10. Peace, A. R.; Jeppesen, J. O.; Stoddart, J. F.; Luo, Y.; Collier, C. P.; Heath, J. R. *Acc. Chem. Res.* **2001**, *34*, 433.
11. Bloembergen, N. *IEEE Journal on Selected Topics in Quantum Electronics* **2000**, *6*, 876.
12. *Nonlinear Optical Properties of Organic Molecules and Crystals* Chemla, D. S,; Zyss, J. (Eds.), Acadamic Press: New York, 1987, Vol. 1 and Vol. 2.
13. Articles in *Chem. Rev.* **1994**, *94*, 1.
14. Kanis, D. R.; Ratner, M. A.; Marks, T. J. *Chem. Rev.* **1994**, *94*, 195.
15. Cheng, L. –T.; Tam, W.; Steveson, S. H.; Meredith, G. H.; Rikken, G.; Marder, S. R. *J. Chem. Phys.* **1991**, *95*, 10631.
16. Cheng, L. –T.; Tam, W.; Marder, S. R.; Steigman, A. E.; Rikken, G.; Spangler, C. W. *J. Chem. Phys.* **1991**, *95*, 10643.

17. (a) Ouder, J. L. *J. Chem.Phys.* **1977**, *67*, 446; (b) Levine, B. F. *J. Chem. Phys.* **1975**, *63*, 115.
18. Dulcic, A.; Sauteret, C. *J. Chem. Phys.* **1978**, *69*, 3453.
19. Ouder, J. L.; Leperson, H. *Opt. Commun.* **1975**, *15*, 258.
20. (a) Singer, J. E.; Sohn, J. E.; King, L. A.; Gordon, H. M.; Katz, H. E.; Dirk, C. W. *J. Opt. Soc. Am. B* **1989**, *6*, 1339; (b) Katz, H. E.; Singer, K. D.; Sohn, J. E.; Dirk, C. W.; King, L. A.; Gordon, H. M. *J. Am. Chem. Soc.* **1987**, *109*, 6561.
21. Eaton, D. F. *Science* **1991**, *253*, 281.
22. (a) Blanchard-Desce, M.; Wortmann, R.; Lebus, S.; Lehn, J. M.; Krämer, P. *Chem. Phys. Lett.* **1995**, *243*, 526; (b) Marder, S. R.; Cheng, L. T.; Tiemann, B. G.; Friedli, A. C.; Blanchard-Desce, M.; Perry, J. W.; Skindhøj, J. *Science* **1994**, *263*, 511.
23. Morley, J. O.; Docherty, V. J.; Pugh, D. *J. Chem. Soc. Perkin. Trans. II* **1987**, 1351.
24. (a) Miller, R. D.; Lee, V. Y.; Moylan, C. R. *Chem. Mater.* **1994**, *6*, 1023; (b) Dirk, C. W.; Katz, H. E.; Schiliing, M. L.; King, L. A. *Chem. Mater.* **1990**, *2*, 700.
25. (a) Bella, S. D. *Chem. Soc. Rev.* **2001**, *30*, 355; (b)Torre, G. D. L.; Vazquez, P.; Lopez, F. A.; Torres, T. *J. Mater. Chem.* **1998**, *8*, 1671; (c) Long, N. J. *Angew. Chem. Int. Ed. Engl.* **1995**, *34*, 21.
26. (a) Kelderman, E.; Starmans, W. A. J.; van Duynhoven, J. P. M.; Verboom, W.; Engbersen, J. F. J.; Reinhoudt, D. N.; Derhaeg, L.; Verbiest, T.; Clays, K.; Persoons, A. *Chem. Mater.* **1994**, *6*, 412; (b) Kelderman, E.; Derhaeg, L.; Heesink, G. J. T.; Verboom, W.; Engbersen, J. F. J.; van Hulst, N. F.; Persoons, A.; Reinhoudt, D. N. *Angew. Chem. Int. Ed. Engl.* **1992**, *31*, 1075.
27. (a) Mignani, G.; Barzoukas, M.; Zyss, J.; Soula, G.; Balegroune, F.; Grandjean, D.; Josse, D. *Organometallics*. **1991**, *10*, 3660; (b) Mignani, G.; Krämer, A.; Puccetti, G.; Ledoux, I.; Soula, G.; Zyss, J.; Meyrueix, R. *Organometallics* **1990**, *9*, 2640.
28. (a) Ray, P. C.; Das, P. K. *Chem. Phys. Lett.* **1995**, *244*, 153; (b) Verbiest, T.; Clays, K.; Samyn, C.; Wolff, J.; Reinhoudt, D.; Persoons, A. *J. Am. Chem. Soc.* **1994**, *116*, 9320; (c) Zyss. J.; Ledoux, I. *Chem. Rev.* **1994**, *94*, 77.

29. Bahl, A.; Grahn, W.; Stadler, S.; Feiner, F.; Bourhill, G.; Bräuchle.; Reisner, A.; Jones, P. G. *Angew. Chem. Int. Ed. Engl.* **1995**, *34*, 1485.
30. (a) Gangopadhyay, P.; Radhakrishnan, T. P. *Angew. Chem. Int. Ed. Engl.* **2001**, *40*, 2451; (b) Verbiest, T.; van Elshocht, S.; Kauranen, M.; Hellemans, L.; Snauwaert, J.; Nuckolls, C.; Katz, J. T.; Persoons, A. *Science* **1998**, *282*, 913.
31. (a) Jain, M.; Chandrasekhar, J. *J. Phys. Chem.* **1993**, *97*, 4044; (b) Kurtz, H. A.; Stewart, J. J.; Dieter, K. M. *J. Comput. Chem.* **1990**, *11*, 82.
32. Ouder, J. L.; Chemla, J. S. *J. Chem. Phys.* **1977**, *66*, 2644.
33. Verbiest, T.; Houbrechts, S.; Kauranen, M.; Clays, K.; Persoons, A. *J. Mater. Chem.* **1997**, *7*, 2175.
34. (a) Singer, K. D.; Sohn, J. E.; King, L. A.; Gordon, H. M.; Katz, H. E.; Dirk, C. W. *J. Opt. Soc. Am. B* **1989**, *6*, 1339; (b) Levine, B. F.; Bethea, C. G. *J. Chem. Phys.* **1975**, *63*, 2666.
35. (a) Clays, K.; Persoons, A. *Phys. Rev. Lett.* **1991**, *66*, 2980; (b) Kielich, S.; Lalane, J. R.; Maryin, F. B. *Phys. Rev. Lett.* **1971**, *26*, 1295.
36. Zyss, J.; Ouder, J. L. *Phys. Rev. A* **1982**, *26*, 2028.
37. (a) Ukachi, T.; Shigemoto, T.; Komatsu, H.; Sugiyama, T. *J. Opt. Soc. Am. B* **1993**, *10*, 1372; (b) Reichoff, K.; Peticolas, W. F. *Science* **1965**, *147*, 611.
38. (a) Sarma, J. A. R. P.; Allen, F. H.; Hoy, V. J.; Howard, J. A. K.; Thaimattam, R.; Biradha, K.; Desiraju, G. R. *Chem. Commun.* **1997**, 101; (b) Russell, V. A.; Ward, M. D. *Chem. Mater.* **1996**, *8*, 1654; (c) Sarma, J. A. R. P.; Rao, J. L.; Bhanuprakash, K. *Chem. Mater.* **1995**, *7*, 1843; (d) Bernstein, J.; Davis, R. E.; Shimoni, L.; Chang, N. L. *Angew. Chem. Int. Ed. Engl.* **1995**, *34*, 1555; (e) Zerkowski, J. A.; MacDonald, J. C.; Whitesides, G. M. *Chem. Mater.* **1994**, *6*, 1250; (f) Etter, M. C. *Acc. Chem. Res.* **1990**, *23*, 120; (g) Twieg, R.; Azema, A.; Jain, K.; Cheng, Y. Y. *Chem. Phys. Lett.* **1982**, *92*, 208; (h) Lipscomb, G. F.; Garito, A. F.; Narang, R. S. *J. Chem. Phys.* **1981**, *75*, 1509; (i) Lipscomb, G. F.; Garito, A. F.; Narang, R. S. *Appl. Phys. Lett.* **1981**, *38*, 663.
39. (a) Hoss, R.; König, O.; Kramer-Hoss, V.; Berger, U.; Rogin, P.; Hulliger, J. *Angew. Chem. Int. Ed. Engl.* **1996,** *35*, 1664; (b) Ramamurthy, V.; Eaton, D. F. *Chem. Mater.* **1994**, *6*, 1128; (c) Cox, S. D.; Gier, T. E.; Stucky, G. D. *Chem. Mater.* **1990**, *2*, 609; (d) Weissbuch, I.; Lahav, M.; Leiserowitz, L.; Meredith, G. R.; Vanherzeele, H. *Chem. Mater.* **1989**, *1*, 114.

40. (a) Gangopadhyay, P.; Radhakrishnan, T. P. *Chem. Mater.* **2000**, *12*, 3362; (b) Gangopadhyay, P.; Rao, S. V.; Rao, D. N.; Radhakrishnan, T. P. *J. Mater. Chem.* **1999**, *9*, 1699; (c) Gangopadhyay, P.; Sharma, S.; Rao, A. J.; Rao, D. N.; Cohen, S.; Agranat, I.; Radhakrishnan, T. P. *Chem. Mater.* **1999**, *11*, 466; (d) Sharma, S.; Radhakrishnan, T. P. *Mol. Cryst. Liq. Cryst.* **1999**, *338*, 257.
41. Anthony, S. P.; Radhakrishnan, T. P. *Chem. Commun.* **2001**, 931.
42. Jayanty, S.; Gangopadhyay, P.; Radhakrishnan, T. P. *J. Mater. Chem.* **2002**, *12*, 2792.
43. Burland, D. M.; Miller, R. D.; Walsh, C. A. *Chem. Rev.* **1994**, *94*, 31.
44. Lalama, S. J.; Sohn, J. E.; Singer, K. D. *SPIE. Proc.* **1985**, *578*, 168.
45. Marks, T. J.; Ratner, M. A. *Angew. Chem. Int. Ed. Engl.* **1995**, *34*, 55.
46. (a) Cui, X.; Pei, R.; Wang, Z.; Yang, F.; Ma, Y.; Dong, S.; Yang, X. *Biosensors & Bioelectronics* **2003**, *18*, 59; (b) Park, S. Y.; Rubner, M. F.; Mayes, A. M. *Langmuir* **2002**, *18*, 9600; (c) Lvov, Y.; Ariga, K.; Onda, M.; Ichinose, I.; Kunitake, T. *Colloids and Surfaces A* **1999**, *146*, 337.
47. Marder, S. R.; Perry, J. W.; Yakymyshyn, C. P. *Chem. Mater.* **1994**, *6*, 1137.
48. (a) Ashwell, G. J.; Jefferies, G.; George, C. D.; Ranjan, R.; Charters, R. B.; Tatam, R. P. *J. Mater. Chem.* **1996**, *6*, 131; (b) Ashwell, G. J.; Jackson, D. P.; Crossland, W. A. *Nature*, **1994**, *368*, 438.
49. (a) A Dictionary of Japanese Art Terms, Bijutsu Co. Ltd., Tokyo, Japan, 1990; (b) Encyclopaedia of Japan, Kodansha, 1983; (c) Tabor, D. *J. Colloid Interface Sci.* **1980**, *75*, 240; (Babylonian lecanomancy-an ancient text on the spreading of oil on water); (d) Fulford, G. D. *Isis* **1968**, *59*, 198.
50. Franklin, B. *Phil. Trans. R. Soc. London.* **1774**, *64*, 445.
51. Giles, C. H.; Forrester, S. D. *Chem. Ind. (London)* **1971**, 42.
52. (a) Pockels, A. *Nature (London)* **1893,** *48,* 152; (b) Pockels, A. *Nature (London)* **1892**, *46*, 418; (c) Pockels, A. *Nature (London)* **1891**, *43*, 437.
53. Langmuir, I. *J. Am. Chem. Soc.* **1917**, *39*, 1848.
54. Langmuir, I. *Trans. Faraday Soc.* **1920**, *15*, 62.
55. Blodgett, K. B. *J. Am. Chem. Soc.* **1934**, *56*, 495.
56. Kuhn, H.; Möbius, D.; Bücher, H. in *Physical Methods of Chemistry* Weissberger, A.; Rossiter, B., (Eds.), Part **3B** Chapter 7, Wiley : New York 1972, Vol. 1.
57. Mann, B.; Kuhn, H. *J. Appl. Phys.* **1971**, *42*, 4398.

58. Gaines Jr., G. L. *Insoluble Monolayers at Liquid-Gas Interfaces* Wiley-Interscience: New York, 1966
59. Tredgold, R. H. *Order in Thin Organic Films* Cambridge University Press: Cambridge, 1994.
60. Ulman, A. *An Introduction to Ultrathin Organic Films*: *From Langmuir-Blodgett to Self assembly* Acadamic Press: London, 1991.
61. Petty, M. C.; Barlow, W. A. *Langmuir-Blodgett Films* Robert, G. G. (Eds.), Plenum Press: New York, 1990.
62. Middleton, S. R.; Iwahashi, M.; Pallas, N. R.; Pethica, B. A. *Proc. R. Soc. (London*) **1984**, *396*, 143.
63. Peterson, I. R. *Molecular Electronics* Ashwell, G. J. (Eds.), Research Studies Press: Taunton, 1992, p. 117.
64. Gray, G. W.; Goodby, J. W. G. *Smectic Liquid Crystals* Leonard Hill: Glasgow, 1984.
65. Pallas, N. R.; Pethica, B. A. *Langmuir* **1985**, *1*, 509.
66. Lavigne, P.; Trancréde, P.; Lamarche, F.; Grandbois, M.; Salesse, C. *Thin Solid Films* **1994**, *242*, 229.
67. Ricceri, R.; Dei, L.; Ottaviani, M. F.; Grando, D.; Gabrielli, G. *Langmuir* **1996**, *12*, 5869.
68. Kwok, D. Y.; Tadros, B.; Deol, H.; Vollhardt, D.; Miller, R.; Cabrerizo-Vílchez, M. A.; Newmann, A. W. *Langmuir* **1996**, *12*, 1851.
69. Sharma, S.; Radhakrishnan, T. P. *Thin Solid Films* **2001**, *382*, 246.
70. Dynarowicz-Łątka, P.; Kita, K. *Adv. Colloid Inter. Sci. B* **1999**, *79*, 1.
71. (a) Chen, K. B.; Chang, C. H.; Yang, Y. M.; Maa, J. R. *ibid*. **2000**, *170*, 199; (b) Rychlicka-rybka, J. *Colloid Surf. A* **1996**, *119*, 29.
72. Dahim, M.; Brockman, H. *Biochemistry* **1998**, *37*, 8369.
73. Neugebauer, C. A. *Handbook of Thin Film Technology* Maissel, L. I.; Glang, R. (Eds.), Chapter 8, McGraw-Hill: New York, 1970.
74. (a) Kimura, F.; Umemura, J.; Takenaka, T. *Langmuir* **1986**, *2*, 96; (b) Bonnerot, A.; Chollet, P. A.; Frisby, H.; Hoclet, M. *Chem. Phys.* **1985**, *97*, 365.
75. Peterson, I. R. *J. Phys. D: Appl. Phys.* **1990**, *23*, 379.
76. Schwartz, D. K. *Surf. Sci. Rep.* **1997**, *27*, 241.
77. Lednev, I. K.; Petty, M. C. *Adv. Mater.* **1996**, *8*, 615.

78. (a) Nishikata, Y.; Kakimoto, M.; Imai, Y. *Thin Solid Films* **1989**, *179*, 191; (b) Nishikata, Y.; Kakimoto, M.; Morikawa, A.; Imai, Y. *Thin Solid Films* **1988**, *160*, 15.
79. Albrecht, O.; Eguchi, K.; Matsuda, H.; Nakagiri, T. *Thin Solid Films* **1996**, *284/285*, 152.
80. Langmuir, I.; Schaefer, V. J. *J. Am. Chem. Soc.* **1938**, *60*, 1351.
81. Whitesides, G. M.; Laibinis, P. E. *Langmuir* **1990**, *6*, 87.
82. (a) Decher, G.; Lvov, Y.; Schmitt, J. *Thin Solid Films* **1994**, *244*, 772; (b) Decher, G.; Hong, J. D.; Schmitt, J. *Thin Solid Films* **1992**, *210/211*, 831.
83. Peng, J. B.; Barnes, G. T.; Gentle, I. R. *Adv. Colloid Interface. Sci.* **2001**, *91*, 163.
84. (a) Bell, G. M.; Combs, L. L.; Dunne, L. J. *Chem. Rev.* **1981**, *81*, 15; (b) Lösche, M. in *Lower Dimensional Systems and Molecular Electronics* Metzer, R. M.; Day, P.; Papavassiliou, G. V. (Eds.), Plenum Press: New York, 1991, Vol. 248, p. 491.
85. Sugahara, M.; Uragami, M.; Yan, X.; Regen, S. L. *J. Am. Chem. Soc.* **2001**, *123*, 7939.
86. (a) Neal, D. B.; Petty, M. C.; Roberts, G. G.; Ahmed, M. M.; Feast, W. J.; Girling, I. R.; Cade, N. A.; Kolinsky, P. V.; Peterson, I. R. *Proc. IEEE Int. Symp. Applications of Ferroelectrics, ISAF'86* **1986**, 89; (b) Kuhn, H.; Möbius, D.; Bücher, H. in *Techniques of Chemistry* Weissberger, A.; Rossiter, B. W. (Eds.), Wiley: New York, 1972, Vol. 1, Pt. 3B, p. 577.
87. Facii, P.; Fontana, M. P.; Dalcanale, E.; Costa, M.; Sacchelli, T. *Langmuir* **2000**, *16*, 7726.
88. Baker, S. M.; Danzer, J.; Desaire, H.; Credo, G.; Flitton, R. *Langmuir* **1998**, *14*, 5267.
89. Nierengarten, J. F.; Eckert, J. F.; Rio, Y.; Carreon, M. D. P.; Gallani, J. L.; Gullion, D. *J. Am. Chem. Soc.* **2001**, *123*, 9743.
90. Tachibana, H.; Yamanaka, Y.; Sakai, H.; Abe, M.; Matsuyoshi, M. *Chem. Mater.* **2000**, *12*, 854.
91. Xu, Y.; Zhang, D.; Liu, Y.; Han, M.; Zhu, D. *Thin Solid Films* **1996**, *284*, 537.
92. Engelking, J.; Ulbrich, D.; Menzel, H. *Macromolecules* **2000**, *17*, 8118.
93. Lednev, I. K.; Petty, M. C. *Adv. Mater. for Opt. and Elec.* **1994**, *4*, 225.

94. Decher, G.; Tieke, B.; Bosshard, C.; Gunter, P. *J. Chem. Soc. Chem. Commun.* **1988**, 933.
95. Mann, R. W.; Szczur, O. *Mol. Cryst. Liq. Cryst.* **2001**, *355*, 305.
96. Nalwa, H. S.; Wantabe, T.; Ogino, K.; Sato, H.; Miyata, S. *J. Mater. Sci.* **1998**, *33*, 3699.
97. Ashwell, G. J.; Zhou, D.; Hamilton, R.; Skjonnemand, K.; Green, A. *Synthetic Metals* **2001**, *121*, 1455.
98. Ashwell, G. J.; Dyer, A. N.; Green, A.; Sato, N.; Sakuma, T. *J. Mater. Chem.* **2000**, *10*, 2473.
99. Ashwell, G. J.; Dawnay, E. J. C.; Kucznski, A. P.; Szablewski, M.; Sandy, I. M. *J. Chem. Soc. Faraday Trans.* **1990**, *86*, 1117.
100. Teerenstra, M. N.; Hagting, J. G.; Schouten, A. J.; Nolte, R. J. M.; Kauranen, M.; Verbiest, T.; Persoons, A. *Macromolecules* **1996**, *29*, 4876.
101. Petty, M. C. *Thin Solid Films* **1992**, *210/211*, 417.
102. Allen, S.; Ryan, T. G.; Hutchings, M. G.; Ferguson, I.; Swart, R.; Froggatt, E. S.; Burgess, A.; Eaglesham, A.; Cresswell, J.; Petty, M. C. *Proc. OMNO 92 Conference,* Ashwell, G. J.; Bloor, D. (Eds.), *Roy. Soc. Chem., London* **1993**, p. 50.
103. Nalwa, H. S.; Kakuta, A. *Appl. Organometallic Chem.* **1992**, *6*, 645.
104. Maslyanitsyn, I. A.; Shigorin, V. D.; Yudin, S. G. *Quantum Electron.* **1997**, *27*, 437.
105. Schwartz, H.; Mazor, R.; Khodorkovsky, V.; Shapiro, L.; Klug, J. T.; Kovalev, E.; Meshulam, G.; Berkovic, G.; Kotler, Z.; Efrima, S. *J. Phys. Chem. B* **2001**, *105*, 5914.
106. Ledoux, I.; Zyss. J. in *Organic Molecules for Nonlinear Optics and Photonics* Messier, J.; Kajzar, F.; Prasad, P. N. (Eds.), Kluwer Academic Publishers: Dordrecht, 1991, Vol. 194, p. 81.
107. Swalen, J. D.; Bjorklund, G. C.; Fleming, W.; Herminghaus, S.; Jungbauer, D.; Jurich, M.; Moerner, W. E.; Reck, B.; Smith, B. A.; Twieg, R.; Wilson, C. G.; Zentel, R. in *Organic Molecules for Nonlinear Optics and Photonics* Messier, J.; Kajzar, F.; Prasad, P. N. (Eds.), Kluwer Academic Publishers: Dordrecht, 1991, Vol. 194, p. 433.

108. (a) Cross, G. H.; Girling, I. R.; Peterson, I. R.; Cade, N. A. *Electron Lett.* **1986,** *22*, 1111; (b) Girling, I. R.; Cade, N. A.; Kolinsky, P. V.; Earls, J. D.; Cross, G. H.; Peterson, I. R. *Thin Solid Films* **1985**, *132*, 101.
109. (a) Kloppner, L. J.; Duran, R. S. *J. Am. Chem. Soc.* **1999**, *121*, 8108; (b) Kloppner, L. J.; Duran, R. S. *Langmuir* **1998**, *14*, 6734; (c) Bodalia, R. R.; Duran, R. S. *J. Am. Chem. Soc.* **1993**, *115*, 11467.
110. Hann, R. A. in *Langmuir-Blodgett Films* Roberts, G. G. (Eds.), Plenum Press: New York, 1990, p. 17.
111. (a) Nalwa, H. S. (Eds.) *Handbook of Organic Conductive Molecules and Polymers* John Wiley: Chichester, 1997, Vols. 1-4; (b) Chandrasekhar, P. *Conducting Polymers: Fundamentals and Applications* Kluwer Academic Publishers: Norwell. 1999.
112. (a) Roth, S. *One Dimensional Metals: Physics and Material Science* VCH: Weinheim, 1995; (b) Conwell, E. M. in *Handbook of Organic Conductive Molecules and Polymers* Nalwa, H. S. (Eds.) John Wiley: Chichester, 1997, Vol. 4, p. 1.
113. Kaufmann, F. B.; Schroeder, A. H.; Engler, E. M.; Kramer, S. R.; Chanbers, J. Q. *J. Am. Chem. Soc.* **1990**, *102,* 483.
114. Sayre, C. N.; Collard, D. M. *J. Mater. Chem.* **1997**, *7*, 909.
115. Ogura, K.; Saino, T.; Nakayama, M.; Shiigi, H. *J. Mater. Chem.* **1997**, *7*, 2363.
116. Křivka, I.; Prokeš, J.; Tobolková, E.; Stejskal, J. *J. Mater. Chem.* **1999**, *9*, 2425.
117. (a) Posudievsky, O. Y.; Biskulova, S. A.; Pokhodenko, V. D. *J. Mater. Chem.* **2002**, *12*, 1446; (b) Guey, W. C.; Yih, H. J.; Sheng, H. S. *J. Mater. Chem.* **2001**, *11*, 2061.
118. Yan, F.; Xue, G. *J. Mater. Chem.* **1999**, *9*, 3035.
119. Cao, H.; Xu, Z.; Sheng, D.; Hong, J.; Sang, H.; Du, Y. *J. Mater. Chem.* **2001**, *11*, 958.
120. Huang, L.; Wang, Z.; Wang, H.; Cheng, X.; Mitra, A.; Yan, Y. *J. Mater. Chem.* **2002**, *12*, 388.
121. Yang, Y.; Wan, M. *J. Mater. Chem.* **2002**, *12*, 897.
122. Matsuo, Y.; Higashika, S.; Kimura, K.; Miyamoto, Y.; Fukutsuka, T.; Sugie, Y. *J. Mater. Chem.* **2002**, *12*, 1592.

123. Dynarowicz-Łątka, P.; Dhanabalan, A.; Oloveira Jr., O. N. *Adv. Colloid Interf. Sci.* **2001**, *91*, 221.
124. Eisenthal, K. B. *Chem. Rev.* **1996**, *96*, 1343.
125. Krüger, P.; Schalke, M.; Wang, Z.; Notter, R. H.; Dluhy, R. A.; Lösche, M. *Biophys. J.* **1999**, *77*, 903.
126. Frommer, J. *Angew. Chem. Int. Ed.Engl.* **1992**, *31*, 1298.
127. Sui, G.; Micic, M.; Huo, Q.; Leblanc, R. M. *Colloid and Surfaces A: Physiochemical and Engineering Aspects* **2000**, *17*, 185.
128. Kuzmenko, I.; Rapaport, H.; Kjaer, K.; Als-Nielsen, j.; Isabella, W.; Lahav, M.; Leiserowitz, L. *Chem. Rev.* **2001**, *101*, 1659.
129. (a) Knoll, W.; Rabe, J.; Philpott, M. R.; Swallen, J. D. *Thin Solid Films* **1983**, *99*, 173; (b) Sastry, M. *Bull. Mater. Sci.* **2000**, *23*, 159.
130. (a) Du, X.; Liang, Y. *J. Phys. Chem. B* **2001**, *105*, 6092; (b) Takenaka, T.; Umemura, J. in *New Developments in Construction and Functions of Organic Thin Films* Kajiyama, T.; Aizawa, M. (Eds.), Elsevier Science: Amsterdam, 1996, p. 145.
131. (a) Flueraru, C.; Schrader, S.; Zauls, V.; Dietzel, B.; Motschmann, H. *Opt. Commun.* **2000**, *182*, 457; (b) Era, M.; Tsutsui, T.; Saito, S. in *New Developments in Construction and Functions of Organic Thin Films* Kajiyama, T.; Aizawa, M. (Eds.), Elsevier Science: Amsterdam, 1996, p. 287.
132. Langmuir, I.; Schaefer, V. J. *J. Am. Chem. Soc.* **1937**, *59*, 2075.
133. Moriizumi, T. *Thin Solid Films* **1988**, *160*¸ 413.
134. Kim, D. K.; Choi, Y. S.; Chang, J. S.; Kwon, Y. S. *Thin Solid Films* **1998**, *327-329*, 612.
135. Charych, D. H.; Nagy, J. O.; Sperck, W.; Bendnarski, M. D. *Science* **1993**, *261*, 585.
136. Li, C.; Huang, J.; Liang, Y. *Langmuir* **2000**, *16*, 7701.
137. Swart, R. M. in *Langmuir-Blodgett Films* Roberts, G. G. (Eds.), Plenum Press: New York, 1990, p. 273.
138. Sastry, M.; Ramakrishnan, V.; Pattarkine, M.; Gole, A.; Ganesh, K. N. *Langmuir* **2000**, *16*, 9142.
139. (a) Chia, S.; Cao, J.; Stoddart, J. F.; Zink, J. I. *Angew. Chem. Int. Ed.* **2001**, *40*, 2447; (b) Martin, A. S.; Sambles, J. R.; Ashwell, G. J. *Phys. Rev. Lett.* **1993**, *70*, 218.

140. Jung, G. Y.; Pearson, C.; Kilitziraki, M.; Horsburgh, L. E.; Monkman, A. P.; Samuel, D. W. I.; Petty, M. C. *J. Mater. Chem.* **2000**, *10*, 163.
141. Yoon, H. C.; Shin, H. K.; Kim, C.; Kwon, Y. S. *Synthetic Metals* **2003**, *137(1-3)*, 1427.
142. Era, M.; Kawafuji, H.; Tsutsui, T.; Saito, S.; Takehara, K.; Isomura, K.; Taniguchi, H. *Thin Solid Films* **1992**, *210/211*, 163.
143. Munn, R. W.; Szczur, O. *Mol. Cryst. Liq. Cryst.* **2001**, *355*, 305.
144. Sugawara, M.; Sazawa, H.; Umezawa, Y. *Langmuir* **1992**, *8*, 609.
145. Baker, S. M.; Danzer, J.; Desaire, H.; Credo, G.; Flitton, R. *Langmuir* **1998**, *14*, 5267.
146. Kawamata, J.; Yuichirou, O.; Yamagishi, A.; Inoue, K. *Nonlinear Optics* **2000**, *25*, 431.
147. Sharma, S.; Chandra, M. S.; Radhakrishnan, T. P. *Langmuir* **2001**, *17*, 8118.
148. Nakamura, K.; Era, M.; Tsutsui, T.; Saito, S. *Jpn. J. Appl. Phys.* **1990**, *29*, L628.
149. (a) Blodgett, K. A. *Phys. Rev.* **1939**, *55*, 391; (b) Blodgett, K. A. *J. Am. Chem. Soc.* **1935**, *57*, 1007.
150. Alfimov, M. V.; Lednev, I. K.; Styrkas. D. A. *Thin Solid Films* **1989**, *179*, 397.
151. Shin, D.; Park, M.; Lim, S. *Thin Solid Films* **1998**, *327-329*, 607.
152. (a) Jelly, E. E. *Nature* **1936**, *138*, 1009; (b) Scheibe, G. *Angew. Chem.* **1936**, *49*, 563.
153. Grundy, M. J.; Musgrove, R. J.; Richardson, R. M.; Roser, S. J. *Langmuir* **1990**, *6*, 519.
154. Wang, W.; Lu, X.; Xu, J.; Jiang, Y.; Liu, X.; Wang, G. *Physica B* **2000**, *293*, 6.
155. Grebelkin, A. L.; Korobeinicheva, N I. K.; Orlova, A.; Repinskii, S. M.; Sveshnikova, L. L.; Selyunina, Zh. Yu.; Sagalaeva, N. I.; Shelkovnikov, V. V.; *Z. Nauch. Priklad. Foto.* **1992**, *37*, 232.
156. Miyamato, Y.; Kaifu, K.; Koyano, T.; Saito, M. ; Kato, M.; Kawamura, K. *Thin Solid Films* **1992**, *208*, 62.
157. Wang, Y.; Nichogi, K.; Terashita, S.; Iriyama, K.; Ozaki, Y. *J. Phys. Chem.* **1996**, *100*, 368.
158. Yamada, T.; Kajikawa, K.; Ishikawa, K.; Takezoe, H.; Fukuda, A. *Thin Solid Films* **1993**, *226*, 173.

CHAPTER 2

Stabilization of a Cationic Amphiphile Monolayer by Polyanions in the Subphase and Computational Modeling of the Complex at the Air-Water Interface

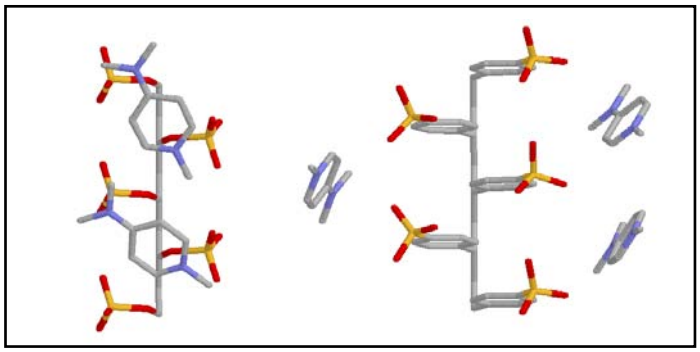

Exploitation of intermolecular interactions with polyelectrolytes introduced in the subphase leads to the stabilization of the Langmuir film of an amphiphile which otherwise does not show any tendency to form a monolayer at the air-water interface. Utility of semiempirical quantum chemical computational modeling in the visualization of the monolayer-polyelectrolyte complexation at the air-water interface is demonstrated. The picture shows optimized geometries of the model complexes formed between amphiphile headgroups and oligomeric unit of different polyelectrolytes used in the study.

Scope

Intermolecular interactions across the air-water interface form the basis for a variety of investigations on monolayers and adsorption phenomena at the interface. In this chapter we present a systematic study of the influence of different anions in the aqueous subphase, on the formation of a monolayer of the cationic amphiphile N-n-octadecyl-4-dimethylaminopyridinium.[1] No monolayer is formed when only the bromide counterion is present. However polyanions such as poly(4-styrenesulfonate) in the subphase not only facilitate the formation of the monolayer but impart strong stability to it. The monolayer stabilization through ionic complex formation at the air-water interface is modeled using semiempirical quantum chemical computations. The significance of including solvation effects in the computations is highlighted.

2.1. Introduction

Intermolecular interactions across the air-water interface have been the focus of a great variety of investigations. H-bonding between amphiphiles spread on the water surface and molecules dissolved in the aqueous subphase has been used to stabilize monolayers,[2,3] promote selective molecular recognition,[4] carry out combinatorial surface chemistry[5] and fabricate nanoporous 2-dimensional assemblies.[6] Extensive use has been made of strong electrostatic interactions between ionic amphiphiles and ions or polyelectrolytes in the subphase. The classic example is the stabilization of fatty acid monolayers by metal ions in the subphase demonstrated by Blodgett.[7] Adsorption of polyelectrolytes from the bulk subphase onto the monolayer assembled at the air-water interface serves as a convenient model system to investigate polyelectrolyte adsorption on solid substrates.[8] Specific structural and morphological changes of ionic amphiphile monolayers resulting from complexation with polyelectrolytes in the subphase have been shown to facilitate photochemical reactions in the monolayer.[9] Biomembrane mimics for ion transport have been fabricated through complexation of cationic amphiphiles with polyanions.[10]

In most of the investigations of the utilization of intermolecular interactions across the air-water interface, the monolayers already possessed reasonable stability when assembled on a subphase of pure water. Hence, the improvement in stability on introduction of the interacting partners in the subphase was usually not very dramatic.

On the other hand, it often occurs that a molecule of special interest on derivatization in the traditional way with a long hydrophobic alkyl chain does not form a stable monolayer on the water surface and hence is not amenable to organized assembly through the Langmuir-Blodgett technique. As noted in Sec. 1.3.15, a common solution to the problem is to mix the amphiphile of interest with other amphiphiles such as fatty acids which are known to form very stable and transferable monolayers.[11] However, even though the composite monolayer achieves satisfactory stability, the number density of the useful amphiphile in the 2-dimensional layer is reduced, leading to less effective utilization of the monolayer in the application of interest (Fig. 2.1). Introduction of intermolecular interactions across the air-water interface, preferably of the strong Coulombic type noted above, provides an attractive alternative.

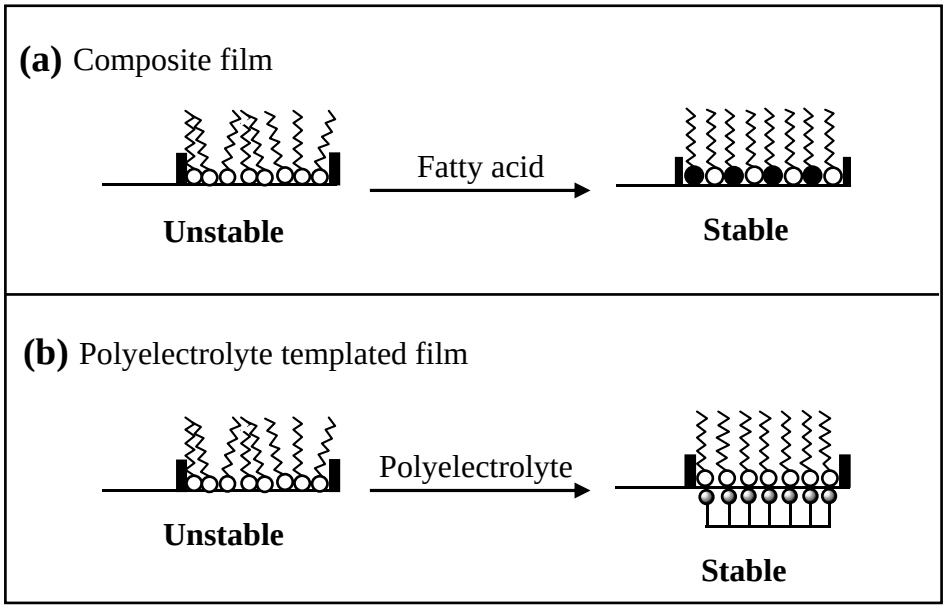

Figure 2.1. *Schematic representation of the formation of **(a)** composite monolayer; **(b)** polyelectrolyte templated monolayer; the number density of the desired chromophore in the 2-D film is considerably reduced in **(a)**, but only marginally in **(b)**.*

The cationic amphiphile, N-*n*-octadecyl-4-dimethylaminopyridinium (ODP^+) has a push-pull chromophore of potential interest in quadratic nonlinear optical applications; AM1/TDHF[12] computed value of the static hyperpolarizability of the headgroup is 6×10^{-30} esu. Adsorption behavior of its soluble analogs having shorter alkyl chains, at the air-water interface has been reported earlier.[13] ODP^+ does not

manifest any tendency towards monolayer formation on the water surface when the counterion is the simple bromide ion which comes along with it from the synthetic protocol used. Introduction of various types of more complex counterions in the subphase are found to lead to the formation of monolayers of ODP^+ with different levels of stability. Specific polyelectrolytes such as poly(4-styrenesulfonate) in the subphase impart high stablility to the monolayers so that these can also be transferred successfully onto suitable substrates. We show further that semiempirical quantum chemical computations provide a convenient framework to gain insight into the structural aspect of complex formation between the ionic amphiphile and the polyelectrolyte. Computations are carried out on model oligomer units of the polyelectrolyte and the headgroup of the amphiphile. The significance of including solvation effects in such computations is demonstrated. We also note that the counterion system, in addition to being the complexing partner for the amphiphiles, acts as a convenient reference to describe different possible orientations of the amphiphiles at the interface. To the best of our knowledge, this is the first demonstration of the utility of such quantum chemical modeling in the visualization of monolayer-polyelectrolyte complexation at the air-water interface.

2.2. Experimental Details

ODP^+Br^- was prepared by the direct reaction of 4-dimethylaminopyridine with 1-bromooctadecane in carbontetrachloride and purified by repeated recrystallizations from acetonitrile. Electronic absorption spectrum of chloroform solution of ODP^+Br^- shows a single peak with λ_{max} at 290 nm.

The counterions we have introduced in the subphase range from simple inorganic ions to organic molecular ions and polyelectrolytes. The different counterions used were generated in solutions from the following salts: (i) sodium sulfate (Na_2SO_4), (ii) potassium malonate ($(K^+)_2MA^{2-}$), (iii) potassium succinate ($(K^+)_2SC^{2-}$), (iv) potassium *p*-nitrophenolate (K^+PNP^-) (v) potassium *p*-toluenesulfonate (K^+PTS^-), (vi) poly(potassium vinylsulfate) ($(K^+)_nPVS^{n-}$; MW = 170,000), (vii) poly(sodium (4-styrenesulfonate)) ($(Na^+)_nPSS^{n-}$; MW = 70,000), (viii) poly(sodium 3:1 (4-styrenesulfonate-*co*-maleate)) ($(Na^+)_n31PSSM^{n-}$; MW ~ 20,000) and (ix) poly

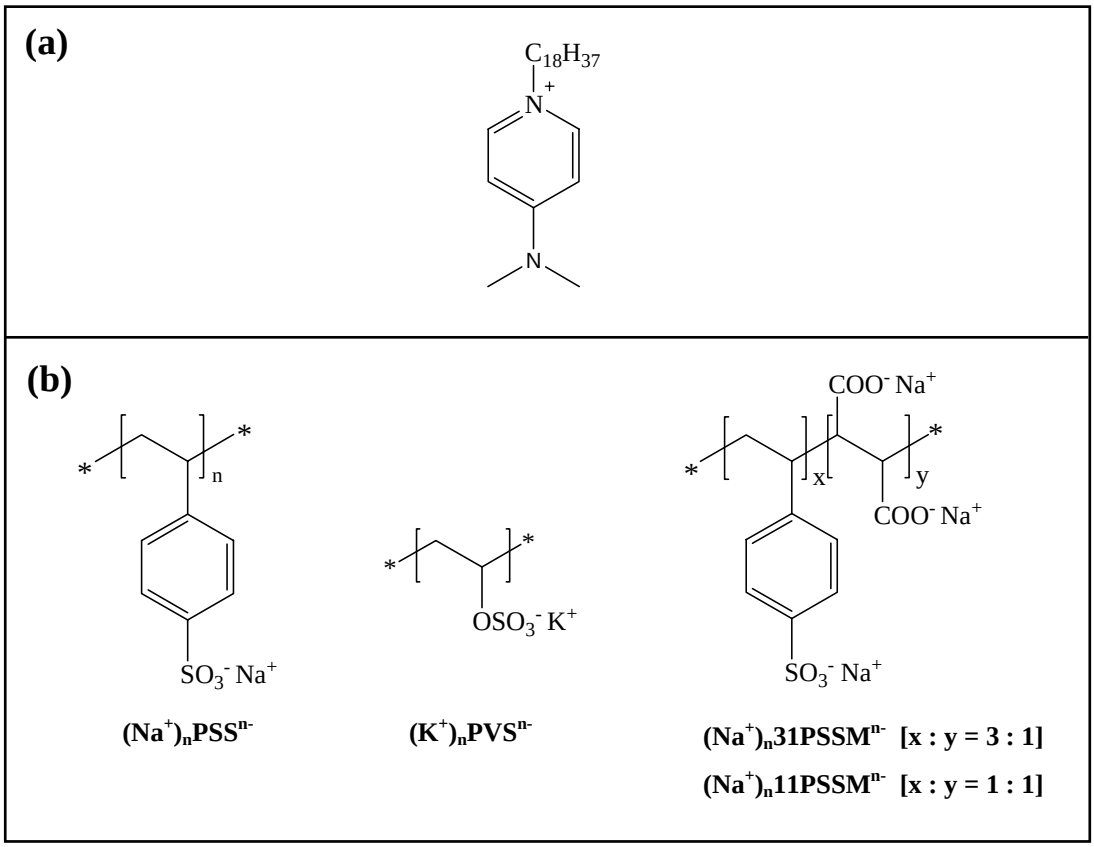

Figure 2.2. *Molecular structure of* ***(a)*** *ODP*$^{+}$ *and* ***(b)*** *the different polyelectrolytes used in this study.*

(sodium 1:1 (4-styrenesulfonate-*co*-maleate)) ($(Na^{+})_n$11PSSM^{n-}; MW ~ 20,000). The polyelectrolytes were purchased from Aldrich Chemical Co. Whereas the other salts were prepared from the respective acids and bases. All the salts were purified by multiple recrystallizations from high purity water and methanol or acetonitrile. The molecular structures of ODP^{+} and the polyelectrolytes are shown in Fig. 2.2. The general procedures used for the fabrication of Langmuir and LB films are given in Appendix B. Electronic spectrum of LB film was recorded in reflectance mode. The sample and the reference uncoated plate were placed with a clean Teflon sheet as the background. The reflectance was converted into absorption using the Kubelka-Munk function. We have attempted to image the Langmuir monolayer by Brewster angle microscopy; however the ODP^{+} system does not show any clear images as the monolayer does not form without polyelectrolyte and the image contrast is very poor when polyelectrolytes such as PSS^{n-} is present.[3]

2.3. Effect of Small Anions and Polyanions on the Stability of ODP^+ Langmuir Film

When ODP^+Br^- is introduced from a chloroform solution on a pure water surface, it does not show any tendency towards uniform spreading. The π-A isotherm **a** in Fig. 2.3 shows that no stable monolayer is formed on compression of the barrier; complete collapse is observed. Isotherms **b** – **f** in Fig. 2.3 are obtained when ODP^+Br^- is spread on a subphase containing PNP^-, SC^{2-}, SO_4^{2-}, MA^{2-} and PTS^- ions, respectively.

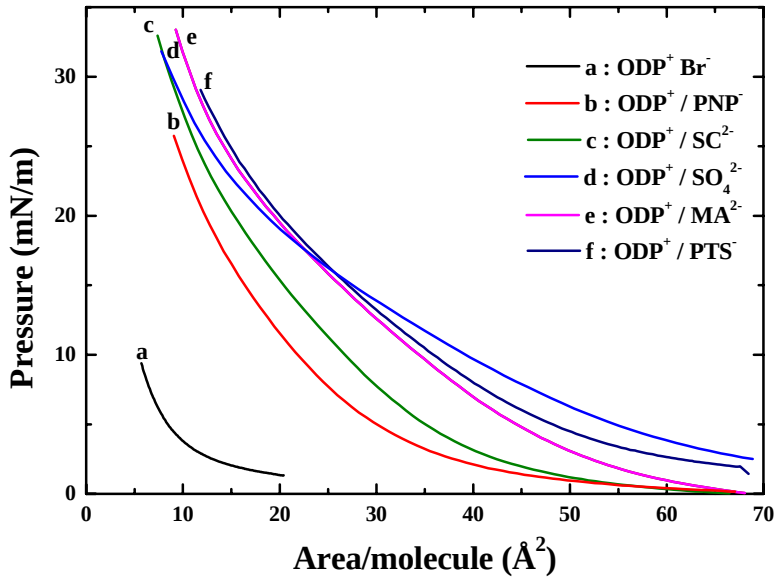

Figure 2.3. *π-A isotherms of ODP^+Br^- spread on* ***(a)*** *subphase of pure water and subphases containing* ***(b)*** *K^+PNP^-;* ***(c)*** *$(K^+)_2SC^{2-}$;* ***(d)*** *Na_2SO_4;* ***(e)*** *$(K^+)_2MA^{2-}$ and* ***(f)*** *K^+PTS^-; x-axis refers to area/molecule of ODP^+.*

These isotherms suggest that the excess counterions in the subphase facilitates the formation of ODP^+ monolayer; however, the gradual and continuous rise of the pressure down to low values of area/molecule indicates the dominance of a liquid-like regime with poor packing and stability. The subtle differences in the isotherms can be qualitatively correlated to the structure of the specific counterions. Between isotherms **b** and **f** the latter is displaced towards higher areas reflecting the larger size of PTS^- relative to that of PNP^-. Isotherm **e** in presence of MA^{2-} appears surprisingly at higher areas compared to isotherm **c** in presence of SC^{2-}. This suggests that SC^{2-} binds two

ODP^+ leading to a more efficient packing whereas MA^{2-} binds only one. A possible explanation for this observation is that the orientation of the carboxylate groups in the same direction is facilitated when they are attached to an ethylene unit as in SC^{2-} rather than when they are on a methylene unit as in MA^{2-}. Isotherm **d** in presence of SO_4^{2-} is quite different from the rest as expected on the basis of its very different structure; we return to this case below. Thus the isotherms in Fig. 2.3 indicate the formation of ODP^+ monolayers with better stabilities than that found on pure water subphase; the molecular areas can be qualitatively correlated to the structures of the relevant counterions in the subphase. Among the different ions, in view of the smaller area/molecule and steepness of the isotherm, SC^{2-} in the subphase appears to support one of the better packing of ODP^+ amphiphiles. Therefore we have considered the logical extension to the deployment of polyelectrolytes in the subphase.

The π-A isotherms recorded for ODP^+ amphiphile with different polyelectrolytes in the subphase are shown in Fig. 2.4 and contrasted with that of ODP^+ on pure water. When the polyelectrolyte $(K^+)_nPVS^{n-}$ is introduced, the isotherm does not improve over those due to the small ions in Fig. 2.3. In fact, isotherm **b** in Fig. 2.4

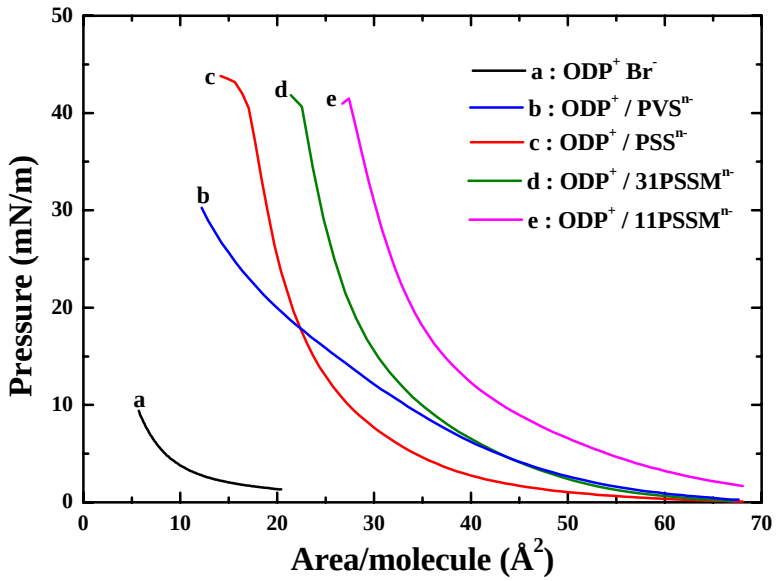

Figure 2.4. *π-A isotherms of ODP^+Br^- spread on **(a)** subphase of pure water and subphase containing **(b)** $(K^+)_n$ PVS^{n-}; **(c)** $(Na^+)_nPSS^{n-}$; **(d)** $(Na^+)_n$ $31PSSM^{n-}$ and **(e)** $(Na^+)_n11PSSM^{n-}$; x-axis refers to area/molecule of ODP^+.*

resembles isotherm **d** in Fig. 2.3, possibly a consequence of the similarity between the binding groups in the two cases. However, isotherms **c** – **e** in Fig. 2.4 due to the polyelectrolytes PSS^{n-}, $31PSSM^{n-}$, $11PSSM^{n-}$ clearly belong to a new group. These isotherms do not show any liquid-like regime; on the contrary, they represent the onset of a close-packed solid region with steep rise of pressure around 10 – 15 mN/m. They also exhibit clear collapse pressures unlike the other isotherms. The area/molecule of ODP^+ extracted from the isotherms in presence of PSS^{n-}, $31PSSM^{n-}$ and $11PSSM^{n-}$ is 25.7, 31.1 and 39.2 $Å^2$, respectively. Interestingly, the relative displacements are clearly related to the fraction of styrenesulfonate units in the three polymers which are 1.0, 0.75 and 0.5 respectively. The area per molecule in each case strongly suggests that the ODP^+ complexes with the sulfonate unit alone in these polyelectrolytes. This is in good agreement with an earlier observation of selective complexation of a cationic amphiphile with copolymer electrolytes[9] and reflects the fact that under the present experimental conditions (pH ~ 5.5) the carboxylic acid groups are in the protonated state and unavailable for complexation. The isotherm in the presence of PVS^{n-} does not show a solid region; however, for the sake of comparison with the other polyelectrolytes, an area/molecule can be extracted by extrapolation of the isotherm near the highest pressures reached; the value obtained is 33.5 $Å^2$. Though our current focus is on intermolecular interactions across the air-water interface, we note that observations such as this provide very useful insight into the details of polyelectrolyte adsorption onto ionic monolayers.

Plots of inverse compressibility ($-d\pi/dA$) shown in Fig. 2.5 reveal the comparison and contrast between the stability of ODP^+ monolayers with SO_4^{2-}, PVS^{n-} and PSS^{n-} in the subphase. The plots in the first two cases are similar suggesting again that the mode of binding of ODP^+ by SO_4^{2-} resembles that of PVS^{n-}. For area/molecule between 25 and 35 $Å^2$, the inverse compressibility in both cases remains nearly constant at a low value corresponding to the liquid-like regime in the π-A isotherms; the final rise stops around 2 mN/m.$Å^2$. On the contrary, in the case of PSS^{n-} ions in the subphase, the inverse compressibility smoothly rises to a much higher value indicating the formation of the solid region. The higher stability of the monolayers with the PSS^{n-} and its copolymer polyelectrolytes in the subphase is further demonstrated by the area-time plots at constant pressure shown in Fig. 2.6. In the case of the subphase with

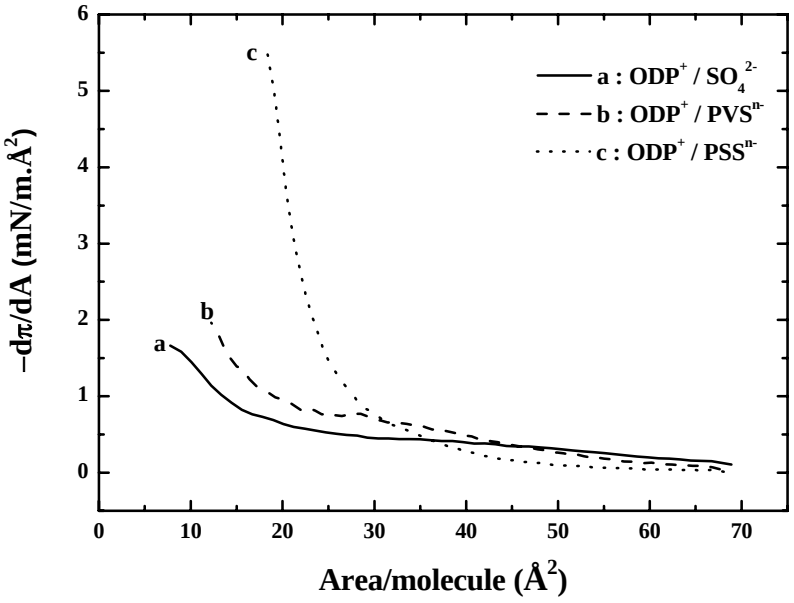

Figure 2.5. *Plots of inverse compressibility versus area/molecule for ODP^+ monolayers when the subphase contains* ***(a)*** *Na_2SO_4;* ***(b)*** *$(K^+)_n$ PVS^{n-} and* ***(c)*** *$(Na^+)_nPSS^{n-}$; x-axis refers to area/molecule of ODP^+.*

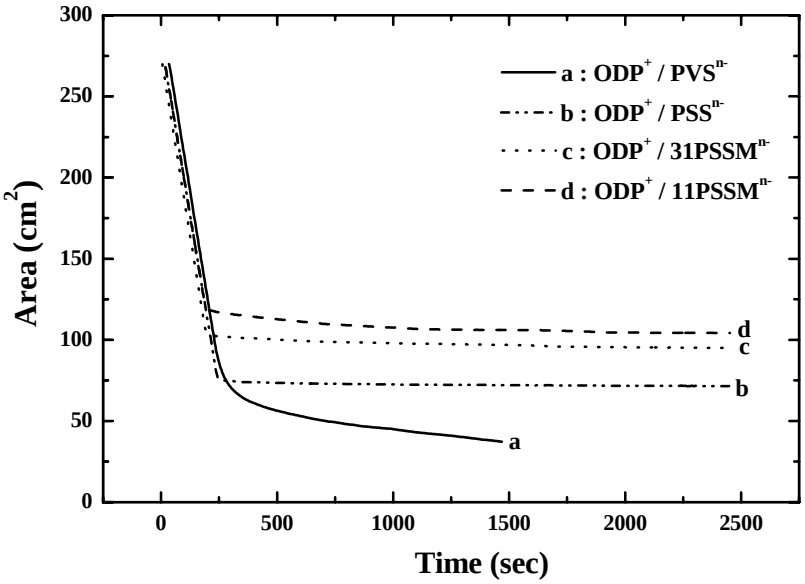

Figure 2.6. *Area-time plots for ODP^+ monolayers under constant pressure with the subphase containing* ***(a)*** *$(K^+)_n$ PVS^{n-} (at 18 mN/m) and* ***(b)*** *$(Na^+)_nPSS^{n-}$;* ***(c)*** *$(Na^+)_n31PSSM^{n-}$ and* ***(d)*** *$(Na^+)_n11PSSM^{n-}$ (at 30 mN/m).*

PVS^{n-}, the monolayer held at a pressure of 18 mN/m shows a slow but steady collapse. However, with PSS^{n-}, $31PSSM^{n-}$ and $11PSSM^{n-}$ in the subphase, even at a higher pressure of 30 mN/m the area remains nearly constant for an extended period of time; among the three there is a minor but clearly discernible improvement in the monolayer stability with increasing content of sulfonate group and the PSS^{n-} case shows negligible collapse. In view of the stability of the ODP^+ monolayer on the subphase containing PSS^{n-}, we have attempted the transfer of the monolayer onto a suitable substrate.

Nearly quantitative transfer (TR ~ 0.9) of a single layer is achieved when a hydrophilic glass or quartz substrate is used. The electronic absorption spectrum of the LB film on quartz is presented together with the solution spectra of ODP^+Br^- (in chloroform) and $(Na^+)_nPSS^{n-}$ (in water) in Fig. 2.7. The presence of ODP^+ in the LB film is clearly established by the peak at 300 nm; the peak at 220 nm and a weak absorption near 260 nm prove the presence of PSS^{n-}. The two shoulders of the 300 nm band suggest the possible presence of J and H aggregates of the ODP^+ amphiphile in the LB film. The small peak near 240 nm appears to be an artifact arising from the Kubelka-Munk transformation of the reflectance spectrum which has a >100% spike at this wavelength.

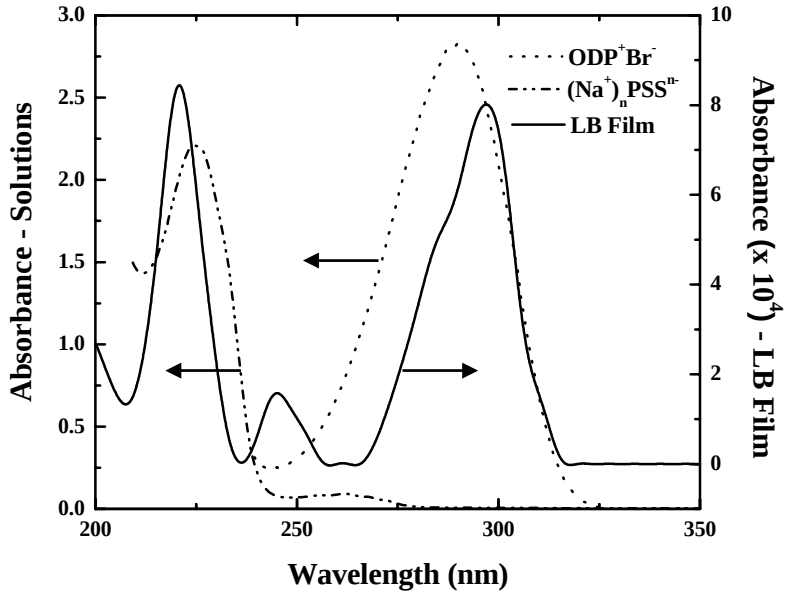

Figure 2.7. *Absorption spectra of ODP^+Br^- (chloroform solution), $(Na^+)_nPSS^{n-}$ (aqueous solution) and LB film of ODP^+/PSS^{n-}.*

The various experiments prove that PSS^{n-} in the subphase lends high stability to the ODP^{+} monolayer whereas PVS^{n-} performs poorly. Since both are strong electrolytes with similar anionic groups and high solubility in water, the basis for this difference is not immediately obvious. The higher molecular weight of PVS^{n-} compared to PSS^{n-} used cannot be the cause, since the polymers, $31PSSM^{n-}$ and $11PSSM^{n-}$ with considerably lower molecular weight do not impart any greater stability to the ODP^{+} monolayer; in fact the ODP^{+} monolayer shows slightly poorer stability in the presence of the latter polyelectrolytes compared to PSS^{n-} (Fig. 2.6). The hydrophobic nature of PSS^{n-} probably facilitates strong stabilization of the amphiphile monolayer and the relatively more hydrophilic $31PSSM^{n-}$, $11PSSM^{n-}$ and PVS^{n-} are less effective. However, among the latter three there is no clear correlation between their stabilizing effect and the hydrophobic nature.[14] We have therefore investigated a molecular level structural model for the complexation of ODP^{+} with PSS^{n-} and PVS^{n-} using the computational studies discussed below, to gain insight into the factors that influence the stabilization of the amphiphile monolayer.

2.4. Computational Modeling of the Complex at the Air-Water Interface

Semiempirical quantum chemical computations on model systems were carried out using the AM1[15] method implemented in the MOPAC93[16] program package. Model systems investigated are $(MDP^{+})_n(R^{5-})$ complexes where MDP^{+} represents ODP^{+} with a methyl group in place of the octadecyl group and R^{5-} represents the pentamer units of PSS^{n-} or PVS^{n-}. Local constraints imposed on the pentanions are described in the following paragraphs. C_{2v} symmetry was imposed locally on the individual MDP^{+} ions. Using appropriately defined z-matrices, the MDP^{+} ions were allowed to rotate and translate freely in the vicinity of the pentanions during the geometry optimizations. The optimizations were carried out with different initial geometries to explore possible pathways on the potential energy surface and final geometries reached consistently are presented. Geometry optimizations were carried out for the complexes without and with the inclusion of solvation effects modeled using the COSMO subroutine.[17] We refer to the former case as the 'gas phase' and the latter as the solvated phase. Earlier studies in our laboratory have shown that the inclusion of solvation effects facilitate the modeling of polymorphism in molecular crystals[18] and a realistic description of

molecular geometries within crystal environments.[19] Since the ODP^+- counterion interaction presumably occurs in the water subphase, the solvated phase calculations employed a dielectric constant of 80 (keyword, EPS = 80). The calculations employed the keyword NSPA = 40 (NSPA: number of geometric segments per atom); increasing the value to 60 or 70 was found to cause only negligible changes in the final results. The area/molecule of the MDP^+ units was extracted from the optimized geometries as follows. The volume of the cluster was determined using the program MOLDRAW[20] and employing the maximum grid of 30,000 points; this program evaluates the molecular volume using van der Waals spheres inscribed around the atoms and taking into account overlap regions. The estimated volumes were reproducible within ~ 3 $Å^3$. The height of the clusters was determined as the distance between mean parallel planes of atoms at the top and bottom when the cluster is viewed along the counterion template chain with the polymethylene backbone at the bottom; a correction due to the van der Waals radii of the atoms in the top and bottom planes was included. Area/molecule of ODP^+ was computed directly from the volume and height of the clusters. Corrections for the uncomplexed anion groups were included as described at the relevant points below. Fig. 2.8 represents schematically the various placements of the MDP^+ ion with respect to the counterion template in the clusters investigated.

The intrinsic persistence length of polyelectrolytes such as PSS^{n-} is ~ 10Å, and complexation with ionic surfactants is known to cause them to stretch out at the air/solution interface.[21] These observations support the following assumptions based on which the clusters represented in Fig. 2.8 were chosen for the computational investigation. (i) The pentameric anion fragment (typically about 10Å long) serves as a reasonable basic model for the polyelectrolyte keeping in view also the computational effort involved. (ii) The pentanions are likely to adopt a conformation wherein their ionic groups are preferentially oriented upwards at the air-water interface so as to facilitate close interaction with the cationic headgroups of the amphiphiles localized at the interface. In fact when pentanion conformations with the monomer groups oriented parallel or alternately antiparallel were used as the initial geometries, the geometry optimizations led to a low equilibrium wedge angle between them, justifying this assumption. (iii) The ionic headgroup of the amphiphile, MDP^+ can be positioned in the regions between the anionic groups or above the backbone. In the former case, three cations can be included in vertical (clusters A and B) or horizontal (cluster C)

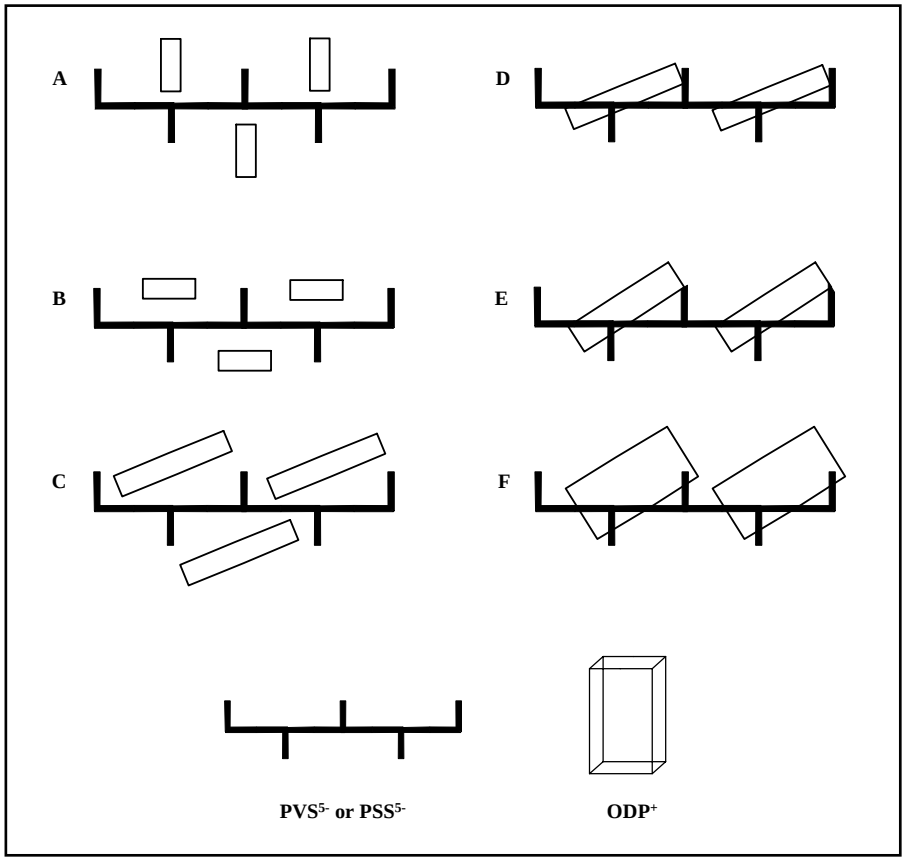

Figure 2.8. *Schematic drawing of the $(MDP^+)_nPVS^{5-}$ and $(MDP^+)_nPSS^{5-}$ clusters considered in the computational study; the top view is shown.*

orientations. In the case of PSS^{5-}, cluster C was found to be unviable due to the limited space available between the bulky *p*-toluenesulfonate groups. When placed over the backbone, the cations are likely to adopt only horizontal orientations (with different possible tilt angles) to facilitate the Coulombic interaction between the strongly positive N^+ of the pyridinium moiety and the anionic groups while accommodating the alkyl chain which is oriented away from the interface; the spatial requirement of such orientations allow the inclusion of only two cations in the clusters D – F.

First, we have optimized the pentanions PVS^{5-} and PSS^{5-} alone. A constraint imposed was that the alternate ionic groups on the polymethylene backbone would open out symmetrically outwards on either side (see Fig. 2.9). This minimizes the repulsions between the groups within the framework of the assumptions listed above. In the case

of PSS^{5-}, we have imposed additionally a parallel orientation of the phenyl ring planes. The calculations were carried out in the 'gas phase' and the 'solvated phase' as noted earlier. A significant difference was noted between the two optimized geometries; inclusion of solvation effects leads to smaller wedge angle between the opened out monomer groups. In the case of PVS^{5-} the angles are 26.6^{o} and 14.5^{o} in the gas and solvated phases, respectively; the relevant angles in PSS^{5-} are 68.6^{o} and 54.0^{o}. This clearly demonstrates the amelioration of the electrostatic repulsions between the groups when solvent effects are taken into account. The optimized geometries for the solvated phase structures are shown in Fig. 2.9.

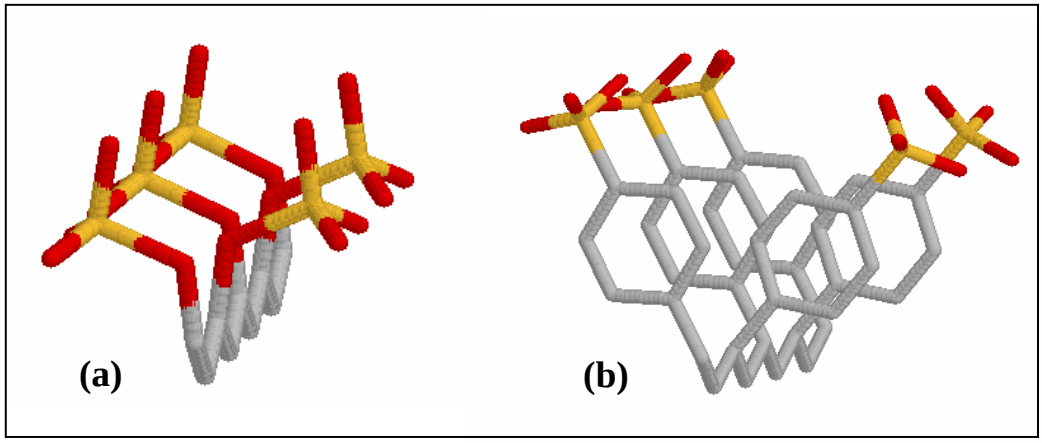

Figure 2.9. *AM1 optimized geometries of* ***(a)*** *PVS^{5-} and* ***(b)*** *PSS^{5-} in the 'solvated phase'; C (●), O (●), S (●).*

Introduction of MDP^{+} enhances the wedge angle in PVS^{5-} as shown by the values for the optimized geometries presented in Table 2.1. The table also provides the computed volume, effective height and area/molecule of MDP^{+} for each of the optimized geometries. In the clusters A – C, a 1:1 ratio between MDP^{+} and the ionic groups in PVS^{5-} is assumed in the computation of area/molecule *i.e.*, the contribution to the area due to two ionic groups on the latter is subtracted out. In the clusters D – F the horizontal MDP^{+} span nearly two anionic groups; hence the ratio is taken as 1:2 (a case of overcompensation of the amphiphile charge; see Ref. 22 for another example) so that in the area calculation the contribution of one ionic group in PVS^{5-} is subtracted out. For the purpose of these subtractions, the area of one ionic group in PVS^{5-} for each of the clusters was obtained by estimating the cluster volume after the removal of MDP^{+}

Table 2.1. *Relevant geometric features of AM1 optimized clusters (Fig. 2.8) with PVS^{5-} and PSS^{5-}; G and S represent the 'gas phase' and 'solvated phase' optimizations (see text for details).*

Anion	Cluster	Wedge angle* (°)				Height (Å)	Area/ molecule (Å^2)
		G	S	G	S	S	S
PVS^{5-}	A	42.3	31.4	883.8	891.8	10.4	24.6
	B	41.7	33.2	885.3	895.1	12.0	20.3
	C	42.3	43.9	888.3	886.6	12.6	19.3
	D	43.9	38.8	732.7	735.6	12.8	22.6
	E	43.9	39.0	731.8	738.2	11.8	23.2
	F	45.2	42.6	732.7	734.0	10.2	29.8
PSS^{5-}	A	60.0	54.7	1220.4	1228.9	10.9	27.5
	B	60.3	54.6	1227.3	1228.4	11.1	25.8
	D	60.0	56.5	1066.3	1072.7	16.1	26.2
	E	57.6	55.3	1069.3	1077.3	15.7	27.0
	F	61.9	55.7	1070.9	1080.1	14.8	29.0

* *See text for the wedge angle of the uncomplexed pentanions.*

ions and estimating the height as described earlier. The results shown in Table 2.1 reiterate the fact that the opening of the wedge angle is relatively less in the solvated phase. Another significant difference between the optimized geometries in the gas and solvated phases is the symmetric nature of the assembly of the MDP^+ ions in the latter case in all the clusters studied. This is illustrated by the optimized geometries of some representative clusters in the two phases shown in Figs. 2.10 and 2.11; it is significant to note that the gas and solvated phase optimizations used the same initial geometry. This strongly suggests that the inclusion of the solvation effect in the computational modeling is essential to obtain a coherent picture of the complexation across the air-water interface. The disorderly structure of the gas phase optimized cluster geometries is incompatible with the ordered nature of monolayers and further makes it impossible to extract any accurate measure of the height of the cluster and hence the area/molecule. Therefore, we have presented in Table 2.1, the area/molecule calculated for only the solvated phase optimized geometries. Comparison of the computed results in Table 2.1 with the experimental value for PVS^{n-} in the subphase shows that cluster F (Fig. 2.10) provides the best description of the ODP^+ - PVS^{n-} complex formation across the air-

water interface. Cluster F displays an over compensation of the amphiphile charge by the polyelectrolyte; the horizontal orientation of the headgroups of ODP^+ dictated by the polyelectrolyte template most likely leads to a poorly packed monolayer and consequent instabilities described earlier.

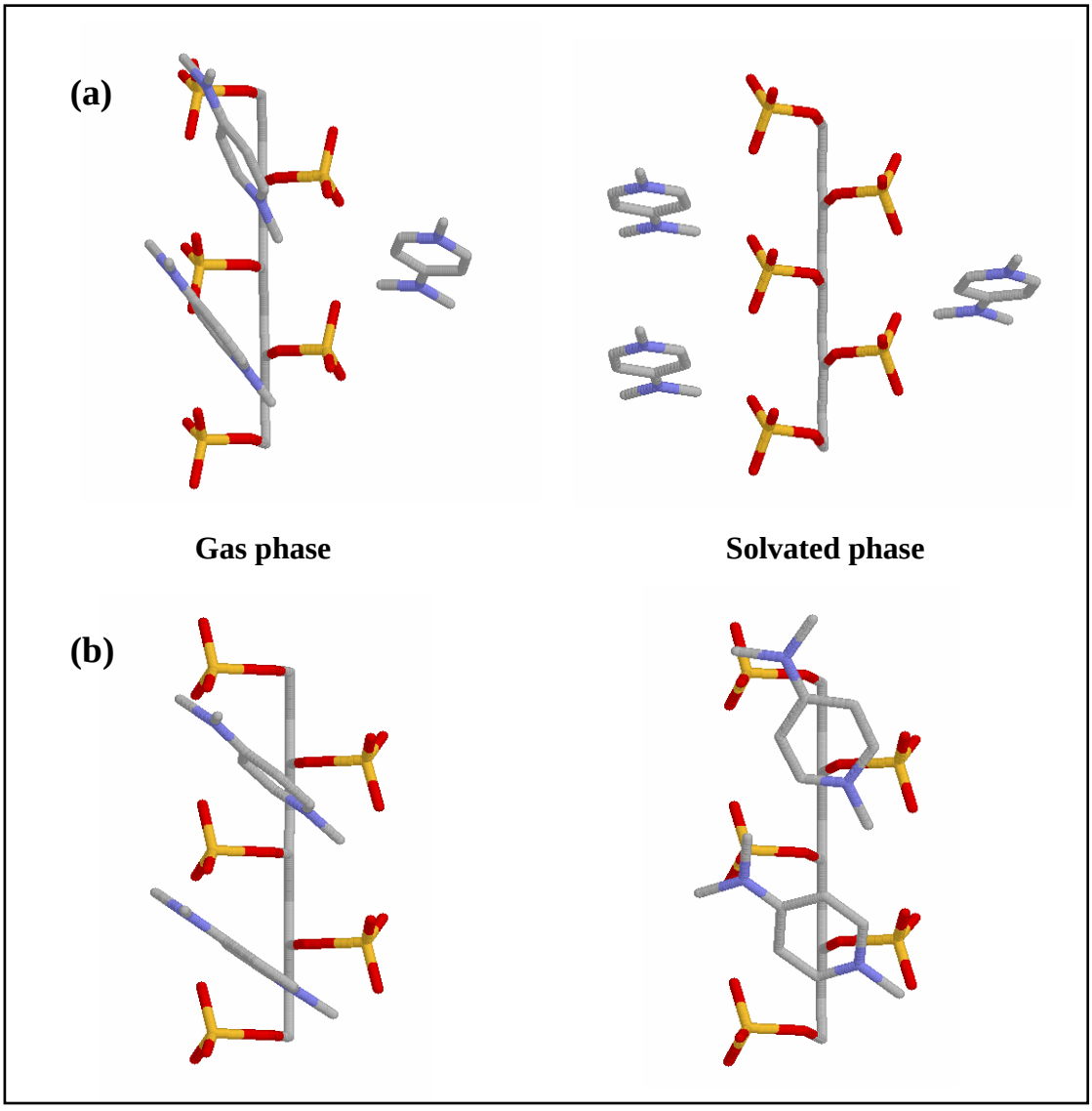

Figure 2.10. *AM1 optimized geometries of the clusters* ***(a)*** *A* ($(MDP^+)_3PVS^{5-}$) *and* ***(b)*** *F* ($(MDP^+)_2PVS^{5-}$) *(see Fig. 2.8) in the 'gas' and 'solvated' phases; C ( ), N ( ), O ( ), S ( ).*

In contrast to PVS^{5-}, the wedge angles in PSS^{5-} are affected much less by the complexation of MDP^{+} especially in the solvated phase. This points to the fact that PSS^{n-} is structurally tuned to complex MDP^{+}. The optimized geometries of the clusters B and D in the gas and solvated phases are shown in Fig. 2.11. Though the area/molecule computed for both the clusters B and D (Table 2.1) are close to the experimental value, the former is in better agreement. Further, cluster B with the MDP^{+} units in the regions between the ionic groups of PSS^{5-}, appropriately oriented for

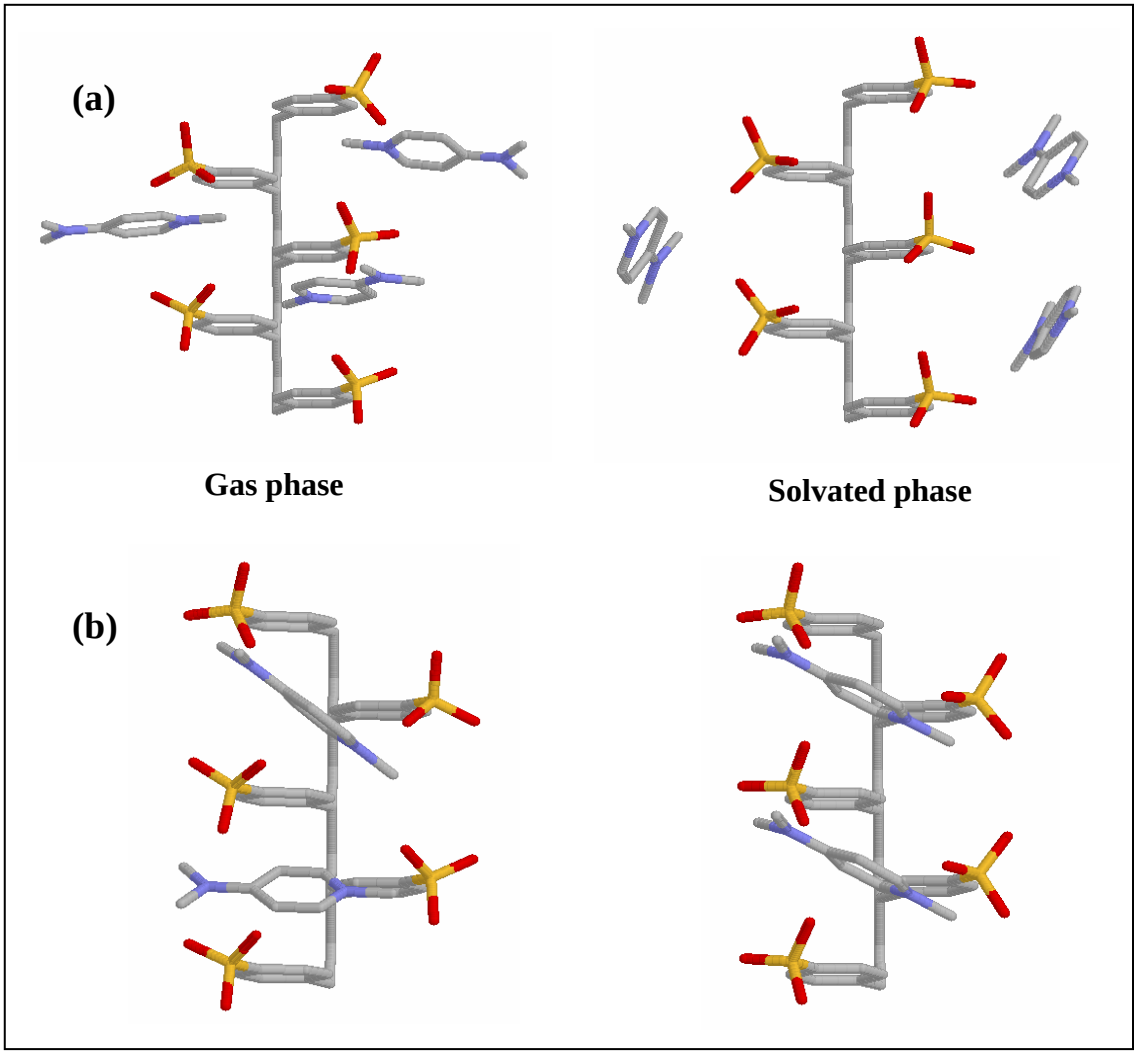

Figure 2.11. *AM1 optimized geometries of the clusters* ***(a)*** *B* $((MDP^{+})_3PSS^{5-})$ *and* ***(b)*** *D* $((MDP^{+})_2PSS^{5-})$ *(see Fig. 2.8) in the 'gas' and 'solvated' phases; C (●), N (●), O (●), S (●).*

enhanced interaction between the N^+ of pyridinium and the anionic groups, shows smaller distortion of the wedge angle of PSS^{5-}. Finally, the vertical disposition of the ODP^+ headgroups in cluster B is likely to lead to a compact packing of the complex and enhanced stability of the ODP^+ monolayers on the subphase containing PSS^{n-}. Thus, cluster B appears to be a more appropriate representation of the ODP^+ - PSS^{n-} complex. Our computations point to the significance of the orientation of the headgroup unit as well as the efficiency of complexation with the polyanion in determining the monolayer stability.

2.5. Summary

ODP^+ which does not exhibit any inclination towards monolayer formation on pure water surface is found to organize into monolayers of varying stability by the introduction of a variety of counterions in the subphase. Polyelectrolytes such as poly(4-styrenesulfonate) in the subphase produce dramatic enhancement of stability of the ODP^+ monolayer facilitating near quantitative transfer onto suitable substrates. Semiempirical quantum chemical calculations including solvation effects are shown to provide a useful description of the complexation of the ionic amphiphile and the counterion template across the air-water interface. Subtle distinctions in the stabilization of the ionic amphiphile monolayer brought about by different polyelectrolytes can be understood within the framework of these computational investigations. The present experimental investigation and computational modeling provide a bulk as well as molecular level view of ionic interactions across the air-water interface and should prove useful in probing the basis of some of the phenomena noted at the beginning of this chapter. The impact of polyelectrolytes on the formation and stabilization of Langmuir films can be exploited in controlling amphiphile organization in transferred LB films. When films are constituted from suitable NLO-phores the polyelectrolyte templating can have considerable influence on the materials attributes such as second harmonic generation capability. Investigations based on these ideas will be presented in Chapter 3.

References

1. Sharma, S.; Chandra, M. S.; Radhakrishnan, T. P. *Langmuir* **2001**, *17*, 8118.
2. (a) Engelking, J.; Ulbrich, D.; Menzel, H. *Macromolecules* **2000**, *33*, 9026; (b) Lackmann, H.; Engelking, J.; Menzel, H. *Mater. Sci. Engg. C* **1999**, *8-9*, 127; (c) Stroeve, P.; van Os, M.; Kunz, R.; *Thin Solid Films* **1998**, *327*, 90; (d) Goedel, W. A.; Wu, H.; Friedenberg, M. C.; Fuller, G. G.; Foster, M.; Frank, C. W. *Langmuir* **1994**, *10*, 4209; (e) Chi, L. F.; Johnston, R. R.; Ringsdorf, H. *Langmuir* **1991**, *7*, 2323; (f) Erdelen, C.; Laschewsky, A.; Ringsdorf, H.; Schneider, J.; Schuster, A. *Thin Solid Films* **1989**, *180*, 153; (g) Shimomura, M.; Kunitake, T. *Thin Solid Films* **1985**,*132*,243.
3. Engelking, J.; Ulbrich, D.; Meyer, W. H.; Schenk-Meuser, K.; Duschner, H.; Menzel, H. *Mater. Sci. Engg. C* **1999**, *8-9*, 29.
4. (a) Talroze, R. V.; Lebedeva, T. L.; Shandryuk, G. A.; Plate, N. A.; Stepina, N. D.; Yanusova, L. G.; Feigin, L. A. *Thin Solid Films* **1998**, *325*, 232; (b) Bohanon, T. M.; Denzinger, S.; Fink, R.; Paulus, W.; Ringsdorf, H.; Weck, M. *Angew. Chem. Int. Ed. Engl.* **1995**, *34*, 58; (c) Ahuja, R.; Caruso, P.; Möbius, D.; Paulus, W.; Ringsdorf, H.; Wildburg, G. *Angew. Chem. Int. Ed. Engl.* **1993**, *32*, 1033; (d) Kawahara, T.; Kurihara, K.; Kunitake, T. *Chem. Lett.* **1992**, 1839.
5. Huo, Q.; Sui, G.; Kele, P.; Leblanc, R. M. *Angew. Chem. Int. Ed. Engl.* **2000**, *39*, 1854.
6. Plaut, D. J.; Lund, K. M.; Ward, M. D. *Chem. Commun.* **2000**, 769.
7. (a) Blodgett, K. A. *Phys. Rev.* **1939**, *55*, 391; (b) Blodgett, K. A. *J. Am. Chem. Soc.* **1935**, *57*, 1007; (c) Blodgett, K. A. *J. Am. Chem. Soc.* **1934**, *56*, 495.
8. (a) Miyano, K.; Asano, K.; Shimomura, M. *Langmuir* **2000**, *7*, 444; (b) Stubenrauch, C.; Albouy, P.; Klitzing, R. V.; Langevin, D. *Langmuir* **2000**, *16*, 3206; (c) Engelking, J.; Wittemann, M.; Rehahn, M.; Menzel, H. *Langmuir* **2000**, *16*, 3407; (d) Ruths, J.; Essler, F.; Decher, G.; Riegler, H. *Langmuir* **2000**, *16*, 8871.
9. (a) Nishiyama, K.; Kurihara, M.; Fujihara, M. *Thin Solid Films* **1989**, *179*, 477; (b) Nishiyama, K.; Fujihara, M. *Chem. Lett.* **1988**, 1257.
10. (a) Niwa, M.; Mukai, A.; Higashi, N. *Macromolecules* **1991**, *24*, 3314; (b) Niwa, M.; Mukai, A.; Higashi, N. *Langmuir* **1990**, *6*, 1432.

11. (a) Munn, R. W.; Szczur, O. *Mol. Cryst. Liq. Cryst.* **2001**, *355*, 305; and references therein; (b) Shin, D.; Park, M.; Lim, S. *Thin Solid Films* **1998**, *327-329*, 607.
12. Dupuis, M.; Karna, S. *J. Comput. Chem.* **1991**, *12*, 487.
13. Haage, K.; Motschmann, H.; Bae, S.; Gründemann, E. *Colloids Surfaces* **2001**, *183-185*, 583.
14. Compared to PVS^{n-} the polyanions $11PSSM^{n-}$ and $31PSSM^{n-}$ possess additionally phenyl and carboxylic acid groups. The hydrophobicity/ hydrophilicity of these groups (extractable from the data in : (a) Dean, P. M. *Molecular Foundations of Drug-Receptor Interaction* Cambridge University Press: Cambridge, **1987**, p. 222; (b) Eisenberg, D.; Weiss, R. M.; Terwilliger, T. C.; Wilcox, W. *Faraday Symp. Chem. Soc.* **1982**, *17*, 109) suggests that PVS^{n-} would be more hydrophobic than the other two. However PVS^{n-} stabilizes the ODP^{+} monolayer the least.
15. Dewar, M. J. S.; Zoebisch, E. G.; Healy, E. F.; Stewart, J. J. P. *J. Am. Chem. Soc.* **1985**, *107*, 3902.
16. *MOPAC93* © Fujitsu Inc.
17. Klamt, A.; Schüürmann, G. *J. Chem. Soc. Perkin Trans.2* **1993**, 799.
18. Sharma, S.; Radhakrishnan, T. P. *J. Phys. Chem. B* **2000**, *104*, 10191.
19. Jayanty, S.; Radhakrishnan, T. P. *Chem. Mater.* **2001**, *13*, 2460.
20. Ugliengo, P.; Viterbo, D.; Chiari, G. *Z. Kristallogr.* **1993**, *207*, 9; *MOLDRAW* Release 1.0, Version E; see the website - *http://www.ch.unito.it/ifm/fisica/moldraw/moldraw.html*
21. Langevin, D. *Adv. Colloid Interface Sci.* **2001**, *89-90*, 467.
22. Ahrens, H.; Baltes, H.; Schmitt, J.; Möhwald, H.; Helm, C. A. *Macromolecules* **2001**, *34*, 4504.

CHAPTER 3

Polyelectrolyte Assisted Deaggregation in a Hemicyanine Dye Langmuir-Blodgett Film : Enhancement and Stabilization of Second Harmonic Generation

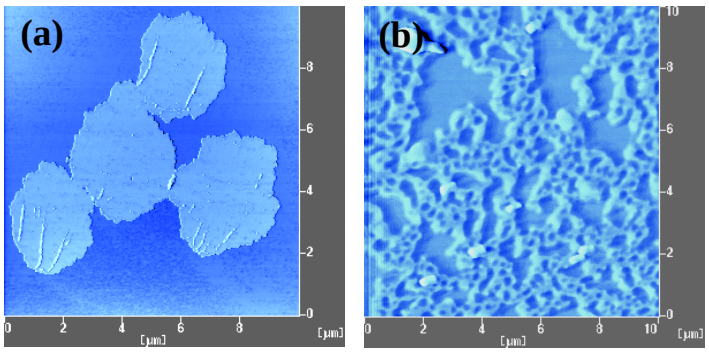

The polyelectrolyte methodology developed in the previous chapter not only helps to stabilize Langmuir films but also effects deaggregation of hemicyanine dye based amphiphiles, leading to enhanced second harmonic generation from the LB films. The degradation of SHG due to laser irradiation is also suppressed by the polyelectrolyte template. AFM images of LB films fabricated with (a) only bromide ion and (b) additionally poly(4-styrenesulfonate) in the subphase, demonstrate the effect of polyelectrolyte templating on the LB film of the hemicyanine dye.

Scope

Molecular aggregation of hemicyanine dye molecules is a problem of fundamental relevance to their linear and nonlinear optical properties. This is an important issue in our investigations of Langmuir-Blodgett films based on the hemicyanine dye and their optical second harmonic generation capability. Therefore in this chapter we present first (Sec. 3.3), our exploration of hemicyanine monomer and dimer structures. We have adopted a novel approach based on crystal structure investigation of model compounds combined with semiempirical quantum chemical computations.[1] Crystal structure of the hemicyanine salt, N-n-butyl-4-[2-(4-dimethylaminophenyl)ethenyl]pyridinium bromide is investigated. The electronic absorption spectra of this compound in the solid state and in solution are modeled using semiempirical computations on the molecule and its dimers extracted from the crystal lattice; the molecular environment in the bulk materials is mimicked by invoking a solvation model following the 'molecules-in-materials' strategy developed in our laboratory. This approach provides insight into the electronic absorption spectral features of Langmuir-Blodgett films of amphiphiles based on hemicyanines reported in earlier studies. More importantly, these modeling studies proved useful in guiding our subsequent efforts at achieving deaggregation in the Langmuir-Blodgett films of the hemicyanine NLO-phore.

Subsequently we describe our investigations of Langmuir-Blodgett films based on the amphiphilic hemicyanine dye, N-n-octadecyl-4-[2-(4-dimethylaminophenyl)-ethenyl]pyridinium bromide. The aggregation of these amphiphiles in Langmuir films on the water surface is influenced by the rate of equilibration of the monolayer after spreading.[2] We have demonstrated that complexation of these cationic amphiphiles at the air-water interface by anionic polyelectrolytes in the subphase has a pronounced effect of deaggregating the amphiphiles and stabilizing the film (Sec. 3.4). This method is shown to be an effective route to achieve complete deaggregation of the dye chromophores in the deposited Langmuir-Blodgett films without reducing the chromophore density in the 2-dimensional lattice. Interestingly, the Langmuir-Blodgett films of the polyelectrolyte complexed amphiphiles show enhanced second harmonic generation,[3] as a consequence of the deaggregation and the larger population of the monomer.

During our investigations of monolayer Langmuir-Blodgett films of the hemicyanine dye, we noticed that the second harmonic generation decays with successive measurements and the associated laser irradiation;[4] this indeed provides a fine illustration of the metastability of Langmuir-Blodgett films. Once again the

Langmuir-Blodgett films of the polyelectrolyte complexed dye are found to be superior in terms of enhanced stability even when subjected to laser irradiation (Sec. 3.5). Poly(4-styrenesulfonate) is shown to arrest the decay most efficiently. Morphological features of the Langmuir-Blodgett films unraveled by atomic force microscopy provided direct insight into the impact of the polyelectrolyte templates. Electronic absorption investigations revealed a close correlation between the trends of second harmonic generation decay and H-aggregate type dimer formation of the NLO-phore. This study provides significant insight into fundamental issues of ultrathin film assembly and introduces an effective strategy towards materials fabrication through this route.

3.1. Introduction

Polymethine dyes possess a push-pull framework[5] and depending on the charge on the unit, they are usually classified into four types (Fig. 3.1),

(a) Cationic streptopolymethine : Cyanine and Hemicyanine dyes.
(b) Anionic streptopolymethine : Oxonol dyes.
(c) Neutral streptopolymethine : Merocyanine dyes
(d) Zwitterionic squaraine-based cyanine dyes.

These dye systems have been extensively used in materials applications and in biology. They are used in optical disks,[6] recording media,[7] and industrial paints for trapping of solar energy;[8] they are also used as laser materials,[9] as photorefractive materials,[10] anti-tumor agents[11] and probes in biological systems.[12] Cyanine dyes have been popular in the field of photography and dye industry for long.[13] The regular cyanine dyes consist of two nitrogen centers (one of which is positively charged) linked through a conjugated chain of an odd number of carbon atoms.

Cyanine dyes with their donor-acceptor framework and extended π-electron conjugation possess large molecular hyperpolarizability, an important prerequisite for developing molecular materials for optical second harmonic generation.[14] Merocyanines and hemicyanines have been popular candidates.[15] Even though merocyanine dyes exhibit strong nonlinear optical response, they are prone to oxidation

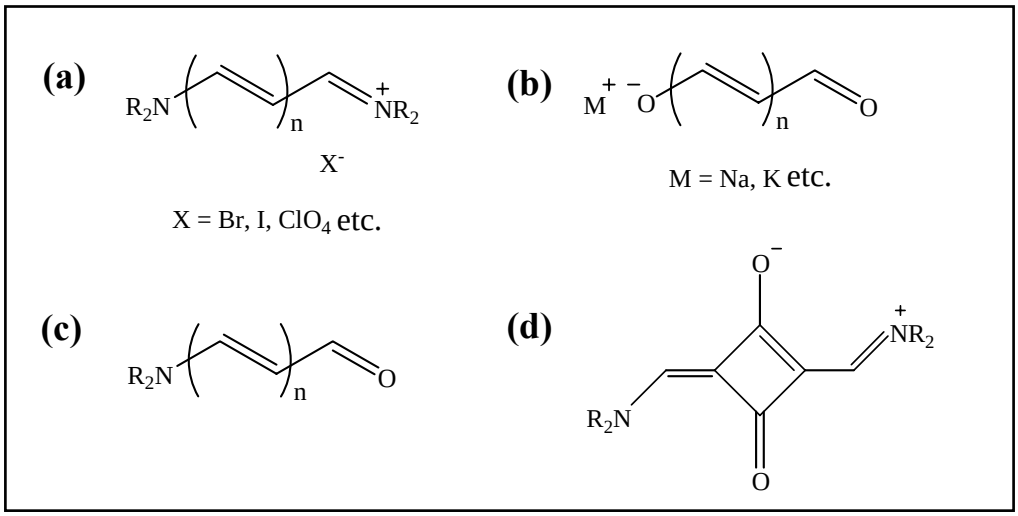

Figure 3.1. *General chemical structures of polymethine dyes:* ***(a)*** *cationic streptopolymethine;* ***(b)*** *anionic streptopolymethine;* ***(c)*** *neutral streptopolymethine and* ***(d)*** *zwitterionic squaraine-based cyanine.*

upon exposure to atmosphere; this has limited their application. Hemicyanine dyes on the other hand are stable in the atmosphere and show SHG response comparable to merocyanine dyes (Fig. 1.9); they are often used as the standard to compare the SHG of new materials;[16] the aggregation problem mentioned earlier, indeed is a difficulty that needs to be addressed.

One of the key challenges in the area of organized molecular assembly is the realization of strong quadratic NLO effects in bulk structures by maximal exploitation of the large molecular responses.[14,17] As mentioned in Sec. 1.2 many strategies have been developed for the fabrication of noncentrosymmetric molecular crystals with optimal supramolecular organization to achieve high second order NLO susceptibility and phenomena such as SHG. Since the Langmuir-Blodgett technique provides a systematic and elegant route to the fabrication of organized molecular assemblies, considerable effort has gone into the fabrication of LB films of hemicyanine based amphiphiles as potential candidates for SHG applications.[18-23] However, the dipolar molecules show a strong predilection towards aggregation in ultrathin films.[18,21,24-27] As noted in Sec. 1.3.15, the aggregate formation can significantly alter the linear and NLO characteristics of these compounds, often with adverse consequences. The

absorption peak shows significant wavelength shifts with respect to the monomer molecule as a result of excitonic interaction in the aggregates (Fig. 1.12).[28] Molecular aggregation usually leads to quenching of the fluorescence, though interesting exceptions are being reported.[29] Molecular aggregation also leads to a reduction in the SHG capability.[20] One source of the problem is the shifting of the electronic states by aggregation which can adversely affect the resonance enhancement effect on SHG at the typical wavelength of 532 nm.

Another fundamental problem associated with LB films which has limited their applications is that, once the molecular assembly obtained through mechanical compression of Langmuir films at the air-water interface is transferred to a solid substrate as LB film, it is no longer necessarily in a thermodynamically stable state.[30] The LB film can undergo molecular level reorganizations with or without external stimuli,[31-33] which can impair its potential functionality.[32,33] An interesting case in point is that of LB films based on quadratic NLO chromophores which exhibit SHG. The laser irradiation involved in the SHG process can itself perturb the molecular assembly in the film with detrimental consequences for its SHG capability. Demonstration of such a phenomenon and development of a suitable solution are of fundamental interest in the design of LB films.

N-*n*-alkyl-4-[2-(4-dimethylaminophenyl)ethenyl]pyridinium bromide is a classic example of an NLO-phore, the amphiphiles of which are prone to extensive aggregation at the air-water interface leading to loss of SHG capability. Previous studies on this system include the impact of protonation[22] and the formation of composites with insoluble polymers[23] and fatty acids.[20,21,33,34] A variety of model structures have been explored to understand the aggregation phenomenon;[18,35] the H-aggregate formation in LB films with associated electronic absorption shift[21,27,36,37] have been investigated by electronic spectroscopy,[36,37] dynamics of emission[26] and SHG.[18-23,38] Investigations based on the extended dipole approximation have shown that, for the small intermolecular distances relevant to these systems, only H-aggregate behavior is manifested regardless of the axial orientation of molecules.[37] Extended dipole approximation has been employed also to analyze the spectral properties of stilbene aggregates in microheterogeneous media and monolayers.[39] The structures of these

aggregates have been modeled through force field approaches utilizing cluster geometries from crystals.[40]

Our studies have focused on N–*n*–octadecyl–4-[2-(4–dimethylamino phenyl)ethenyl]pyridinium bromide ($ODEP^+Br^-$) and the impact of some synthetic and natural polyelectrolytes introduced in the subphase on the deaggregation, enhancement of SHG and stabilization of LB films to laser irradiation. In the first phase of the study we have used polyelectrolytes possessing similar binding sites but located at different distances and in the second phase, polyelectrolytes with different kinds of binding sites and levels of rigidity.

3.2. Experimental and Computational Details

3.2.1. *Synthesis and characterization*

ODEP$^{\pm}$Br$^-$

$ODEP^+Br^-$ was synthesized following the procedure reported earlier (Scheme 3.1).[41] 0.50 g (1.50 mmol) of 1-bromooctadecane was added to 0.15 ml (1.51 mmol) of 4-methylpyridine and stirred at 125^{o}C for 5 h. 0.60 g (1.41 mmol) of N-*n*-octadecyl-4-methylpyridinium bromide obtained was mixed with 0.23 g (1.40 mmol) of 4-(N,N-dimethylamino)benzaldehyde and 0.10 ml of piperidine in methanol and refluxed for 3 h. On cooling the reaction mixture to 30^{o}C, 0.59 g (72% yield) of $ODEP^+Br^-$ precipitated out as a red crystalline solid. It was filtered, dried and recrystallized several times from methanol. M. P. /^{o}C = 216-218 (dec.); FTIR (KBr) : $\bar{\upsilon}$/cm^{-1} = 2916.6, 2849.1, 1643.5, 1593.35, 1163.2, 833.3; UV-Vis (chloroform) : λ_{max}/nm = 497.5, 285.0; ^{1}H-NMR ($CDCl_3$) : δ/ppm = 0.88 (t, 3H), 1.25 (m, 30H), 1.95 (m, 2H), 3.08 (s, 6H), 4.68 (t, 2H), 6.68-6.72 (d, 2H), 6.80-6.89 (d, 1H), 7.50-7.55 (d, 2H), 7.57-7.66 (d, 1H), 7.82-7.85 (d, 2H), 8.89-8.92 (d, 2H); ^{13}C-NMR ($CDCl_3$) : δ/ppm = 14.07, 22.66, 26.10, 29.06, 29.36, 29.65, 31.59, 31.88, 40.08, 60.36, 111.98, 116.44, 122.41, 122.75, 130.65, 143.02, 143.41, 152.39, 154.18.

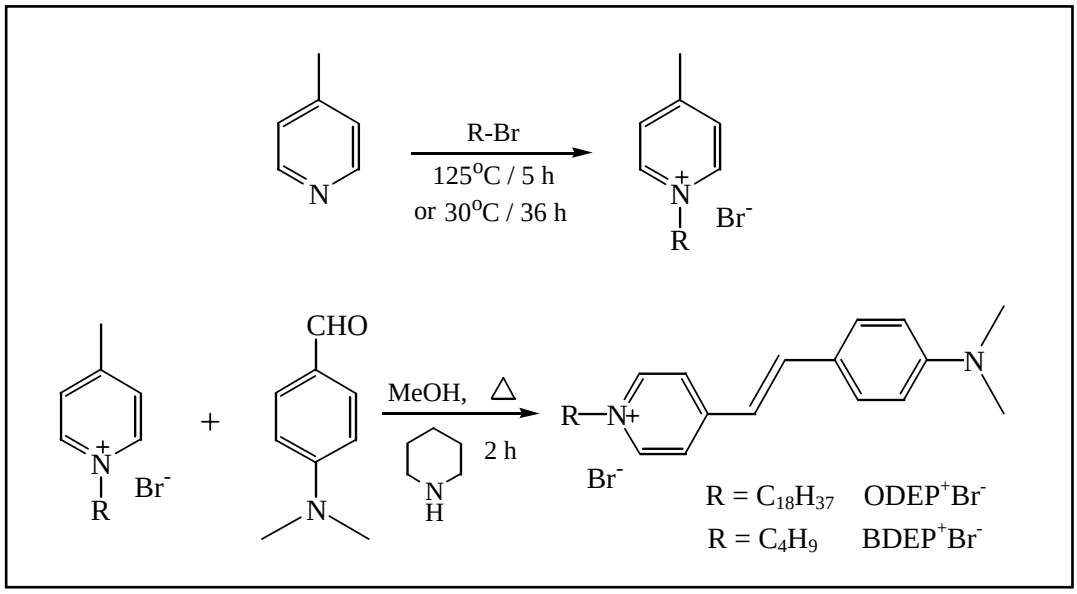

Scheme 3.1

BDEP$^{\pm}$Br^{-}

$BDEP^{+}Br^{-}$ was synthesized following the same procedure (Scheme 3.1) as the previous reaction except that the reaction was carried out at room temperature in the first step. 0.21 ml (2.19 mmol) of 1-bromobutane was added to 0.24 ml (2.20 mmol) of 4-methylpyridine and stirred at 30°C for 36 h. 0.20 g (0.87 mmol) of N-*n*-butyl-4-methylpyridinium bromide obtained was mixed with 0.145 g (0.87 mmol) of 4-(N,N-dimethylamino)benzaldehyde and 0.10 ml of piperidine in methanol and refluxed for 2 h. On cooling the reaction mixture to 30°C, 0.17 g (54% yield) of $BDEP^{+}Br^{-}$ precipitated out as a red crystalline solid. It was filtered, dried and recrystallized several times from methanol. M. P. /°C = 230 (dec.); FTIR (KBr) : $\bar{\upsilon}$/cm^{-1} = 3016.9, 1641.6, 1575.9, 1157.4, 823.7; UV-Vis (chloroform) : λ_{max}/nm = 497.5, 285.0; ^{1}H-NMR ($CDCl_3$) : δ/ppm = 0.95 (t, 3H), 1.41 (m, 2H), 1.95 (m, 2H), 3.06 (s, 6H), 4.66 (t, 2H), 6.65-6.70 (d, 2H), 6.80-6.89 (d, 1H), 7.50-7.54 (d, 2H), 7.57-7.65 (d, 1H), 7.84-7.88 (d, 2H), 8.94-8.97 (d, 2H); ^{13}C-NMR ($CDCl_3$) : δ/ppm = 13.51, 19.39, 33.48, 40.07, 60.09, 112.00, 116.39, 122.38, 122.72, 130.67, 143.05, 143.46, 152.41, 154.20.

3.2.2. *Langmuir and Langmuir-Blodgett film studies*

The polyelectrolytes used in the studies presented in this chapter are poly(sodium 4-styrenesulfonate) ($(Na^+)_nPSS^{n-}$; MW = 70,000), poly(sodium 3:1 (4-styrenesulfonate-*co*-maleate)) ($(Na^+)_n31PSSM^{n-}$; MW ~ 20,000), poly(sodium 1:1 (4-styrenesulfonate-*co*-maleate)) ($(Na^+)_n11PSSM^{n-}$; MW ~ 20,000), sodium salt of carboxymethyl cellulose ($(Na^+)_nCMC^{n-}$; MW = 90,000) and sodium salt of deoxyribonucleic acid ($(Na^+)_nDNA^{n-}$; highly polymerized CT DNA) (Fig. 3.2). The Langmuir films were formed by spreading the solution of $ODEP^+Br^-$ in chloroform on the aqueous subphase containing the polyanion ($ODEP^+$: monomer unit of the polyanion ~ 1 : 8), allowing equilibration for 90-120 min. The general procedures used for the Langmuir and LB film preparation and characterization are given in Appendix B.

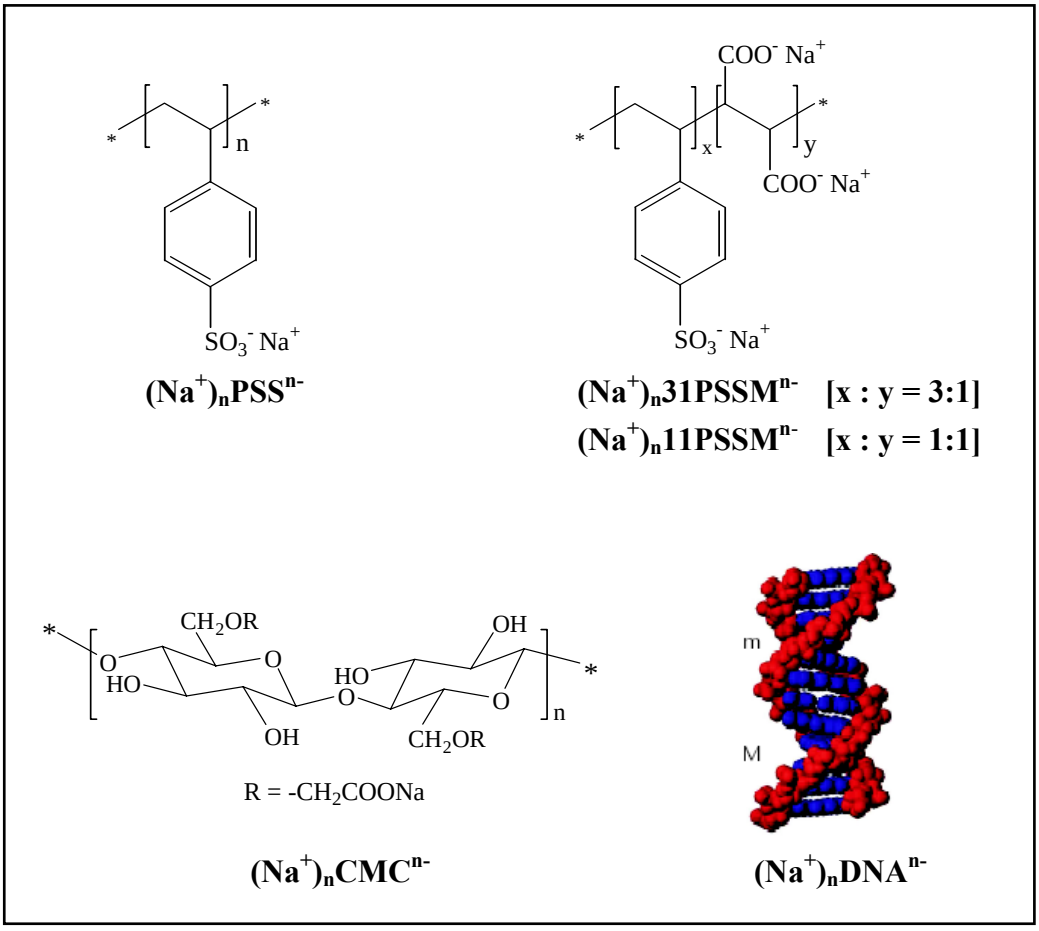

Figure 3.2. *Molecular structures of the various polyelectrolytes used in the studies presented in this chapter.*

Incident angle dependence of the SHG intensity of the films was measured using a ns-pulsed 1064 nm beam from an Nd-YAG laser. Details of the equipment and the experimental procedure are presented in Appendix E. Both p-p and s-p polarization measurements were carried out and the SHG fringe patterns were analyzed using standard protocols.[42]

3.2.3. *Crystal structure determination*

X-ray diffraction data were collected on an Enraf-Nonius MACH3 diffractometer. MoK_α radiation with a graphite crystal monochromator in the incident beam was used. Data was reduced using Xtal3.4;[43] Lorentz and polarization corrections were included. Empirical absorption correction was applied using ψ–scan data. All non-hydrogen atoms were found using the direct method analysis in SHELX-97 [44] and after several cycles of refinement the positions of the hydrogen atoms were calculated and added to the refinement process. Graphics were handled using ORTEX6a.[45] More details are given in Appendix D.

3.2.4. *Semiempirical computations*

Semiempirical quantum chemical computations were carried out using the AM1[46] method in the MOPAC93 program package.[47] The microenvironment of the molecule in the crystal and the solution phase were both simulated using the solvation model COSMO;[48] the parameter, NSPA (number of segments per atom) was set equal to 60 in all calculations. The concept of modeling molecules-in-materials using such an approach has been developed in our laboratory.[49,50] Computations were carried out on geometries of the molecule and its supramolecular assemblies extracted from the crystal structure; H atom positions alone were optimized. In the relevant cases, the butyl group was replaced by octadecyl chain and optimized fully. The absorption energies were obtained from configuration interaction (CI) calculations invoking the full set of 400 singlet configurations involving 6 molecular orbitals bracketing the HOMO/LUMO.

3.3. Modeling Molecular Aggregation of Hemicyanine Chromophore by a Combined Spectroscopic, Crystallographic and Computational Approach

We have addressed the fundamental problem of aggregate formation of the hemicyanine chromophore by analyzing the electronic spectral features of $BDEP^+Br^-$ using inputs from crystallographic and computational investigations. The simple method we have developed involves the use of supramolecular clusters in molecular crystals of the hemicyanine dye as models for the aggregates and computation of their electronic structure using semiempirical computations incorporating solvation modeling which normally mimics the molecular environment in solution but is used here to provide a rough representation of the influence of the crystal lattice. A comparison of the electronic absorption spectra of the solution and microcrystalline solid clearly suggests the utility of the latter approach in modeling the electronic structure of molecular aggregates. Previous studies in our laboratory on 4-nitroaniline based systems have provided important insight into the correlation of molecular association in crystals and Langmuir/LB films.[51] Our approach is similar to that of Whitten and coworkers in the case of stilbenes,[40] to the extent that we use supramolecular clusters from crystals to model the aggregate behavior; however the utilization of semiempirical quantum chemical computations including environment effects and the modeling of the spectroscopic features based on these clusters is a new channel of exploration.

3.3.1. *Electronic absorption spectroscopy*

The electronic absorption spectra of $BDEP^+Br^-$ in chloroform solution and in the solid state are presented in Fig. 3.3. The peak at 497.5 nm present in the solution spectrum is characteristic of the monomer, independent $BDEP^+$ chromophore.[21,26,27,37] Similar monomer peaks have been observed in LB films as well, where the hemicyanine dye has been deaggregated by admixing with fatty acids.[21,26] Spectra of $BDEP^+Br^-$ recorded in solvents of different polarity clearly revealed the negative solvatochromism of this molecule suggesting a strongly polar ground state. The absorption spectrum of the microcrystalline solid is broad and deconvolution indicates peaks at 460.2, 399.4, 327.2 and 278.7 nm. The new peaks at 399.4 and 327.2 nm appear to originate from the supramolecular aggregates present in the crystalline material. The absorption peaks

near 340 nm in the spectra of Langmuir/LB films of other amphiphiles having the same headgroup as $BDEP^+$ have been attributed[21,27,37] to molecular aggregates. To gain insight into the types of clusters that are relevant to model these spectral features, we have carried out single crystal X-ray diffraction analysis of $BDEP^+Br^-$.

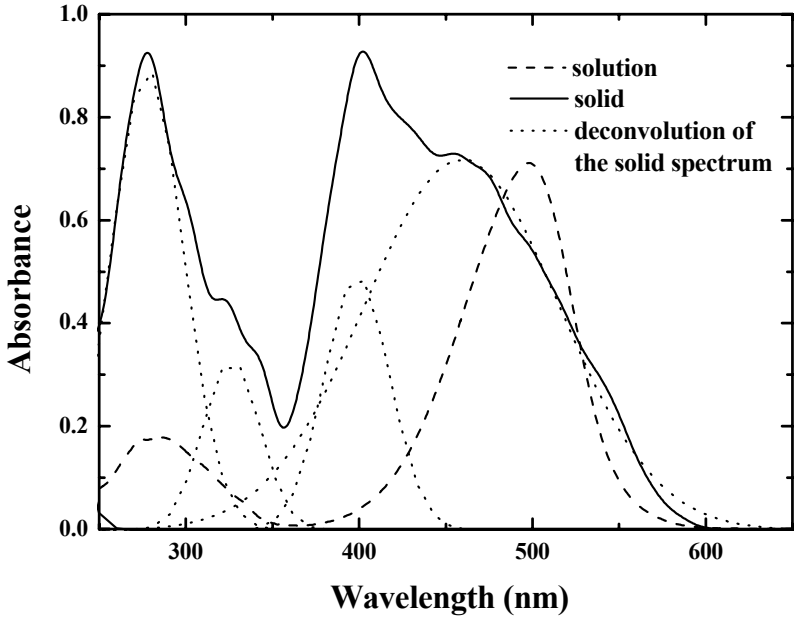

Figure 3.3. *Electronic absorption spectra of $BDEP^+Br^-$ in solid and solution states.*

3.3.2. *Single crystal X-ray structure analysis*

Several salts of N-methyl-4-[2-(4-dimethylaminophenyl)ethenyl]pyridinium have been reported to form noncentric crystal lattices.[52] X-ray analysis of crystals of $BDEP^+Br^-$ grown by slow evaporation of methanolic solutions showed that they belong to the monoclinic $P2_1/c$ space group.

The basic crystallographic data are collected in Table 3.1. The asymmetric unit consists of two molecules. The molecular structure is shown in Fig. 3.4; since the structure of the two molecules in the asymmetric unit is very similar only one is shown. It should be mentioned that the second bromide ion in the asymmetric unit resides close to the dimethylaminophenyl group of the molecule shown in the figure. The aromatic region of the molecule is nearly planar with a very small twist of ~ 4^o around the central double bond. The butyl chain is all-*trans*. Fig. 3.5 provides a view of the packing of

Table 3.1. *Crystallographic data of $BDEP^+Br^-$*

Molecular formula	$C_{19}H_{25}N_2Br$
Formula weight	361.32
Crystal system	Monoclinic
Space group	$P2_1/c$ (No.14)
a, Å	12.222 (10)
b, Å	17.521 (17)
c, Å	17.13 (2)
β, deg.	90.58 (9)
Z	8
$\rho_{calc.}$, g cm^{-3}	1.308
λ (Å)	0.71703
μ, cm^{-1}	22.50
Number of unique reflections	6433
Number of reflections with $I \geq 2\sigma_I$	3139
Number of parameters	397
GOF	1.002
T_{min}, T_{max} (empirical absorption correction)	0.7942, 0.9995
R (for $I \geq 2\sigma_I$)	0.0621
wR^2	0.1336

molecules in the crystal of $BDEP^+Br^-$. The organic cation forms square channels running along the ***a*** axis with the bromide ions packed inside these channels. This packing motif appears to be facilitated by the strong Coulombic interactions likely to be present in this ionic solid. The crystal structure provides a basis to visualize possible molecular associations in different states of $BDEP^+Br^-$ such as the solid, LB films and solution. We analyze below, the electronic spectrum of $BDEP^+Br^-$ in solution and in the solid state using semiempirical computations on the geometry of $BDEP^+Br^-$ and its dimers extracted from the crystal structure. We show that these computations also provide a model to understand the aggregate structures in LB films reported previously.

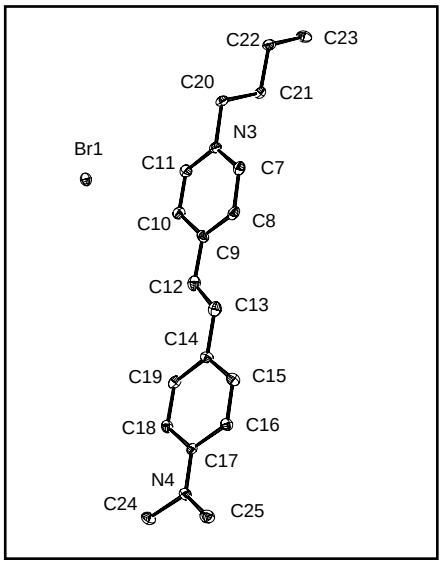

Figure 3.4. *Molecular structure of $BDEP^{+}Br^{-}$ from single crystal X-ray analysis; 10% probability thermal ellipsoids are indicated and H atoms are omitted for clarity. Structure of only one molecule in the asymmetric unit is shown.*

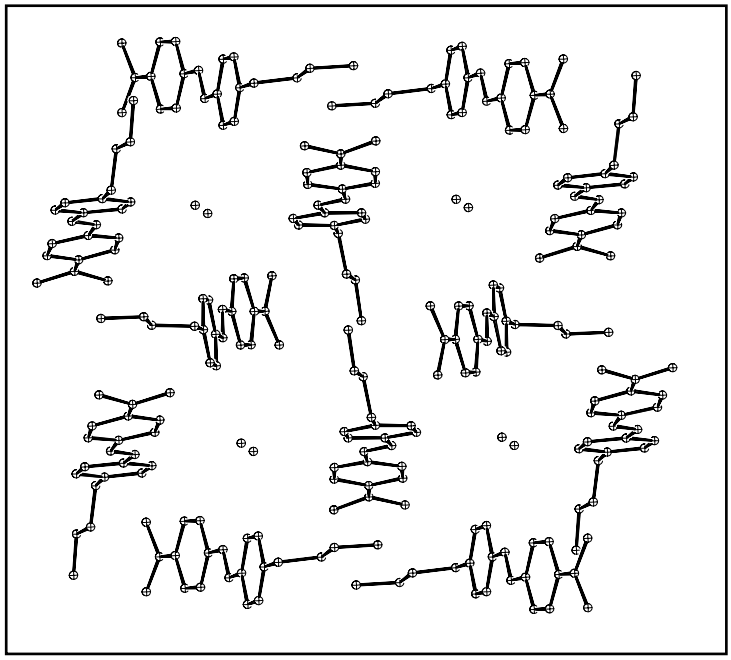

Figure 3.5. *Packing of molecules in $BDEP^{+}Br^{-}$ crystals viewed approximately along the **a** axis; H atoms are omitted for clarity. The spheres inside the channels are the bromides and the distance between the two ions shown within each cavity is 5.907 Å.*

3.3.3. *Computational modeling*

AM1/CI computations were carried out on the monomer, the cationic part of $BDEP^{+}Br^{-}$, as well as the antiparallel and parallel dimer structures (Fig. 3.6) present in the crystal. Calculations employed different dielectric constants within the COSMO option. The computed λ_{max} and oscillator strength for the absorptions are collected in Table 3.2; those with oscillator strength < 0.25 are not shown. At all values of the dielectric constant, the lowest energy absorptions in both the dimers are found to be blue shifted with respect to the monomer. Based on a close examination of the computed absorption maxima and the peaks in the experimental spectra, the models that explain the experimental data are presented in Table 3.3. The agreement between the experimental values and the model calculations is quite good.

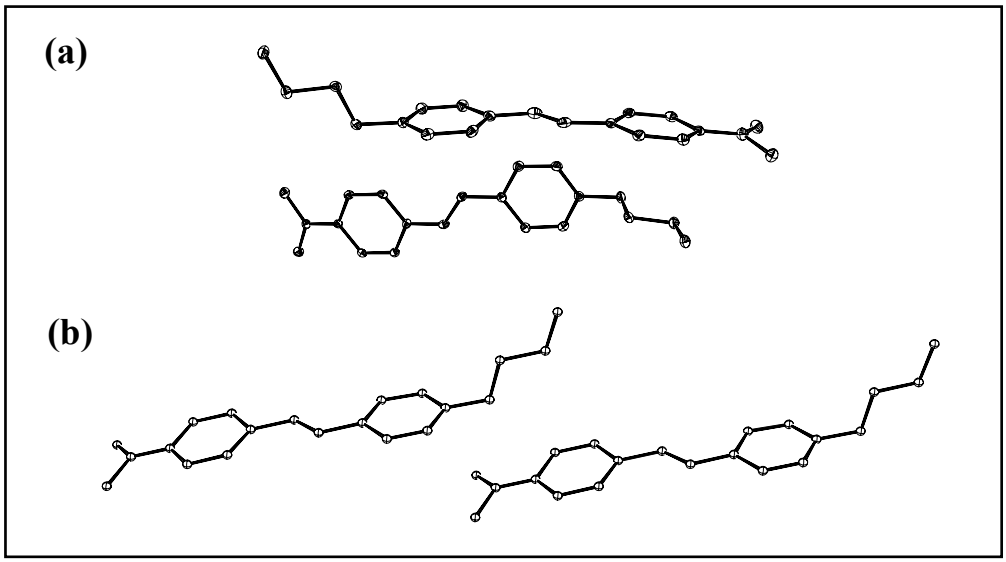

Figure 3.6. ***(a)*** *Antiparallel and* ***(b)*** *parallel dimer structures of the cations present in* $BDEP^{+}Br^{-}$ *crystals.*

The table also presents the data on LB films compiled from previous reports;[18,21] the data correspond to the hemicyanine dye based amphiphiles in pure form as well as composites with arachidic acid. Inspection of the experimental and computed data in Table 3.3 leads to the following conclusions. The monomer peaks are present in the solution, solid state and LB film spectra. The antiparallel dimer explains the additional peaks in the solid state spectrum. Parallel dimer serves as a suitable model for the new

Table 3.2. *Peak maximum (λ_{max}) and oscillator strength (f) of the electronic absorptions of monomer, antiparallel (Fig. 3.6a) and parallel (Fig. 3.6b) dimers of the cationic part of $BDEP^+$ computed using the AM1/CI method under different dielectric constants, ε in the COSMO routine.*

Structure	λ_{max} (nm) [f]				
	ε = 1	**ε = 2**	**ε = 3**	**ε = 4**	**ε = 5**
Monomer	506.6 [0.86] 281.3 [0.32]	476.4 [0.88] 294.4 [0.57]	450.2 [0.95] 290.9 [0.61]	435.8 [1.00] 288.6 [0.60]	426.9 [1.03] 287.0 [0.54]
Dimer (antiparallel)	455.2 [0.90] 393.6 [0.60]	394.9 [0.87] 344.7 [0.58]	371.3 [0.88] 325.7 [0.59]	361.4 [0.90] 315.9 [0.61]	361.8 [0.96] 310.0 [0.62]
Dimer (parallel)	466.5 [1.08] 363.9 [0.76]	403.3 [1.07] 345.0 [0.75]	379.2 [1.12] 337.5 [0.73]	369.1 [1.17] 333.5 [0.72]	368.0 [1.22] 331.3 [0.72]

Table 3.3. *Modeling of the electronic absorption peaks of $BDEP^+$ in chloroform solution and in the solid state and of similar chromophores in LB films, using selected computed λ_{max} from Table 3.2; M = monomer, AD = antiparallel dimer, PD = parallel dimer.*

Sample	λ_{max} (nm)		Model
	Experiment	**AM1/CI Calculation**	
Solution (chloroform)	497.5 285.0	506.6 281.3	M (ε=1)
LB Film	477.0,[a] 460.0[b] 339.0[a] 263.0[a]	476.4, 450.2[#] 368.0,* 331.3* 294.4, 290.9[#]	M (ε=2) [#]M (ε=3) *PD (ε=5)
Solid	460.2 399.4 327.2 278.7	476.4 394.9* 344.7* 294.4	M (ε=2) *AD (ε=2)

[a]*Ref. 21. The peaks at 339.0 and 263.0 nm are found in LB films of the pure hemicyanine dye and the peaks at 477.0 and 263.0 nm in LB films of the dye mixed with arachidic acid.*

[b]*Ref. 18. LB films of pure hemicyanine dye; the absorption in the UV region is not mentioned in this paper.*

peaks observed in the spectrum of the LB film. It should be noted that, even though the parallel dimer has the appearance of a traditional J-aggregate, the peaks are blue shifted. This result obtained from a rigorous quantum chemical computation, is consistent with the experimental observation of only blue shifted aggregate peaks in the LB films of these dyes. This has been rationalized based on the fact that the simple point dipole approximation is not appropriate at short intermolecular distances where consideration of the extended dipole approximation predicts H-aggregate type behavior irrespective of molecular orientations.[37] It is seen that the molecular environment in the solution is modeled by a low dielectric constant close to that of the solvent. The dielectric constant required to model the solid state is quite reasonable given the fact that the refractive index of organic crystals is typically 1.5 - 2.0.[50] The molecular environment in the LB films is modeled using a low dielectric constant in the case of the hemicyanine dye mixed with the fatty acid, but by a relatively higher dielectric constant than that in the solution and solid states for the case of the pure dye; this is indicative of a more polarizable structure present in the LB films of the pure dye.

3.4. Polyelectrolyte Assisted Deaggregation and SHG Enhancement in the Langmuir and LB Films of a Hemicyanine Based Amphiphile

In this section we present an investigation of the polyelectrolyte complexation approach to address the problem of chromophore aggregation in LB films of the hemicyanine based amphiphile. Analysis of the electronic absorption spectra of the dye-polyelectrolyte LB film, based on the study of molecular clusters presented in the previous section indicates that the polyelectrolyte complexation is an efficient route to achieve complete deaggregation of the dye molecules in the LB film. SHG measurements on the LB films fabricated with and without the polyelectrolytes in the subphase clearly establish the positive impact of the polyelectrolyte in enhancing the SHG response through effective deaggregation. The hemicyanine based amphiphile, $ODEP^{+}Br^{-}$ was used for these studies. The polyelectrolytes used in the present study are $(Na^{+})_nPSS^{n-}$, $(Na^{+})_n31PSSM^{n-}$ and $(Na^{+})_n11PSSM^{n-}$ (Fig. 3.2.). At the pH of the experiment, 5.5, it is likely that only the sulfonate groups are ionized but not the carboxylic acid groups. Therefore the distance between the anionic sites becomes progressively larger from PSS^{n-} to $31PSSM^{n-}$ to $11PSSM^{n-}$.

3.4.1. *Langmuir film studies*

Introduction of polyelectrolytes in the aqueous subphase has a strong effect on the initial pressure equilibration of $ODEP^+Br^-$ at the air-water interface *i.e.*, reaching ~ 0 mN/m after spreading. When only Br^- is present in the subphase, two different rates of equilibration were observed rather randomly in different experiments; one taking ~ 40 min and the other ~ 60 min after spreading, to reach 0 mN/m. When PSS^{n-} is present, the equilibration is slower and perfectly reproducible. This general feature is observed with other polyelectrolytes also. The pressure equilibration of the $ODEP^+$ monolayer with Br^- alone in the subphase and with PSS^{n-} also introduced in the subphase are shown in Fig. 3.7.

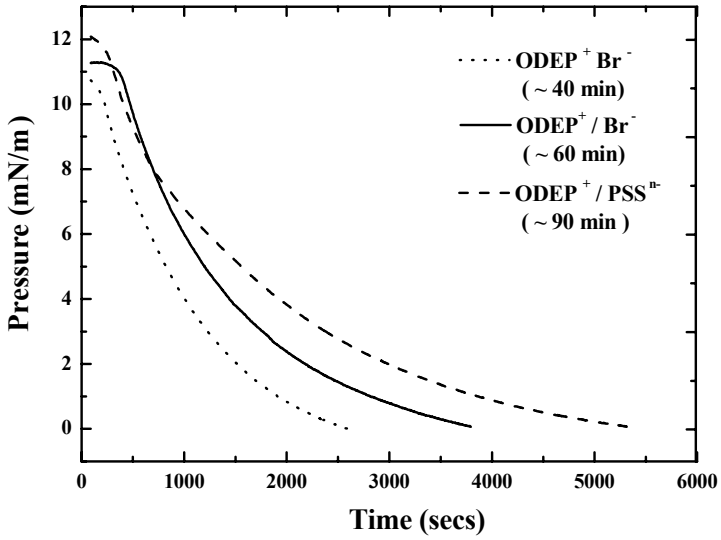

Figure 3.7. *Pressure relaxation on spreading $ODEP^+$ at the air-water interface without and with PSS^{n-} in the subphase; two situations observed in the former are shown.*

The pressure-area isotherms of the resulting Langmuir film are also sensitive to the equilibration time and the presence of polyelectrolytes in the subphase. The isotherms of $ODEP^+$ with Br^- alone in the aqueous subphase (under two different conditions) as well as with the polyelectrolytes PSS^{n-}, $31PSSM^{n-}$ and $11PSSM^{n-}$ are shown in Fig. 3.8. The extrapolated area/molecule for the $ODEP^+Br^-$ in the two different cases are 40.2 and 48.0 $Å^2$; the former value, corresponding to the quicker

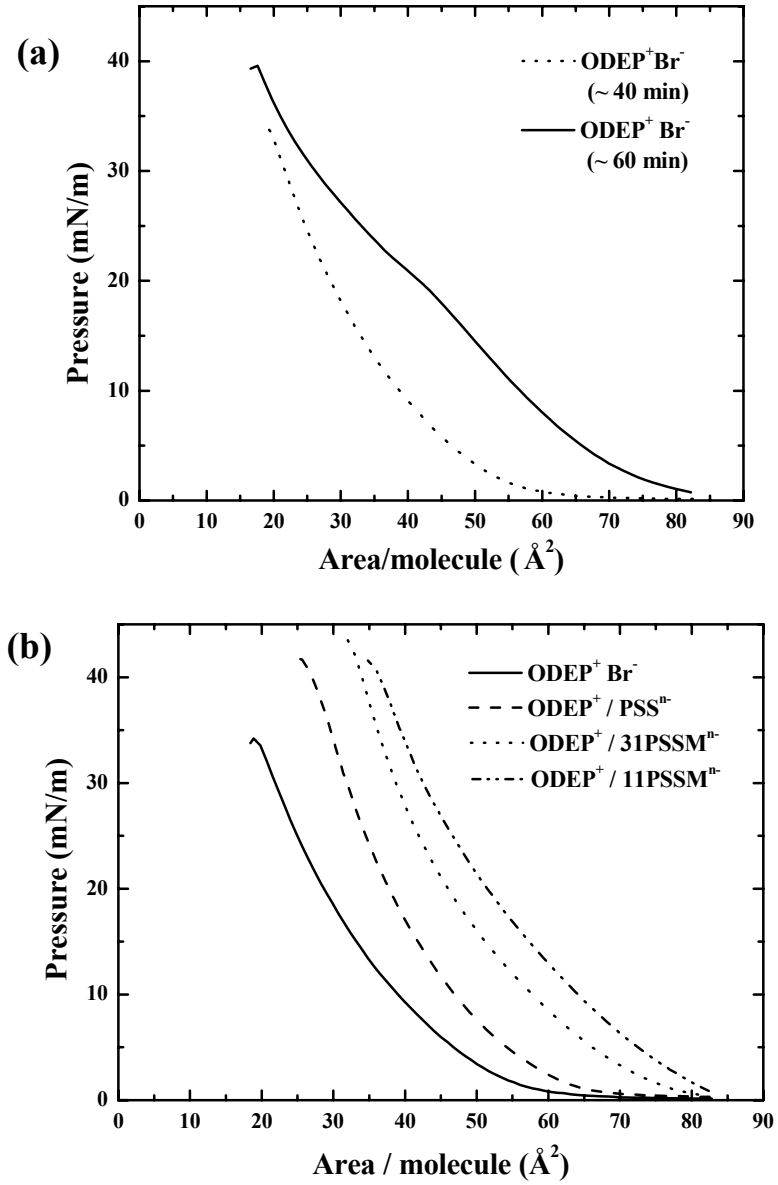

Figure 3.8. *Pressure–area isotherms for ODEP$^+$ with* ***(a)*** *Br$^-$ (different equilibration times) and* ***(b)*** *various polyelectrolytes in the aqueous subphase.*

equilibration is close to that reported for similar amphiphiles.[18,35] In the case of PSS^{n-}, 31PSSM^{n-} and 11PSSM^{n-} it is 45.6, 52.4, and 60.6 Å^2 respectively.

The systematic shift of the area/molecule of the ODEP$^+$ follows the expected trends in the distance between binding sites of the polyelectrolytes. This also strongly

indicates the complexation between the cationic amphiphile headgroup and the sulfonate groups on the polyelectrolyte, promoted most likely by the electrostatic interactions. The sharper slopes and higher collapse pressures of the isotherms in presence of the polyelectrolytes are indicative of the improved stabilization of the $ODEP^+$ monolayer. The reduced hysteresis and reproducibility of the isocycles in the presence of PSS^{n-} (Fig. 3.9) also point to the role of polyanions in the stabilization of the cationic amphiphile monolayer. Area-time creep plots suggest comparable temporal stability in the case of all polyelectrolytes.

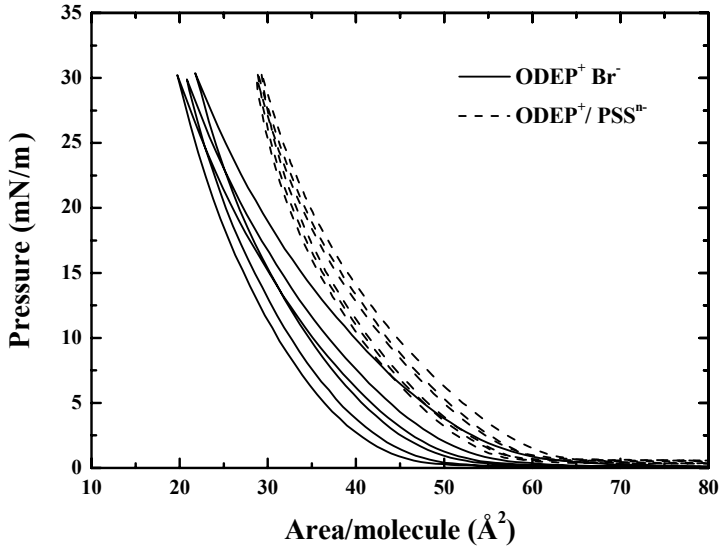

Figure 3.9. *Successive pressure-area isocycles of $ODEP^+$ without and with PSS^{n-} in the subphase.*

Brewster angle microscopy

The morphology of the monolayer at the air-water interface was studied using Brewster angle microscopy (BAM). Appendix C gives details of the instrumentation. $ODEP^+Br^-$ forms a stable film at the air-water interface. Therefore a smooth surface is obtained in the compressed state (Fig. 3.10a); however some cracks are visible. Compressed monolayers formed in presence of PSS^{n-} in the subphase show nearly circular domain features (Fig. 3.10b) and in the presence of $11PSSM^{n-}$, a smooth film with no domain structure is observed (Fig. 3.10c). These observations suggest that the morphology of the compressed monolayer at micron scale is strongly affected by the presence of polyelectrolytes in the subphase.

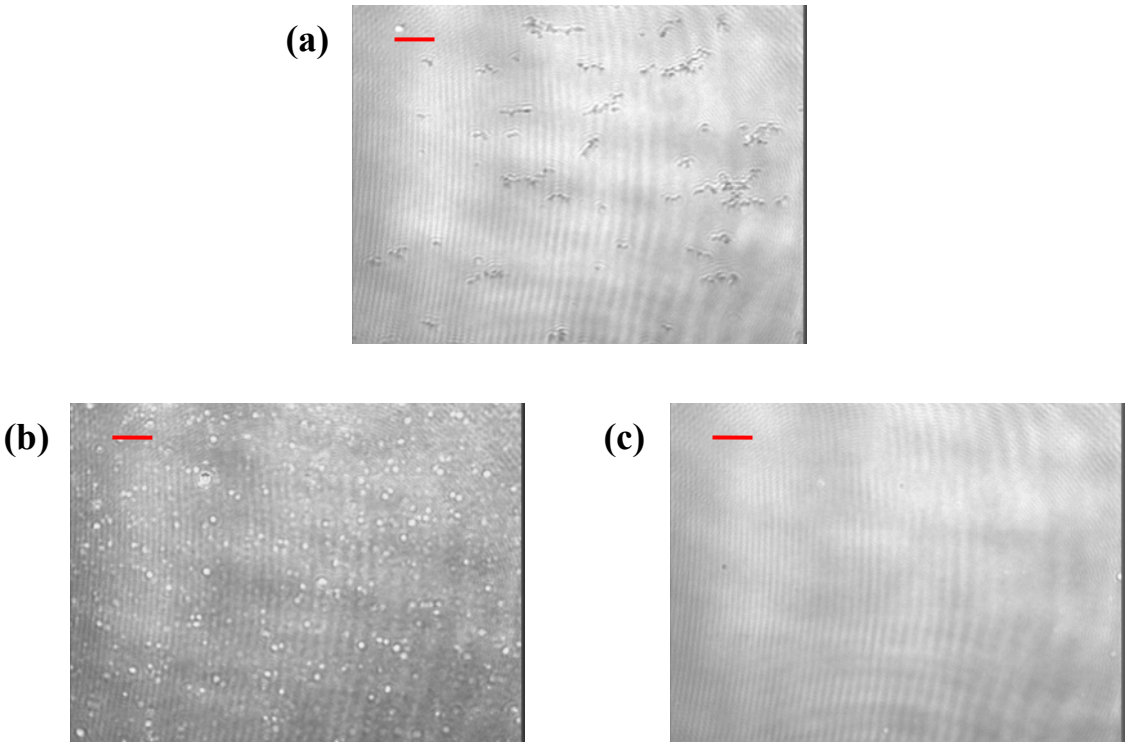

Figure 3.10. *BAM images of $ODEP^+$ (at 25 mN/m) with* ***(a)*** *only Br^- and additionally* ***(b)*** *PSS^{n-} and* ***(c)*** *$11PSSM^{n-}$ in the aqueous subphase. Scale bar is 20 µm.*

3.4.2. *Langmuir-Blodgett film studies*

The Langmuir layer was held at a pressure of 30 mN/m for about 15 min before transferring onto the substrate. Monolayer and multilayer LB films of $ODEP^+$ amphiphile were deposited on hydrophilic glass/quartz substrates. The transfer ratios were typically 0.9-1.0 in the case of monolayers and 0.5-1.0 in the case of multilayers.

Electronic absorption spectroscopy

Monolayer LB films of $ODEP^+$ without and with the polyelectrolytes in the subphase, coated on hydrophilic quartz substrates were characterized by their electronic spectra (Fig. 3.11). All the spectra show absorption near 275 nm; however, the position of the peaks in the visible range is very much dependent on the presence or absence of polyelectrolytes in the subphase. We have observed that the spectra of films coated

without the polyelectrolytes in the subphase are quite sensitive to the time taken for the monolayers to reach equilibrium pressure (~ 0 mN/m) after spreading (Fig. 3.11a). The highest wavelength peak exhibited by films which equilibrated in ~ 40 min is at 354 nm. When the equilibration was slower (~ 60 min) the spectrum showed multiple

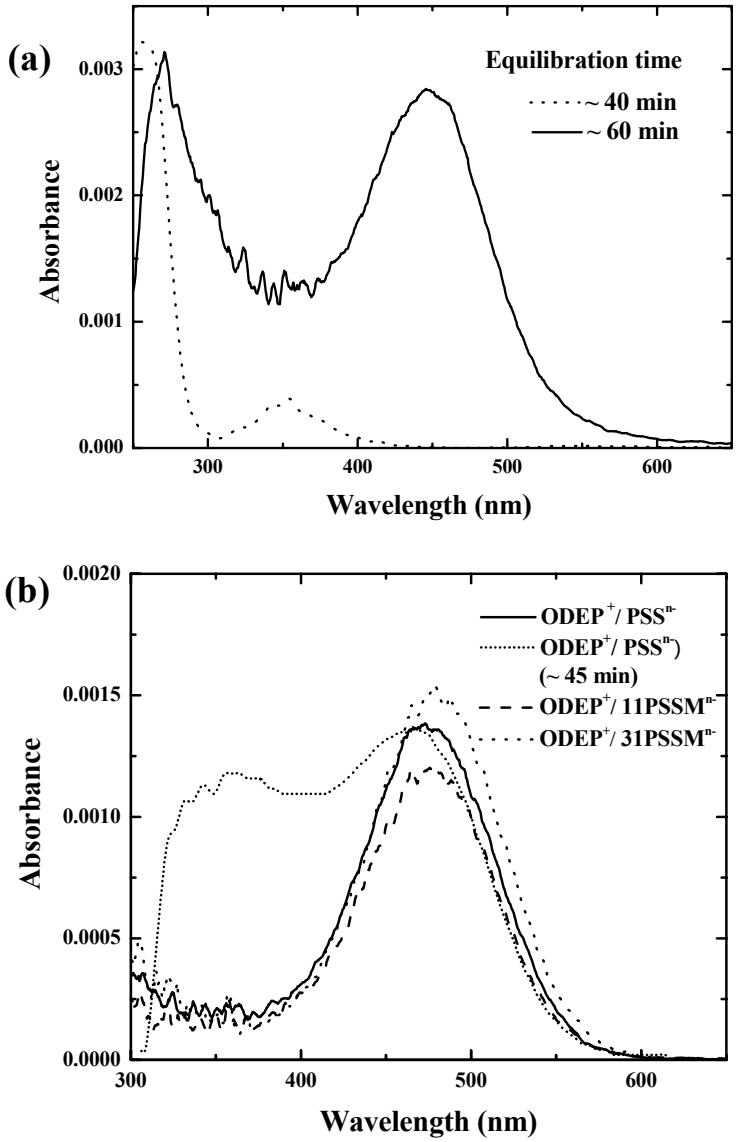

Figure 3.11. *Electronic absorption spectra of monolayer LB films fabricated from* ***(a)*** *$ODEP^+Br^-$ Langmuir films which equilibrated over different time scales, and* ***(b)*** *$ODEP^+$ with different polyelectrolytes in the subphase; spectrum of the film with PSS^{n-} deposited before equilibration is reached (at 45 min) is also shown.*

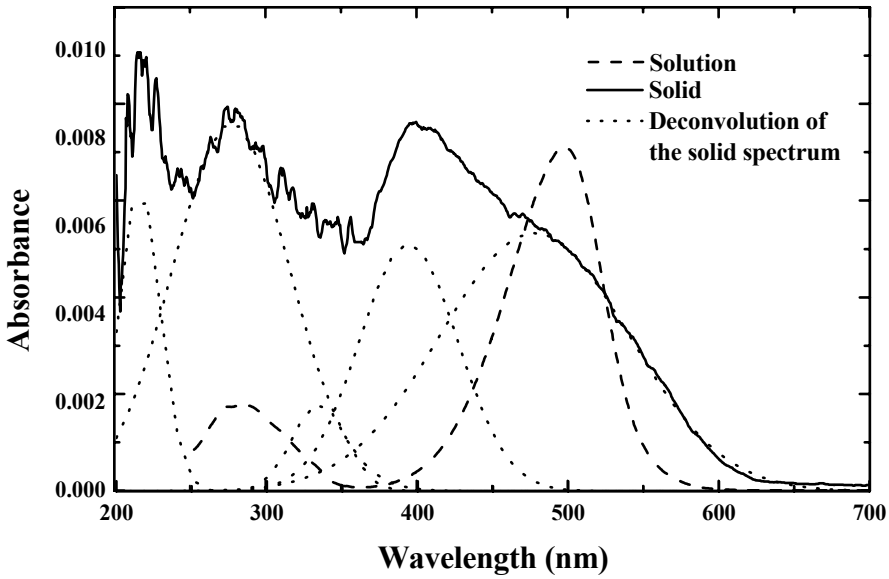

Figure 3.12. *Electronic absorption of ODEP$^+$Br$^-$ in the solid state and in solution; deconvolution of the solid state spectrum is also shown.*

absorptions; deconvolution indicates peaks at 356 and 445 nm. We find that the rate of equilibration varies from one experiment to another and it has not been possible to identify any definitive mechanism to control this rate. On the other hand, in practically all the experiments we have carried out with the polyelectrolytes in the subphase, the pressure equilibration of the monolayer occurs slowly, taking 60 - 90 min. Not unexpectedly, the corresponding LB films exhibit the long wavelength absorption at ~ 475 nm consistently and there is no sign of absorption near 350 nm (Fig. 3.11b). It may be noted also that if the film is deposited before pressure equilibration is achieved, the peak near 350 nm remains (Fig. 3.11b). Earlier studies[18,20,21,27,29,35,37] on hemicyanine dye based LB films have attributed the long wavelength absorption in the 470 - 480 nm range to the monomer absorption and the peak near 350 nm to the H-aggregate structures. The electronic absorption spectra of ODEP$^+$ in solution and solid state are provided in Fig. 3.12. Deconvolution of the solid state spectrum indicates new peaks additional to that of solution, which can be attributed to molecular aggregates. In Sec. 3.3.3, we have discussed our investigation of BDEP$^+$Br$^-$, the butyl analog of ODEP$^+$, along with semiempirical AM1/COSMO/CI[46-48] computational modeling of the spectral features using molecular clusters from the crystal.[1] Table 3.4 shows that this model

study also sheds light on the origin of the spectral features of $ODEP^+$. The peaks at 330 - 400 nm and 450 - 500 nm can be assigned to the chromophore dimers and monomer respectively. When the film is fabricated without polyelectrolyte in the subphase the dimer peak is always observed; the monomer peak appears when the equilibration is slow (Fig. 3.11a). If the film is formed in presence of polyelectrolyte, but deposited before pressure equilibration, the dimer peak remains (Fig. 3.11b). The only case where this peak disappears completely is when the film of $ODEP^+$ / PSS^{n-} (or with other polyelectrolytes) is fully equilibrated before transfer. This study shows that $ODEP^+$ is completely deaggregated and present as monomers when properly complexed with PSS^{n-} or other polyelectrolytes.[3] The electronic spectra therefore demonstrate that a relatively slow equilibration of the Langmuir layer can lead to partial deaggregation of the headgroups in the case of the pure dye, but a more complete and effective inhibition of the aggregation is achieved using the polyelectrolytes in the subphase.

Table 3.4. *Electronic absorption peaks of $ODEP^+$ in chloroform solution, in the solid state and in LB films and the modeling using results of AM1/COSMO/CI computations on molecular geometries from the crystal structure of $BDEP^+Br^-$ (Sec. 3.3.3); M = monomer, AD = antiparallel dimer, PD = parallel dimer.*

Sample	λ_{max} / nm		Model (ε used in the COSMO)
	Experiment	AM1/COSMO/CI Calculation	
Solution	497.5 285.0	506.6 281.3	M (ε=1)
Solid	477.7 394.0, 334.7 276.2, 215.6	476.4[#] 394.9,* 344.7* 294.4,[#] 214.4[#]	[#]M (ε=2) *AD (ε=2)
LB Film (without polymer)	445.0[a] 356.0,[a] 351.0[b] 271.0,[a] 256.0[b]	450.2[#] 368.0,* 331.3* 290.9[#]	[#]M (ε=3) *PD (ε=5)
LB Film (with polymer)	473.0 270.0	476.4 294.4	M (ε=2)

[a]*Slow equilibration;* [b]*Fast equilibration*

Second harmonic generation studies

The primary goal of investigation of the hemicyanine by LB film is its SHG capability. In order to assess the impact of the polyelectrolyte templating, we have investigated the SHG produced by the LB films of $ODEP^+$. The samples were fabricated by deposition on both sides of hydrophilic glass substrate. Fringe pattern[38] of the different films, recorded by rotation around the vertical axis in the p-p polarization geometry, are shown in Fig. 3.13. The film fabricated without the polyelectrolytes in the subphase is from the Langmuir layer which equilibrated slowly and therefore has the least amount of aggregation under this condition. The relative intensities clearly demonstrate the SHG enhancement in the LB films of polyelectrolyte complexed $ODEP^+$. We have analyzed the SHG data recorded in p-p and s-p geometries using well-known fitting procedures (see Appendix E).[3,42] The fitting of the fringe pattern in p-p geometry are shown in Fig. 3.14. The nonlinear susceptibility components, χ_{zzz} and χ_{zxx} extracted from these analysis are collected in Table 3.5. The values in pm/V are estimated assuming an approximate thickness (l_s) of 5 nm for all the LB films and 22.4 μm as the coherence length at normal incidence (l_c^Q) of Y-cut quartz.[53]

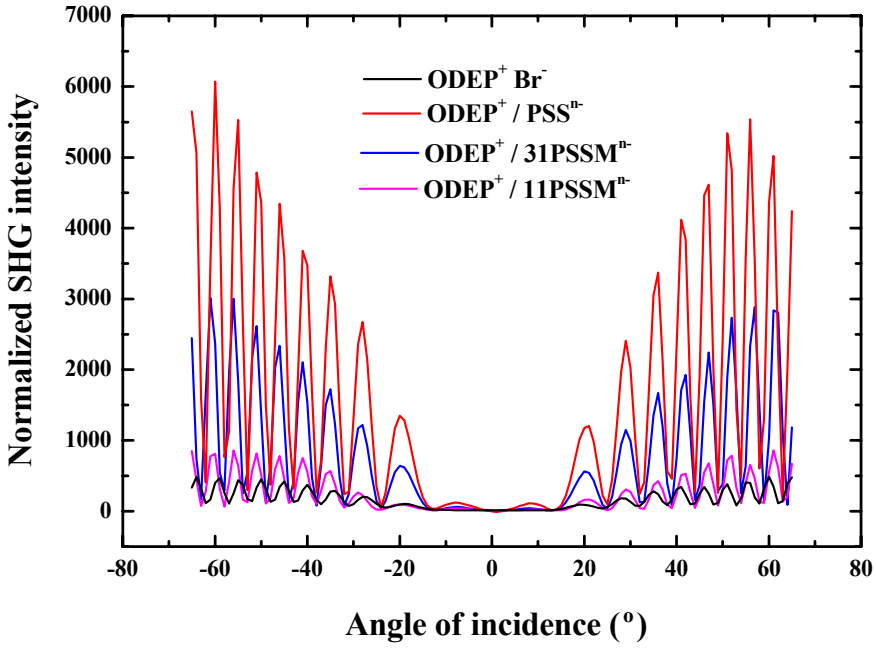

Figure 3.13. *SHG fringes of single layer LB films of $ODEP^+$ fabricated without and with different polyelectrolytes in the subphase; intensities are normalized with respect to Y-cut quartz for comparison.*

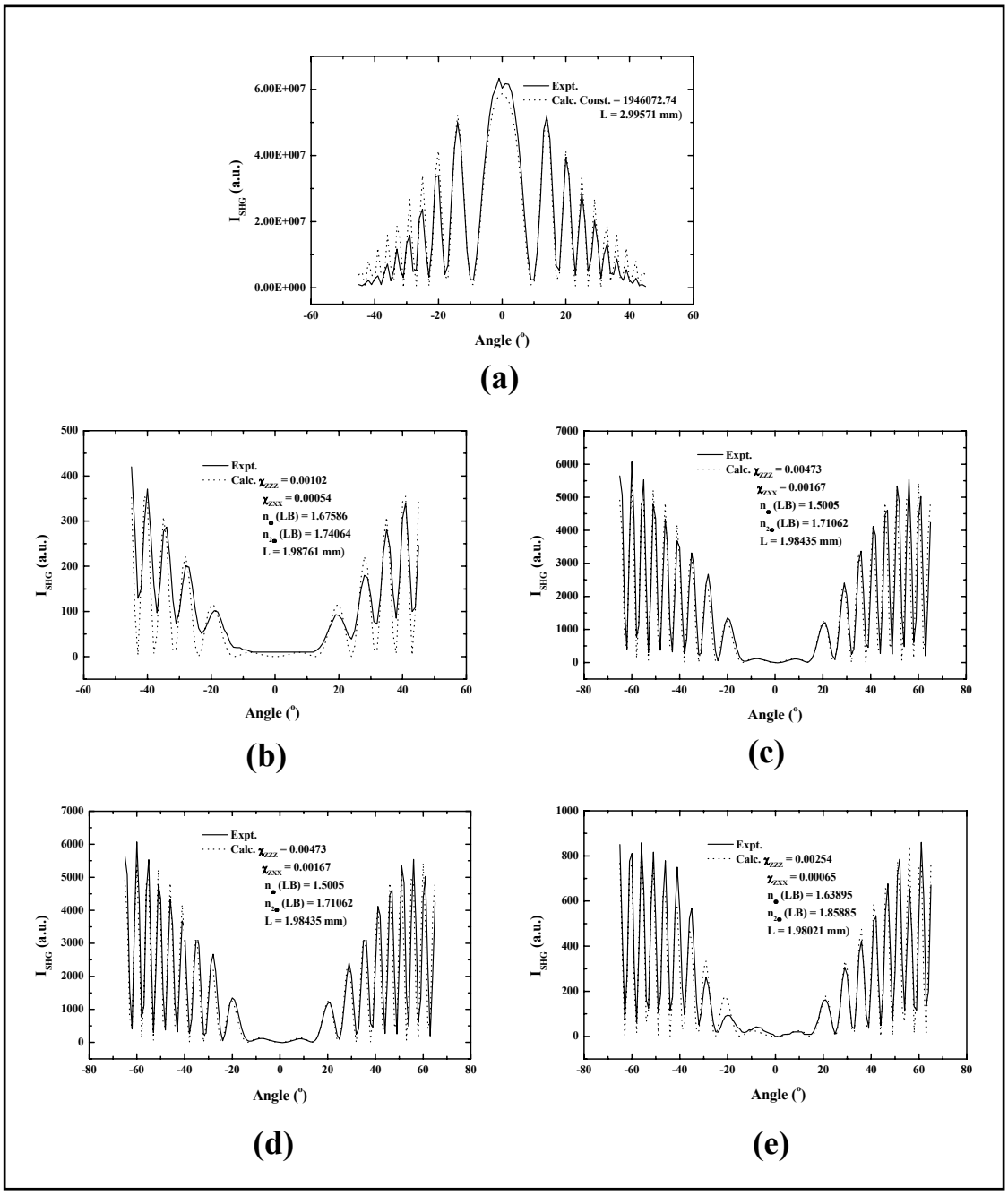

Figure 3.14. *Fitting of the SHG fringe pattern in p-p polarization, of* ***(a)*** *Y-cut quartz and monolayers of* ***(b)*** *$ODEP^+Br^-$;* ***(c)*** *$ODEP^+/PSS^{n-}$;* ***(d)*** *$ODEP^+/31PSSM^{n-}$ and* ***(e)*** *$ODEP^+/11PSSM^{n-}$. The full set of parameters obtained by the fitting procedure is given in the respective plots. See Appendix E for details of the fitting procedure.*

Table 3.5. *Second order NLO susceptibilities of the different monolayer LB films.*

Sample	χ_{zzz} (pm/V)	χ_{zxx} (pm/V)
$ODEP^+Br^-$	2.9	1.5
$ODEP^+$ / PSS^{n-}	13.5	4.8
$ODEP^+$ / $31PSSM^{n-}$	12.5	3.1
$ODEP^+$ / $11PSSM^{n-}$	7.2	1.9

$ODEP^+$ complexed with PSS^{n-} shows nearly four-fold increase over the uncomplexed $ODEP^+$. When the equilibration is fast the film has more chromophore aggregation and would show even lower SHG. The SHG enhancement in polyelectrolyte complexed $ODEP^+$ may be attributed to the reduction of chromophore aggregation. The SHG enhancement on polyelectrolyte templating is very significant since the film of uncomplexed $ODEP^+$ is already partially deaggregated due to the slow equilibration as discussed above. The lower enhancement of SHG in the case of the two copolymer electrolytes may be attributed to the relatively lower densities of the amphiphile in the 2-dimensional lattice. The low SHG observed in films containing aggregate structures, in spite of parallel orientation of the hemicyanine molecules in the dimers suggested by the modeling data in Table 3.4, may result from unfavorable orientation between the dimers or absence of long range order. The adverse impact of molecular aggregation on the SHG has been generally attributed to the shifting of the electronic absorption from ~ 450 nm to ~ 350 nm and the consequent reduction of resonance enhancement of SHG at 532 nm.[54]

We have carried out preliminary investigation of multilayer LB films using PSS^{n-} in the subphase. For comparison, multilayers were fabricated without the polyelectrolyte in the subphase. In the latter case, the upstrokes show nearly quantitative deposition (TR ~ 0.9 - 1.0), but the deposition during downstrokes are considerably less (TR ~ 0.1 - 0.3) indicating a near Z-type deposition. When the polyelectrolyte is present, this pattern is modified with the deposition during the upstrokes remaining similar but that during the downstrokes becoming more prominent (TR ~ 0.5 - 0.7). The electronic absorption intensities are consistent with the transfer

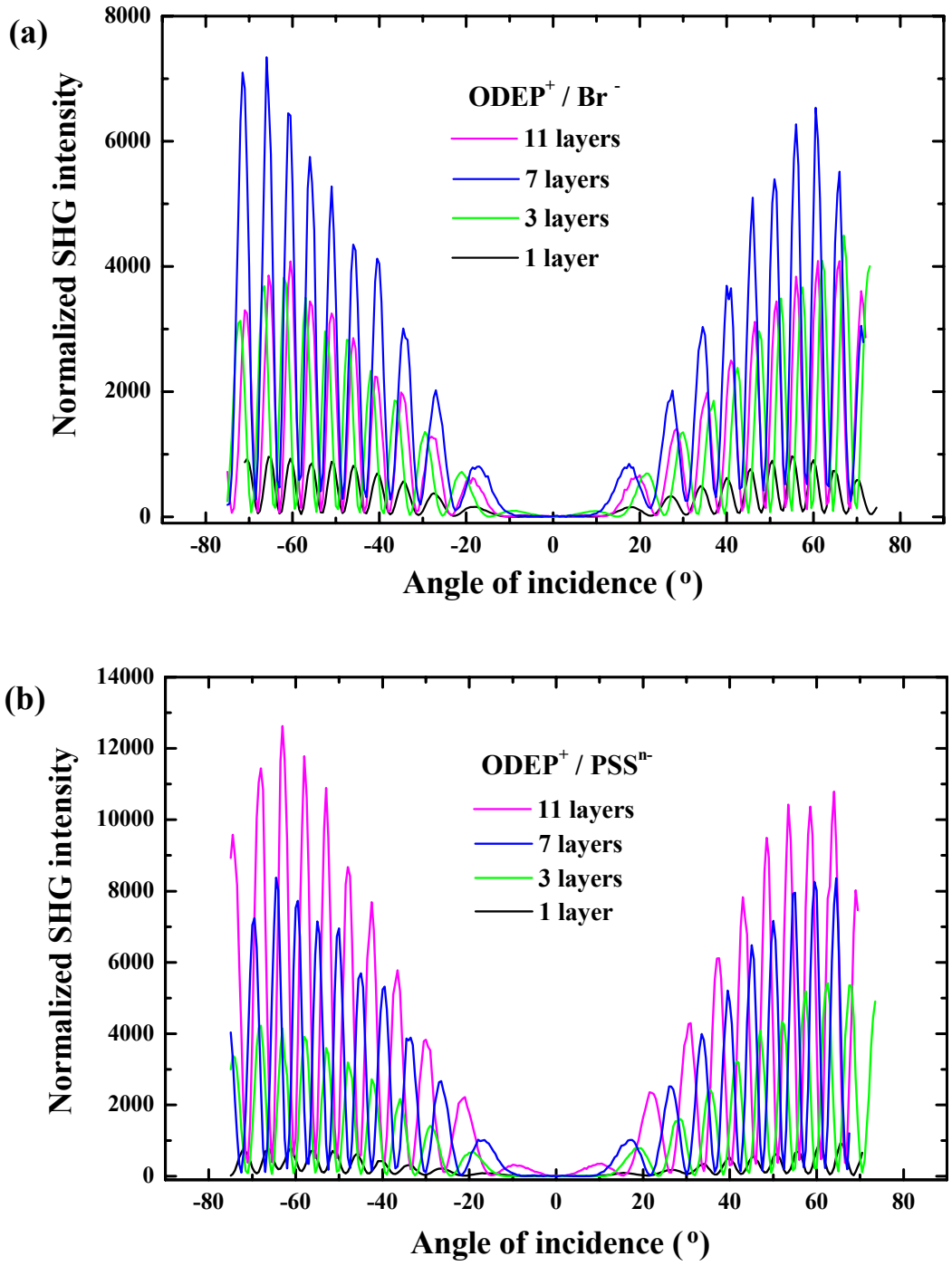

Figure 3.15. *SHG fringes recorded for mono and multilayer LB films of $ODEP^+$ fabricated **(a)** without and **(b)** with PSS^{n-} in the subphase; the SHG intensities are normalized with respect to Y-cut quartz.*

ratios. The fringes recorded for different number of layers in the two cases are shown in Fig. 3.15. The SHG intensities observed for the various multilayers are collected in Table 3.6; these are estimated from the fringe envelope maxima normalized with respect to the quartz signal. The SHG does not follow the quadratic dependence on the number of layers expected for well ordered X or Z type films. The drop in SHG of the pure dye at larger number of layers possibly arises due to reorganization of the Z-type films on continued transfer.

Table 3.6. *SHG intensities of multilayer LB films of $ODEP^+Br^-$ and $ODEP^+/PSS^{n-}$ estimated from the fringe envelope maxima normalized with respect to the quartz signal.*

No. of layers	$ODEP^+Br^-$		$ODEP^+ / PSS^{n-}$	
	p-p	s-p	p-p	s-p
3	61.5	2.77	80.7	8.77
7	96.9	6.00	119	10.7
11	61.2	5.97	179	14.5

In spite of the stronger tendency towards Y-type deposition, the films formed in the presence of the polyelectrolyte exhibit higher SHG intensity for the different number of layers. This suggests that even though the presence of the polyelectrolyte changes the LB film deposition pattern from that in the case of the dye without polyelectrolyte, the overall molecular orientations achieved are more conducive to an enhanced SHG response. Our earlier modeling of the complexation of a cationic amphiphile headgroup by PSS^{n-} (Chapter 2) has revealed a favorable orientation of the headgroup imposed by the polyanion. We believe that a similar effect may be operating in the present case as well.

The study presented in this section reveals that the polyelectrolyte templating is very effective in preventing aggregation of the hemicyanine amphiphiles and that deaggregation can be profitably used in the enhancement of their SHG capability. In the next section we investigate the stability imparted to these films by natural polyelectrolytes like DNA^{n-} and CMC^{n-}, as well as synthetic ones like PSS^{n-}, when the films are subjected to laser irradiation.

3.5. Laser Induced SHG Decay in the Hemicyanine LB Film : Arresting by Polyelectrolyte Templating

As described in the previous sections, amphiphiles based on the prototypical NLO-phore, hemicyanine dye are usually in an aggregated state in their Langmuir[27,37,55] and LB films,[26] causing their SHG capability to diminish or vanish altogether.[3,18-22,38,41,54,56] However, slow equilibration following spreading on the water surface was found (Sec. 3.4) to result in LB films with reduced aggregation and improved SHG.[2,3] In this section we describe a systematic investigation of the pronounced decay of SHG of this film in successive measurements involving the laser irradiation; this illustrates the metastable nature of the LB film. The polyelectrolyte methodology which has been effective in stabilizing the pyridinium amphiphile (Chapter 2) and deaggregating the hemicyanine dye without diluting the NLO-phore (Sec. 3.4), is now shown to be an effective strategy to arrest the SHG degradation in the hemicyanine LB film as well. Morphological features of the LB films observed by atomic force microscopy reveal the impact of the polyelectrolyte. Electronic absorption studies provide insight into the molecular level interactions that trigger the SHG decay.

The current study is also based on the hemicyanine amphiphile, $ODEP^+Br^-$. The polyelectrolytes used in this study are $(Na^+)_nPSS^{n-}$, $(Na^+)_nCMC^{n-}$ and $(Na^+)_nDNA^{n-}$ (Fig. 3.2). These polyelectrolytes have different types of interacting sites and rigidity. The general procedures for the Langmuir and LB films preparation are given in Appendix B. The films coated on fused silica were used for the SHG experiments (Appendix E). Electronic absorption studies were carried out on the same samples. AFM images of films deposited on mica were recorded in the dynamic force (non-contact) mode (Appendix C).

3.5.1. *Langmuir film studies*

The isotherms of $ODEP^+Br^-$ on pure water and with $(Na^+)_nPSS^{n-}$, $(Na^+)_nCMC^{n-}$, and $(Na^+)_nDNA^{n-}$ added in the subphase are shown in Fig. 3.16. The extrapolated area per molecule in the case of Br^- alone and PSS^{n-} are 48.0 and 45.4 $Å^2$ respectively. These areas and the isotherm behavior are consistent with our previous observations. The considerably larger area per molecule (94.6 $Å^2$) in the case of DNA^{n-} and isotherm

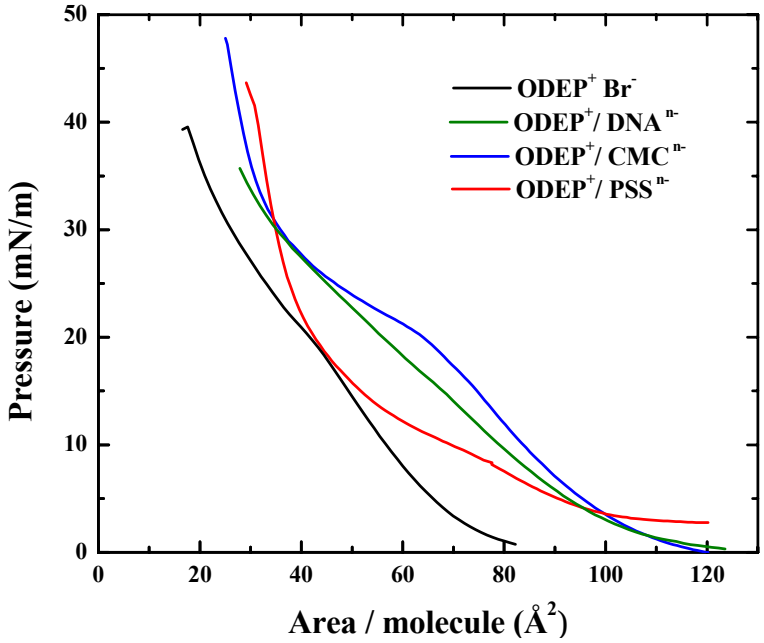

Figure 3.16. *Pressure–area isotherms of ODEP$^+$ with Br$^-$ alone and with different polyelectrolytes in the aqueous subphase.*

structure can be understood based on the structural rigidity of the polyelectrolyte. Strong electrostatic interactions are likely to exist between the phosphate group on the DNA^{n-} and the cationic amphiphile. The distance between the two phosphate groups on a helix is 3.4 Å and that between the two adjacent helices in the duplex is ~ 11 Å.[57] The two helices are joined together with strong hydrogen bonds between them, which impart high rigidity to the double helix. Because of the helical structure, not all phosphate groups are likely to be accessible for interaction with the cationic amphiphile. Only those phosphate groups, which are towards the same side at the air-water interface will readily interact with the ODEP$^+$. So we believe that in the case of DNA^{n-}, its structural complexity and rigidity coupled with strong interactions of available sites with the cationic amphiphile leads to the large spacing between the latter in the monolayer.

In the case of CMC^{n-}, there is a clear signature of a phase transition. The cellulose backbone is assumed to possess a homogeneous substitution of primary alcoholic groups. When the polyelectrolyte approaches the ODEP$^+$ monolayer, all carboxylic groups are accessible for complexation since the pyranose rings are in a face-on conformation. However, upon compression of the monolayer, the rings will flip to

an edge-on conformation leading to a large decrease in area and the phase transition in the π-A isotherm; similar effects have been reported earlier.[58] Interestingly, the extrapolated area per molecule before (101.6 $Å^2$) and after (44.3 $Å^2$) the transition are comparable to that of DNA^{n-} and PSS^{n-} respectively. Based on these observations we assume that the rigidity of CMC^{n-} is intermediate between that of PSS^{n-} and DNA^{n-}.

3.5.2. *Langmuir-Blodgett film studies*

LB films were transferred on to hydrophilic substrates by vertical dipping; transfer ratios were typically ~ 0.8. The transferred monolayer LB films exhibit SHG. However the SHG is found to be susceptible to different extents of decay upon repeated measurements, suggesting metastability in the film. This was monitored by successive SHG measurements alternating with electronic absorption spectroscopy of the films.

Second harmonic generation studies

SHG from the monolayer LB films was measured soon after deposition, allowing sufficient time for drying. The fringe recording takes about 13 min during which time the sample is continuously subjected to laser irradiation at 1064 nm. The measurements were repeated several times with electronic absorption being recorded after each run; the whole experiment was completed in ~ 5 h. As demonstrated with other polyelectrolytes (Sec. 3.4.2),[2,3] LB films of $ODEP^+$ fabricated with CMC^{n-}, DNA^{n-} and PSS^{n-} in the subphase showed considerable enhancement of SHG; the value of $ODEP^+/PSS^{n-}$ is an order of magnitude higher than that of $ODEP^+Br^-$ (Fig. 3.17a). The more significant observation now is that the SHG from the LB film of $ODEP^+Br^-$, showed a steady decline with each new measurement and by the seventh run, it leveled off at approximately 10% of the initial value (Fig. 3.17b). The variation of the SHG signal (fringe pattern) with repeated experiments is shown in Fig. 3.18a. LB films of $ODEP^+/CMC^{n-}$ and $ODEP^+/DNA^{n-}$ on the other hand, showed considerable improvement in retaining the original SHG intensity and $ODEP^+/PSS^{n-}$ showed negligible change throughout (Fig. 3.17b). The steady SHG signal in the case of $ODEP^+$ with PSS^{n-} is shown in Fig. 3.18b. The dramatic effect of the polyelectrolyte templating on arresting the SHG decay is clearly evident from these observations.

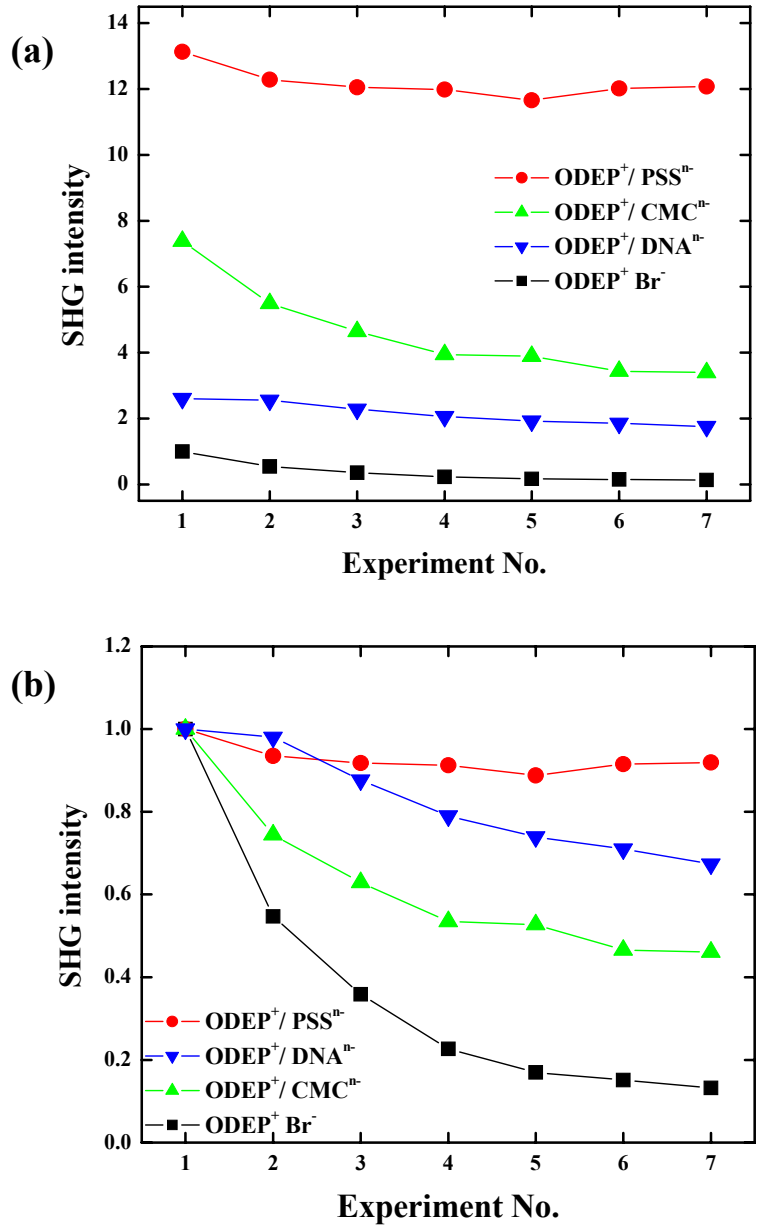

Figure 3.17. *Second harmonic intensity of $ODEP^+$ based LB films from consecutive experiments.* ***(a)*** *Values are scaled with respect to the initial value in each case; the relative magnitude of different films is highlighted by scaling all the initial values with respect to that of $ODEP^+Br^-$;* ***(b)*** *Values are scaled with respect to 1.0 for the initial value in each case to highlight the difference in the variations. The lines connecting points are only a guide to the eye.*

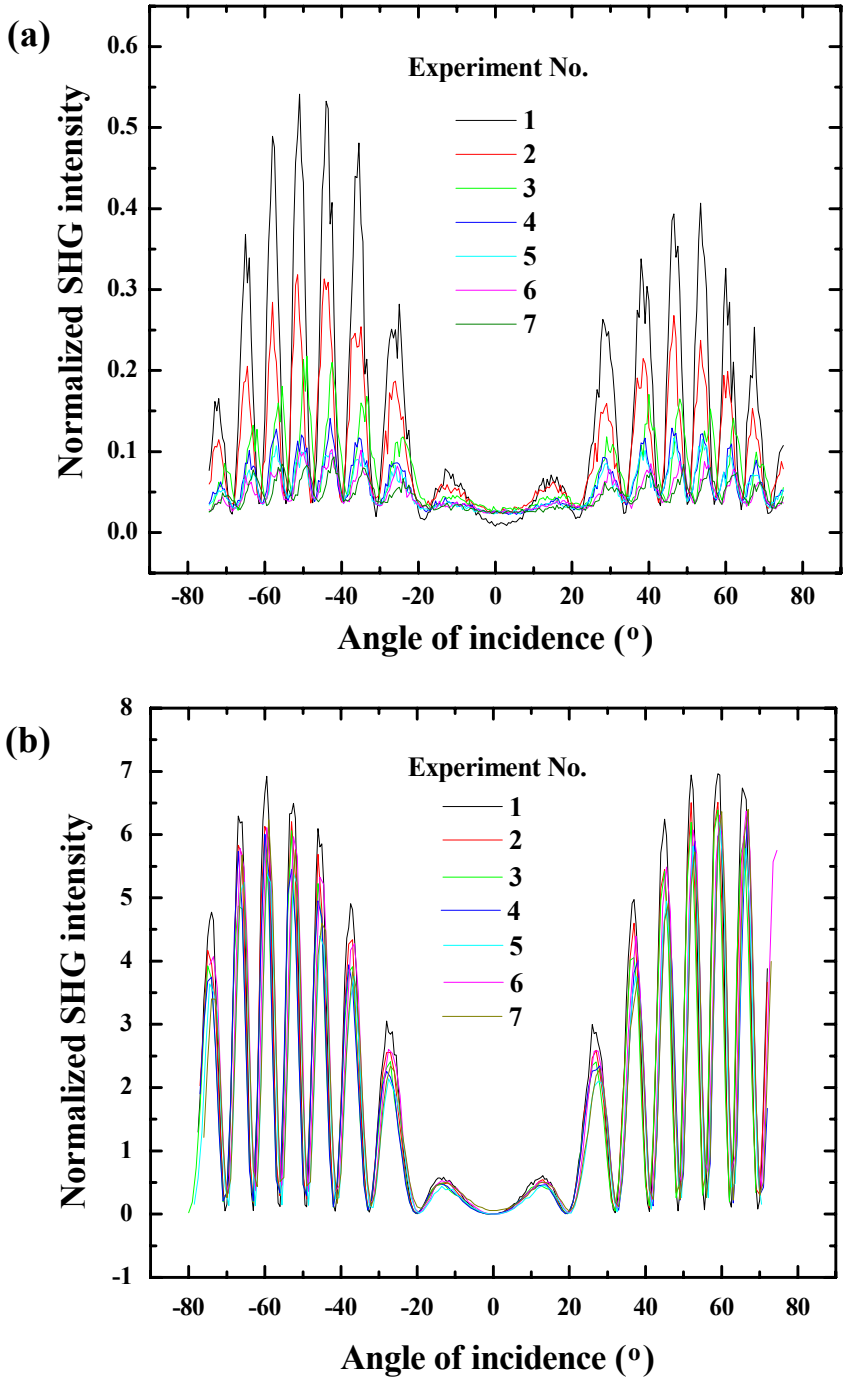

Figure 3.18. *SHG fringe pattern for* ***(a)*** *ODEP$^+$ Br$^-$;* ***(b)*** *ODEP$^+$ / PSS^{n-} in consecutive experiments; the SHG intensities are normalized with respect to Y-cut quartz.*

Atomic force microscopy

AFM images reveal marked contrast between the morphology of the different LB films (Fig. 3.19) and provide a graphic illustration of the impact of the polyelectrolytes. The line profiles for each image are shown in Fig. 3.20.

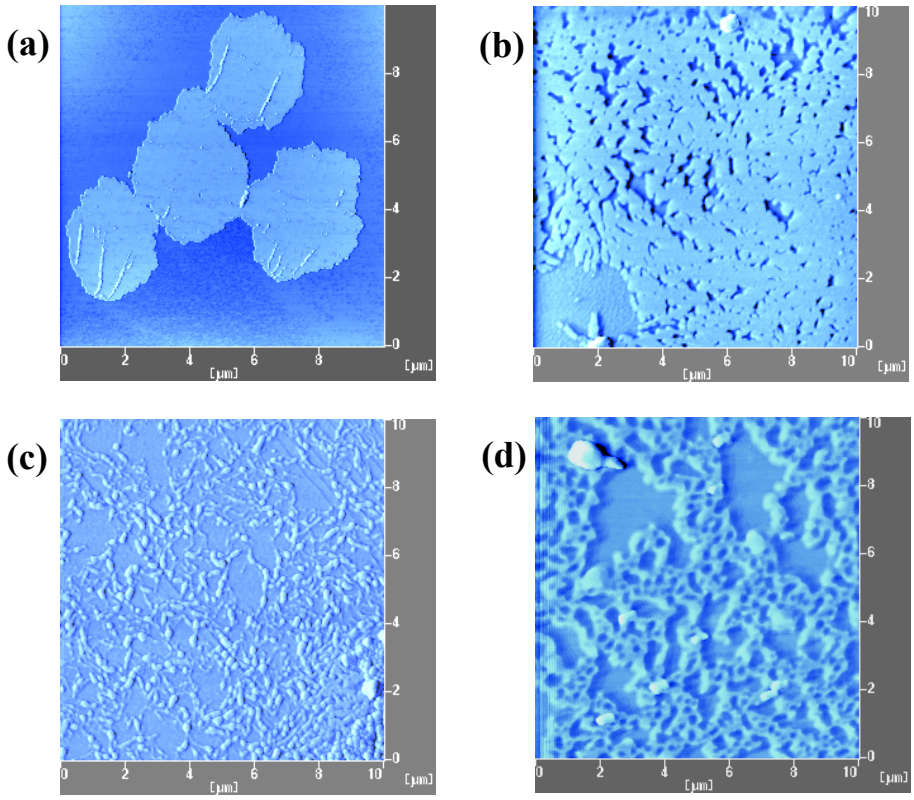

Figure 3.19. *AFM images of* ***(a)*** *$ODEP^+Br^-$;* ***(b)*** *$ODEP^+/DNA^{n-}$;* ***(c)*** *$ODEP^+/CMC^{n-}$ and* ***(d)*** *$ODEP^+/PSS^{n-}$ LB films.*

$ODEP^+Br^-$ films show 'flower-like' features with diameters of several μm and thickness of ~ 2.5 nm; this morphology is consistently observed in a number of samples examined. The thickness is compatible with a monolayer of partially tilted amphiphiles. The structure shows clear rupturing in the films of $ODEP^+/DNA^{n-}$ which progresses further in $ODEP^+/CMC^{n-}$; the thicknesses range from 4.5 - 5.5 and 5.5 - 6.5 nm respectively. The $ODEP^+/PSS^{n-}$ film shows a distinct structure best described as an extended network, with threads typically 120 - 150 nm wide and 3.0 - 3.5 nm high. The

polyelectrolyte templates add to the thickness of the films. The increase in thickness of $ODEP^+/DNA^{n-}$ and $ODEP^+/PSS^{n-}$ are consistent with the diameters of the respective polyanions (~ 2.5 nm and ~ 1.0 nm); in the latter case some interdigitation between the aromatic rings in $ODEP^+$ and PSS^{n-} cannot be discounted. The larger increase in thickness with CMC^{n-} and its step-like structure (Fig. 3.20c) suggests the possibility of multilayer formation. We are not aware of any earlier report of AFM images of hemicyanine based LB films and more significantly, of such dramatic morphological modifications in LB films of NLO-phores. The evolution in the patterns with the different polyelectrolytes closely parallels the SHG trends portrayed in Fig. 3.17a; $ODEP^+Br^-$ and $ODEP^+/PSS^{n-}$ are the extreme situations. From the pictures in Fig. 3.19 and the SHG data, we infer that the probability of molecular aggregation is high in the

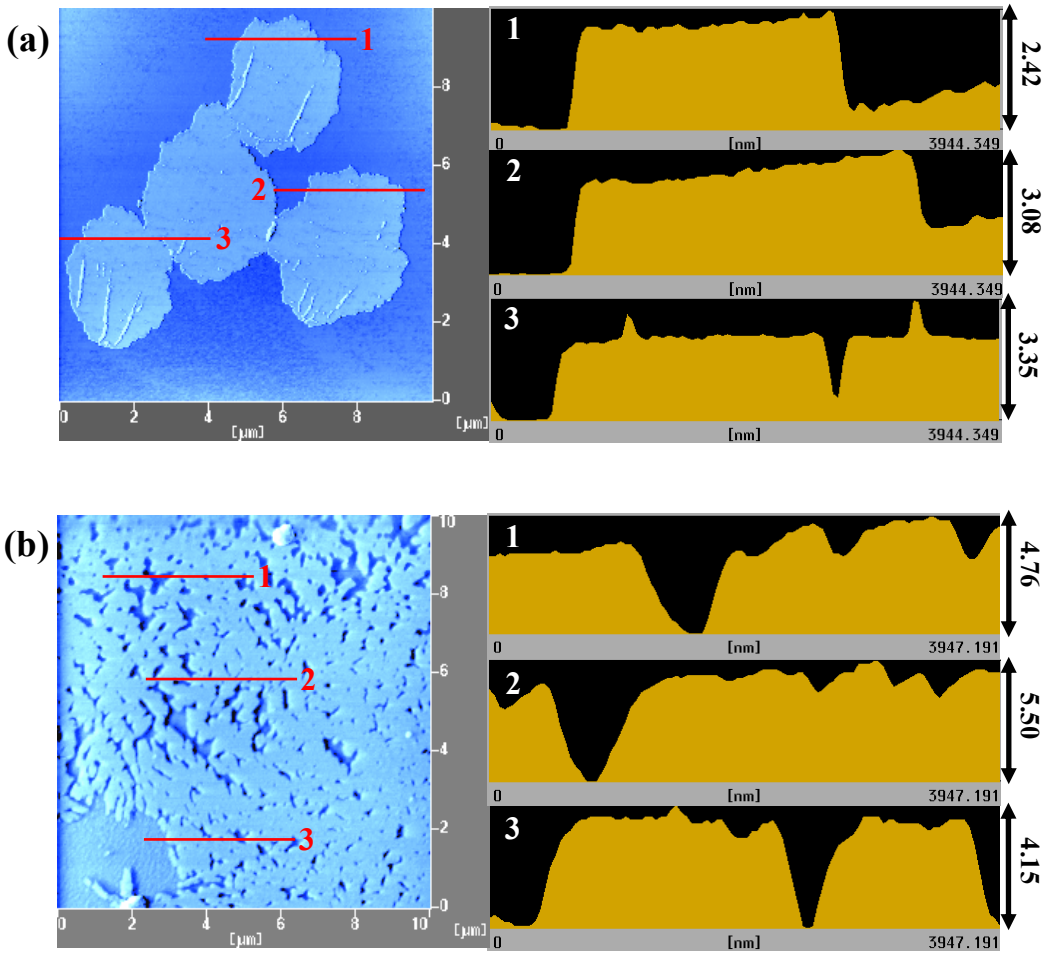

(Continued in the next page)

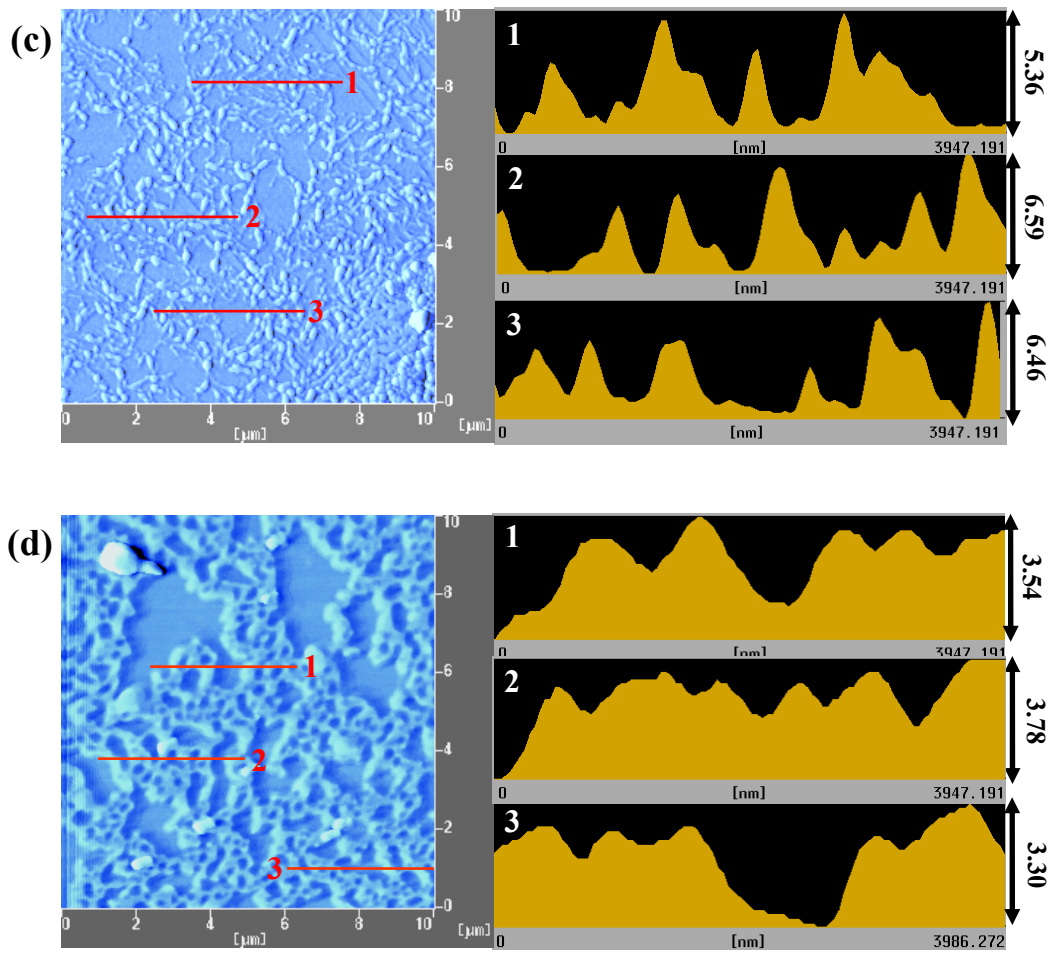

Figure 3.20. (Continued): *AFM images of* ***(a)*** *$ODEP^+Br^-$;* ***(b)*** *$ODEP^+/DNA^{n-}$;* ***(c)*** *$ODEP^+/CMC^{n-}$ and* ***(d)*** *$ODEP^+/PSS^{n-}$ LB films and the thickness profiles along the lines.*

domain structures in the $ODEP^+Br^-$ film, but becomes less likely as these 'flowers' break up under the influence of the polyelectrolytes. The impact is strongest with PSS^{n-}, possibly because of the presence of aromatic rings which engage the hemicyanine headgroup in stabilizing interactions.

Electronic absorption spectroscopy

Insight into the molecular level events which accompany the SHG decay in the LB films is provided by electronic absorption studies. In Sec. 3.4, we have explored in

detail the aggregation of $ODEP^+$ in Langmuir films leading to the formation of π-dimers and diminished SHG response from the LB film.[20,21,23,34,38,55] Temporal instability of Langmuir films of a close derivative of $ODEP^+$ has been monitored through their electronic spectra,[27,37] which revealed the growth of a dimer absorption at ~ 340 nm with concomitant reduction of the monomer absorption at ~ 480 nm. In Sec. 3.4, we showed that the dimer peak in LB films of $ODEP^+Br^-$ was completely suppressed when the films were formed with polyelectrolytes in the subphase. The absorption spectra of the current LB films recorded immediately after fabrication and after each SHG measurement are displayed in Fig. 3.21.

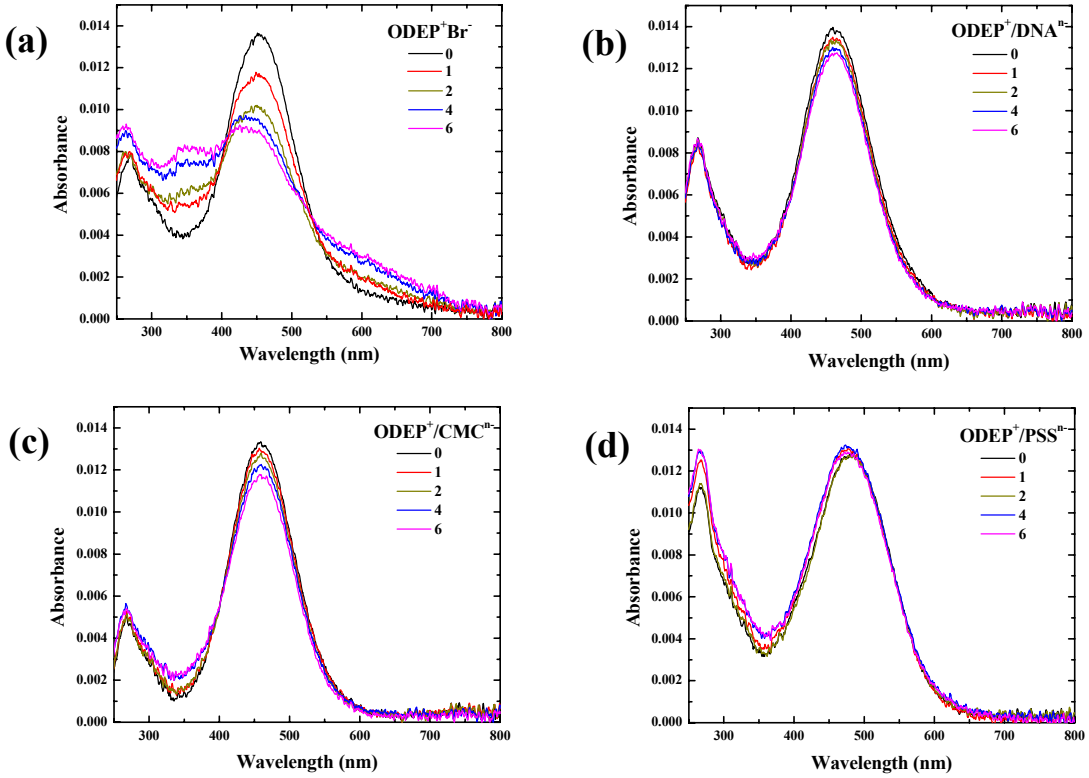

Figure 3.21. *Electronic absorption spectra of the $ODEP^+$ based LB films before the first SHG experiment (0) and after SHG experiments (1, 2, 4, 6).* ***(a)*** *$ODEP^+Br^-$;* ***(b)*** *$ODEP^+/DNA^{n-}$;* ***(c)*** *$ODEP^+/CMC^{n-}$ and* ***(d)*** *$ODEP^+/PSS^{n-}$.*

Fig. 3.21a clearly shows the presence of a weak dimer peak before any laser irradiation of the $ODEP^+Br^-$ LB film. Figs. 3.21b and 3.21c show that the dimer peak is less prominent in $ODEP^+/DNA^{n-}$ and $ODEP^+/CMC^{n-}$. In the case of $ODEP^+/PSS^{n-}$ (Fig.

3.21d), deconvolution (Fig. 3.22) unambiguously indicates that any peak assigned in the range 320 - 400 nm attributable to the dimer has negligible intensity; the finite absorption around 350 nm arises from the broad polyelectrolyte absorption centered near 260 nm.[59] A similar spectral signature of the polyelectrolyte is shown by $ODEP^{+}/DNA^{n-}$; CMC^{n-} does not absorb in the UV-Vis range. Repeated laser irradiations produce continuous changes in the monomer/dimer regions of the spectrum of $ODEP^{+}Br^{-}$. On the other hand, little variations are evident in the spectra of $ODEP^{+}/CMC^{n-}$ and $ODEP^{+}/DNA^{n-}$; the monomer peak shows marginal decline. $ODEP^{+}/PSS^{n-}$ is remarkably resilient to change with no dimer absorption evident all through. We have monitored different areas of the LB film (with a 2 x 2 mm^2 slit) upto 1 cm away from the laser irradiation spot and found that the spectral changes happen uniformly throughout this region.

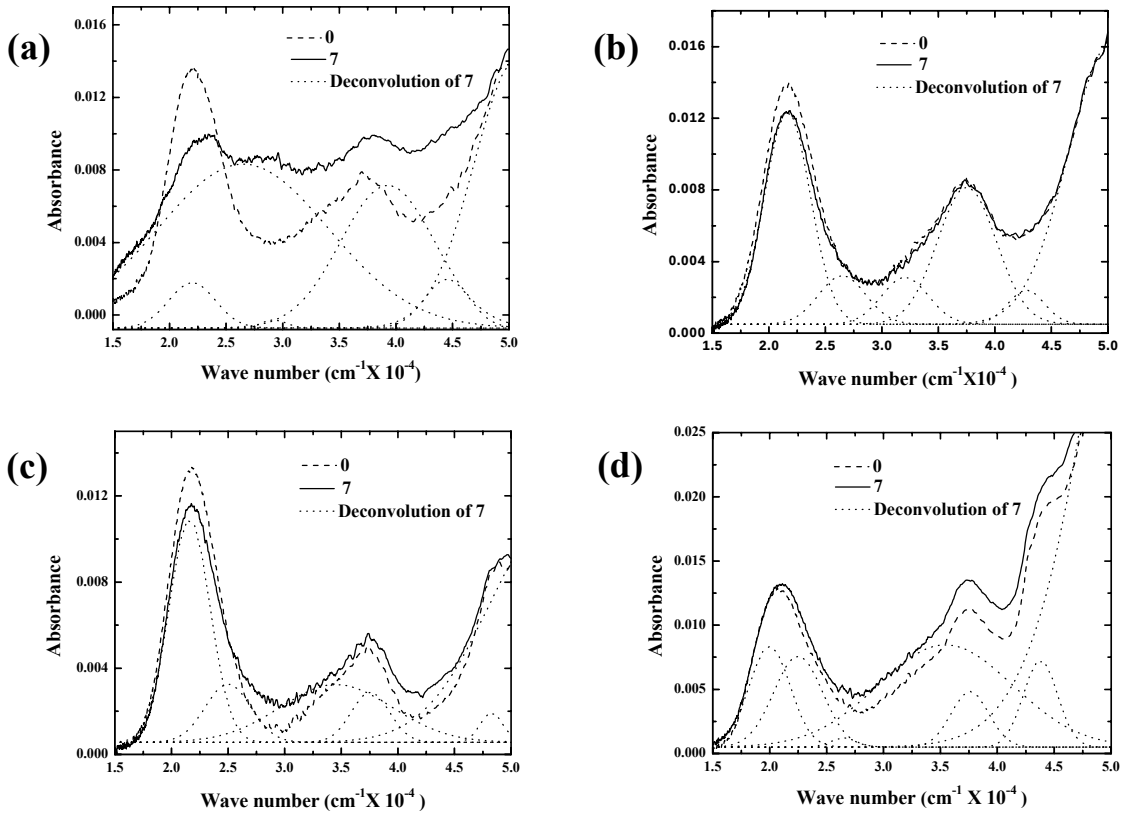

Figure 3.22. *Deconvolution of the electronic absorption spectra of LB films of* ***(a)*** *$ODEP^{+}Br^{-}$;* ***(b)*** *$ODEP^{+}/DNA^{n-}$;* ***(c)*** *$ODEP^{+}/CMC^{n-}$ and* ***(d)*** *$ODEP^{+}/PSS^{n-}$ after the seventh SHG experiment (7); initial spectrum (0) is also shown.*

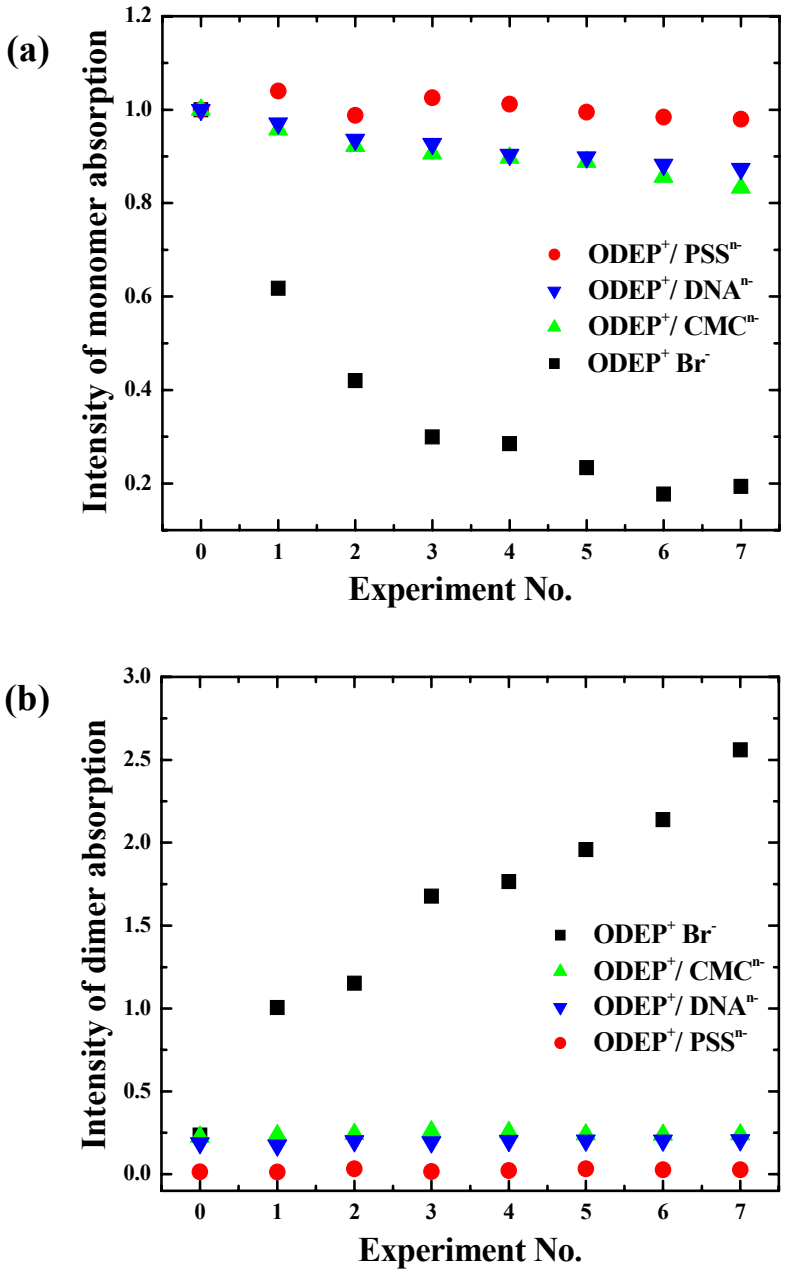

Figure 3.23. *Intensity of the **(a)** monomer and **(b)** dimer electronic absorption of the ODEP$^+$ based LB films before the first SHG experiment (0) and after SHG experiments (1 - 7); in each system, the monomer and dimer intensities are scaled with respect to the initial intensity of the monomer absorption.*

The deconvolution of the spectra (plotted on cm^{-1} *i.e.*, energy scale) of the various LB films after seven laser irradiations (associated with SHG experiments) is shown in Fig. 3.22; the initial spectra are shown for comparison. The peakpositions were determined by deconvolution of the initial spectrum and kept fixed for subsequent analysis so that the changes in the specific peaks can be analyzed; independent deconvolutions of each spectrum showed that the peak positions varied very little throughout. The correlation coefficients in all cases were better than 0.98. The deconvolution indicates that the absorption at 280 - 290 nm is common to all spectra. In the case $ODEP^+/PSS^{n-}$ and $ODEP^+/DNA^{n-}$, the intensity in these regions is higher as these polyelectrolyes have their own absorption in this region. The peaks of special interest are those obtained by deconvolution in the range 300 - 500 nm. In $ODEP^+Br^-$ these occur at 454 nm and 377 nm (Fig. 3.21a and 3.22a) and can be assigned to the monomer and dimer absorptions respectively, based on earlier reports. The intensities of the monomer / dimer peaks in the different systems are shown in Fig. 3.23. The growth of the dimer accompanying the monomer disappearance and the isobestic points (Fig. 3.21a) rule out any chemical degradation upon laser irradiation and demonstrate vividly, the steady increase of H-aggregates in $ODEP^+Br^-$ film. Figs. 3.17 and 3.23 illustrate the clear correlation between the electronic absorption in the different films and their SHG variation.

3.5.3. *Computational modeling*

Further insight into the molecular aggregation in the LB film comes from semiempirical computations on $ODEP^+$ and its dimers. Computations were carried out using the AM1 method[46]. The monomer geometry was built from the crystal structure of the butyl derivative (Sec. 3.3.2) and full optimization of the hydrocarbon chain (Fig. 3.24a). A number of dimer configurations were explored by placing two optimized monomers with headgroups parallel (H-aggregate) at different interplanar distances and with different extent of slip. The final geometry we have obtained satisfying the spectroscopic results, has an interplanar distance of ~ 3.8 Å and displacement of 6.0 Å (Fig. 3.24b). If we assume close packing along the orthogonal direction in a 2-dimensional lattice with a spacing of about 6.3 Å (Fig. 3.24a), the area per molecule will be ~ 38 $Å^2$; this is in good agreement with the value from the π-A isotherms (Fig. 3.8a). The vertical height of ~ 30 Å (Fig. 3.24b) is in the range of thickness of the LB

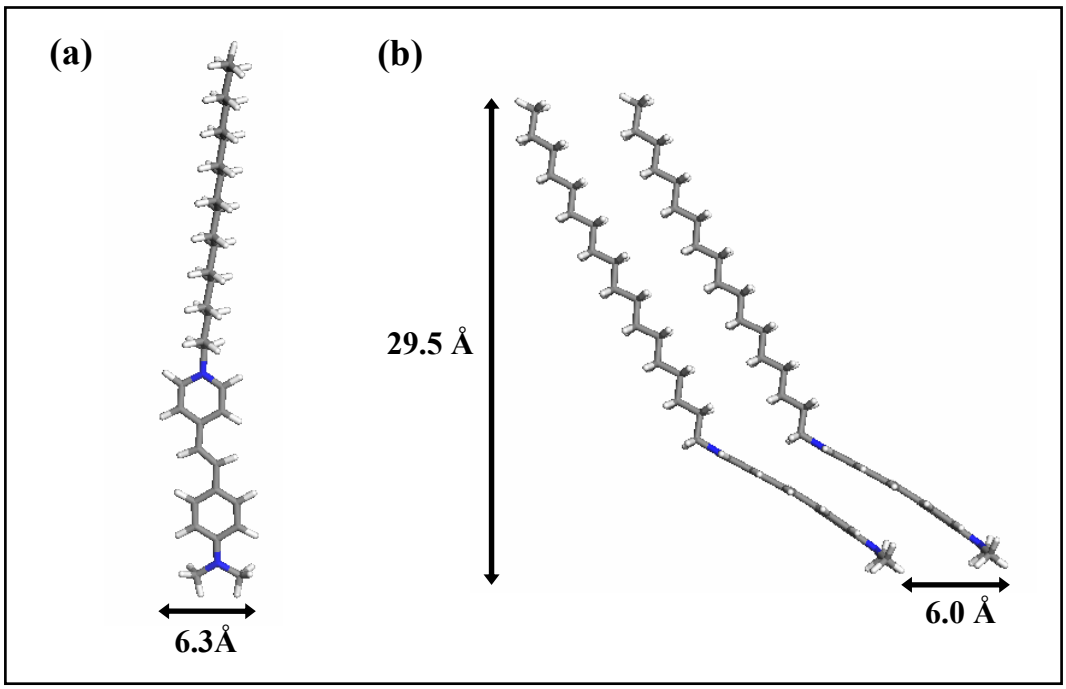

Figure 3.24. ***(a)*** *Optimized structures of ODEP$^+$ (see text for details) and* ***(b)*** *the model dimer of ODEP$^+$; C ( ), N ( ), H ( )*

films (Fig. 3.19a), taking into account the polyelectrolyte layer. Excited state energieswere computed using the CI routine in MOPAC. The environment of the molecules was mimicked[49,50] using the COSMO option,[48] imposing dielectric constants in the range 2-4. The computed absorption with oscillator strength > 0.5 in the UV range are collected in Table 3.7 and show good correlation with the experimental data. The computational study provides a simple model to correlate the various inferences from the pressure-area isotherms, the AFM images and spectroscopic studies.

Table 3.7. *Electronic absorption spectra of the model monomer and dimer.*

Structure	**λ_{max}/nm (f)**		
	ε = 2	**E = 3**	**ε = 4**
Monomer	475.7 (1.61) 294.0 (1.01)	450.1 (1.62) 290.8 (1.05)	435.9 (1.63) 288.6 (1.03)
Dimer	390.0 (2.64) 408.8 (0.88)	373.2 (1.88) 394.7 (0.73)	364.0 (1.83) 366.7 (0.75)

3.5.4. *SHG decay and impact of polyelectrolytes*

The SHG investigation, electronic spectroscopy and AFM studies of the LB films augmented by the computational modeling studies presented above provide a general picture of the whole phenomenon. It can be inferred that laser irradiation perturbs the metastable molecular organization in the LB film of $ODEP^{+}Br^{-}$ leading to H-aggregate formation and consequent SHG decay while the whole process is effectively suppressed by the polyelectrolyte templating. The impact of the laser irradiation may be attributed to thermal effects from either the absorption of the SHG which falls within the range of monomer absorption or to two-photon processes excited by the fundamental beam. The observed effect of the laser beam on the LB film suggests that either waveguiding in the monolayer structure or the thermal effect leads to cooperative interactions. The binding with the polyanion in the templated systems and the fracturing of the domain structure (Fig. 3.19) prevent the dimerization process. We have examined the temporal changes in the LB films by following the electronic absorption of films not subjected to laser irradiation. In none of the cases is any variation observed in the monomer-dimer composition for up to ~ 24 h. However, the dimer peak emerges subsequently; again the process is considerably suppressed in the case of films formed with the polyelectrolytes. Interestingly, absorption spectral changes similar to that obtained by the laser irradiation could be induced in the $ODEP^{+}/Br^{-}$ film by keeping it at $60^{o}C$ for a few days. It is most likely that the laser irradiation essentially accelerates the dimerization process in the $ODEP^{+}Br^{-}$ monolayer films through thermal effects. Further explorations to gain a more elaborate picture of this interesting phenomenon are under progress.

3.6. Summary

We have addressed the fundamental issues of molecular aggregation and thermodynamic instability in the context of LB films for SHG applications. The simple methodology of polyelectrolyte templating is shown to be an effective strategy to address these problems.

In Sec. 3.3 we investigated the molecular aggregation of hemicyanine dye, a system of great interest in NLO applications. The crystal structure of a model compound was investigated to provide a basis for modeling aggregate structures. We employed an approach based on semiempirical quantum chemical computations (incorporating solvation modeling) of molecular and supramolecular structures from the crystal, to gain significant insight into the electronic absorption features of the solution and the solid state of the dye molecule. The analysis provided structural models to explain the monomer and aggregate electronic absorption spectra of previously reported LB films based on the hemicyanine chromophore.

Explorations of the Langmuir and LB films of the cationic hemicyanine amphiphile, $ODEP^{+}Br^{-}$ are presented in Sec. 3.4. The role of equilibration time in the formation of aggregates at the air-water interface was revealed. We demonstrated that the introduction of polyelectrolytes in the aqueous subphase is a simple strategy for achieving efficient deaggregation of the amphiphiles at the air-water interface. The deaggregation leads to the enhancement of the SHG response from the LB films.

In Sec. 3.5 the decay of the SHG response of $ODEP^{+}Br^{-}$ LB film under laser irradiation was unraveled, providing a demonstration of the metastability of LB films. The method of polyelectrolyte-templating was shown to be capable of arresting this phenomenon. Electronic absorption spectroscopy coupled with AFM investigations provided significant molecular level and morphological insight into the phenomena involved.

The experimental and computational approaches developed in the present study are useful in exploring and modeling aggregation phenomena in LB films. The method of polyelectrolyte templating is of general applicability for ionic amphiphiles since it does not involve any chemical modification of the molecule of interest and does not impair the density of the active species in the 2-dimensional layer of the LB film. The present findings support the development of the LB technique as a viable and practical method for the realization of molecular electronic and photonic systems and devices.

References

1. Chandra, M. S.; Radhakrishnan, T. P. *Mol. Cryst. Liq. Cryst.* **2003**, *403*, 77.
2. Chandra, M. S.; Ogata, Y.; Kawamata, J.; Radhakrishnan, T. P. *J. Nonlin. Opt. Phys. Mater.* **2004**, *13*, 347.
3. Chandra, M. S.; Ogata, Y.; Kawamata, J.; Radhakrishnan, T. P. *Langmuir* **2003**, *19*, 10124.
4. Chandra, M. S.; Krishna, M. G.; Mimata, H.; Kawamata, J.; Nakamura, T.; Radhakrishnan, T. P. *Adv. Mat.* (In press).
5. Nair, V.; Cooper, C. S. *J. Org. Chem.* **1981**, *46*, 4759.
6. (a) Sturmer, D. P. in *Kirk-Othmer Encyclopedia of Chemical Technology* (3rd Ed.), Interscience: New York, 1979, p 393; (b)West, W.; Gilman, P. B. in *The Theory of the Photographic Process* James, T. J., (Eds.), Macmillian: New York, 1977, p. 277.
7. Kietzmann, R.; Ehert, A.; Spitler, M.; Willig, F. *J. Am. Chem. Soc.* **1993**, *115*¸ 1930.
8. Saito, K.; Yokoyama, H. *Thin Solid Films* **1994**, *234*, 526.
9. (a) Lanzafame, J. M.; Muenter, A. A.; Brumbaugh, D. V. *Chem. Phys.* **1996**, *210*, 79; (b) Möbius, D. *Adv. Mater.* **1995**, *7*, 437.
10. Wurthner, F.; Wortmann, R.; Matschiner, R.; Lukaszuk, K.; Meerholz, K.; Denardin, Y.; Bittmer, R.; Brauchle, C.; Sens, R. *Angew. Chem. Int. Ed. Eng.* **1998**, *28*, 2765.
11. Kawakami, M.; Koya, K.; Ukai, T.; Tatsuta, N.; Ikegawa, A.; Ogawa, K.; Shishidi, T.; Chen, L. B. *J. Med. Chem.* **1998**, *41*, 130.
12. Soper, S. A.; Mattingly, Q. L. *J. Am. Chem. Soc.* **1994**, *116*, 3744.
13. Williams, C. H. G. *Trans. R. Soc. Edinburg* **1856**, *21*, 377.
14. Zyss, J.; Nicoud, J. -F. *Curr. Opin. Solid State Mater. Sci.* **1996**, *1*, 533.
15. (a) *Non-Linear Optical Materials* Kuhn, H.; Robillard, J., (Eds.), CRC Press: Boca Raton, FL, 1992.; (b) *Introduction to Non-Linear Optical Effects in Molecules and Polymers* Prasad, P. N.; Williams, D. J., (Eds.), Wiley: New York, 1991.
16. Petty, M. C. *Thin Solid Films* **1992**, *210/211*, 417.
17. Long, N. J. *Angew. Chem. Int. Ed. Engl.* **1995**, *34*, 21.

18. Li, F.; Jin, L.; Huang, C.; Zheng, J.; Guo, J.; Zhao, X.; Liu, T. *Chem. Mater.* **2001**, *13*,192.
19. Ashwell, G. J. *J. Mater. Chem.* **1999**, *9*, 1991.
20. Carpenter, M. A.; Willand, C. S.; Penner, T. L.; Williams, D. J.; Mukamel, S. *J. Phys. Chem.* **1992**, *96*, 2801.
21. Scildkraut, J. S.; Penner, T. L.; Willand, C. S.; Ulman, A. *Opt. Lett.* **1988**, *13*, 134.
22. Marowsky, G.; Chi, L. F.; Möbius, D.; Steinhoff, R.; Shen, Y. R.; Dorsch, D.; Rieger, B. *Chem. Phys. Lett.* **1988**, *147*, 420.
23. Hayden, M.; Kowel, T.; Srinivasan, M. P. *Opt. Commun.* **1987,** *61*, 351.
24. Würthner, G.; Yao, S.; Debaerdemaeker, T.; Wortmann, R. *J. Am. Chem. Soc.* **2002**, *124*, 9431.
25. Ashwell, G. J.; Skjonnemand, K.; Paxton, G. A. N.; Allen, D. W.; Mifflin, J. P. L.; Li, X. *J. Mater. Chem.* **2001**, *11*, 1351.
26. Han, K.; Lu, X.; Xu, J.; Zhou, G.; Ma, S.; Wang, W.; Cai, Z.; Zhou, J. *J. Phys. D* **1997**, *30*, 2923.
27. Evans, C. E.; Bohn, P. W. *J. Am. Chem. Soc.* **1993**, *115*, 3306.
28. Kasha, M.; Rawls, H. R.; El-Bayoumi, M. A. *Pure Appl. Chem.* **1965**, *11*, 371.
29. (a) An, B., Kwon, S., Jung, S. & Park, S. Y. *J. Am. Chem. Soc.* **2002**, *124*, 14410.; (b) Luo, J.; Xie, Z.; Lam, J. W. Y.; Cheng, L.; Chen, H.; Qiu, C.; Kwok, H. S.; Zhan, X.; Liu, Y.; Zhu, D.; Tang, B. Z. *Chem. Commun.* **2001**, 1740; (c) Levitus, M.; Schmieder, K.; Ricks, H.; Shimizu, K. D.; Bunz, U. H. F.; Garcia-Garibay, M. A. *J. Am. Chem. Soc.* **2001**, *123*, 4259; (d) Deans, R.; Kim, J.; Machacek, M. R.; Swager, T. M. *J. Am. Chem. Soc.* **2000**, *122*, 8565.
30. (a) Petty, M. C. *Langmuir-Blodgett Films*: *An Introduction* University Press: Cambridge, 1996, p. 43; (b) Schwartz, D. K. *Surface Science Reports*, **1997**, *27*, 241.
31. (a) Wang, Y. ; Nichogi, K.; Terashita, S.; Iriyama, K.; Ozaki, Y. *J. Phys. Chem.* **1996**, *100*, 368; (b) Schönhoff, M.; Chi, L. F.; Fuchs, H.; Lösche, M. *Langmuir* **1995**, *11*, 163; (c) Grebelkin, A. L.; Korobeinicheva, I. K.; Orlova, N. A.; Repinskii, S. M.; Sveshnikova, L. L.; Selyunina, Zh. Yu.; Sagalaeva, N. I.; Shelkovnikov, V. V. *Z. Nauch. Priklad. Foto.* **1992**, *37*, 232.
32. (a) Xu, J.; Lu, X.; Han, K.; Zhou, G.; Zhang, Z. *Langmuir* **1997**, *13*, 3187; (b) Yamada, T.; Kajikawa, K.; Ishikawa, K.; Takezoe, H.; Fukuda, A. *Thin Solid*

Films **1993**, *226*, 173; (c) Miyamato, Y.; Kaifu, K.; Koyano, T.; Saito, M.; Kato, M.; Kawamura, K. *Thin Solid Films* **1992**, *208*, 62.

33. (a) Wang, W.; Lu, X.; Xu, J.; Jiang, Y.; Liu, X.; Wang, G. *Physica B*, **2000**, *293*, 6; (b) Stroeve, P.; Saperstein, D. D.; Rabolt, J. F. *J. Chem. Phys.*, **1990**, *92*, 6958.
34. Girling, I. R.; Cade, N. A.; Kolinsky, P. V.; Jones, R.; Peterson, I. R.; Ahmed, M. M.; Neal, D. B.; Petty, M. C.; Roberts, G. G.; Feast, W. J. *J. Opt. Soc. Am. B* **1987**, *4*, 950.
35. Li, F.; Huang, C.; Jin, L.; Wu, D.; Zhao, X. *J. Mater. Chem.* **2001**, *11*, 3002.
36. Alfimov, M. V.; Lednev, I. K.; Styrkas, D. A. *Thin Solid Films* **1989**, *179*, 397.
37. Evans, C. E.; Song, Q.; Bohn, P. W. *J. Phys. Chem.* **1993**, *97*, 12302.
38. Kajikawa, K.; Kigata, K.; Takezoe, H.; Fukuda, A. *Mol. Cryst. Liq. Cryst.* **1990**, *182A*, 91.
39. (a) Song, X.; Geiger, C.; Farahat, M.; Perlstein, J.; Whitten, D. G. *J. Am. Chem. Soc.* **1997**, *119*, 12481; (b) Song, X.; Geiger, C.; Leinhos, U.; Perlstein, J.; Whitten, D. G. *J. Am. Chem. Soc.* **1994**, *116*, 10340.
40. Vaday, S.; Geiger, H. C.; Cleary, B.; Perlstein, J.; Whitten, D. G. *J. Phys. Chem.* **1997**, *101*, 321.
41. Girling, I. R.; Cade, N. A.; Kolinsky, P. V.; Earls, J. D.; Cross, G. H.; Peterson, I. R. *Thin Solid Films* **1985**, *132*, 101.
42. (a) Kuzyk, M. G.; Singer, K. D.; Zahn, H. E.; King, L. A. *J. Opt. Soc. Am. B* **1989**, *6*, 742; (b) Mizrahi, V.; Sipe, J. E. *J. Opt. Soc. Am. B* **1988**, *5*, 660; (c) Jerphagnon, J.; Kurtz, S. K. *J. Appl. Phys.* **1970**, *41*, 1667.
43. Hall, S. R.; King, G. S. D.; Stewart, J. M. (eds.), *Xtal3.4*, University of Western Australia: Crawley, 1995.
44. Sheldrick, G. M. *SHELX-97*, University of Göttingen: Göttingen, 1997.
45. McArdle, P. *J. Appl. Cryst.* **1995**, *28*, 65.
46. Dewar, M. J. S.; Zoebisch, E. G.; Healy, E. F.; S Stewart, J. J. P. *J. Am. Chem. Soc.* **1985**, *107*, 3902.
47. *MOPAC93* © Fujitsu Inc.: Tokyo.
48. Klamt, A.; Shüürmann, G. *Perkin Trans. 2* **1993**, 799.
49. Sharma, S.; Radhakrishnan, T. P. *J. Phys. Chem. B* **2000**, *104*, 10191.
50. Jayanty, S.; Radhakrishnan, T. P. *Chem. Mater.* **2001**, *13*, 2460.

51. (a) Sharma, S.; Radhakrishnan, T. P. *J. Phys. Chem. B* **2003**, *107*, 147; (b) Sharma, S.; Radhakrishnan, T. P. *ChemPhysChem* **2003**, *4*, 67.
52. Marder, S. R., Perry, J. W., Yakymyshyn, C. P. *Chem. Mater*. **1994**, *6*, 1137.
53. Van Cott, K. E; Guzy, G.; Neyman, P.; Brands, C.; Heflin, J. R.; Gibson, H. W.; Davis, R. M. *Angew. Chem. Int. Ed.* **2002**, *41*, 3236.
54. Ashwell, G. J.; Hargreaves, R. C.; Baldwin, C. E.; Bahra, G. S.; Brown, C. R. *Nature* **1992**, *357*, 393.
55. Scheelen, A.; Winant, P.; Persoons, A. In *Organic Molecules for Nonlinear Optics and Photonics* Messier, J.; Kajzer, F.; Prasad, P. N., (Eds.), Kluwer: The Netherlands, 1991, p. 497.
56. (a) Sato, O.; Baba, R.; Hashimoto, K.; Fujishima, A. *J. Phys. Chem.* **1991**, *95*, 9636; (b) Cross, G. H.; Girling, I. R.; Peterson, I. R.; Cade, N. A.; Earls, J. D. *J. Opt. Soc. Am. B*, **1987**, *4*, 962.
57. *Cell Biology* DeRobertis, E. D. P.; Saez, F. A.; DeRoberties Jr., E. M. F., (Eds.), W. B. Saunders Company: Tokyo, 1975.
58. Engelking, J.; Menzel, H. *Thin Solid Films* **1998**, *327-329*, 90.
59. Sharma, S.; Chandra, M. S.; Radhakrishnan, T. P. *Langmuir* **2001**, *17*, 8118.

CHAPTER 4

Polyelectrolyte Templated Polymerization in Langmuir Film : Nanoscopic Control of Polymer Chain Organization

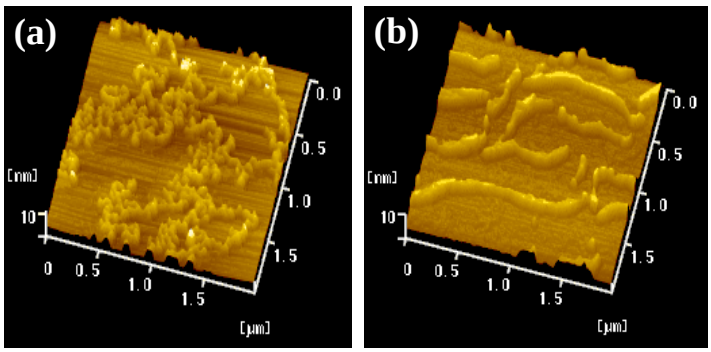

Polymerization of amphiphilic aniline at the air-water interface is strongly influenced by polyelectrolyte templating introduced from the aqueous subphase leading to highly aligned chains of polyaniline in the deposited Langmuir-Schaefer films. The picture shows AFM images of monolayer LS films of the polyaniline : (a) network structure without polyelectrolyte templating and (b) aligned chains in presence of carboxymethyl cellulose.

Scope

Polyelectrolytes introduced in the aqueous subphase are shown to have a profound impact on the kinetics of polymerization of N-n-octadecylaniline at the air-water interface. This can be attributed to changes effected in the monomer reorientation behavior and molecular organization in the Langmuir film; considerable modification is observed in the morphology of the monomer and polymer Langmuir films. The polyelectrolyte complexation is found to be an elegant and efficient methodology to achieve enhanced alignment of the polyaniline chains in the transferred Langmuir-Blodgett (Langmuir-Schaefer) film.[1] Polymerization of N-n-octadecylaniline at a liquid-liquid (hexane-water) interface is also investigated; polyelectrolytes are found to influence the morphology and enhance the mechanical stability of the resulting polyaniline films.

4.1. Introduction

Molecular assembly mediated by covalent as well as noncovalent interactions and its control at the nanoscopic level are of fundamental relevance to supramolecular chemistry, polymer chemistry and molecular scale electronics, photonics and patterning. The Langmuir-Blodgett technique is especially suited to exercise such control; it also facilitates efficient monitoring. A fine example is the synthesis of conjugated polymers at the air-water interface[2,3] and investigation of the kinetics through the measurement of surface pressure or monolayer area changes.[2,4-7] In the previous chapters, we have demonstrated the utility of polyelectrolyte complexation in stabilizing otherwise unstable Langmuir films[8] and the role of polyelectrolyte templates in efficient deaggregation leading to enhanced[9] and stable[10] second harmonic generation in LB films based on the hemicyanine dye. Polyelectrolytes have been extensively employed as dopants and templates in the synthesis of conducting polymers.[11,12] They impart higher solubility and processability to the polymers and play a critical role in modifying their morphology and conducting properties.[12] A logical extension of the studies cited above suggests that the covalent assembly of molecules through polymerization at the air-water interface can be regulated and modulated by noncovalent interactions with polyelectrolytes introduced from the subphase.

In this chapter, we present our investigations of the polymerization of N-*n*-octadecylaniline (NOA) assembled as a Langmuir film on water surface and demonstrate the influence of polyelectrolytes introduced from the subphase, on the morphology of the Langmuir film, kinetics of the polymerization and the polymer chain organization in the transferred Langmuir-Schaefer film. Polymerized N-*n*-alkylaniline cannot sustain the neutral quinonoid (emeraldine base) and the corresponding protonated (emeraldine salt) forms. Perhaps owing to this limitation, polymers of N-alkylaniline (alkyl = butyl - dodecyl) synthesized in the bulk phase[13,14] have shown low conductivity. However we note that NOA possesses several advantages for the kind of exploration we have planned – easy synthesis, stable protonated monomer and polymer states and steric/structural features well-suited for organization at the air-water interface. We envisaged that, under the usual aniline polymerization conditions, polyelectrolytes would exercise strong control on the orientation of the protonated monomer as well as the organization of the polymer which is likely to form in either the fully protonated (with ammonium groups) or even further oxidized (bipolaronic) form. We have investigated also, the polymerization of NOA at the liquid-liquid (organic-aqueous) interface to examine the possibility of fabricating free-standing films and the utility of polyelectrolytes in this regard. The polyelectrolytes are expected to improve the mechanical stability of the final product.

4.2. Experimental Details

4.2.1. *Synthesis and Characterization*

NOA was prepared as shown in Scheme 4.1. 1-bromooctadecane (1.0g, 3.0 mmol) in 20 ml toluene was added to a stirred solution of aniline (0.32 g, 3.3 mmol) in 30% aqueous sodium hydroxide containing catalytic amount of N,N,N,N-tetrabutylammonium bromide. The reaction mixture was stirred at 70-80^{o}C for 7 days. The toluene phase was washed with sodium chloride solution and evaporated. The resultant solid was purified by several recrystallizations from hexane. Yield : 0.82 g (80%); M.P./^{o}C = 50-52; FT-IR (KBr pellet): $\bar{\upsilon}$/cm^{-1} = 3396.9, 2916.6, 2847.2, 1604.9, 1510.4, 1468.0, 1315.6, 748.5, 690.6; ^{1}H-NMR ($CDCl_3$): δ/ppm = 0.90 (t, 3H), 1.27 (s, 30H), 1.60 (m, 2H), 3.10 (t, 2H), 6.72 (m, 3H), 7.13 (m, 2H) (amine proton is

not observed); ^{13}C NMR ($CDCl_3$) : δ/ppm = 148.6, 129.2, 117.0, 112.7, 44.0, 31.9, 29.7, 27.2, 22.7, 14.1.

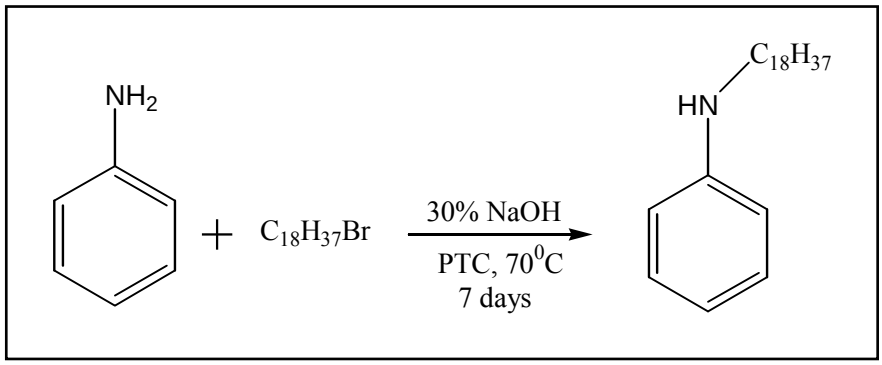

Scheme 4.1

4.2.2. *Langmuir and Langmuir – Blodgett / Schaefer film fabrication and characterization*

Langmuir films were formed by spreading a solution of NOA (0.04 μmol) in chloroform on an aqueous subphase (220 ml) containing sulfuric acid (0.10 M) or sulfuric acid (0.10 M) and a polyelectrolyte (~ 0.20 μmol based on the acid groups). The polyelectrolytes used in this study are poly(potassium vinylsulfate) (PVS, MW = 170,000) and sodium salt of carboxymethyl cellulose (CMC, MW = 90,000); under the acidic conditions employed, the polyelectrolytes are likely to be largely in the polyacid form (Fig. 4.1).

Ammonium peroxydisulfate was used as the oxidizing agent for polymerization. Polymerization reactions were carried out at different target pressures. Details of these studies are provided in the next section. The morphology changes during the polymerization process were monitored using Brewster angle microscopy. Monolayers of the polymer, poly(N-*n*-octadecylaniline) (PNOA) were transferred to freshly cleaved mica plates by the horizontal dipping procedure (LS method) for AFM imaging. 24-layer films were deposited on hydrophilic glass plates by vertical dipping, for optical absorption studies. The general procedure for LB film fabrication is given in Appendix B and details of the microscopy studies are described in Appendix C.

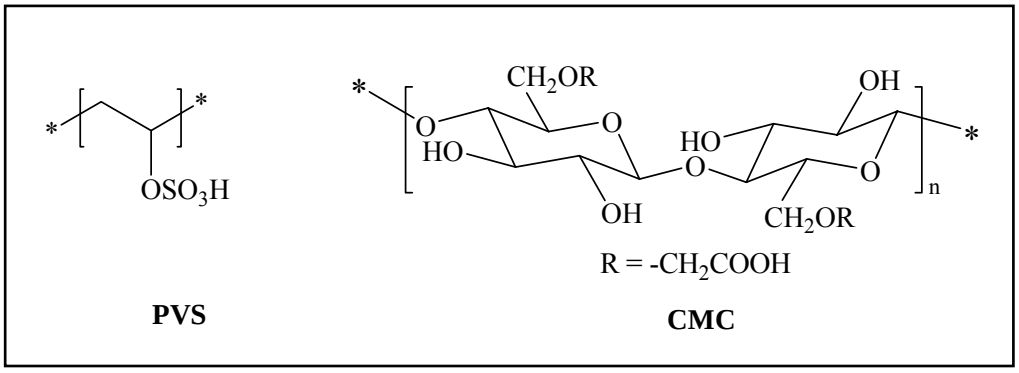

Figure 4.1. *Molecular structures of the polylectrolytes used in the studies presented in this chapter.*

4.2.3. *Polymerization at the air-water interface*

The polymerization of NOA (Scheme 4.2) in the Langmuir film at the air-water interface was investigated using two different procedures. We have initially followed an approach reported earlier (Method I, Fig. 4.2a)[4-6] in which the oxidizing agent is added to the subphase prior to the introduction of the monomer: After spreading, the monolayer was compressed immediately to the target pressure and the reaction was studied at that pressure. We found that, in this procedure the kinetics is sensitive to the barrier speed and is subject to errors due to delays in initial compression. Therefore we have developed a new procedure for further studies (Method II, Fig. 4.2b). The monomer was spread on the acidic subphase and compressed to the desired target pressure. Subsequently, the oxidizing agent (typically ~1.0 ml of 1.7 M solution) was injected into the subphase using a surgical needle inserted through the compressed

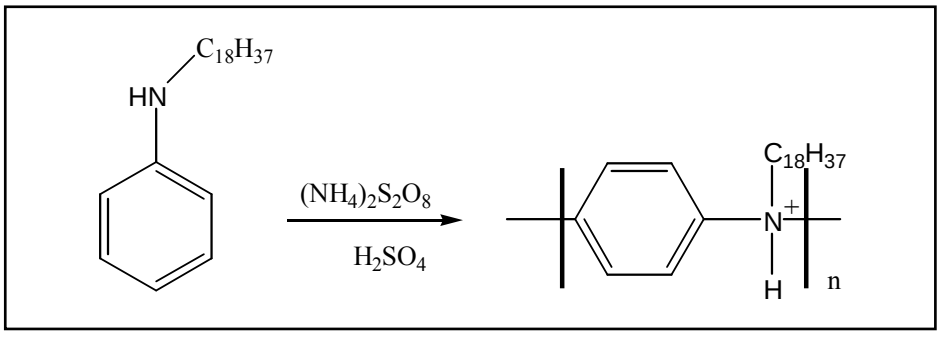

Scheme 4.2

monolayer; this had no adverse impact on the integrity of the film. In this procedure, the monomers in the monolayer are organized before initiating the polymerization and the kinetics is followed from the beginning; conceptually this is similar to the double compartment method reported previously.[7]

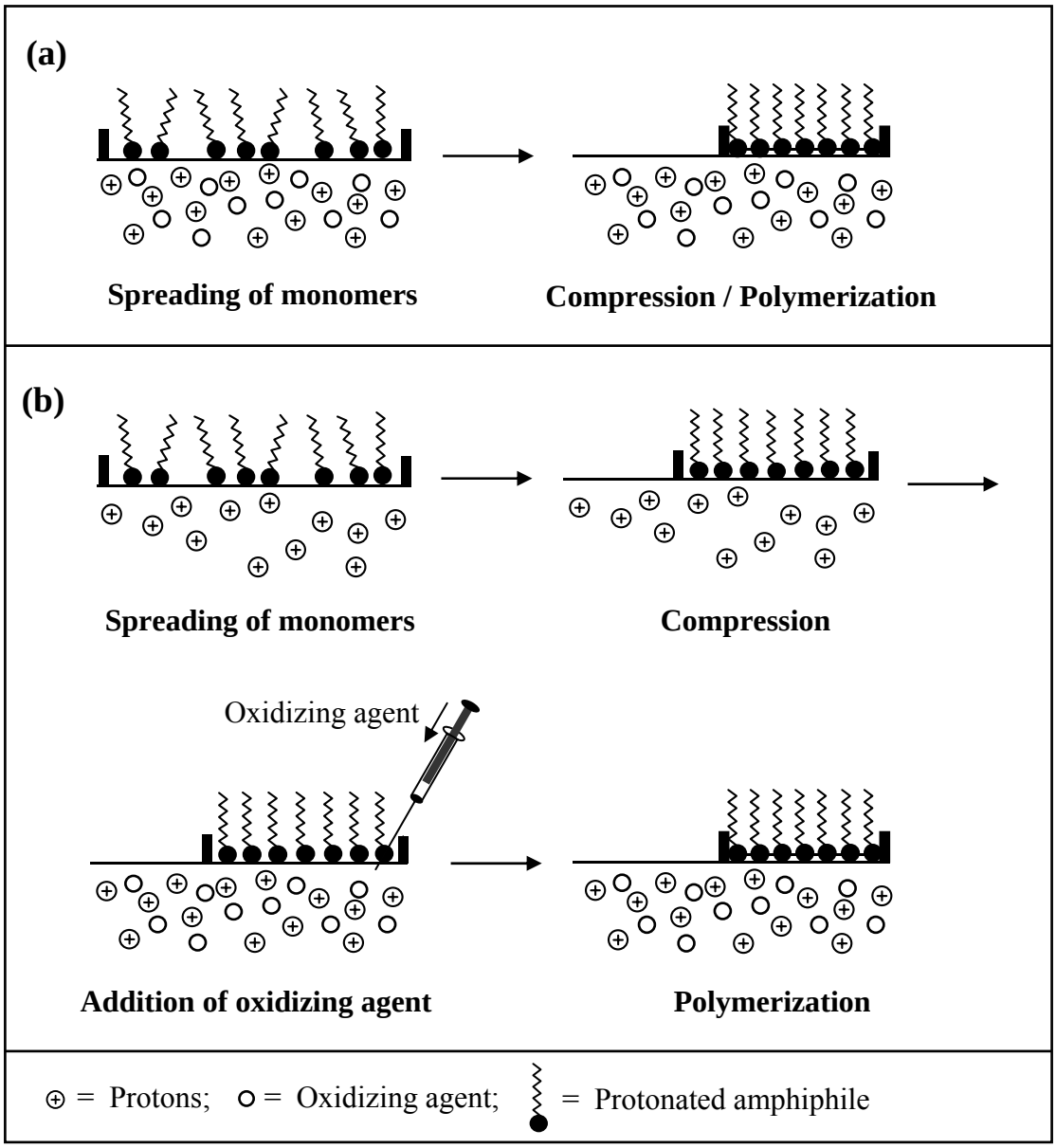

Figure 4.2. *Schematic representation of the polymerization of NOA at the air-water interface;* ***(a)*** *Method I and* ***(b)*** *Method II (see text for details).*

4.2.4. *Bulk polymerization at the organic – aqueous interface*

NOA was dissolved in hexane (0.009 M) and carefully introduced on the surface of an aqueous solution in a round bottom flask containing sulfuric acid (1.0 M) and ammonium peroxydisulfate (0.03 M). The reaction setup was protected from mechanical disturbances at the interface. A thin layer of the green polymer is found to develop slowly at the interface within 2-3 h. The thickness of the film increases visibly over a period of 2 weeks. The reaction slows down and stops when the thickness of the film at the interface grows sufficiently to prohibit the interaction between the two liquid phases. The hexane solution on top was removed carefully without damaging the film. The film surface was washed thoroughly with hexane to remove traces of the unreacted monomer and the film was removed carefully and washed further with pure water. It could be retained as a free-standing film or on a substrate support. In parallel experiments to study the impact of the polyelectrolyte on the stability of the polymer, the polyelectrolyte was also added to the aqueous phase before introducing the organic phase on top.

4.3. Polymerization Kinetics

The polymerization reaction was carried out at constant pressure and temperature. Under the constant pressure condition, the polymerization process is accompanied by significant changes in the monolayer area or equivalently, by the barrier movement (Fig. 4.3). This provides a handle to estimate the rate of the reaction as discussed below.

The rate of the reaction at the 2-dimensional interface can be formulated within the spirit of the 'ideal gas equation'. At constant temperature,

$$\pi (A - A_{\infty}) = C\, n$$

where π, A and n are the surface pressure, area and number of monomers during the course of the reaction; A_{∞} is the final area and C is a constant of proportionality, related to the temperature. The rate can be expressed as,

$$\text{Rate} = \frac{dn}{dt} = \frac{1}{C}\frac{d}{dt}\left[\pi(A - A_{\alpha})\right]$$

Using the initial values, n_0, π_0 and A_0, the expression can be written as,

$$\text{Rate} = \frac{n_0}{\pi_0(A_0 - A_{\alpha})}\frac{d}{dt}\left[\pi(A - A_{\alpha})\right]$$

It may be noted that in a constant pressure experiment, $\pi = \pi_0$, however, due to small pressure fluctuations $\pi \sim \pi_0$. If the fluctuations are negligible, the equation can be further simplified to,

$$\text{Rate} = \frac{n_0}{(A_0 - A_{\alpha})}\frac{d}{dt}\left[A - A_{\alpha}\right] \quad = \frac{n_0}{(A_0 - A_{\alpha})}\frac{dA}{dt}$$

It should be noted that the rate varies through the reaction and this can be followed by the area-time curves.

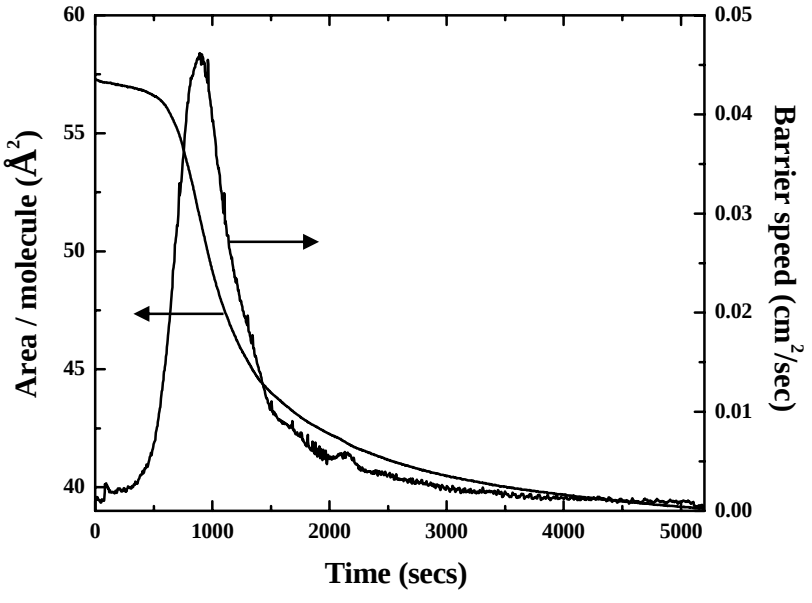

Figure 4.3. *Area and barrier speed as a function of time during the polymerization of protonated NOA in the Langmuir film (with only sulfate ions in the subphase).*

4.4. Polyelectrolyte Assisted Polymerization of NOA and Polymer Chain Organization in PNOA

The Langmuir film offers a unique environment to investigate the polymerization of amphiphilic monomers confined to a 2-dimensional lattice at the air-water interface. The advantage of polymerization in a Langmuir film is that the molecules can be held in a well - defined orientation at the interface while the polymerization kinetics is continuously monitored. Polymerization kinetics in a Langmuir film has been shown to be sensitive to the applied surface pressure,[7] temperature,[15] concentration of the reagents introduced from the subphase[5] and even the orientation and conformation of the molecules.[6] We have chosen to study the polymerization of NOA at the air – water interface. This molecule differs from the classical systems used in polyaniline formation, as the hydrocarbon chain is attached at the reaction site of the monomer. As noted earlier, even though this may impair the conducting property of the final polymer, there would be a strong dependence of the polymerization process in the Langmuir film on the orientation and organization of the molecules. We are particularly interested in the influence of various polyelectrolytes in the subphase, on the polymerization process.

4.4.1. *Polymerization in the Langmuir film*

NOA does not form a stable monolayer on the surface of pure water. Acidification of the subphase with sulfuric acid (but not hydrochloric acid) imparts stability to the monolayer as revealed by the pressure-area isotherm (Fig. 4.4a); this could be attributed to the stabilization of the cationic amphiphile (protonated NOA) layer by the effectively bidentate dianions; similar effects have been noted in Sec. 2.3.[8] The π - A isotherms of protonated NOA with sulfate in the subphase indicates a transition near 23 mN/m. From the extrapolated areas below and above the transition, 101.6 and 75.8 $Å^2$/molecule respectively, the transition can be ascribed to a reorientation of the headgroup.[16,17] There is a small, but finite pressure even when the barrier is fully open. Introduction of polyelectrolytes in the subphase increases the residual pressure slightly, but more significantly it shifts the isotherms to higher areas and smoothens the transition; the extrapolated areas are 96.7, 94.1 $Å^2$/molecule in the

case of PVS and CMC respectively. The increase of residual pressure and isotherm shift occur due to the amphiphile – polyelectrolyte complexation.[8,9] The complexation also effects a cooperative motion of the headgroups leading to smoothening of the transition. A combination of electrostatic and H-bonding interactions depending on the level of ionization of the polyacids is likely to lead to the complexation between the headgroup of the amphiphile and the polyelectrolyte.

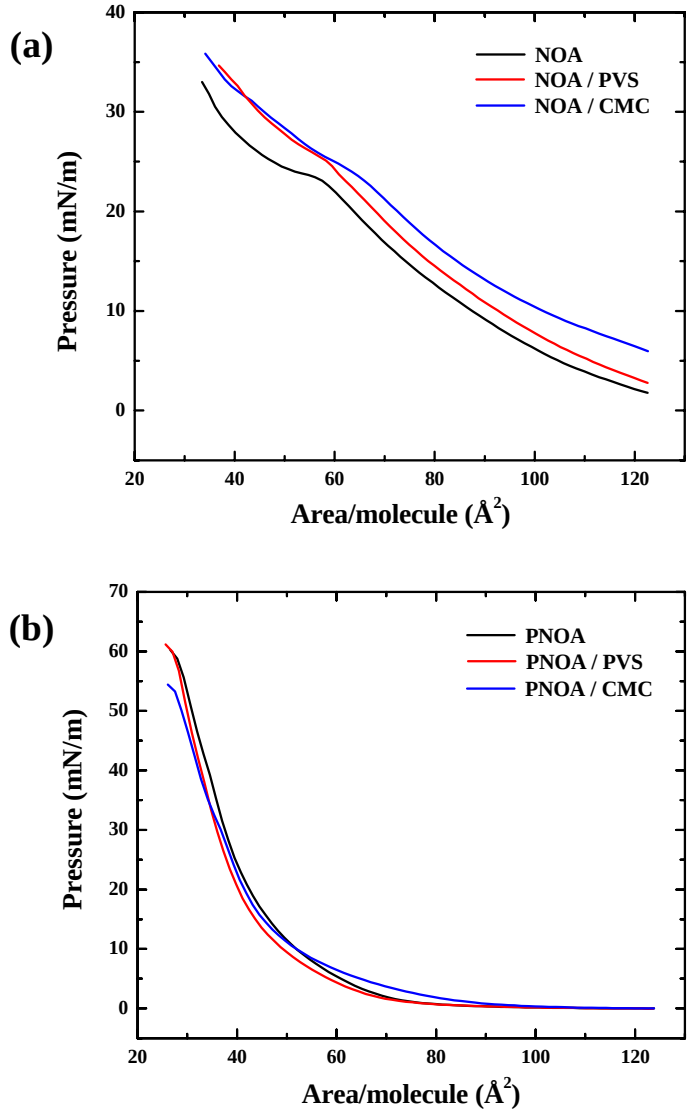

Figure 4.4. *Pressure-area isotherms of protonated* ***(a)*** *NOA and* ***(b)*** *PNOA monolayers without and with polyelectrolytes in the subphase.*

As mentioned in Sec. 4.2.3 we have carried out the polymerization reaction at the air-water interface in two different ways. In Method I, the monolayer was compressed immediately after spreading, to a certain target pressure, which was maintained throughout the reaction by automated movement of the barrier. Barrier speed of ≥ 50 cm^2/min was used. Reactions studied at different pressures, 15 – 33 mN/m showed that the maximum value of the peak rate was obtained at 25 mN/m (Fig. 4.5). This may be attributed to the suitable molecular orientation and flexibility of the reorienting monolayer at this pressure. A drawback of this experimental procedure is that the reaction starts immediately after the spreading as the oxidizing agent is readily available in the subphase; this could lead to errors in the estimated reaction rates. The rates are also found to depend on the barrier speed employed. This method is not suitable to investigate the effect of polyelctrolytes in the subphase since the equilibration of the interaction between the ionic amphiphiles and polyelectrolyte is a slow event and interferes with the polymerization process.

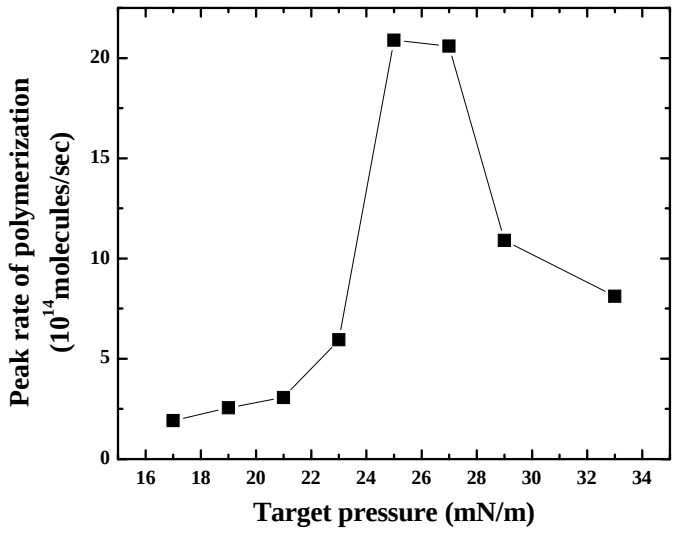

Figure 4.5. *Peak rate of polymerization of NOA with only sulfate ions in the subphase, carried out at various target pressures.*

Method II that we have developed, in which the oxidizing agent is injected into the compressed monolayer without harming the integrity of the film, allowed us to initiate the polymerization on a pre - oriented monolayer and to follow the kinetics from the very beginning. The polymerization reaction appears to be initiated approximately 15 min after the introduction of the oxidizing agent into the subphase as indicated by the

reduction in mean molecular area. The area decrease is mainly due to the covalent bond formation between the monomers upon reaction. We have carried out this reaction before (20 mN), after (30 mN) and at the point of the phase transition, with and without polyelectrolytes in the subphase. Area change and barrier movement during the polymerization at the target pressure corresponding to the phase transition in the absence of polyelectrolytes in the subphase are shown in Fig 4.3. The reaction rates are estimated as described in Sec. 4.3. The rates vary through the course of the reaction; the peak rates of polymerization observed at different target pressures, without and with the polyelectrolytes in the subphase are collected in Table 4.1. In the absence of polyelectrolytes, the peak rate is highest when the pressure is close to that of the transition, indicating that the reaction is slowed down in the rigid states below and above this point. This is consistent with the results from Method I as well (Fig. 4.5). Significantly, the polyelectrolytes reduce the rates in general and the peak rate decreases with increasing pressure. These observations point to the control of the monomer motion and reorientation by the cooperative impact of the polyelectrolyte.

Table 4.1. *Peak rate of polymerization of NOA at 25^{o}C and different target pressures, with only sulfate and additionally different polyelectrolytes introduced in the subphase.*

Pressure (mN/m)	**Rate (10^{13} molecules sec^{-1})**		
	Sulfate	**PVS**	**CMC**
20	2.24	1.66	1.40
~ 23	2.61	1.30	1.15
30	1.40	1.06	0.89

The π-A isotherms of PNOA are shown in Fig. 4.4b. The prominent features are the steeper curves, lower extrapolated areas and higher collapse pressures compared to those of the monomers. The contraction of area results from the formation of covalent bonds between the monomers in the polymer. The steeper curves and higher collapse pressures reveal the enhanced stiffness and stability of the polymer monolayer. Interestingly, the isotherms are nearly independent of the presence or type of polyelectrolyte indicating that the polymer backbone is the same in all cases.

Brewster angle microscopy

We have examined the influence of polyelectrolytes on the monolayer by BAM imaging at different points along the π-A curve through the polymerization process. Selected images for the polymerization carried out at 20 mN/m are presented in Fig. 4.6. The polyelectrolytes impart some degree of organization to the monomer domains prior to polymerization (row [1]). The change of morphology on polymerization (rows [2] to [3]) is quite marked in the absence of polyelectrolytes; the polyelectrolytes tend to

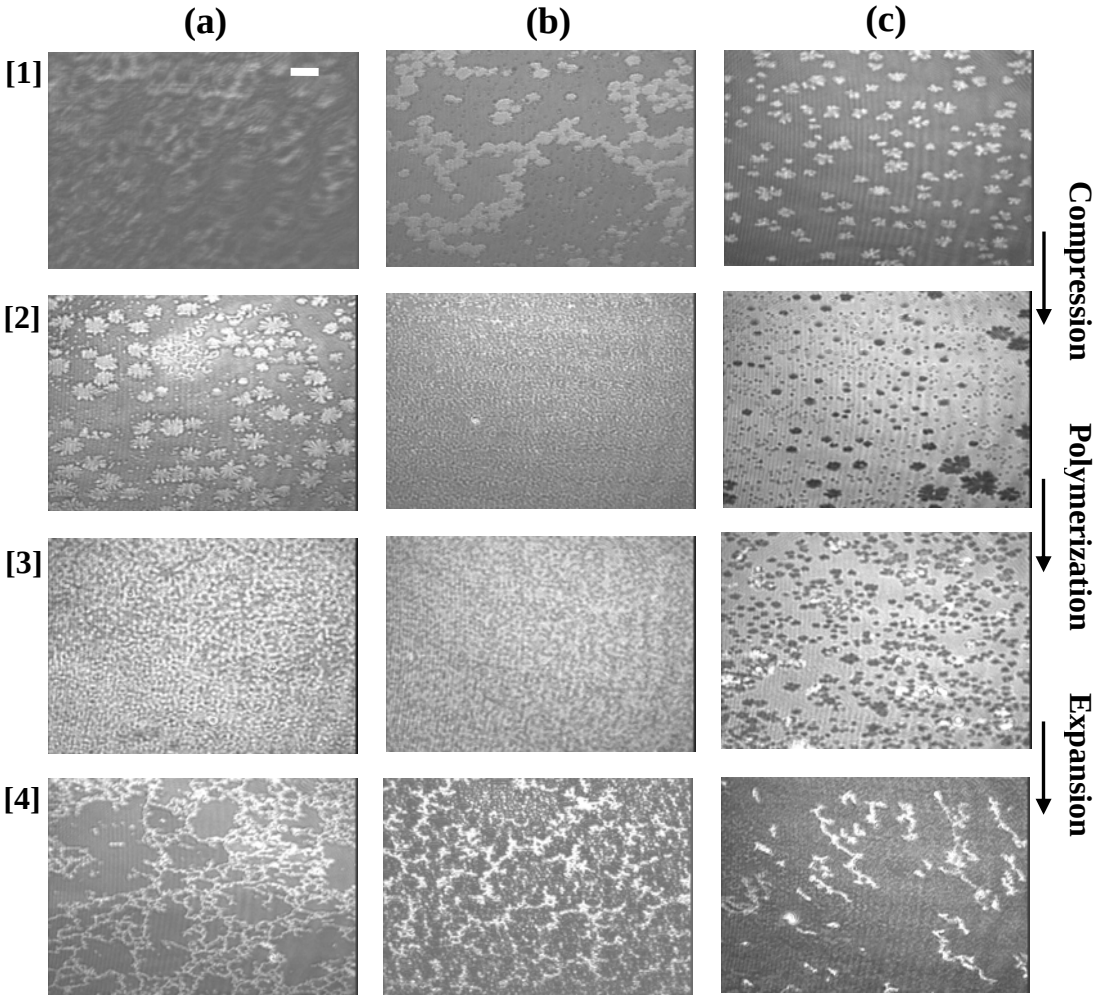

Figure 4.6. *BAM images of Langmuir films. Rows [1], [2] : protonated NOA monolayer at 0 and 20 mN/m; rows [3], [4] : PNOA monolayer at 20 and 0 mN/m; with* ***(a)*** *only sulfate and additionally* ***(b)*** *PVS and* ***(c)*** *CMC in the subphase. The scale bar is 20 µm and the same in all images.*

homogenize the monomer and polymer monolayers smearing out contrast. The most significant impact of the polyelectrolytes is evident upon expansion of the polymer monolayer (row [4]), in terms of considerable reduction in chain entanglement. It is important to note that these morphological features are on the scale of several μm.

4.4.2. *Langmuir-Blodgett/Schaefer film studies*

The amphiphilic polynailine (PNOA) formed on the water surface was transferred onto solid substrates for further characterizations.

UV-Visible-near IR spectroscopy

Multilayer films of PNOA (polymerized at 20 mN/m) deposited on glass showed a broad electronic absorption spectrum with peaks at ~ 305, 445 and 565 nm (Fig. 4.7); the spectrum is largely independent of the counterions in the subphase. The high energy peak is due to π-π* transition whereas the visible peaks have been previously assigned to the polaronic state due to ammonium functionality[18] and the pernigraniline form[6] respectively. The absence of strong absorption above 625 nm indicates a low population of quinonoid structures and bipolaronic states.[13,14,18] We infer that PNOA is in the fully protonated state with mostly benzenoid rings (Scheme 4.2).

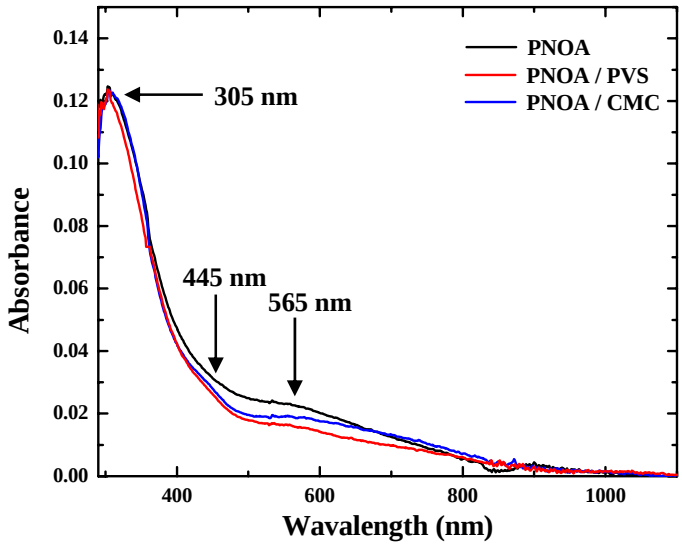

Figure 4.7. *Absorption spectra of PNOA formed with only sulfate and additionally, PVS and CMC in the subphase.*

Atomic force microscopy

Monolayer films deposited on mica immediately after polymerization (at 20 mN) by the LS method were examined using AFM in differential force (noncontact) mode. The 3-dimensional images are shown in Fig. 4.8, and the 2-dimensional images along with the line profiles, in Fig. 4.9. In the absence of polyelectrolytes (Fig. 4.8a, 4.9a), a complex network structure is observed with threads typically 3.5 – 4.0 nm high and 30 – 50 nm wide. There are occasional threads with double thickness possibly arising due to bilayer defect structures. Films fabricated in presence of polyelectrolytes

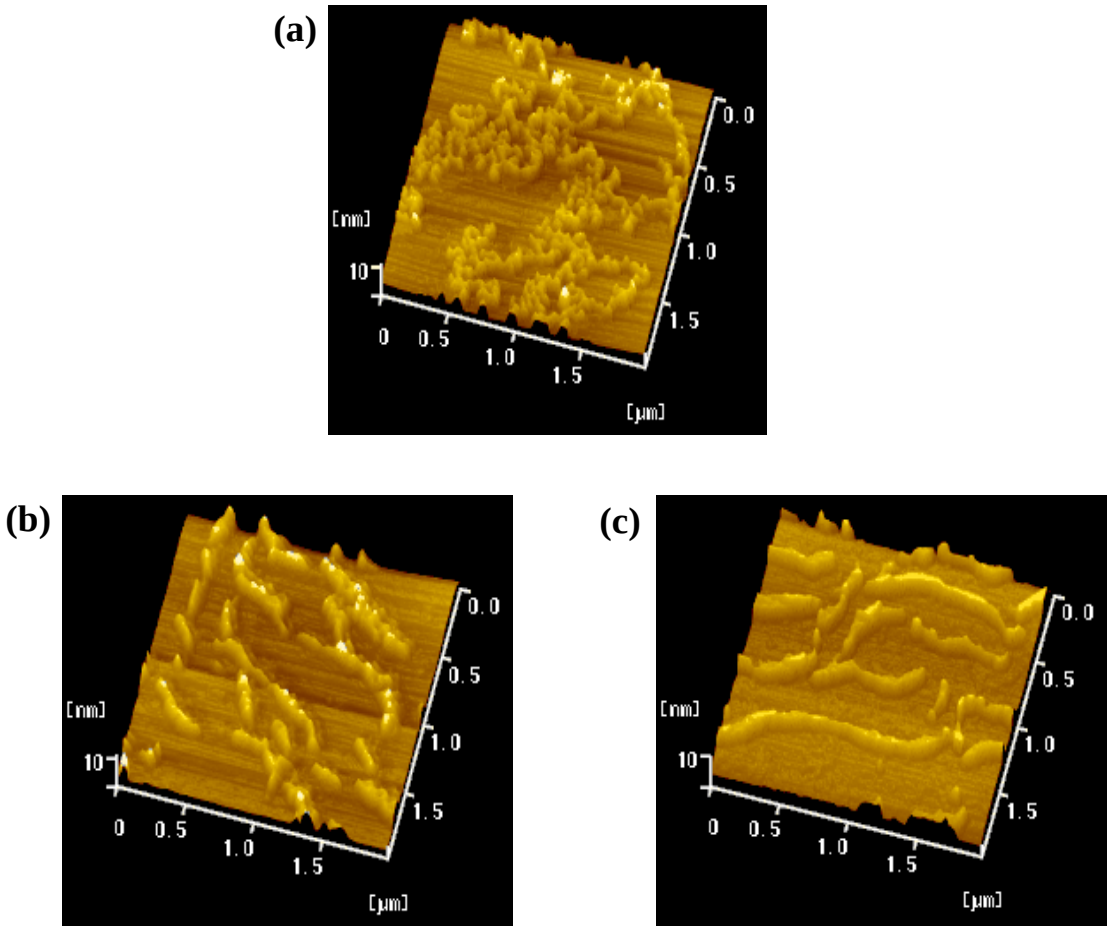

Figure 4.8. *AFM topography images of monolayer LS films of PNOA fabricated with* ***(a)*** *only sulfate and additionally* ***(b)*** *PVS and* ***(c)*** *CMC in the subphase. Image size : 2µm x 2µm x 10nm.*

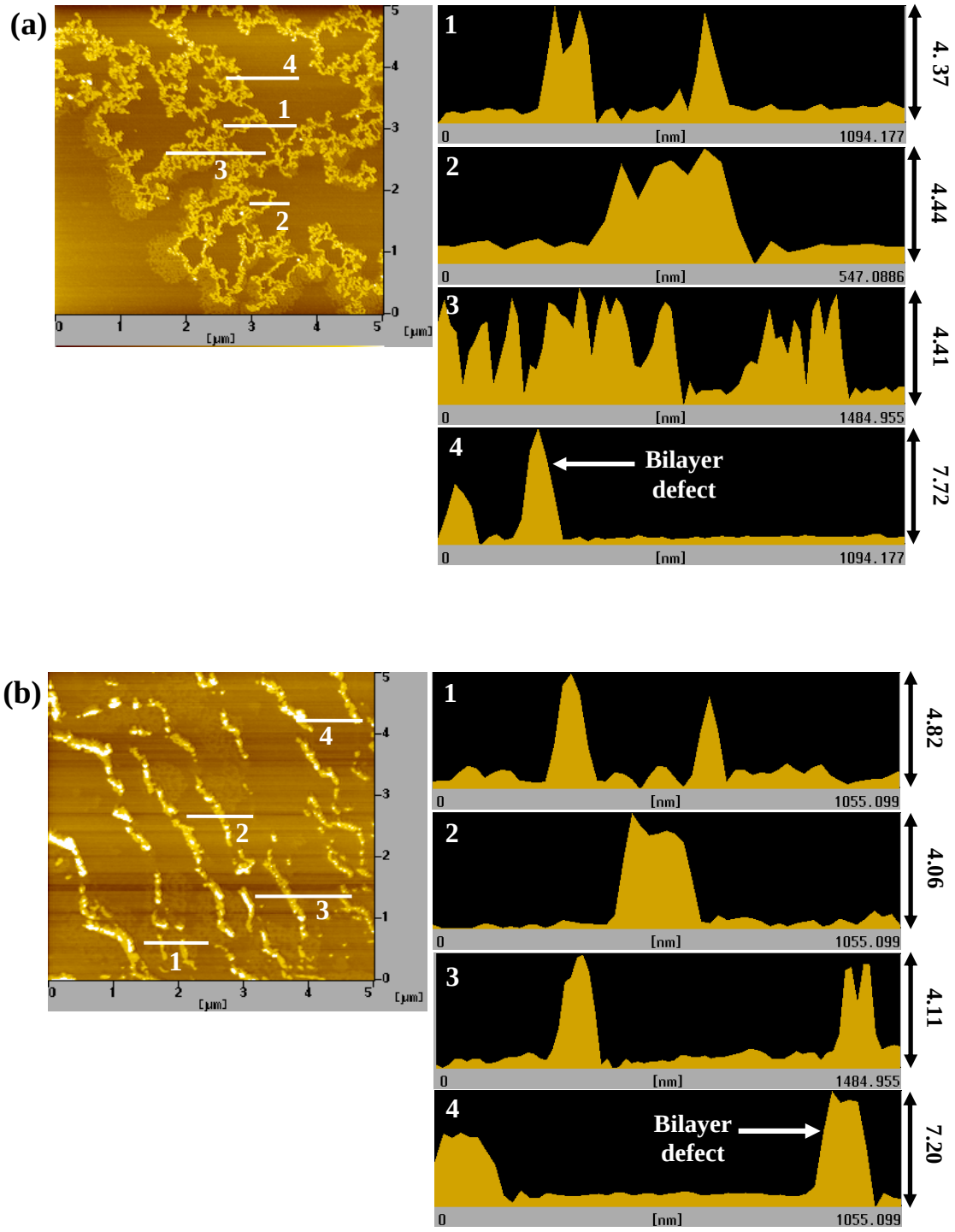

Figure 4.9. (Continued in the next page)

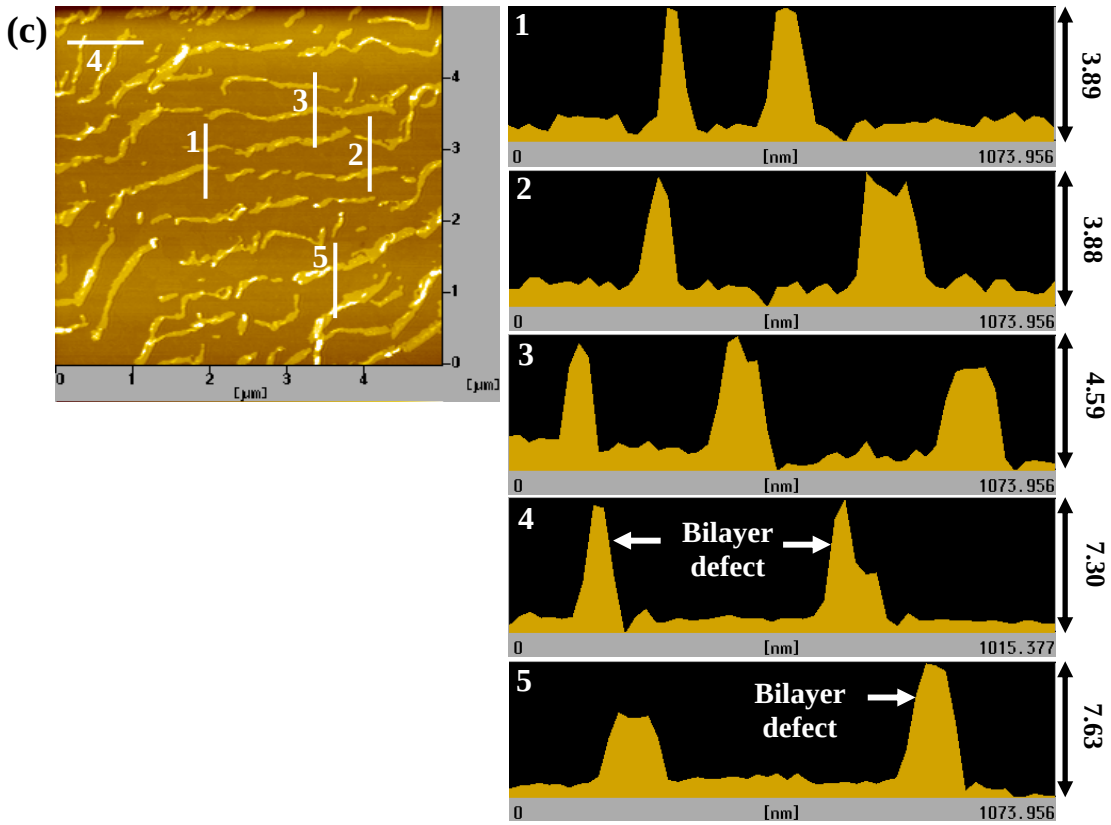

Figure 4.9. (Continued): *AFM topography images of monolayer LS films of PNOA fabricated with* ***(a)*** *only sulfate and additionally* ***(b)*** *PVS and* ***(c)*** *CMC in the subphase. Image size : 5 x 5 µm*^{2}*. The thickness profiles along different lines are shown for each image.*

are dramatically different, showing enhanced alignment of extended polymer chains. Templating by amphiphiles is known to align arrays of conjugated polymers.[19] In the present case, the pre-organized NOA amphiphiles possibly align the complexed polyelectrolytes which in turn enforce orderly growth of the PNOA chains during polymerization. Figs. 4.8b and 4.9b show threads, 4.0- 4.5 nm high and 40 – 50 nm wide in the case of PNOA formed with PVS in the subphase. Figs. 4.8c and 4.9c show threads, 3.8 – 4.2 nm high and 50 – 60 nm wide formed with CMC. The molecular modeling studies we have carried out to get some insight into the features observed in the AFM images are presented in the following section.

4.4.3. *Molecular modeling*

Useful information on the structural dimensions of individual polymer chains can be obtained by force field calculations on oligomer units of reasonable length. We have carried out such an exercise for PNOA, PVS and CMC in an effort to understand the morphological features observed in AFM. All molecular modeling computations were carried out using the Accelrys MS Modeling 3.0.1 program. The monomer geometries were optimized and extended in steps to decamer units using the 'polymer build' option, with geometry optimization at each stage using the Forcite module.

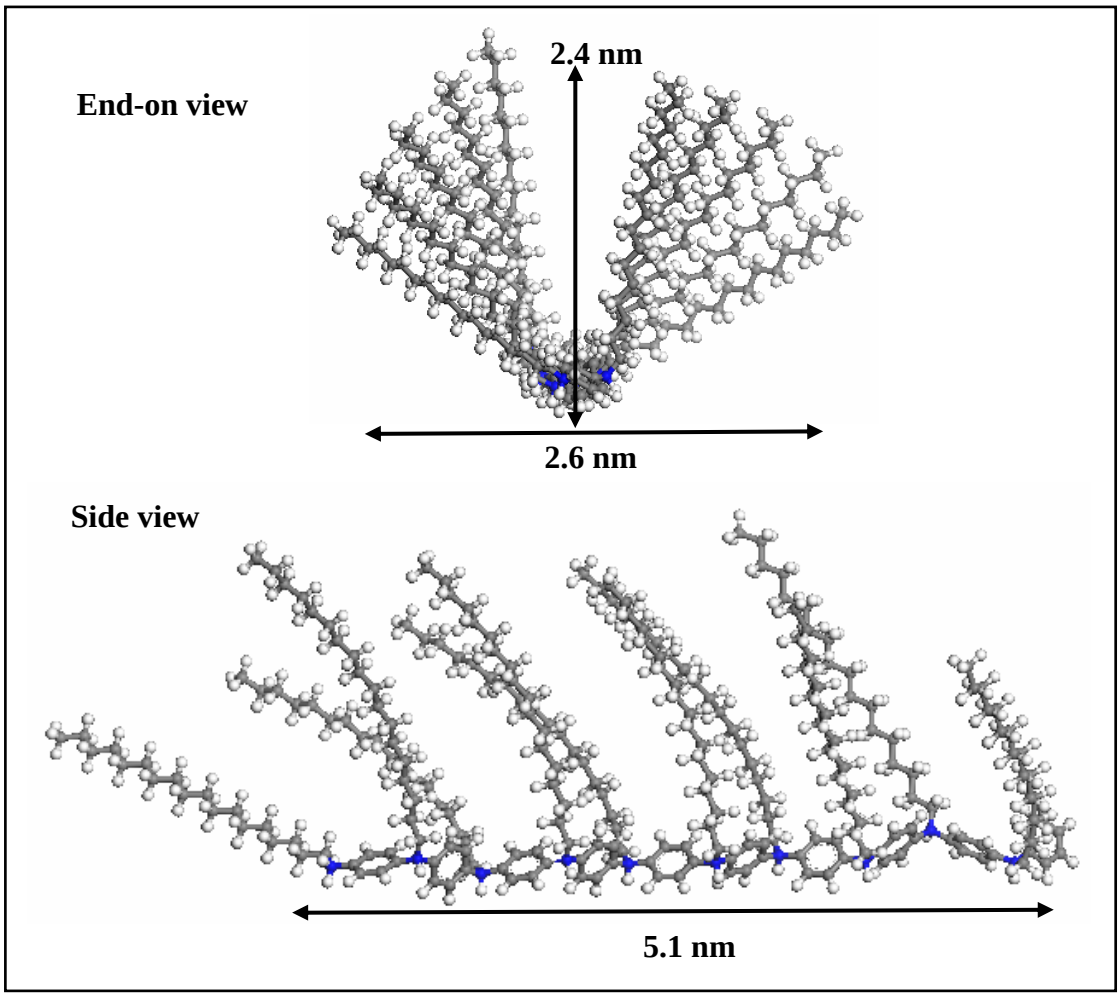

Figure 4.10. *Optimized geometry of fully protonated PNOA; (top) end-on view and (bottom) side view. The average monomer length is estimated to be 0.51 nm; C ( ), N ( ), H ( )*

We have chosen the initial conformations for optimization in such a way that PNOA decamer is fully protonated and the hydrocarbon chains are oriented towards one side of the polyaniline backbone (Fig. 4.10). For PVS and CMC, the acid groups were placed alternately on either side of the backbone and optimized (Fig. 4.11). Different views of the fully optimized geometries and approximate dimensions estimated from them are shown in the respective figures.

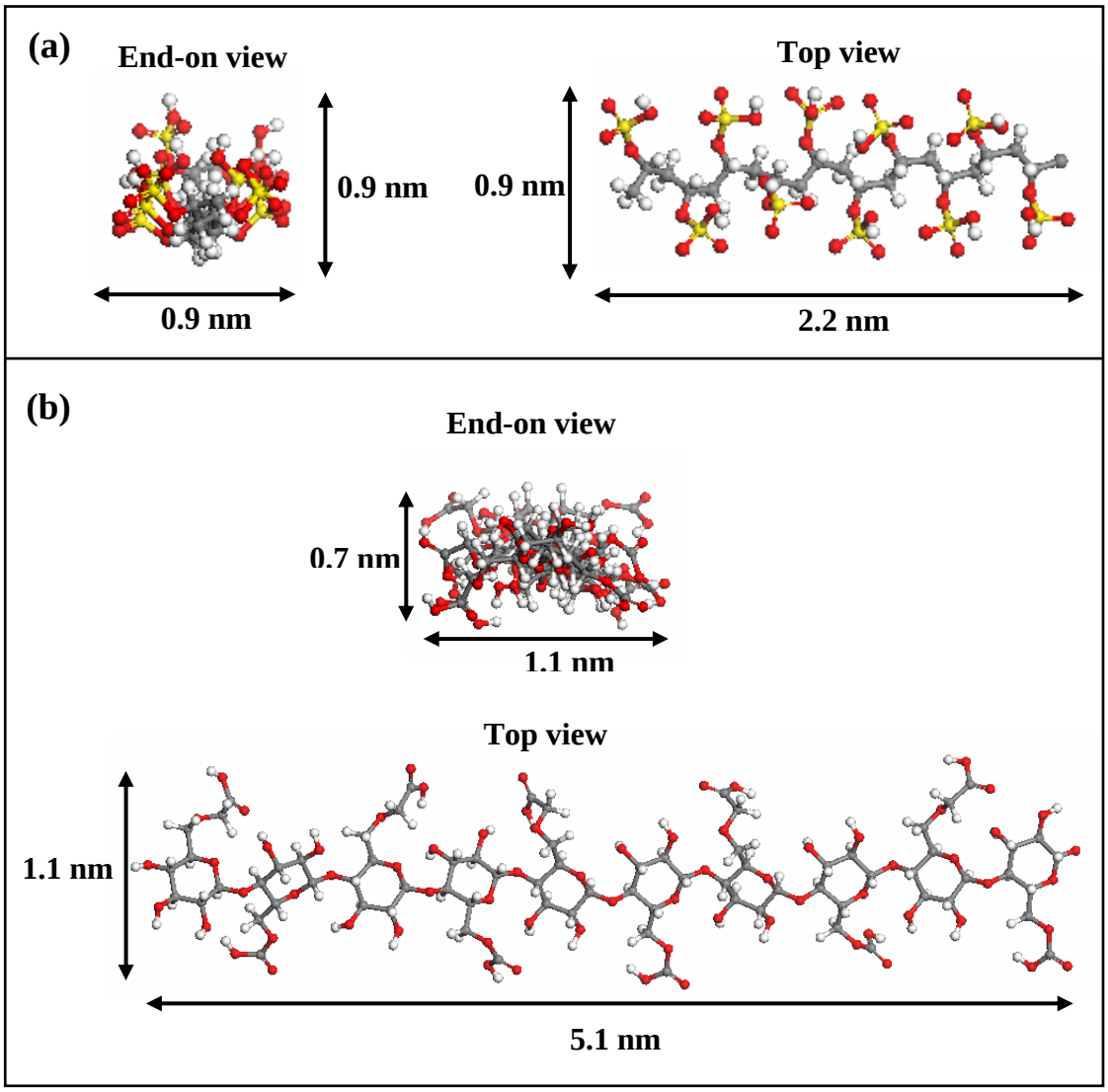

Figure 4.11. *Optimized geometries of* ***(a)*** *PVS and* ***(b)*** *CMC; end-on and top views are shown; the average monomer length is estimated to be 0.22 nm and 0.51nm respectively; C ( ), O ( ), S ( ), H ( ). The estimated length of PVS is consistent with that in Sec. 2.4.*

Molecular modeling of fully protonated PNOA (Fig. 4.10) decamer shows the polyaniline chain with the hydrocarbon groups splayed out wedge-like; the cross-sectional dimensions are ~ 2.4 x 2.6 nm^2. Based on this, the threads in Fig. 4.8a can be visualized as a monolayer of 12 – 20 PNOA chains with sulfate counterions, assembled laterally forming a tape-like structure. The polyelectrolyte decamer models indicate cross-sectional dimensions of ~ 0.9 x 0.9 nm^2 for PVS and ~ 0.7 x 1.1 nm^2 for CMC; the latter is in good agreement with an earlier model.[17] These estimates and the observed widths of the threads in Figs. 4.8b and 4.8c suggest plausible structures for the templated systems, consisting of PNOA chains on top of PVS and laterally placed with the CMC. These figures show that the threads are segmented with lengths in the range 0.6 – 1.6 μm. The average molecular weights of PVS and CMC correspond to chains ~ 0.2 μm long. Therefore the segment length appears to be built from 3 – 8 polyelectrolyte chains, along with the templated PNOA chain. If the PNOA chains are taken to be ~ 1.0 μm long, it would correspond to about 1960 monomers.

4.4.4. *Poly(4-styrenesulfonate) as the polyelectrolyte template for polymerization*

We have also studied the influence of sodium salt of poly(4-styrenesulfonate) (PSS) on the polymerization kinetics of NOA at the air-water interface and chain alignment in the LS films. We found that the effects due to PSS are rather complicated. The π-A isotherms are quite different from those shown in Fig. 4.4; the area per molecule is higher and the collapse pressure is lower. The polymerization rates are slower compared to the case of other polyelectrolytes. The absorption spectrum shows peaks shifted from those shown in Fig. 4.7. Most significantly, AFM study of the LS films reveals that PSS does not impart any organization in the chain alignment in the final polymer. It forms close packed features which are 150-200 nm long, 50-80 nm wide and 3.5-4.5 nm high (Fig 4.12). We believe that all these effects stem from additional π-stacking interactions of PSS with the polyaniline. These observations suggest that very strong interactions between the polyelectrolyte and the anilines may prove counterproductive.

The choice of the polyelectrolyte is important; while the impact of PVS and CMC are beneficial, PSS produces ambiguous effects. Judicious choice of the polyelectrolyte facilitates the fabrication of highly aligned polymer chains in the

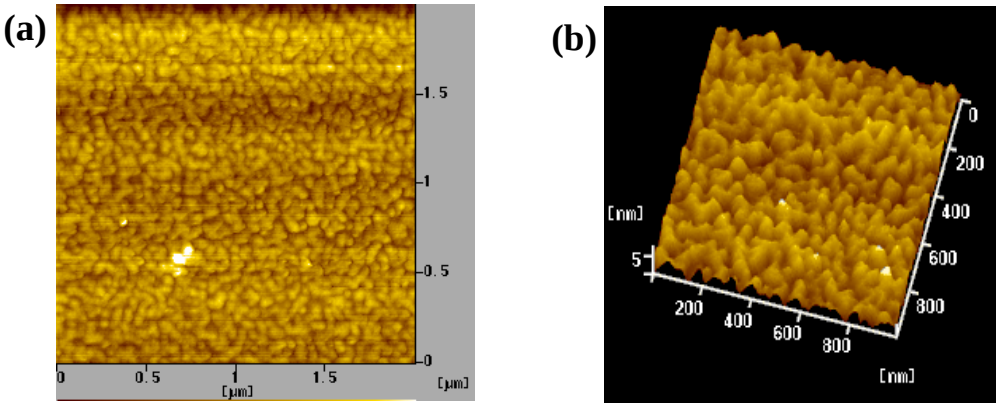

Figure 4.12. *AFM topography images of monolayer LS films of PNOA fabricated with PSS in the subphase :* ***(a)*** *2-dimensional;* ***(b)*** *3-dimensional.*

transferred ultrathin films. Control of polymerization in monolayers at the air-water interface using the simple and efficient technique of polyelectrolyte complexation has significant implications for the fabrication of organized polymer assemblies for molecular electronic and photonic applications and nanolevel patterning.

4.5. Synthesis of PNOA at the Organic – Aqueous Interface

Following our study of the synthesis of PNOA monolayers at the air-water interface, we have considered the bulk synthesis of this polymer at the liquid-liquid (aqueous-organic) interface. Free-standing films are of interest from the point of view of applications. We have developed a new procedure to prepare PNOA at the organic – aqueous interface which allowed the incorporation of polyelectrolytes as well. The detailed procedure of PNOA synthesis at the hexane-water interface is presented in Sec. 4.2.4.

The PNOA formed at the liquid-liquid interface is highly stable in the atmosphere and non-hygroscopic; the latter is significant in view of earlier reports to the contrary.[14] The film thickness can be tuned by varying the concentration of NOA in the organic phase. This method facilitates the preparation of films with desired area and excellent uniformity. This procedure can be employed to prepare PNOA with

polyelectrolyte templating as well using the polyions introduced in the aqueous layer. The films formed without polyelectrolyte templating are found to be extremely brittle, so that they cannot be removed easily from the reaction system. Presence of polyelectrolyte imparts considerable improvement in mechanical stability, so that though brittle, free-standing films can be easily isolated.

PNOA synthesized at the organic-aqueous interface is insoluble in most of the organic solvents; it has partial solubility in DMSO and NMP. This is in contrast with PNOA prepared in the bulk medium which has moderate solubility in the common organic solvents and suggests that PNOA synthesized at the liquid-liquid interface possesses higher molecular weight compared to the polymer prepared in the bulk. The films we have prepared were characterized by spectroscopy and microscopy studies.

4.5.1. *Electronic and vibrational spectroscopy*

UV-Visible-near IR spectrum of PNOA film (Fig. 4.13) shows peaks at 350, 430 and 750 nm and a broad absorption band at 800-1100 nm. These spectral characteristics are indicative of a moderately oxidized polymer. The peak at 350 nm arises due to the π - π^* absorption and the bands at 430 and 1000 - 1100 nm are related to

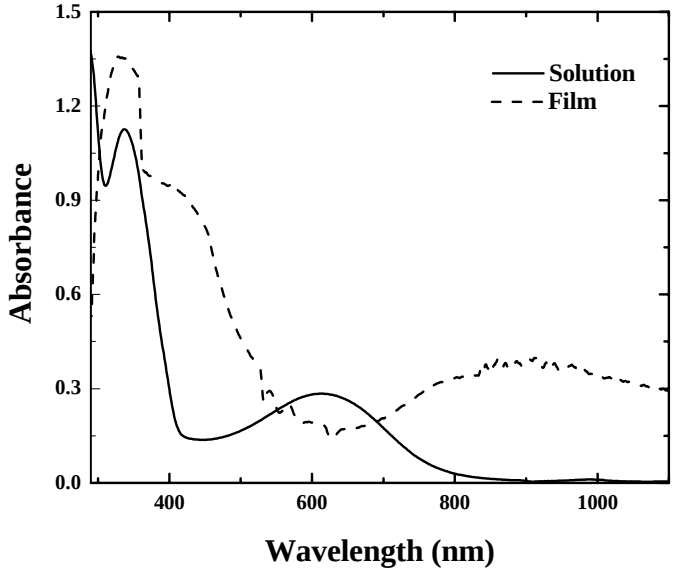

Figure 4.13. *Electronic absorption spectrum of PNOA synthesized at the aqueous-organic interface in the form of free-standing film and as solution in DMSO.*

polaron transition (benzenoid form). The peak around 750 nm can be attributed to bipolaron transition (quinonoid form).[14] The DMSO solution of the polymer shows absorption peaks at 350 and 620 nm. Absence of peak near 750 nm suggests that the low molecular weight fraction of the polymer that is soluble, does not sustain the quinonoid form.

The FT-IR spectrum shows the characteristic peaks of poly(N-*n*-alkylaniline)s. Absorption in the 3000-2800 cm^{-1} region is characteristic of C-H stretching vibrations. The ring stretch vibration of quinonoid and benzenoid forms are observed at 1580 and 1494 cm^{-1} respectively. The C-N stretch and C-H bend appear at 1400 – 1250 cm^{-1}. The band in the 820 – 800 cm^{-1} region is characteristic of the C-H out of plane bending vibration of the para-substituted benzene ring confirming that the expected head-to-tail coupling polymerization at the para carbon and nitrogen positions occur in the polymer formation. The relative weakness of the band around 750 cm^{-1} (C-H out-of-plane bending vibration of a terminal benzene ring) accounts for the high molecular weight of the polymers. The observed intensity ratio of the bands of the quinonoid and benzenoid forms is characteristic of moderately oxidized polymers, consistent with the observations from the UV-Visible-near IR spectra.

To verify if the PNOA film is formed in a protonated state, we have subjected it to acid and base treatments. Treatment with 1 M sulfuric acid caused no visible changes on the film. However, when treated with 1 M sodium hydroxide, the film color changed from green to a purple violet, possibly a result of deprotonation. This color change was found to be reversible upon washing the film again with pure water.

4.5.2. *Scanning electron microscopy*

Scanning electron microscope images of the PNOA film grown at the aqueous-organic interface are shown in Fig. 4.14. When prepared with no polyelectrolytes in the aqueous subphase, the film shows a honey-comb like porous surface but with no symmetric structure. The pore size is around ~ 2.5 μm. When synthesized with PVS in the aqueous phase, the film has different morphology when viewed on either surface (Fig. 4.14b and 4.14c). The surface exposed to the organic layer shows a morphology similar to that in Fig. 4.14a, but with pore sizes decreased to ~ 1.5 μm. More

significantly, no pores are visible on the surface exposed to the aqueous phase. Upon scratching this surface however, pores become apparent (Fig. 4.14d). This suggests that the polyelectrolyte forms a thin layer covering the lower surface of the polymer film exposed to the aqueous phase. These observations reveal the participation of the polyelectrolyte in the polymer formation and suggest a basis for the extra stability of the polyelectrolyte-polymer complex film.

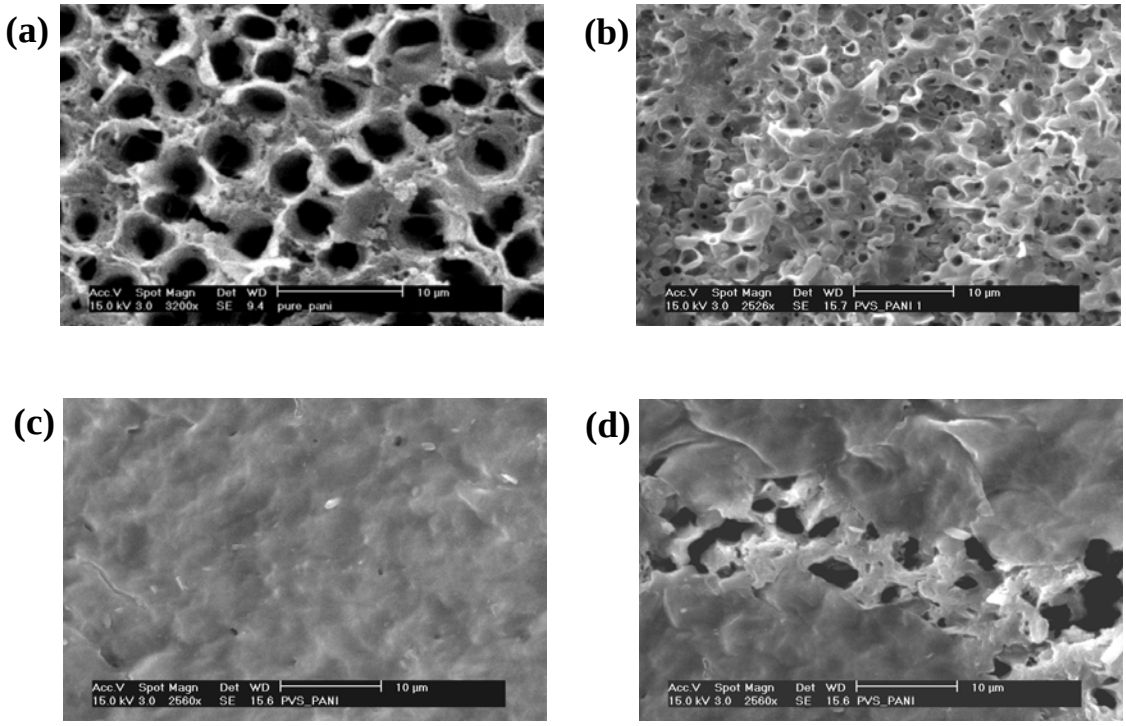

Figure 4.14. *SEM images of PNOA film synthesized at the aqueous – organic interface with* ***(a)*** *only sulfate and* ***(b) - (d)*** *additionally PVS in the subphase;* ***(b)*** *and* ***(c)*** *are the images of the surfaces in contact with the organic and aqueous phases respectively and* ***(d)*** *the image of the surface shown in (c) upon scratching.*

4.6. Summary

In this chapter we have presented the kinetics of polymerization of an amphiphilic aniline at the air-water interface and microscopy investigation through the process as well as on the end product. The critical role of polyelectrolyte templating from the aqueous subphase, on the polymerization kinetics and morphology of the

Langmuir film as well as the polymer LS film were investigated. The BAM studies revealed the influence of polyelectrolytes on the organization of the monomer and polymer monolayers. Significant reduction occurs in the polymerization rates due to polyelectrolyte templating. The AFM images of the polymer LB film formed, with and without polyelectrolyte templating demonstrated that the polyelectrolytes impart greater alignment to the polymer chains. Our study has shown that an optimal choice of the polyelectrolyte is necessary to exercise such control on the alignment of the conjugated polymer chains.

Polymerization studies carried out at the aqueous-organic interface resulted in free-standing and non-hygroscopic films which are of potential interest in practical applications. The polyelectrolyte templating is once again found to be beneficial, since it significantly increased the mechanical stability of the final polymer. Further studies should focus on exploring the possibility of achieving electrical conductivity in the ultrathin and thin films of these conjugated polymers.

References

1. Chandra, M.S.; Radhakrishnan, T. P. (*Communicated*).
2. Kloeppner, L. J.; Duran, R. S. *J. Am. Chem. Soc.* **1999**, *121*, 8108.
3. Hong, K.; Rubner, M. F. *Thin Solid Films* **1988**, *160*, 187.
4. Bodalia, R. R.; Duran, R. S. *J. Am. Chem. Soc.* **1993**, *115*, 11467.
5. Duran, R. S.; Zhou, H. C. *Thin Solid Films* **1992**, *210/211*, 356.
6. Kloeppner, L. J.; Duran, R. S. *Langmuir* **1998**, *14*, 6734.
7. Duran, R. S.; Zhou, H. C. *Polymer* **1992**, *210/211*, 4019.
8. Sharma, S.; Chandra, M. S.; Radhakrishnan, T. P. *Langmuir* **2001**, *17*, 8118.
9. (a) Chandra, M. S.; Ogata, Y.; Kawamata, J.; Radhakrishnan, T. P. *J. Nonlin. Opt. Phys. Mat.* **2004**, *13*, 347; (b) Chandra, M. S.; Ogata, Y.; Kawamata, J.; Radhakrishnan, T. P. *Langmuir* **2003**, *19*, 10124.
10. Chandra, M. S.; Krishna, M. G.; Mimata, H.; Kawamata, J.; Nakamura, T.; Radhakrishnan, T. P. *Adv. Mat.* (in press).
11. (a) Nagarajan, R.; Tripathy, S.; Kumar, J.; Bruno, F. F.; Samuelson, L. *Macromolecules* **2000**, *33*, 9542; (b) Liu. W.; Cholli, A. L.; Nagarajan, R.; Kumar, J.; Tripathy, S.; Bruno, F. F.; Samuelson, L. *J. Am. Chem. Soc.* **1999**, *121*, 11345; (c) Sudhakar, M; Stoecker, P. W.; Viswanathan, T. *Recent Res. Dev. Polym. Sci.* **1998**, *2*, 173; (d) Liu, J.; Yang, S. C. *Chem. Commun.* **1991**, 1529.
12. Jayanty, S.; Prasad, G. K.; Sreedhar, B.; Radhakrishnan, T. P. *Polymer* **2003**, *44*, 7265.
13. Watanabe, A.; Mori, K.; Iwabuchi, A.; Iwasaki, Y.; Nakamura, Y. *Macromolecules* **1989**, *22*, 3521.
14. Chevalier, J. -W.; Bergeron, J. -Y.; Dao, L. H. *Macromolecules* **1992**, *25*, 3325.
15. (a) Shibata, A.; Ossa, A.; Hashimura, Y.; Yamashita, S.; Ueno, S.; Yamashita, T. *Langmuir* **1990**, *6*, 217; (b) Letts, S. A.; Fort, T.; Lando, J. B. *J. Colloid Interface Sci.* **1976,** *56,* 64.
16. Heesemann, J. *J. Am. Chem. Soc.* **1980,** *102*, 2167.
17. Engelking, J; Menzel, H. *Thin Solid Films* **1998**, *327-329*, 90.
18. Zhao, B.; Neoh, K. G.; Kang, E. T.; Tan, K. L. *Chem. Mater.* **2000**, *12*, 1800.
19. Hoeben, F. J. M.; Jonkheijm, P.; Meijer, E. W.; Schenning, A. P. H. J. *Chem. Rev.* **2005**, *105*, 1491.

CHAPTER 5

Overview of the Present Work and Future Prospects

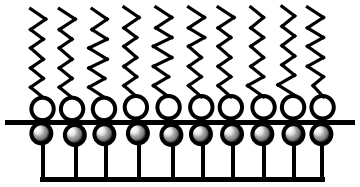

Polyelectrolyte templating

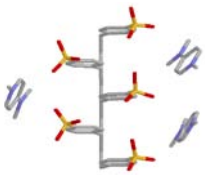

Modeling amphiphile – polyelectrolyte complexes

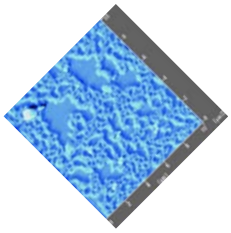

Stabilizing organization of NLO-chromophore based amphiphiles in LB films

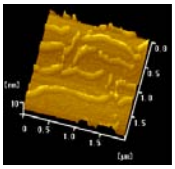

Organizing conjugated polymer chains in LB films

5.1. Overview of the Present Work

Development of various techniques for the organized assembly of atoms and molecules is of fundamental interest in various disciplines ranging from materials science to biology. Molecular materials are emerging as important candidates to meet the challenges of modern technology, as they afford superior flexibility in their design and fabrication. Organization of molecules into bulk materials, exploiting the full potential of the molecular responses for the materials application continues to be a difficult endeavor as it involves the careful control and optimization of a range of noncovalent intermolecular interactions. Langmuir-Blodgett technique is an elegant and efficient tool for the controlled assembly of molecules into ultrathin films. It is a promising route for the fabrication of molecular scale structures and devices with applications such as sensors[1] and electronic[2] or photonic[3] components and as models for biological membranes.[4] The LB technique provides a powerful tool to study intermolecular interactions at the air-water interface. Even though Langmuir-Blodgettry is a simple and elegant approach to fabricate molecular materials it is often plagued by difficulties like (i) instability of the amphiphile monolayer at the air-water interface; (ii) aggregation of the dipolar headgroups impairing the materials attributes being sought and (iii) thermodynamic instability of the transferred films. The delicate nature of LB films, usually held together by weak dispersion forces, has precluded their deployment in device applications, unless special post-deposition treatments are restored to. A common solution to address some of these problems has been the fabrication of composite films containing the amphiphile of interest in a specific application and an inert amphiphile which is known to form very stable films. This approach however has the disadvantage of reducing the number density of the active amphiphile headgroups in the 2-dimensional lattice leading to less effective utilization of the ultrathin films in the application of interest.

The main objective of this thesis was the exploration of the utility of a simple templating methodology in the fabrication of Langmuir and LB films. We have addressed specifically, the issue of instability and molecular aggregation and the control of polymerization process in the ultrathin films. Polyelectrolytes introduced from the aqueous subphase act as efficient templates for the assembly of ionic amphiphiles at the air-water interface. The utility of the polyelectrolytes in stabilizing Langmuir films and

achieving enhanced and stable second harmonic generation capability in the LB films through effective molecular deaggregation was demonstrated. The polyelectrolyte templates were also shown to exert a profound influence on the kinetics of polymerization in Langmuir films leading to improved polymer chain alignment in the deposited LB films.

The exploitation of intermolecular interactions across the air-water interface using polyelectrolytes introduced from the subphase has added a new dimension to the methods developed to circumvent some of the fundamental problems in the fabrication of LB films. Our investigation of N-*n*-octadecyl-4-dimethylaminopyridinium (ODP^+) - its tendency not to form monolayer at the air-water interface and the dramatic stabilization of its Langmuir films by various anions including polyanions – demonstrated the utility of exploiting the relatively strong Coulombic interactions in amphiphile-polyelectrolyte complexation. The systematic study with different kinds of anions in the aqueous subphase has provided a deeper understanding of the role of the molecular structure and positioning of the binding sites on the anions, in the stabilization of these films. The computational investigations including solvation effects suggest a new approach to model the complexation of ionic amphiphile headgroups and the polyion template. Subtle distinctions in the stabilization of the ionic amphiphile monolayer brought about by different polyelectrolytes could be understood within the framework of these computational investigations.

N-*n*-octadecyl-4-[2-(4-dimethylaminophenyl)ethenyl]pyridinium ($ODEP^+$), a system of great interest in quadratic nonlinear optical applications provided the logical second step to test our idea of polyelectrolyte complexation in the context of a real application. Molecular aggregation of this hemicyanine based amphiphile is a serious handicap in realizing the full SHG capability of its bulk assemblies. Our semiempirical quantum chemical computations incorporating solvation modeling on molecular and supramolecular structures from the crystal structure of the butyl derivative, $BDEP^+Br^-$ provided significant insight into the electronic absorption features of the chromophore group in isolated and aggregated states in solution, solid and LB films. The Langmuir film study of $ODEP^+Br^-$ revealed that the aggregation is dependent on the rate of equilibration of the monolayer at the air-water interface. Faster equilibration leads to aggregated forms which carry over to the LB films as well and produce reduced SHG.

Polyelectrolyte complexation from the aqueous subphase slows down the equilibration rate and leads to non-aggregated structures. With this approach, we were able to demonstrate enhanced SHG capability in the polyelectrolyte complexed LB films.

The metastability of the LB films of $ODEP^{+}Br^{-}$ and the decay of its SHG upon multiple laser irradiations was another important observation in our investigations of these LB films. Measurement of electronic absorption spectra after each laser irradiation which demonstrated the growth of the dimer peak at the expense of the monomer absorption provided valuable insight into the molecular level events accompanying SHG decay. The beneficial impact of polyelectrolyte templating could once again be illustrated by the arresting of the SHG decay in the templated $ODEP^{+}$ films. AFM imaging of the LB films gave an unprecedented view of hemicyanine LB films and strong morphological variations they are subjected to, as a result of the incorporation of polyelectrolyte supports. The images and spectroscopic features of the LB films coupled with molecular mechanics and semiempirical computations allowed us to project a structural model for the $ODEP^{+}$ monolayer films.

Polyelectrolyte templating from the aqueous subphase can strongly influence the organization and orientation of the amphiphilic units at the air-water interface. We have exploited this possibility in controlling the polymerization of the amphiphilic aniline (NOA) in Langmuir film. The novel protocol we have developed allowed us to follow accurately the kinetics of the polymerization at the air-water interface. The sequence of events during polymerization was monitored using Brewster angle microscopy. Impact of polyelectrolyte complexation was evident in the rates of polymerization as well as the Langmuir film morphology. The most significant influence of the polyelectrolyte was the extension and alignment imposed on the chains of the polyaniline as revealed by AFM investigation of the transferred Langmuir-Schaefer films. Investigation of the polyaniline synthesis at the aqueous-organic interface, further corroborates the role of polyelectrolyte in the polymerization process.

Investigations presented in this thesis have clearly demonstrated that polyelectrolyte templating is a simple tool to achieve enhanced stability in Langmuir and LB films and exercise control on the noncovalent and covalent assembly of molecules at the air-water interface. Our studies have provided examples of beneficial

impact on NLO chromophore assembly and conjugated polymer synthesis. We believe that this methodology provides a powerful approach to enhance the suitability of LB films for the fabrication of molecular scale devices and applications such as nanolevel patterning.

5.2. Future Prospects

The polyelectrolyte methodology we have developed as an alternative to the fabrication of composite films of different amphiphiles, for the stabilization and control of monolayer organization at the air-water interface, holds promise in several other potential applications. The methodology affords sufficient flexibility to fabricate LB films of any amphiphile with headgroups designed for electronic, magnetic or optical applications. The technique can be adapted to monitor molecular recognition events at the interface, an issue of great interest in surface chemistry and catalysis, and to fabricate 2-dimensional assemblies as mimics for biomembranes. The complexation of ionic amphiphiles can be used to probe the nature of polyelectrolytes as the binding would be site-specific. An immediate goal would be to explore anionic amphiphiles stabilized by polycationic systems. The methodology can be made very versatile if intermolecular interactions other than the strong ionic ones can be exploited. These would include hydrogen bonding and π-π interactions; the utility of these weaker forces in this context remains to be demonstrated.

In the area of NLO materials based on polyelectrolyte templated LB films, we have made only a beginning with the hemicyanine dye. The structure of $ODEP^+$ is quite amenable to several interesting modifications. The existing hydrocarbon chain attachment on the pyridinium nitrogen is not necessarily the best suited for headgroup orientation at the air-water interface. Moving the chain attachment to the other end (dimethylamino) would open up new possibilities of molecular orientation and facilitate better interaction between the polyelectrolyte from the subphase and the ionic site on the amphiphiles. This will also enable substitution of different kinds of groups on the pyridine nitrogen. An interesting possibility is to incorporate metal ions so that novel NLO and light emission properties can be explored. A vast repertoire of molecular systems possessing strong quadratic or other NLO responses is known. Choice of

optimal polyelectrolytes to stabilize monolayers of amphiphiles based on these headgroups would be a rewarding exercise to undertake. It would also be of great interest to explore the use of polyelectrolyte templated LB films in waveguiding and NLO applications other than SHG.

Preliminary investigations on fabrication of multilayer films have shown that polyelectrolyte complexation encourages the formation of Y-type films. Y-type films are the most common in multilayer LB films and are known to be much more stable than X or Z-type of films. However they are detrimental for properties such as SHG which require noncentrosymmetric organization of the NLO-phore units. Interestingly, even though Y-type films are formed with soft polymers like poly(4-styrenesulfonate) the SHG of the multilayer films was found to increase quadratically with the number of layers. Detailed investigations are required to unravel the basis of this surprising observation; it is possible that the polyelectrolyte template layer screens the electrostatic interactions between the layers of the NLO-phore and facilitates parallel orientation of the dipole assemblies. If proved, this would be a significant advantage of adopting polyelectrolyte templating methodology.

Our investigation of aniline polymerization modulated by polyelectrolytes in the subphase demonstrates that the templating methodology provides a convenient handle on molecular level organization and chemical reaction. This concept can be developed into a general route for the synthesis of single macromolecule chains and nanoparticles. In addition to facilitating controlled assembly, this technique provides for efficient monitoring of the process kinetics. The products of these processes, coupled polymer chains or polymer-nanoparticle composites are of great current interest in a number of applications.

The polyelectrolyte templating or ‘gluing’ is a versatile accessory to the popular technique of Langmuir-Blodgettry. We have demonstrated instances where it has allowed fine control of molecular interactions and assemblies and enabled the realization of enhanced materials attributes. Extension of these ideas to molecular devices and related applications could be important challenges for future research.

References

1. Roberts, G. G. in *Langmuir-Blodgett Films*, Roberts, G. G. (Eds.), Plenum Press: New York, 1990, p. 317.
2. Paloheimo, J.; Kuivalainen, P.; Stubb, H.; Vuorimaa, E.; Lathi, P. –Y. *Appl. Phys. Lett.* **1990**, *56*, 1157.
3. (a) Zhao, S.; Reichert, W. M. *Langmuir* **1992**, *8*, 2785; (b) Swalen, J. D. *J. Molecular Electronics* **1986**, *2*, 155.
4. Swart, R. M. in *Langmuir-Blodgett Films* Roberts, G. G. (Eds.), Plenum Press: New York, 1990, p. 273.

Appendices

APPENDIX A

Instrumentation for Characterization of New Materials

Melting temperatures of solids were determined using capillary melting point apparatus (Superfit, India); values reported are uncorrected. Infrared spectra were recorded on a Jasco5300 FTIR spectrometer. All the spectra were calibrated against polystyrene absorption at 1601 cm^{-1}. Samples were recorded as KBr pellets. Electronic absorption (UV-Vis) spectra were recorded on a Hitachi Model U-3300 or Shimadzu model UV 3101 PC UV-Visible spectrophotometer. Specular reflectance (8^o incidence) or diffuse reflectance spectra of solid samples and LB films on quartz or glass substrates were recorded using the integrating sphere (ISR 3100) accessory. ^1H and ^{13}C NMR spectra were recorded on Bruker AC 200 MHz NMR spectrometer. ^1H NMR (200 MHz) spectra were measured with TMS ($\delta = 0$) as internal standard. ^{13}C NMR (50 MHz) spectra were recorded using the solvent peaks as the internal standard. Sartorius BP211D balance was used for high precision weighing.

APPENDIX B

Langmuir and Langmuir-Blodgett Film Fabrication

Pressure-area (π-A) isotherms were investigated on a Nima Model 611M (USI Co. Ltd. Model FDS-23 trough was used in a few experiments) LB trough using a Wilhelmy plate for pressure sensing (Fig. B1). The components of the trough were described in Sec. 1.3.3. The Nima trough dimensions are 30 x 10 x 0.35 cm^3. Millipore MilliQ water (resistance > 18 MΩ) was used for the subphase in all experiments; typically ~ 220 ml of water was taken in the trough. Experiments employing the polyelectrolytes used typically ~ 1.8 μM (based on monomer molecular weight) solutions. Solution of amphiphiles in chloroform (Uvasol grade, EMerck) was spread on the subphase keeping the mole ratio of amphiphiles to the counterions in the subphase ~ 1 : 8; a systematic investigation of different ratios in the case of pyridinium amphiphile and $(Na^+)_nPSS^{n-}$ showed this to be the optimal one to achieve the best improvement in monolayer stability. However, 1 : 5 ratio was found to be more suitable for the amphiphilic anilines and hence employed in the experiments in Chapter 4. All experiments were carried out at 25°C. After spreading the amphiphile solution, a minimum wait period of 30 min to a maximum of 120 min depending on the monolayer material was allowed for the adsorption of the polyelectrolyte at the interface and

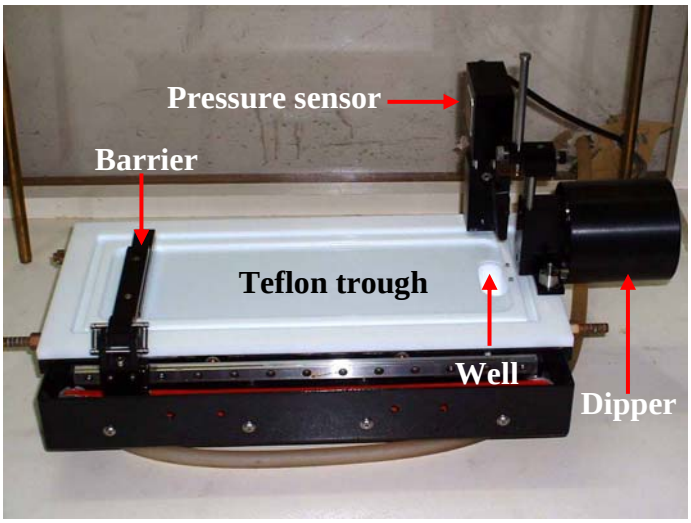

Figure B1. *Langmuir-Blodgett trough used in our laboratory.*

equilibration of the surface pressure. The π-A isotherms were recorded using a barrier speed of 50 cm^2/min. All pressure-area experiments were repeated on fresh subphases 3 - 5 times to confirm reproducibility.

Langmuir-Blodgett films were deposited either on glass or quartz substrates. Hydrophilic surface for the monolayer deposition was prepared using the following protocol employing high purity water in all operations. The substrate was cleaned with detergent followed by several rinsings in water; it was sonicated in fresh lots of water three times for 15-20 min each. The surface was made hydrophilic by immersing in aqueous sodium hydroxide for 12 h or treating with pirhana solution (H_2O_2 : H_2SO_4 = 3 : 7) for 90 min followed by sonication and rinsing in water. Hydrophobic surface was prepared by exposing the slides to vapors of hexamethyldisilazane for 12 h. The LB film was coated on the substrate by the vertical dipping procedure employing a dipping speed of 5 mm/min with the monolayer held typically at a pressure of 25 or 30 mN/m. Alternatively, films were coated using the horizontal lifting (Langmuir-Schaefer) procedure carried out manually. Freshly cleaved mica plates coated by the horizontal dipping were used for AFM imaging.

APPENDIX C

Microscopy Techniques

(a) *Brewster angle microscope*

Brewster angle microscopy allows the *in situ* study of thin films at the gas/liquid or solid/gas interfaces. The principle of the method is illustrated in Fig. C1.

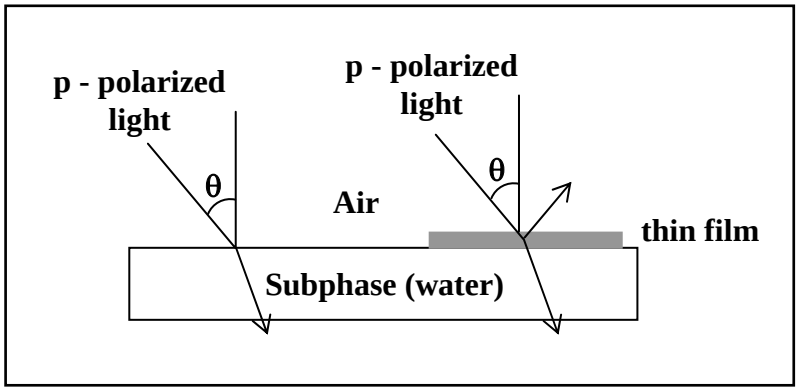

Figure C1. *Principle of Brewster angle microscopy.*

When a beam of p-polarized light (plane of polarization parallel to the plane of incidence) is incident on the surface at a specific angle, θ (Brewster angle), such that

$$\tan \theta = \frac{n_{subphase}}{n_{air}}$$

(n's are the refractive indices) it is completely transmitted; no reflection occurs and the view from the top of the surface looks dark. Introduction of a thin film at the interface between the two phases alters the optical property of the surface and a small amount of the incident light is reflected. This provides an efficient way to image the monolayer on the water surface.

The equipment used in our experiments, Nanofilm Model BAM 2Plus is shown in Fig. C2. The wavelength and power of the laser used are 532 nm and 20 mW respectively. Using the 20x objective lens, an ultimate resolution of ~ 1 μm can be achieved in the images.

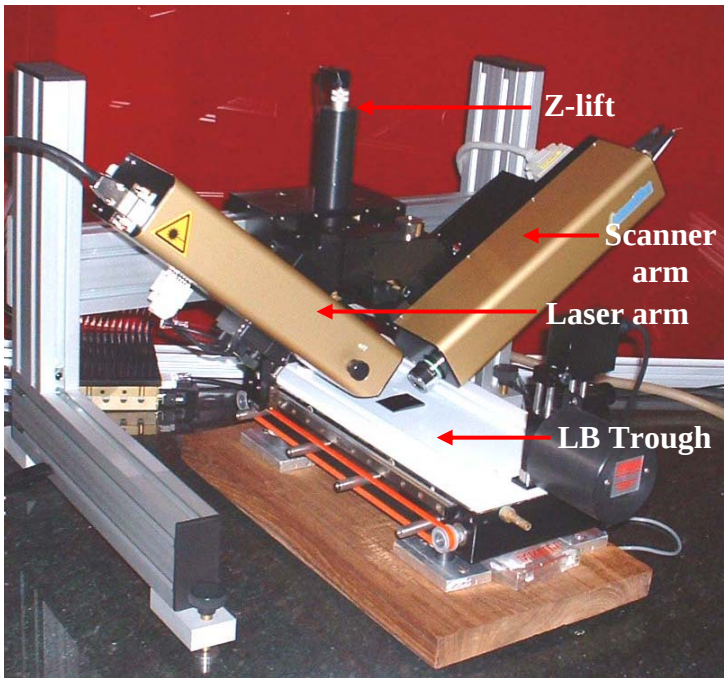

Figure C2. *Brewster angle microscope used in our laboratory, the picture shows also the LB trough positioned under the BAM.*

(b) ***Atomic force microscope***

AFM images of Langmuir-Blodgett and Langmuir-Schafer films deposited on mica substrates were recorded on a SEIKO Model SPA 400 atomic force microscope. All images presented were recorded in the dynamic force (non-contact) mode using a tip having a force constant of 20 N/m. Topography as well as phase images were recorded, typically using a 20 μm scanner. Line profiles were analyzed using the software supplied by the microscope manufacturer.

(c) ***Scanning electron microscope***

Morphology of free-standing polymer films studied in Chapter 4 was examined using a Philips XL 30 ESEM scanning electron microscope. Gold coating was provided on the films prior to examination.

APPENDIX D

X-ray Crystallography

X-ray diffraction data was collected on an Enraf-Nonius MACH3 diffractometer at 293 K. MoK_α radiation (λ = 0.71073 Å) with a graphite crystal monochromator in the incident beam was used. Standard CAD4 centering, indexing and data collection programs were used. The unit cell dimensions were obtained by a least square fit of 24 centered reflections in the neighborhood of $\theta = 10^o$. Intensity data were collected using the ω scan method at a scan speed of 4.12^o/min to a maximum 2θ of 50^o. The scan width $\Delta\theta$ for each reflection was $0.80 + 0.35 \tan\theta$. During data collection the intensities of three standard reflections were monitored every 1.5 h of X-ray exposure, no decay was observed. In addition three orientation standards were monitored every 250 reflections to check the effects of crystal movement. Data was reduced using Xtal 3.4;[1] Lorentz and polarization corrections were included. All non-hydrogen atoms were found using the direct method analysis in SHELX-97[2] and after several cycles of refinement the positions of the hydrogen atoms were calculated and added to the refinement process. Empirical absorption correction was applied using ψ scan data. Refinement proceeded to convergence by minimizing the function $\sum w(F_o^2 - F_c^2)$. A final difference Fourier map showed the largest difference peak and hole to be acceptably small. The R indices were calculated as $R = \sum \left| (|F_0| - |F_c|) \right| / \sum |F_0|$ and $wR^2 = \left[\sum w(F_0^2 - F_c^2)^2 / \sum (F_0^2)^2 \right]^{1/2}$. Graphics were handled using ORTEX6a.[3]

The fractional atomic coordinates (x 10^4) and isotropic displacement parameters, U_{eq} (Å^2 x 10^3) of $BDEP^+Br^-$ are provided in Table D1. U_{eq} is defined as one third of the trace of the orthogonal U_{ij} tensor. Estimated standard deviations (esd) are given in parenthesis.

References

1. *Xtal 3.4*, Hall, S. R.; King, G. S. D.; Stewart, J. M. (Eds.), University of Western Australia, Perth, Australia, **1995**.
2. *SHELX-97*, Sheldrick, G. M. University of Göttingen, Göttingen, Germany, **1997**.
3. McArdle, P. *J. Appl. Cryst.* **1995**, *28*, 65.

Table D1

	x	y	z	U_{eq}
Br(1)	9284(1)	2164(1)	2441(1)	62(1)
Br(2)	4453(1)	2166(1)	2504(1)	86(1)
N(3)	9377(4)	4904(3)	3008(3)	56(1)
N(4)	884(4)	4694(3)	1313(3)	59(2)
N(5)	5541(4)	2984(3)	-55(3)	53(1)
N(6)	14011(4)	1332(3)	-162(3)	53(1)
C(7)	8694(6)	5497(4)	2891(4)	63(2)
C(8)	7595(6)	5373(4)	2728(4)	66(2)
C(9)	7191(6)	4620(5)	2682(4)	63(2)
C(10)	7925(6)	4029(4)	2782(4)	67(2)
C(11)	8976(6)	4179(4)	2951(4)	64(2)
C(12)	6043(7)	4446(5)	2486(4)	75(2)
C(13)	5302(7)	4960(5)	2372(4)	71(2)
C(14)	4139(6)	4846(4)	2128(4)	54(2)
C(15)	3492(6)	5478(4)	2026(4)	57(2)
C(16)	2429(5)	5440(3)	1757(4)	54(2)
C(17)	1952(5)	4735(4)	1577(3)	47(2)
C(18)	2581(6)	4084(4)	1710(4)	58(2)
C(19)	3652(6)	4142(4)	1982(4)	57(2)
C(20)	10540(5)	5034(4)	3205(4)	57(2)
C(21)	10739(5)	5166(4)	4064(3)	56(2)
C(22)	11926(5)	5394(4)	4223(4)	64(2)
C(23)	12162(6)	5482(4)	5086(4)	75(2)
C(24)	407(6)	3961(4)	1094(4)	75(2)
C(25)	310(6)	5377(4)	1066(4)	73(2)
C(26)	5975(6)	2862(4)	657(4)	60(2)
C(27)	7052(6)	2689(4)	751(4)	60(2)
C(28)	7752(5)	2639(3)	111(4)	48(2)
C(29)	7275(5)	2765(3)	-625(4)	51(2)
C(30)	6182(6)	2926(4)	-686(4)	55(2)
C(31)	8911(5)	2440(3)	217(4)	52(2)
C(32)	9642(5)	2384(3)	-352(4)	51(2)
C(33)	10770(5)	2148(3)	-273(4)	48(2)
C(34)	11281(5)	1981(3)	444(4)	51(2)
C(35)	12347(5)	1721(4)	480(4)	52(2)
C(36)	12960(5)	1594(3)	-199(4)	47(2)
C(37)	12443(5)	1785(4)	-917(3)	51(2)
C(38)	11390(5)	2046(4)	-938(3)	52(2)
C(39)	4380(5)	3207(4)	-164(4)	61(2)
C(40)	4248(5)	4065(4)	-232(4)	55(2)
C(41)	3078(5)	4273(4)	-446(4)	64(2)
C(42)	2892(5)	5131(4)	-460(4)	71(2)
C(43)	14480(5)	1056(4)	565(4)	68(2)
C(44)	14585(5)	1130(4)	-880(4)	64(2)

APPENDIX E

Measurement of Second Harmonic Generation from LB Films

Incident angle dependence of the SHG intensities of the films was measured using a pulsed beam from a repetitively Q-switched Nd-YAG laser (Lee, Model 818TQ, 1.0 kHz) at a wavelength of 1064 nm with a pulse duration of 100 or 140 ns and a peak power of 5.1 kW. Top view of the setup is shown in Fig. E1. Since the dynamic range of the boxcar system is not very wide, neutral density filters were used to control the light intensity. The samples were mounted on a motor-controlled rotational stage. The angle of incidence of the laser beam on the film, θ, was rotated from 0 to 75°. In the p-p and s-p polarization measurements (Fig. E2) p-polarized (perpendicular to the rotation axis) and s-polarized (parallel to the rotation axis) fundamental laser beams were used and the p-polarized second harmonic light was detected by a photomultiplier tube (Hamamatsu, Model R212). The signal from the photomultiplier tube was sent to a boxcar averager (Stanford Research, Model SR250). All the instruments were controlled by a personal computer.

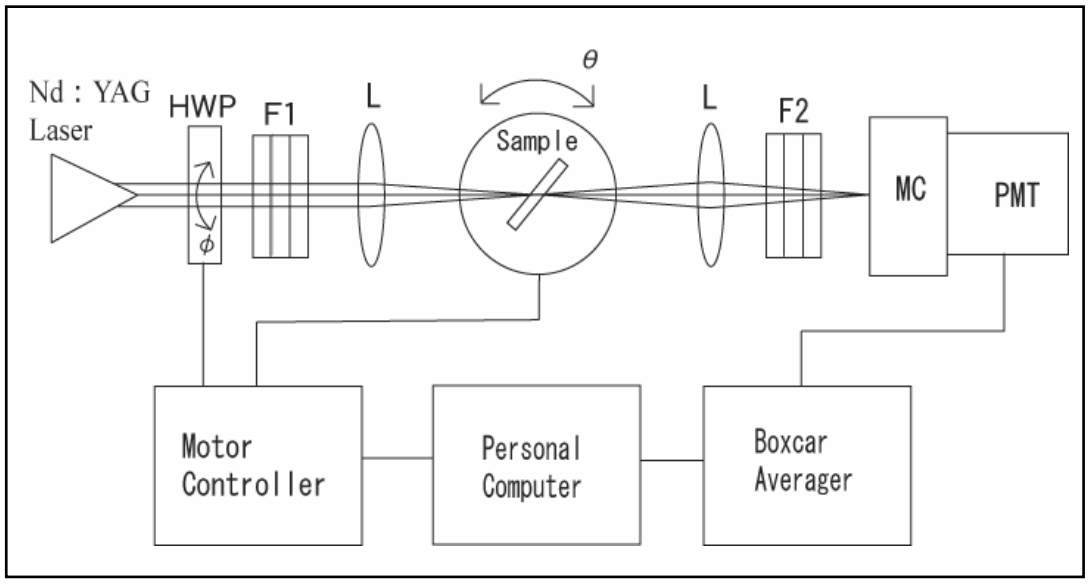

HWP: Half wave plate, F1, F2: Filters, L: Lens, MC: Monochromator, PMT: Photomultiplier tube

Figure E1. *Setup for the measurement of SHG from LB films.*

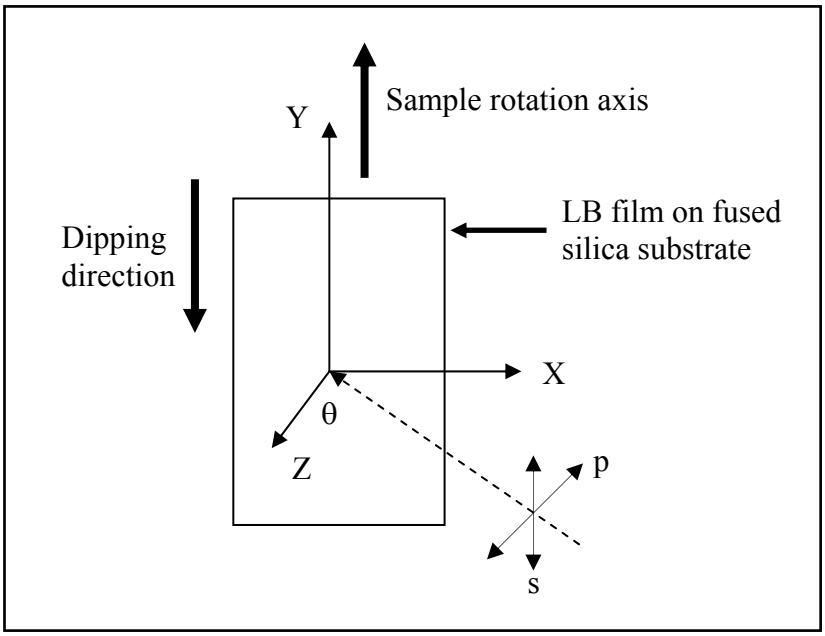

Figure E2. *Geometry of the LB film sample placement and fundamental laser beam polarization.*

SHG fringe analysis

When a sample such as LB film coated on both sides of a fused silica plate or a Y-cut quartz crystal, is placed in the setup shown in Fig. E1 and rotated, the SHG produced from the front and back surfaces interfere, producing a fringe pattern (see for example, Fig. 3.13). The laser beam intensity (P_ω) was estimated using the quartz data and the χ_{xxx} value of quartz. The equations for fitting were taken from the references, 1-3 and are listed below.

Quartz

P_ω was estimated by fitting the fringe pattern ($P_{2\omega}^{quartz}$ versus θ) using the following equation :

$$P_{2\omega}^{quartz} = [A\,(P_\omega)^2\,B] \,/\, [(n_\omega^2 - n_{2\omega}^2)^2]$$

A is an instrument constant

$$B = t_\omega^4\, T_{2\omega}\, (\chi_{xxx})^2 (\cos^2\theta_\omega' \cos\theta_{2\omega}' - \sin^2\theta_\omega' \cos\theta_{2\omega}' - \cos\theta_\omega' \sin\theta_\omega' \sin\theta_{2\omega}')^2 \sin^2[\Phi(\theta')]$$

where,

$t_\omega = 2\cos\theta / (n_\omega\cos\theta + \cos\theta_\omega')$

$T_{2\omega} = 2\, n_{2\omega}\cos\theta_{2\omega}'\,[C/D]$

$C = (n_\omega\cos\theta + \cos\theta_\omega')(n_{2\omega}\cos\theta_\omega' + n_\omega\cos\theta_{2\omega}')$

$D = (n_{2\omega}\cos\theta + \cos\theta_{2\omega}')^3$

$\Phi(\theta') = [\pi/2]\,[4L/\lambda]\,[n_\omega\cos\theta_\omega' - n_{2\omega}\cos\theta_{2\omega}']$

and $\theta_\omega' = \sin^{-1}(\sin\theta/n_\omega)$; $\theta_{2\omega}' = \sin^{-1}(\sin\theta/n_{2\omega})$

The nonlinear coefficient χ_{xxx} was taken as 0.30 pm/V and the refractive indices n_ω (1.53413) and $n_{2\omega}$ (1.54702) are taken from the literature.[3] The wavelength, λ is 1064 nm.

The value of $A(P_\omega)^2$ and L, the thickness of the quartz crystal (path length) are the fitting parameters.

LB films

The fringes recorded for the LB films are fitted subsequently using the following equations for the s-p and p-p geometries.

$P_{2\omega}^{p\text{-}p} = [A\,(P_\omega)^2\,B] / [(n_\omega^2 - n_{2\omega}^2)^2]$

where $B = t_\omega^4\, T_{2\omega}\,(\chi_{zzz}\sin^2\theta_\omega''\sin\theta_{2\omega}'' + 3\chi_{zxx}\cos^2\theta_\omega''\sin\theta_{2\omega}'')^2\sin^2[\Phi(\theta')]$

$t_\omega = 2\cos\theta / (n_\omega\cos\theta + \cos\theta_\omega')$

$T_{2\omega} = 2\, n_{2\omega}\cos\theta_{2\omega}'\,[C/D]$

$C = (n_\omega\cos\theta + \cos\theta_\omega')(n_{2\omega}\cos\theta_\omega' + n_\omega\cos\theta_{2\omega}')$

$D = (n_{2\omega}\cos\theta + \cos\theta_{2\omega}')^3$

$\Phi(\theta') = [\pi/2]\,[4L/\lambda]\,[n_\omega\cos\theta_\omega' - n_{2\omega}\cos\theta_{2\omega}']$

$P_{2\omega}^{s\text{-}p} = [A\,(P_\omega)^2\,B] / [(n_\omega^2 - n_{2\omega}^2)^2]$

where $B = t_\omega^4\, T_{2\omega}\,(\chi_{zxx}\sin\theta_{2\omega}'')^2\sin^2[\Phi(\theta')]$

$t_\omega = 2\cos\theta / (n_\omega\cos\theta_\omega' + \cos\theta)$

$T_{2\omega} = 2\, n_{2\omega}\cos\theta_{2\omega}'\,[C/D]$

$C = (n_\omega\cos\theta_\omega' + \cos\theta)(n_\omega\cos\theta_\omega' + n_{2\omega}\cos\theta_{2\omega}')$

$D = (n_{2\omega}\cos\theta_{2\omega}' + \cos\theta)^3$

$$\Phi(\theta') = [\pi/2]\,[4L/\lambda]\,[n_{\omega}\cos\theta_{\omega}' - n_{2\omega}\cos\theta_{2\omega}']$$

and $\theta_{\omega}' = \sin^{-1}(\sin\theta/n_{\omega})$; $\theta_{2\omega}' = \sin^{-1}(\sin\theta/n_{2\omega})$;
$\theta_{\omega}'' = \sin^{-1}(\sin\theta/ n_{\omega}'')$; $\theta_{2\omega}'' = \sin^{-1}(\sin\theta/ n_{2\omega}'')$

The value of $A(P_{\omega})^2$ was obtained from the quartz data fitting. The refractive indices n_{ω} and $n_{2\omega}$ for the glass substrate are taken to be 1.5149 and 1.5247 respectively. The wavelength, λ is 1064 nm.

The value of the substrate thickness, L, the refractive indices n_{ω}'' and $n_{2\omega}''$ of the LB film at frequencies ω and 2ω respectively and the susceptibility tensor components, χ_{ZZZ} and χ_{ZXX} of the LB film are the fitting parameters for the p-p polarization data. For the s-p polarization data L, n_{ω}'', and χ_{ZXX} are the fitting parameters.

In all the analysis carried out, the agreement between the parameters obtained from the p-p and s-p data fittings for any given sample was found to be satisfactory.

References

1. Kuzyk, M. G.; Singer, K. D.; Zahn, H. E.; King, L. A. *J. Opt. Soc. Am. B* **1989,** *6,* 742.
2. Mizrahi, V.; Sipe, J. E. *J. Opt. Soc. Am. B* **1988,** *5,* 660.
3. Jerphagnon, J.; Kurtz, S. K. *J. Appl. Phys.* **1970,** *41,* 1667.

Publications and Presentations

PUBLICATIONS

1. Sharma, S.; **Chandra, M. S.**; Radhakrishnan, T. P. *Langmuir* **2001**, *17*, 8118.
Stabilization of a Cationic Amphiphile Monolayer by Polyanions in the Subphase and Computational Modeling of the Complex at the Air-Water Interface.

* 2 Ramakrishnan, M.; Kenoth, R.; Ravikanth, K.; **Chandra, M. S.**; Radhakrishnan, T. P.; Swamy, M. J. *FEBS Lett.* **2002**, *531*, 343.
N-Myristoylethanolamine - Cholesterol (1:1) Complex : First Evidence from Differential Scanning Calorimetry, Fast-Atom-Bombardment Mass Spectrometry and Computational Modeling.

3. **Chandra, M. S.**; Radhakrishnan, T. P. *Mol. Cryst. Liq. Cryst.* **2003**, *403*, 77.
Molecular Aggregation in a Hemicyanine Dye: Modeling by a Combined Crystallographic and Computational Approach.

4. **Chandra, M. S.**; Ogata, Y.; Kawamata, J.; Radhakrishnan, T. P. *Langmuir* **2003**, *19*, 10124.
Polyelectrolyte Assisted Deaggregation and SHG Enhancement in Hemicyanine Langmuir-Blodgett Film.

5. **Chandra, M. S.**; Ogata, Y.; Kawamata, J.; Radhakrishnan, T. P. *J. Nonlin. Opt. Phys. Mater.* **2004**, *13*, 347.
Enhanced SHG in Polyelectrolyte Complexed Hemicyanine Dye Langmuir-Blodgett Films.

6. **Chandra, M. S.**; Krishna, M. G.; Mimata, H.; Kawamata, J.; Nakamura, T.; Radhakrishnan, T. P. *Adv. Mat.* (In press)
Laser induced SHG Decay in a Langmuir-Blodgett Film : Arresting by Polyelectrolyte Templating.

7. **Chandra, M. S.**; Radhakrishnan, T. P. (*Communicated*)
Polyelectrolyte Templated Polymerization in Langmuir Film : Nanoscopic Control of Polymer Chain Organization.

* *Not included in the thesis.*

PRESENTATIONS AT INTERNATIONAL FORUMS

1. **Chandra, M. S.**; Ogata, Y.; Kawamata, J.; Radhakrishnan, T. P.
   AsiaNano 2002 (Asian Symposium on Nanotechnology and Nanoscience) at Nippon Kagaku Miraikan, Tokyo, November, **2002**.
   Polyelectrolyte Assisted Deaggregation and SHG Enhancement in Hemicyanine Based LB Films.

2. **Chandra, M. S.**; Ogata, Y.; Kawamata, J.; Radhakrishnan, T. P.
   Poster presented at the 7th International Conference on Organic Nonlinear Optics (ICONO7) / International Conference on Organic Photonics and Electronics, Sorak, Korea, November, **2003**.
   Enhanced SHG in Polyelectrolyte Complexed Hemicyanine Dye Langmuir-Blodgett Films.

3. **Chandra, M. S.**
   Seminar at Yamaguchi University, Yamaguchi, Japan, November, **2003.**
   Polyelectrolyte assisted stabilization and deaggregation of ionic amphiphiles in Langmuir and Langmuir-Blodgett films.

4. **Chandra, M. S.**; Kawamata, J.; Radhakrishnan, T. P.
   Poster presented at the 6th International Tropical Conference on Optical Probes of Conjugated Polymers and Biosystems, Bangalore, India, January, **2005.**
   Stable and Enhanced Second Harmonic Generation in Organic Ultrathin Films : Role of Polyelectrolyte Templating.